Mémoire

Auteur : Dessart, Antoine
Promoteur(s) : De Becker, Michaël
Faculté : Faculté des Sciences
Diplôme : Master en sciences spatiales, à finalité approfondie
Année académique : 2024-2025
URI/URL : http://hdl.handle.net/2268.2/22967

Faculty of Sciences

Department of astrophysics, geophysics and oceanography

Master Thesis

SMEM0029-1

Three-phase astrochemical investigation of glycine precursors in dark molecular clouds

---

A thesis conducted to obtain the degree of Master in Space Sciences, Research Focus

Author:
Antoine Dessart
Liège University

Supervisor:
Michaël De Becker
Liège University

Reading Committee:
Michaël De Becker
Denis Grodent
Valérie Van Grootel
Lauriane Soret
Liège University

Academic year 2024-2025

Contents

Acknowledgments

Before letting you discover the work I have carried with heart throughout this academic year, there are several acknowledgments I would like to address.

Before anyone else, I would like to express all my gratitude to both Maria Groyne, PhD student at the University of Liège, and Michaël De Becker, head of the MEGA group at the University of Liège, for their critical advise and supervision all along this year that allowed me to dig as deep as possible into this more than interesting topic. I could not have wished for a better supervising team.

After that, I would like to thank the reading committee composed of Michaël De Becker, Denis Grodent, Valérie Van Grootel and Lauriane Soret for their attentive reading of my work. I hope you will enjoy reading this manuscript as much as I appreciated writing it.

I am grateful to the following people for their careful proofreading of my work and for all their comments, which allowed me to improve this document as much as I could: Maria Groyne, Michaël De Becker, Christophe Dessart and Marc Grodent.

I would also like to thank the Physics Department at the University of Liège, where I completed my Bachelor's degree — a crucial step without which I would not have been able to pursue such an engaging Master's program. My sincere gratitude goes as well to all the members of the Department of Astrophysics, Geophysics and Oceanography at the University of Liège, for the warm and welcoming atmosphere as well as for the high-quality teaching provided throughout these past two years.

Last but no least, my family deserves also my gratitude for all their care and support during my studies, as well as my friends since my beginning at the University, Vincent Ernst and Théotime Vande Populiere. This Master's thesis marks the conclusion of the past five years of my life, and I could not have gone through it without all of you.

Abstract

The origin of life on Earth remains one of the most captivating scientific questions. To explain the emergence of life, one must first understand how the molecular building blocks necessary for the first living cell appeared. This thesis contributes to the investigation of the exogenous origin of these building blocks—that is, their synthesis in astrophysical environments and subsequent delivery to Earth via cometary and asteroidal impacts. The focus is placed on the potential formation of amino acids - particularly glycine - in dark molecular cloud environments.

Building on the gas-phase study by Groyne (2023), this work extends the investigation using a static (i.e. with fixed physical parameters over time) three-phase astrochemical model that incorporates not only gas-phase chemistry, but also reactions occurring on and within interstellar dust grains, including their surfaces and icy mantles. This modeling is performed using the ***Nautilus*** code (Ruaud et al., 2016). After presenting this rate-equation-based model and comparing it to results obtained with the ***Astrochem*** code in Groyne (2023), this study offers a detailed analysis of the chemical behavior of key glycine precursors, as identified in various formation pathways proposed in the literature.

Finally, a comparison with observational data from the literature is conducted, highlighting the limitations of this simplified model in reproducing observed ice abundances. Although a static, rate-equation-based approach may not be optimal for modeling ice compositions, this study provides valuable initial insights into the chemical behavior of glycine precursors, laying the groundwork for future research using more comprehensive and dynamic models.

Chapter 1

Introduction to the field of Astrochemistry

In this introductory section, the field of Astrochemistry will be introduced along with its various connections with other research fields. The two main guidelines to follow, i.e. molecular complexity and astrophysical filiation, will also be introduced, as well as a brief census of molecular species that have been discovered so far in the interstellar medium.

1.1 What is Astrochemistry? What lies behind this field of research?

Before diving into the core of the work that I have carried out throughout this academic year, it is essential to get everyone on the same page and to clearly define the field we are studying. Following De Becker (2013), Astrochemistry can be defined as *"the science devoted to the study of the chemical processes at work in astrophysical environments, including the interstellar medium, comets, circumstellar and circumplanetary regions"*.

Our research field is at the **crossroad of two disciplines** giving it its name, namely Astrophysics and Chemistry. The first is focusing on the physics behind the evolution of astronomical objects, while the second is linked to the study of the formation and evolution of molecular species within a given environment. Astrochemistry is thus a multidisciplinary scientific domain using both fields in a complementary way, extending the application field of Chemistry to space and being a significant input for Astrophysics[1]. A next step in our definition of the field is to differentiate Chemistry from Molecular Spectroscopy. There is often confusion between those and it is therefore useful to define them properly. The first has already been defined, whereas the second could be seen as a technique allowing a qualitative and quantitative study of molecular species through their interaction with electromagnetic radiations (absorption and emission) within a given environment (astrophysical or not). This technique is thus an **extremely useful tool** for Astrochemistry, because it allows the census of molecular populations.

Another link to be highlighted is the one to Astrobiology, which is of prime impor-

[1]Indeed, the molecular content of an astrophysical environment (interstellar cloud, protoplanetary disk, planetary nebulae, ...) is completely dependent on its physical properties. As we will see in Chapter 2, chemical reactions (moreover astrochemical reactions) depend a lot on the density and temperature conditions.

tance in the context of the present work. Several key questions in Astrobiology can be tackled with the help of Astrochemistry such as the origin of the building blocks of life (sugars, nucleic acids, amino acids, ...), i.e. endogenous or exogenous, but also the origin of the homochirality problem[2], the problem of bio-signatures (with the help of molecular spectroscopy) as discussed in Seager et al. (2013) and Seager et al. (2016), and also the RNA (RiboNucleic Acid) world hypothesis to explore the gap between biotic and abiotic systems (Gilbert, 1986; Ayukawa et al., 2019). This is of course not an exhaustive list, but these are some questions that can be explored with the help of Astrochemistry.

We may say that *Astrochemistry is the natural multidisciplinary answer that modern science has developed to address scientific questions that are totally out of the scope of existing individual scientific disciplines* (De Becker, 2013). A summary of all those various connections is presented in Figure 1.1.

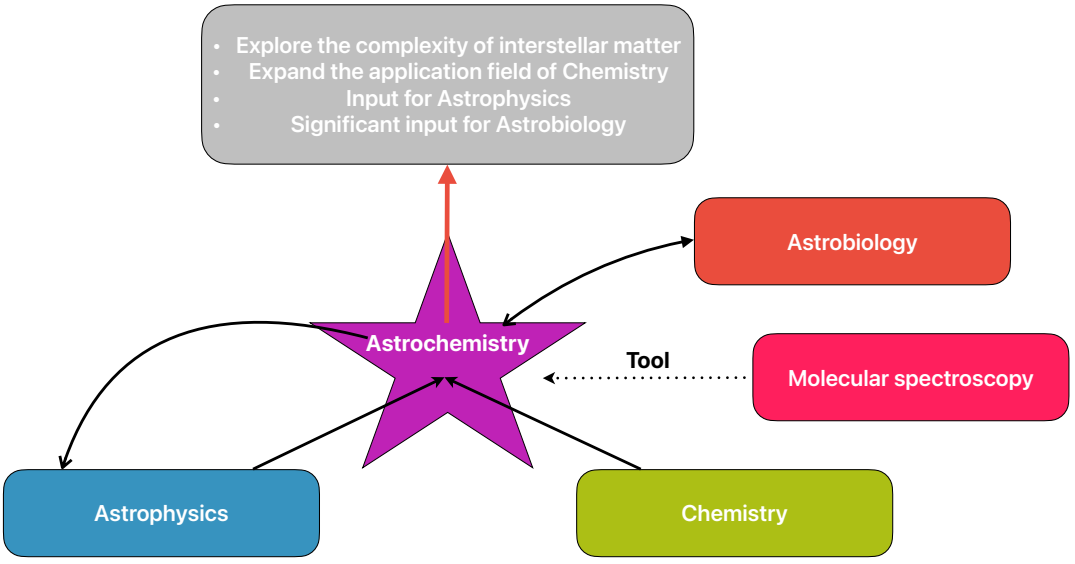

Figure 1.1: Schematic view of the interdisciplinary dynamical exchanges implied in the astrochemical field of research.

Beside those considerations, on a more practical point of view, it is also important to emphasize some challenges an astrochemist may encounter. Unlike classical Chemistry, which takes place in laboratories under terrestrial conditions, Astrochemistry deals with chemical processes occurring in space under highly **unusual physical conditions**. In particular, temperature and density—two fundamental parameters in our study—differ significantly. In most laboratory experiments, standard conditions of pressure and temperature are assumed, namely 101325 Pa and 273.15 K. While experiments can to some extent be conducted at higher or lower values, they are limited by what is achievable on Earth. Under atmospheric conditions, the density at sea level[3] is approximately 10^{19}

[2]Most of the amino acids and the sugars active in our biochemistry are respectively of the L-form and D-form. Even if they are much rarer, other enantiomers can also be found in living organisms as discussed for example in Fujii (2002) and Genchi (2017). A question that may be asked is the following: *Where does this enantioselectivity comes from? Is it linked to some astrophysical considerations?* It may be, through a phenomenon called **asymmetric photolysis** as for example discussed in Cerf and Jorissen (2000) or Jorissen and Cerf (2002).

[3]Throughout this work, I may occasionally misuse the term *density*. Unless otherwise specified, *density*

molecules/cm^3. By contrast, the highest densities observed in the ISM correspond to approximately 10^6 molecules/cm^3, typical of the densest molecular clouds—the primary astronomical objects of interest in this study. This represents a decrease of about 10^{13} orders of magnitude compared to terrestrial conditions. Furthermore, such low densities are associated with extremely low temperatures, typically ranging from 10 K to 20 K. In addition to these density and temperature differences, molecular clouds are continuously exposed to intense radiation fields, primarily in the ultraviolet (UV) range, as well as to energetic cosmic rays, as discussed in Chapter 2.

Considering these factors, such environments present a unique and challenging setting for chemical studies. One might even assume that these astrophysical conditions are entirely inhospitable to molecular formation, a view famously expressed nearly a century ago (1926) by Sir Arthur Stanley Eddington (1882–1944): "*It is difficult to admit the existence of molecules in interstellar space, because once a molecule is dissociated it seems to be no chance for atoms to join again*". However, as we will explore in Section 1.3, molecules do indeed exist in space. Moreover, it must be understood that such ISM-like conditions are very difficult to reproduce in laboratory, even with the best technologies at our disposal[4]. Furthermore, as discussed in Section 1.3, the molecular content of interstellar clouds is rich, notably made of species present in rather low relative abundances, which makes spectral molecular lines often difficult to characterize through spectroscopy.

All of those challenges complicate the work of astrochemists, and they must usually restrict their studies to specific cases. For example, we might mention the study of interstellar ices present inside molecular clouds, as discussed in Chapter 2, through experimentation and simulation on interstellar ice analogues[5] or the study of the molecular content of meteorites or cometary coma, known to possess a quite appreciable amount of organic molecules (including notably amino acids).

As a conclusion to this section, we may say that astrochemists aim to understand the molecular complexity that can be achieved in various astronomical environments, through observational studies, computational molecular modeling (as done in this master thesis) and laboratory experiments.

1.2 Two guidelines: molecular complexity and astrophysical filiation

It is legitimate to ask ourselves: *what do we mean by molecular complexity*? It is already possible to get, intuitively, a glimpse of its signification. Let's take the H_2 molecule, the most abundant molecule in the universe. One senses that this molecule is more simple than for example H_2O. The CO molecule, the second most abundant molecule in the universe, a priori also more complex than H_2. Our opinion seems thus to be based upon the number of different constituting atoms, as well as the number of chemical bonds within the molecule.

should be understood as *numerical density*.

[4]Some setups are able to achieve these low temperature and pressure levels, such as the one at the Laboratory for Astrophysics at the Leiden University (`https://home.strw.leidenuniv.nl/~linnartz/setups.html`)

[5]Interstellar ice analogues are synthetic ices, containing elements which are known to be contained in interstellar ices, aiming at reproduce the icy mantles surrounding dust grains.

We will restrict the discussion to the reasoning proposed by Mil'man (1989), which is based on information theory, and where it is considered that "*the complexity of a molecular compound can be approximated by the amount of information required to fully and unambiguously characterize it*". Following this principle, we will consider several criteria in order to establish the level of complexity of a given molecular species:

(i) The number of constituting atoms

(ii) The number and diversity of functional groups[6]

(iii) The presence of a stereogenic center[7]

In order to investigate molecular complexity, two (complementary) approaches may be followed: (i) we can either climb the complexity ladder, following **the bottom-up approach**, in which we study the simplest compounds in order to understand how they can become more and more complex to achieve eventually the highest complexity that we know, i.e. DNA, RNA and proteins, (ii) or we can go down this ladder following **the top-down approach** where we start with the more complex molecules to find out their precursors. In the context of this work, the first approach will be explored, as discussed with much more details in Chapter 3.

The second guideline to be addressed is the concept that we call **astrophysical filiation**, which is linked to the transformation of astrophysical environments, and thus to the changes of the physical parameters affecting chemical reactions. A schematic view of the connection between various astronomical environments is shown in Figure 1.2. In this work, we focus exclusively on the interstellar medium (ISM), with a particular emphasis on molecular clouds. However, it is important to remember that many other astrophysical environments are equally relevant, as **they are all interconnected**. The collapse of a molecular cloud leads to stellar formation, and only a small fraction of the original cloud, not incorporated into the newly formed star, will give rise to a protoplanetary disk. This disk will eventually evolve into planets, asteroids and comets. Some asteroids and comets may become meteorites, enriching planetary surfaces with molecular material. Stars, through their radiation fields, influence the molecular composition of interstellar clouds, particularly the diffuse ones. As they reach the end of their life cycle, the ejected planetary nebula/supernova remnants may further impact the surrounding interstellar medium, primarily through hydrodynamic shocks that alter both density and temperature. While stellar evolution and planetary formation extend beyond the scope of this master thesis, these processes are deeply intertwined. This broader astrophysical lineage highlights the strong connections between various fields of study relevant to Astrochemistry.

[6]Mainly found in organic compounds, and can be simply defined as specific groupings of atoms within a molecule, that possess their own reactivity properties, regardless of the other atoms inside the molecule. Examples that will be of great interest to us are the carboxylic acid group R−COOH and the amine group R−NH_2, contained in each amino acid. Let us note that the "R-" stands for the rest of the molecule.

[7]A **stereogenic center** is another word for **chiral carbon**, which is a carbon atom bound to four different groups.

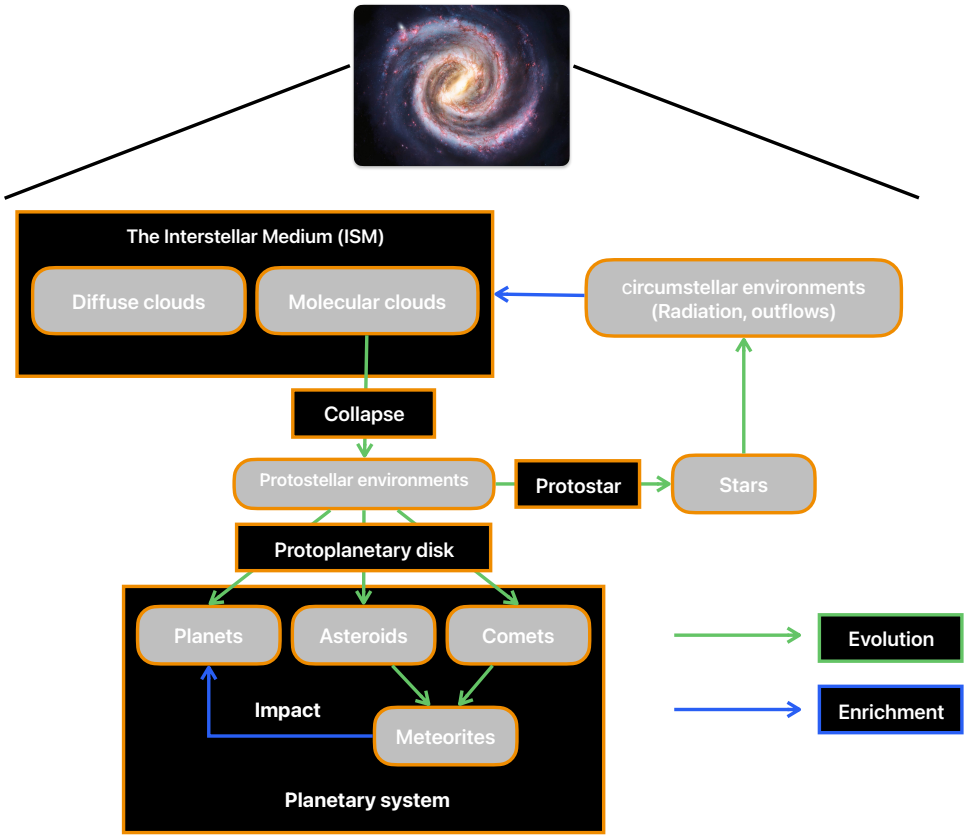

Figure 1.2: Filiation between astrophysical environments relevant in the case where we limit ourselves to the galactic environment. Adapted from De Becker (2023-2024).

1.3 Census of the molecular entities discovered in the interstellar medium

On the contrary to what Sir Eddington might have thought, **molecules do exist in space**. Particularly, they exist in the ISM, as it has been proven thanks to molecular spectroscopy[8]. Since the first molecular detection in gas phase, namely the CH molecule (Swings and Rosenfeld, 1937), a lot of molecules have been detected in the ISM, including several complex organic species, such as the first isomer of glycine, i.e. syn-glycolamide $NH_2C(O)CH_2OH$ (Rivilla et al., 2023). As years go by, more and more molecules will continue to be discovered in the ISM, thanks to new technological developments included in new observatories (on the ground and in space) such as the Atacama Large Millimeter/submillimeter Array in the radio domain or the James Webb Space Telescope in the infrared. A census of the **currently** detected molecules in the ISM is presented in Table 1.1 (adapted[9] from De Becker 2013).

[8]Mainly (more than 80%) through the detection of bands in the radio part of the electromagnetic spectrum, which carries information about the rotational modes of a given molecule and constitutes a very specific signature. The rest has been detected mostly in the infrared domain (vibrational modes), and a very small amount in the ultraviolet and visible domains.

[9]Thanks to *the Astrochemist* website, created and maintained by D. E. Woon, `https://www.astrochymist.org/`

2 atoms	AlCl, AlF, AlO, C_2, CF^+, CH, CH^+, CN, CN^-, CO, CO^+, CP, CS, FeO, NaS, MgS, CaO, H_2, HCl, HF, NH, KCl, N_2, NO, NO^+, NS, NaCl, O_2, OH, OH^+, PN, SH, SH^+, SO, SO^+, SiC, SiN, SiO, SiS, P, TiO, ArH^+, NS^+, VO, HeH^+, NCS, PO^+, SiP, FeC
3 atoms	AlNC, AlOH, C_3, C_2H, C_2O, C_2P, C_2S, CO_2, H_3^+, CH_2, H_2Cl^+ , H_2O, H_2O^+, H_2S, HCN, HCO, HCO^+, HCS^+, HCP, HNC, HN_2^+, HNO, HOC^+, KCN, MgCN, NH_2, N_2H^+, N_2O, NaCN, OCS, SO_2, c-SiC_2, SiCN, SiNC, SiCSi, FeCN, TiO_2, CCN, S_2H, HCS, HSC, NCO, NCS, CaNC, MgC_2, HSO, CaC_2
4 atoms	l-C_3H, c-C_3H, C_3N, C_3O, C_3S, C_3H^+, H_3O^+, C_2H_2, H_2CN, H_2CO, H_2CS, HCCN, HCCO, $HCNH^+$, HCNO, HOCN, $HOCO^+$, HNCO, HNCS, HSCN, NH_3, SiC_3, PH_3, H_2O_2, HMgNC, MgCCH, NCCP, CNCN, HONO, HCCS, HNCN, $HCCS^+$, H_2NC, HCNS, $HOCS^+$, HNSO
5 atoms	C_5, CH_4, c-C_3H_2, l-C_3H_2, H_2CCN, H_2C_2O, H_2CNH, H_2COH^+, C_4H, C_4H^-, HC_3N, HCCNC, HCOOH, NH_2CN, SiC_4, SiH_4, HCOCN, HNCNH, HC_3N^-, CH_3O, $NCCNH^+$, CH_3Cl, MgC_3N, NH_2OH, HC_3O^+, HC_3S^+, H_2CCS, C_4S, HCCCO, HCOSH, HCSCN, NaCCCN, MgC_3N^+, HC_3N^+, NC_3S, HC_3S, t-HCSSH
6 atoms	c-H_2C_3O, C_2H_4, CH_3CN, CH_3NC, CH_3OH, CH_3SH, l-H_2C_4, HC_3NH^+, $HCONH_2$, C_5H, HC_2CHO, HC_4N, CH_2CNH, C_5N^-, C_5S, SiH_3CN, z-HNCHCN, MgC_4H, HC_3CO^+, CH_2CCH, H_2CCCS, HCSCCH, MgC_5N, CH_5^+, $HCCNCH^+$, CH_3CO^+, C_5O, c-C_5H, HCCCCS, HMgCCCN, MgC_4H^+, H_2CCCH^+, H_2CCCN, HOCOOH, H_2CNCN, NCCHCS, c-C_3H_2S
7 atoms	c-C_2H_4O, CH_3C_2H, H_3CNH_2, CH_2CHCN, H_2CHCOH, C_6H, C_6H^-, HC_4CN, CH_3CHO, CH_3NCO, HC_5N^-, HC_5O, $HOCH_2CN$, HNCHCCH, HC_4NC, CH_2CHCCH, C_3HCCH, H_2C_5, MgC_5N, CH_2CCCN, NC_4NH^+, MgC_5N^+, $NCCONH_2$, HC_5N^+, HNC_5, $CH_2(CN)_2$, HCCCHCN, CH_3CHS
8 atoms	H_3CC_2CN, $H_2COHCOH$, CH_3OOCH, CH_3COOH, C_6H_2, CH_2CHCHO, CH_2CCHCN, C_7H, NH_2CH_2CN, $(NH_2)_2CO$, CH_3SiH_3, $(NH_2)_2CO$, CH_2CHCCH, $HCCCH_2CN$, MgC_6H, HC_5NH^+, $C_2H_3NH_2$, Z-$(CHOH)_2$, HCCCHCCC, C_7N^-, CH_3CHCO, MgC_6H^+, Z-NCCHCHCN
9 atoms	CH_3C_4H, CH_3OCH_3, CH_3CH_2CN, CH_3CONH_2, CH_3CH_2OH, C_8H, HC_6CN, C_8H^-, CH_2CHCH_3, CH_3CH_2SH, CH_3NHCHO, HC_7O, H_3C_5CN (2 isomers), HCCCHCHCN, H_2CCHC_3N, C_5H_4, $H_2CCCHCCH$, OHCHCHCHO, $CH_2CHCHNH$, $HCCCH_2CCH$, HC_7N^+, CH_3SCH_3
10 atoms	CH_3COCH_3, CH_3CH_2CHO, CH_3C_5N, CH_3OCH_2OH, C_6H_4, HC_2CCHC_3N, HC_7NH^+, $C_2H_5NH_2$, C_2H_5NCO, t-$CH_3CHCHCN$, c-$CH_3CHCHCN$, $CH_2C(CH_3)CN$, $NH_2C(O)CH_2OH$
>10 atoms	HC_8CN, CH_3C_6H, $CH_3OC_2H_5$, $HC_{10}CN$, C_6H_6, C_2H_5OCHO, C_3H_7CN, CH_3COOCH_3, $C_2H_5OCH_3$, CH_3CHCH_2O, C_6H_5CN, CH_3COCH_2OH, C_{60}, C_{60}^+, C_{70}, c-C_5H_5CN, $C_{10}H_7CN$ (2 isomers), c-C_5H_6, c C_9H_8, $NH_2CH_2CH_2OH$, CH_3C_7N, i-C_3H_7OH, n-C_3H_7OH, CH_2CCHC_4H, g-CH_2CHCH_2CN, $HC_{11}N$, C_5H_5CCH (2 isomers), C_6H_5CCH, CH_3C_7N, c-CH_2CHCH_2CN, c-$C_5H_4CCH_2$, c-C_9H_7CN, $C_{10}H^-$, $C_{10}H$, E-1-C_4H_5CN, $(CH_3)_2CCH_2$, $CH_3OCH_2CH_2OH$, 1-$C_{12}H_7CN$, 5-$C_{12}H_7CN$, $C_{16}H_9CN$ (3 isomers), $C_{24}H_{11}CN$, 2-C_4H_5CN
Deuterated	HD, H_2D^+, HDO, D_2O, DCN, DCO, DNC, N_2D^+, NHD_2, ND_3, HDCO, D_2CO, CH_2DCCH, CH_3CCD, D_2CS, NH_3D^+

Table 1.1: Temporary census of interstellar molecules until June 4, 2025.

Objective and insight into the following chapters

The origin of the molecules necessary for the emergence and development of life has been a fascinating topic at the heart of scientific inquiry for decades. Two origins, potentially complementary, have been thoroughly studied for decades, i.e. the endogenous (production in situ on Earth) and exogenous origin (production in some astrophysical environments). This master thesis aims at participating at the exploration of the latter, by **studying some of the most promising precursors (cf. Chapter 3) towards the simplest of all** 20 **natural amino acids**, i.e. glycine NH_2CH_2COOH.

The main goal of the present study could then be stated in the following way:

Achieving a detailed overview of the chemical processes that govern the formation and destruction of various glycine precursors in molecular clouds, both in the gas and solid phases, using an astrochemical modeling tool.

The present study aims to add a layer of complexity on top of the thorough work carried out a couple of years ago by Groyne (2023), in which all precursors (illustrated in Figure 1.3) were studied in a pure gas phase context with the help of the ***Astrochem*** model, used to **simulate molecular clouds**. Important components of the ISM that were omitted in the previous work are dust grain particles, known to be one of the major components of interstellar environments. These grains, in dark, dense, and cold environments such as molecular clouds, are known to be surrounded by icy mantles, in which interesting (organic) chemistry may be at work.

In order to achieve this objective, the following "work plan", subdivided into chapters, will be followed.

First of all, in order to have the theoretical background necessary to perform this work, Chapter 2 will describe the basic knowledge about the ISM, dust grains, chemical reactions and amino acids. Chapter 3 will then extend a bit the theoretical framework by discussing, strongly based on Groyne (2023), the chemical pathways that could be envisaged for the formation of glycine.

Having the theory in mind, the practical part of this work will begin with Chapter 4, in which the astrochemical modeling tool is introduced. For this study, the ***Nautilus*** three-phase astrochemical kinetic modeling code (Ruaud et al., 2016) has been chosen. It will allow us to compute the temporal evolution of the abundance of various molecular species. In addition, the software will also be used to make an assessment of the relative

contribution of the dominant formation and destruction pathways of each molecule. As in Groyne (2023), dark molecular cloud environments will be simulated, considering a homogeneous cell not evolving with time of constant density, temperature, visual extinction and cosmic-rays ionization rate.

Before diving into the objective of this master thesis, i.e. the full 3-phase (gas, dust surface and dust icy mantle) study of glycine precursors (Chapter 6), we will try to reproduce the results of Groyne (2023), to make an assessment of the reproducibility of these results using ***Nautilus***. This model will then be used as the foundation for a more comprehensive astrochemical study, as detailed in Chapter 6. Moreover, the 3-phase study will allow us to **explore all the capabilities of this code**, to understand its functioning and its main limitations affecting the results.

In the last part of this work, an **assessment of the validity of the results** presented in Chapter 6 will be carried out by making a comparison with observational values. This will be done in Chapter 7.

As the work upon which it has been built (Groyne, 2023), this master thesis aims to be one more step toward a long-term and deep study of the formation of amino acids in interstellar environments. The potential improvement of the work will be presented at the end of this document, in Chapter 9.

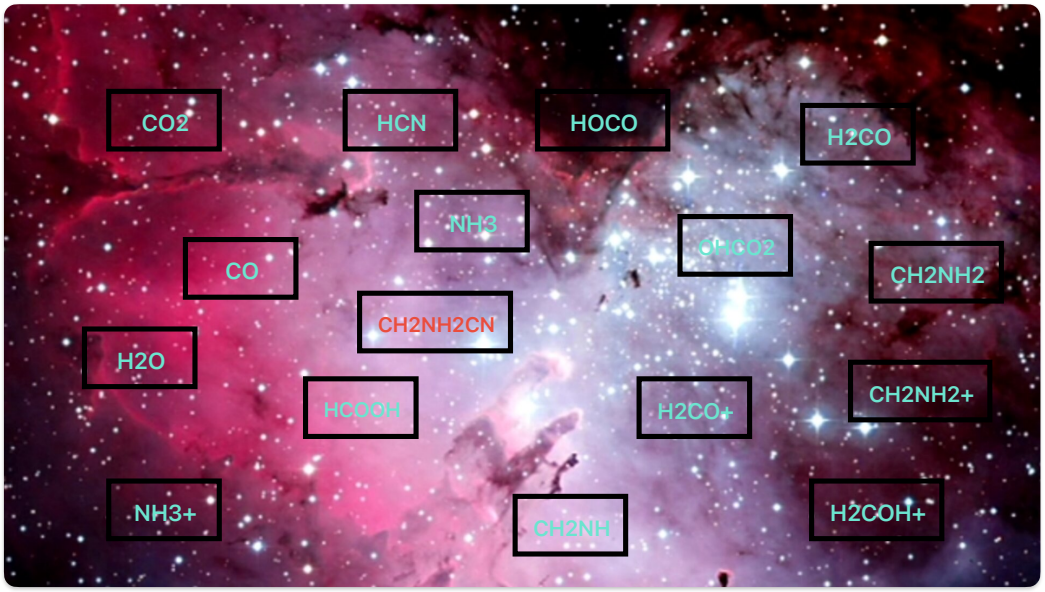

Figure 1.3: Summary of the precursors studied in the framework of the pathways from Chapter 3. In blue, the ones which have been studied. In red, the only one which was not available. The image of the Eagle nebula has been taken from `https://www.esa.int/ESA_Multimedia/Videos/2011/12/M16_the_Eagle_Nebula`.

Chapter 2

Theoretical considerations and scientific context

This chapter provides an overview of key scientific concepts essential for understanding the work presented in this study. We begin by introducing the structure and composition of the interstellar medium. Next, we outline some general properties of interstellar dust grains. We then delve into the chemical reactions that occur in the ISM, in gas-phase, on grain surfaces and in icy mantles. Finally, we conclude with a brief review of molecular clouds and their chemistry, followed by a discussion on the nature and current detection status of amino acids in space.

2.1 The interstellar medium

Before going deeper into concepts linked to Astrochemistry, it is paramount to know and understand the region of the Milky Way we are going to study. In this section, the basics concerning the ISM's composition and phases will be introduced.

The interstellar medium, or simply ISM, is one of the most important components of a galaxy. It corresponds in fact to *"everything in the galaxy that is between stars"* (Draine, 2011). It is usually restricted to the galactic disk since it is there that most of the galactic matter can be found. *Why is the ISM so important*? It serves as the birthplace of new stars, which themselves are major energy sources within a galaxy. However, the ISM is not only crucial for Astrophysics but also plays a fundamental role in Astrochemistry. Through the concept of astrophysical filiation, the initial composition of a molecular cloud undergoes significant processing throughout the various stages of stellar formation and evolution (as briefly discussed in Section 1.2), driven by evolving physical conditions such as radiation fields, temperature and density. Throughout its lifetime, a star continuously emits electromagnetic radiation and ejects stellar material, influencing the surrounding ISM in ways that depend on its type and evolutionary phase. At the end of its life cycle, part of the star's matter is returned to the ISM, enriching it with newly synthesized elements and molecules. These processes highlight the ISM's fundamental role in both Astrophysics and Astrochemistry, making it a key component of this study.

2.1.1 The composition of the ISM

As said before, the interstellar matter is composed of the material that is found between stars. The following list, based on the one established by Draine (2011), emphasizes the

constituents **that are of interest in this study**:

- **Interstellar gas**: Composed of protons, electrons, atoms, ions and molecules found in gas phase with a quasi thermal velocity distribution. Such a component accounts for about 6.7 10^9 $M_\odot$ of the total galactic mass (which is of the order of 10^{12} $M_\odot$), a fraction of a percent.

- **Interstellar dust**: Small particles in the solid phase completely mixed with the gaseous component (crucial interplay between both components), with a size often lower than 1 μm. The composition may vary depending on the location in the ISM. The dust component represents only about 1% (in mass) of the gas component, but it is of prime importance for Astrochemistry.

- **Cosmic rays**: Highly energetic charged particles (ions and electrons), with a non-thermal velocity distribution, which are very often ultra-relativistic. Those particles can be of galactic or extragalactic origin, and must have been accelerated in some astrophysical environment[1].

The primary matter components of interest to us are gas and dust, as they provide the environments where chemical reactions occur, as discussed in Sections 2.3.2 and 2.4.

2.1.2 The different phases of the ISM

As a next step in our presentation of the ISM, we will emphasize that it is organized in several phases, making it absolutely **not homogeneous**.

The ISM consists of various regions, each characterized by **distinct physical conditions**. The Hot Ionized Medium (HIM) consists of shock-heated gas at $\sim 10^5$ K, containing highly ionized species and filling about 50% of the galactic disk. The Warm Ionized Medium (WIM) and HII regions[2], ionized by OB-type stars, have temperatures of $\sim 10^4$ K and densities between 0.2 and 10^4 H atoms/cm^3, occupying about 10% of the ISM. The Warm and Cool Neutral Media (WNM and CNM) are composed mainly of neutral hydrogen, with temperatures of ~ 5000 K and ~ 100 K, and densities of ~ 0.6 cm^{-3} and ~ 30 cm^{-3}, respectively, with a volume filling factor around 0.4. The **Diffuse Molecular Gas** is a transitional phase between the CNM and molecular clouds, with densities of ~ 100 cm^{-3}, temperatures between 10 K and 50 K, and significant H_2 presence due to self-shielding (attenuation of photo-dissociation). The **Dense Molecular Gas (or Molecular Clouds)** consists of gravitationally bound clouds with densities ranging from 10^3 cm^{-3} to 10^6 cm^{-3} and temperatures of 10 to 20 K. These environments are **molecule-rich**, primarily composed of H_2 and CO (along with many others), with a high extinction making them appear as "dark clouds".

Important remark:
Do not be misled by the low volume filling factors of interstellar clouds (10^{-3} and 10^{-4}, respectively), as dense dark molecular clouds are of crucial importance to us due to the remarkably rich chemistry occurring within them (see Section 2.5).

[1] For the galactic cosmic rays, processes such as Diffusive Shock Acceleration (DSA) within supernova remnants have been proposed.

[2] Using the usual spectroscopic notation, HII means ionized hydrogen.

2.2 Generalities about interstellar dust grains

Since dust grains will be central in this work, thanks to their reaction properties, we will review in this section some of their features as well as their evolution in the ISM.

2.2.1 Evidences pointing towards interstellar dust grains

We now know that microscopic (even submicroscopic) dust particles can be found all over the ISM, especially in the densest regions (Pagani et al., 2010). Those dust particles are, in fact, extremely important in respect of the chemistry in the ISM, thanks to the chemical reactions taking place at their surface (as discussed in Section 2.4). Several observational evidences strongly suggest the presence of interstellar dust (Draine, 2011) such as:

- **Wavelength-dependent attenuation (extinction) of starlight**: The dimming of stars by an absorbing medium was first noted by Barnard (1907, 1910) and later confirmed by Trumpler (1930), who attributed it to cosmic dust. Dust absorbs UV/visible light and re-emits it in the mid- and far-IR, causing **reddening** of stars.
- **Polarization of starlight**: Discovered by Hall (1949), this polarization is linked to interstellar dust grains aligning with the magnetic field. The effect increases with reddening and follows a predictable law (see Draine 2011). Notably, dust-induced polarization has been proposed as a factor in asymmetric photolysis, relevant to enantioselectivity in biochemistry.
- **Thermal infrared emission from dust**: Heated by starlight, dust grains re-emit in the IR, contributing significantly to the bolometric luminosity of spiral galaxies.

2.2.2 Size, shape and composition of dust

A strong observational evidence that was not mentioned in Section 2.2.1 is the **depletion of some elements in gas-phase**. By taking as a standard set the relative element abundances measured in hot stars[3], it is possible to observe that some elements are greatly depleted (as measured within a diffuse interstellar cloud) in comparison to our standard set. We are mostly talking about elements capable to form so called refractory (heat-stable & resistant) solids (Fe, Mg, Si, Ni, but also elements like carbon and oxygen which can be found both in gas-phase and inside grains). In order to illustrate what has just been said, Table 2.1 (inspired from Draine 2011 and simplified for the need of illustration[4]) shows the abundances of elements both in gas-phase and within dust grains towards the O9.5V star ζ Ophiuchi, as compared to standard solar photospheric values.

Another illustration is given in Figure 2.1, where the relative abundance of some elements in respect of solar photospheric abundances is plotted as a function of the condensation temperature T_{cond}[5]. This example allows us to infer relevant information about the composition of dust grains: silicates, e.g. of pyroxene ($Mg_xFe_{1-x}SiO_3$) or olivine composition ($Mg_2Fe_{2-2x}SiO_4$) with $0 < x < 1$[6], oxides of silicon, magnesium and iron (e.g. SiO_2, MgO, Fe_3O_4), carbon solids (graphite, amorphous carbon and diamonds), hydrocarbons

[3] Dust particles cannot survive such temperatures and their constituting atoms must be in gas-phase.

[4] The values found in this table are the central (rounded) values of the confidence interval. We did not consider the error bars because they are of no interest in the context of this illustration.

[5] Defined as the temperature below which 50% of atoms are in the solid-phase.

[6] x is the magnesium fraction in the solid. If x equal 1, then no iron is present in the molecule.

X	$(N_X/N_H)_\odot$ [ah]	$N_{X,gas}/N_H$ [h]	$N_{X,dust}/N_H$ [h]	$\%_{gas}$	$\%_{dust}$
C	295	135 [b]	160	45.8%	44.2%
N	74	74 [j]	0	100%	0%
O [c]	537	295 [b]	242	55%	45%
Mg	44	5 [d]	39	11.7%	88.3%
Al	3	0.005 [e]	2.995	0.17%	99.83%
Si	36	2 [c]	34	5.5%	94.5%
S	15	15 [j]	0	100%	0%
Ca	2	0.00004 [g]	1.99996	0.002%	99.998%
Fe	35	0.13 [d]	34.87	0.37%	99.63%
Ni	2	0.003 [f]	1.997	0.15%	99.85%

[a] Asplund et al. (2009)
[b] Cardelli et al. (1993)
[c] Cardelli et al. (1994)
[d] Savage et al. (1992)
[e] Morton (1975)
[f] Federman et al. (1993)
[g] Crinklaw et al. (1994)
[h] Expressed in part per million (ppm)
[i] The quantity of oxygen trapped within dust grains is strongly dependent on the line of sight considered.
[j] Those values may of course be discussed, as done in Jenkins (2009), but the important message is that the quasi totality of nitrogen and sulfur are found in gas phase.

Table 2.1: Table comparing the abundances in gas-phase from the solar photospheric reference values and from a diffuse cloud towards the star ζ Ophiuchi (the abundances being expressed compared to the hydrogen abundance). The abundances inside the grains are inferred from the two other columns. The percentage of a given element (X) in gas-phase or trapped within dust grains is also given.

(like polycyclic aromatic hydrocarbons or PAHs), carbides (and particularly silicon carbide) and metallic iron. Other elements might enter the composition, like titanium and chromium, but their abundances are quite low compared to other elements.

The size of such grains covers a very wide range, going from a few $\mathring{A}$ to several μm, and their shapes are absolutely not symmetrical (they are **too small to be spherical**). In fact, based on the data available to us, it is impossible to build a unified grain model. Some models that seem to reproduce quite well the observed extinction from the near-IR to the UV are based on the following considerations: (i) Dust is made of only two materials, i.e. amorphous silicates and carbonaceous materials (ii) Dust grains are considered spherical (iii) A power-law size distribution for the grains is assumed (here we consider[7] $dn/da \propto a^{-3.5}$ for $a_{min} < a < a_{max}$). Of course, these are not the only class of models, as discussed in Draine (2011), but it is quite enough for our brief introduction to dust grains.

2.2.3 Icy mantles around dust grains

When the astrophysical environment is cold enough (like in interstellar clouds), atoms and molecules may condensate onto dust grains (carbonaceous and silicates) in order to form

[7] Frequently referred to as the Mathis-Rumpl-Nordsieck, or "MRN", distribution (Mathis et al., 1977).

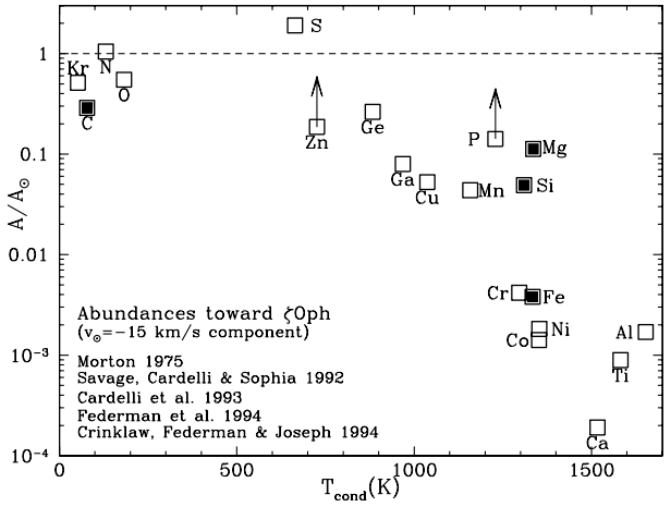

Figure 2.1: Gas-phase abundances in the diffuse cloud towards ζ Ophiuchi relative to solar photospheric abundances (from Draine 2011 and references therein). The darkened squares represent the major grain constituents.

icy mantles. Such mantles may be relatively thick, forming sometimes more than 100 monolayers. The thickness of such mantles is the **result of the competition between accretion and desorption**. Observations of icy mantles have shown that they mostly consist of water (H_2O), carbon monoxide (CO), carbon dioxide (CO_2), methanol (CH_3OH), ammonia (NH_3) and methane (CH_4) (Boogert et al., 2015). Mantles and their surfaces are of tremendous importance for chemistry in the ISM, as discussed in Section 2.4.

2.2.4 Basis about the formation, destruction and evolution of dust grains

Formation of dust particles

Dust grains do not form and evolve within the environment where we see them now. It is indeed possible to show that dust formation and growth within interstellar clouds would take a very long time, exceeding the age of the universe. They can only form within **much denser environments** than molecular clouds.

The following are considered to be the two main sources of interstellar dust: (i) **Stellar winds from cool evolved stars** (ii) **Supernova ejecta**. In the dense (10^{19} H atoms/m^3), relatively cool (1000-2000 K) atmospheres of evolved stars, dust forms through gas-phase condensation onto nucleation clusters. The composition depends on the O/C ratio: **O-rich stars** (O/C $>$ 1) produce **silicate dust**, with H_2O, SiO, and metals like Fe and Mg while **C-rich stars** (C/O $>$ 1) produce **carbonaceous dust**, with hydrocarbons like C_2H and C_2H_2. Supernovae, particularly type II, can generate **even larger amounts of dust** due to high post-shock densities, enabling grain growth through aggregation.

Destruction and evolution of dust particles

Several processes may be responsible for the alteration/destruction of dust grains once ejected in the ISM, such as:

- **Irradiation by the mean interstellar radiation field**: This radiation, especially the UV emission from massive hot stars, is able to alter the chemical composition

as well as the optical properties of hydrogenated carbons by removing much of their hydrogen. Such a process affects mostly carbonaceous dust grains, the silicates being not so sensitive to the radiation field.

- **Shock waves**: After the passing of a shock wave, the atoms, ions and molecules from the hot post-shock gas might strike dust grains and cause the erosion of the surface, ejecting one atom at the time. This process is called **sputtering** and can cause structural and chemical changes of the grain. Grain-grain collisions might also occur, leading to more dramatic structural changes since the grains will break into pieces (**shattering** of the grains) and the material composing them will be redistributed, possibly leading to grains with larger radii[8].

- **Cosmic rays**: High energy particles such as cosmic rays might indeed dust. During a collision between a dust grain and a cosmic ray particle, sputtering of the dust surface may happen.

To conclude this section, let us mention that the fate of dust particles within a molecular cloud is to be involved within the planetary formation process (agglomeration of dust particles forming more and more massive bodies). During this process, dust particles far enough from the central forming star (beyond the so-called **snow line** of water) and shielded from the radiation field are able to keep their icy water-based mantles, **preserving therefore their rich molecular content**. These mantled grains may then be incorporated within comets and asteroids, if not in planets. Such grains surrounded by icy mantles are thus witnesses of the pristine conditions reigning at the epoch of the young solar system, which makes them extremely interesting to study.

2.3 Gas-phase processes

We will now close this astrophysical parenthesis and focus our minds on the world of chemistry. In this section, some considerations about chemical kinetics will be addressed. Energetic aspects will also be discussed as well as several types of gas-phase chemical reactions that may take place in the ISM.

2.3.1 Chemical kinetics and energetic considerations

In this work, the chemical transformations occurring in the ISM will be studied in the framework of **chemical kinetics**[9]. Let us begin with a quick contextualization before addressing the gas-phase reactions in Subsection 2.3.2. Chemical kinetics can be defined as the study of the rates at which chemical reactions occur and of the factors affecting them, such as temperature, density, and catalysts. It provides insight into reaction mechanisms and helps predict how quickly reactants transform into products under various conditions.

When we use this chemical kinetics approach, we will have to solve sets of differential equations (one equation for each species considered), called reaction rate equations or simply **rate equations**, in order to understand the rates of formation and destruction of the chemical species involved in the reactions. Let us emphasize that with this approach,

[8]This is what happens for example within a protoplanetary disk during planetary formation.

[9]The other main framework in which chemical transformations may be studied is **chemical thermodynamics**. It will not be detailed here, but some thermodynamical considerations will be addressed during our discussion about energy activation barriers and chemical equilibrium.

all the intermediate reactions have to be taken into account if we want to study kinetics as best as possible. In order to illustrate such rate evolutions, we can consider three kinds of general chemical reactions, with their respective rate equations:

1. Unimolecular reaction: $A \longrightarrow B$

$$\frac{-dn(A)}{dt} = kn(A) \tag{2.1}$$

2. Bimolecular reaction: $A + B \longrightarrow C$

$$\frac{-dn(A)}{dt} = kn(A)n(B) \tag{2.2}$$

3. T(h)ermolecular[10] reaction: $A + B + M \longrightarrow C + M$[11]

$$\frac{-dn(A)}{dt} = kn(A)n(B)n(M) \tag{2.3}$$

In these equations, k is what we call the reaction rate coefficient, also called **rate constant**), and is THE important quantity when talking about kinetics since it allow its quantification. We will see in this section that k contains the information about the temperature dependence. Concerning the units of the rate constant, they depend in fact on what we call the kinetic order of the reaction. It is generally not possible to predict this order, except in the case of elementary processes[12] where it is simply equal to the molecularity of the reaction, i.e. the number of partners involved in the reaction[13].

The study of reaction kinetics is thus of prime importance, especially in the context of astrochemistry, since it allows to understand in which conditions a molecular compound might be formed as well as the velocity at which this reaction is taking place.

Important remark:

The equations presented above are simple cases, presented as illustrations, and things can become more complex when considering astrophysical environments, as some species can be involved in several reactions, potentially of different orders, at the same time (parallel and consecutive reactions). One understands that **such a classical approach is impossible to put into play in the context of astrochemistry in interstellar clouds**. We have in that case thousands of reactions all interconnected, taking place at the same time in a cold and diffuse (as compared to Earth) environment. Since the equations cannot be solved analytically, we have to proceed by numerical methods to solve simultaneously all our equations. That is the purpose of astrochemical models, as will be discussed in Chapter 4.

[10] The "h" is usually included when we want to emphasize the energetic aspect of the reaction.

[11] M has an energetic purpose, it just plays a catalytic role as it is recovered unchanged after the reaction. For example, dust grains will play this role as we will discuss in Section 2.4.

[12] Processes with no known intermediate steps.

[13] In our restrictive case of astronomical environments, reactions involving three partners are extremely rare, especially if we consider molecular clouds where the densities are extremely low compared to Earth-like conditions.

The rate of a chemical reaction depends primarily on: (i) **Density** (n) and (ii) **Temperature** (T). According to collision theory, the reaction rate (here of a bimolecular reaction) can be expressed as follows:

$$v_A = -\frac{dn(A)}{dt} = \sigma\sqrt{\frac{8k_BT}{\pi\mu}}e^{-\frac{E_A}{k_BT}}n(A)n(B) \tag{2.4}$$

where σ is the collisional cross-section [cm^2], μ the reduced mass [g], and E_A the activation energy [K][14]. The exponential term, derived from Boltzmann statistics, highlights how only molecules with sufficient kinetic energy can react. Everything that is found before the density product is forming the expression of the rate coefficient. This formulation shows the **strong dependence of reaction rates on density and temperature**: higher n leads to more collisions, while higher T increases the fraction of effective collisions.

Note about activation energy barriers

The activation energy barrier determines whether a reaction can occur, as it represents the minimum kinetic energy required for colliding molecules to react. This concept is crucial in Astrochemistry, where the cold environments of molecular clouds severely limit which reactions can take place. A reaction progresses from reactants to products through an activated complex, an intermediate state where bonds are simultaneously breaking and forming. The energy barrier E_A corresponds to the energy difference between the reactants and this intermediate state. It can somehow be interpreted as the energy required to extract electrons from their existing chemical bonds, which constitutes a requirement to make them available to participate in new chemical bonds. In an exothermic reaction ($\Delta E < 0$), energy is released, whereas in an endothermic reaction ($\Delta E > 0$), energy must be supplied from the surroundings. Not all reactions have an activation barrier; radical-radical reactions, for example, proceed without one since radicals already possess unpaired electrons, **making them immediately available and highly reactive**. This is particularly relevant in Astrochemistry, where such barrierless reactions can dominate in cold interstellar environments.

2.3.2 Gas-phase chemical reactions

We will now present different kinds of gas-phase reactions for elementary processes (inspired from De Becker 2013 and Babb 2024) that may take place in the ISM. As we will see, the dominance of a certain reaction will depend on the environment considered.

Photo-chemical reactions

Photo-chemical reactions are reactions induced by the absorption of a photon (typically a FUV photon, regarding the typical bonding energies between atoms). Two main subtypes of such reactions exist: photo-dissociations and photo-ionizations.

Let us begin with the first ones. **Photo-dissociation** reactions are of the type:

$$\mathrm{AB} + \mathrm{h}\nu \longrightarrow \mathrm{A} + \mathrm{B}$$

[14] Usually, this quantity is expressed in Kelvin in the literature. One would thus have to multiply it by k_B to get true energy units.

i.e. the absorption of a photon possessing the right energy can dissociate a molecule. It is immediate that, **in order for such reactions to take place, the medium must be diffuse enough to let the photons go through**. For a study about the importance of FUV photons in photo-dissociation regions, one is referred to Tielens and Hollenbach (1985a,b). Typically, only molecular clouds are dense enough to prevent FUV photons to go very deep within them. These considerations lead to the very important concept of **self-shielding**, which is discussed with more details in Section 2.5. Note also that, as discussed in Section 2.2.1, dust particles play also a role in the absorption of stellar light, as they absorb it and re-emit it in the infrared (reddening of the star light). Typical values of k_{pd}, the photo-dissociation rate constant, are of the order of 10^{-9} to 10^{-10} s^{-1}.

The second kind of photo-chemical reactions are the **photo-ionization** reactions:

$$A + h\nu \longrightarrow A^+$$

in which, as in the previous case, $h\nu$ represents the energy of the photon[15]. In that case, the absorbed photons do not have enough energy to break bonds, but they have sufficient energies to ionize atoms or molecular compounds, depending on the ionization potential.

Neutral-Neutral reactions

Neutral-Neutral reactions have the following form:

$$A + B \longrightarrow C + D$$

i.e. the reaction of two neutral molecules gives two new neutral molecules. Such reaction results from the attractive interaction of the molecules through Van de Waals forces, effective at short distances. Not counting the inhibiting influence of activation barriers, typical values of k_{nn} are of the order of 10^{-12} to 10^{-14} cm^3/s. When barriers are considered, k_{nn} can drop further by several orders of magnitude at low temperature. These reactions are predominant within warm environments, since they usually possess large activation energies. Indeed, in that case chemical bonds have to be broken. In cold environments like molecular clouds, we thus see that only reactions involving light partners or radicals may occur since they possess low (or not at all) activation barriers.

It is important to understand that we did not consider a reaction of the type:

$$A + B \longrightarrow C$$

i.e. the addition of two compounds, but we directly considered the loss of a fragment. This is because when the reaction of two molecules occur, the formed compound is in an excited state, not stable at all. It must thus evacuate this excess of energy one way or another. This is done through the loss of a fragment, which takes away the energetic excess. This is typically what happens for small species, but when bigger species are considered, they might find a way to store the excess of energy within their vibration modes. As we will see in the next Section 2.4, dust grains will have a tremendous importance for that since they have this capacity to take away the excess of energy, thus stabilizing the reaction product and allowing for the formation of more complex species.

[15] In this expression, h is the Planck constant and ν the frequency of the photon.

Ion-molecule reactions

We are here talking about reactions of the type:

$$A^+ + B \longrightarrow C^+ + D$$

Such reactions are especially important in the context of Astrochemistry in cold environments, since they are much quicker than neutral-neutral processes[16]. They do not suffer from any strong temperature dependence, which gives k_{im} values of the order of 10^9 cm$^3/s$ which are several orders of magnitude higher than for neutral-neutral reactions. **They can thus basically happen wherever ions are present**. Let us note that through this type of reaction, cationic chains can be envisaged, which mainly terminate with the capture of an electron (see next type of reactions).

Dissociative electronic recombination reactions

We have:

$$A^+ + e^- \longrightarrow A^* \longrightarrow C + D$$

i.e. the capture of an electron by an ion leads to an electronically unstable neutral compound, which therefore dissociates to give (at least) two fragments. For such reactions, we have k_{de} values of the order of 10^{-7} cm^3/s. Such processes allow the formation of many small neutral molecules which cannot be formed through the simple addition of two simple species (for example, $H_3^+ + e^- \longrightarrow H_2 + H$). In the same way as previously discussed (neutral-neutral reactions), such reactions must be dissociative for light species, but **may not** be dissociative for large molecules.

Cosmic-ray induced reactions

The nature of cosmic rays have already been described in Section 2.1.1. Such particles are indeed of great importance in Astrochemistry (see for example Indriolo and McCall 2013) and in our context. Therefore, we have to emphasize the capability of such energetic particles to interact with molecular compounds. Cosmic-ray induced processes are central in the case of molecular clouds, since the probability of encounter with a partner is much higher than in diffuse clouds. As we will see, cosmic rays constitute an important source of energy within molecular clouds, since such clouds are opaque to external UV photons. Three types of cosmic-ray induced reactions can be envisaged:

1. **Cosmic-ray induced dissociation**: This process consists in the breaking of a chemical bond due to the interaction with an energetic particle. This acts as a significant destruction agent within molecular clouds, since extinction prevents UV photons to go deep in the cloud. It must be emphasized that it is (usually) not **primary cosmic rays** that lead to dissociation, but **secondary cosmic rays**. This can be simply explained thanks to energetic considerations. Primary cosmic rays possess a huge energy[17], thus a low cross-section leading to low reaction rates ($k_{CRd} \approx 10^{-17}$ cm^3/s). Typical secondary cosmic rays are helium cations He^+, resulting from the cosmic-ray induced ionization of neutral He in the cloud. During this process, the primary cosmic ray transfers a small fraction of its energy to He. The energetic He^+ can thus behave as a cosmic ray, but at lower energies than primary ones, leading to a greater cross-section. Secondary cosmic rays lead thus to processes with significantly higher reaction rates ($k_{CRd} \approx 10^{-9}$ cm^3/s).

[16] Very strong polarization-induced interaction between reactant molecules.

[17] Typically, energies below the knee of the usual cosmic-ray power-law spectrum ($E \approx 10^{15}$ eV).

2. **Cosmic-ray induced ionization**: This is similar to photo-ionization, but in this case the electron is ejected through the interaction with a cosmic ray. For instance, this process leads to the presence of energetic He^+ (see above). The ionization of He by primary cosmic rays is quite not highly efficient ($k_{CRi} \approx 10^{-18}$ cm^3/s), but we must not forget that He is an abundant species. This process allows thus cosmic rays to produce ions deeply within dense clouds, and ions are important since they are involved in reactions with relatively high reaction rates enhancing thus the chemistry taking place in the cloud.

3. **Cosmic-ray induced photo-reactions**: Finally, it as been proposed that **cosmic rays act as an in-situ source of UV photons in molecular clouds** (Prasad and Tarafdar, 1983). Indeed, electrons generated thanks to cosmic-rays interaction have the capability to excite atomic hydrogen present in the cloud, which will radiatively relax through the emission of UV photons. These photons will then be involved in photo-chemical processes as the ones described previously. They will also act as a desorption agent for chemical species onto dust grains, as discussed in Section 2.4.

Charge transfer reactions

During such reactions:

$$A^+ + B \longrightarrow A + B^+$$

no chemical bonds are broken, we just have an exchange of the electric charge between the partners. Reaction rates are quite high for this process ($k_{ct} \approx 10^{-9}$ cm^3/s).

Radiative association reactions

In that case, the reactions are of the following form:

$$A + B \longrightarrow AB^* \longrightarrow AB + h\nu$$

The excess of energy is taken away by the photon, allowing the stabilization of the product. The kinetics of those reactions are fully governed by the life-time of the activated complex AB^*. Knowing that the excess of energy is initially stored within the vibrational modes of the compound, only the large species will lead to high reaction rates. For small species, typical values of k_{ra} are found between 10^{-16} and 10^{-20} cm^3/s.

Associative detachment reactions

During associative detachment reactions:

$$A^- + B \longrightarrow AB + e^-$$

an anion and a neutral compound react to form a new molecule, which is stabilized by the emission of an electron. Due to the rareness of anions in the ISM (only a few have been detected, see Table 1.3), such reactions are not of prime importance. They are thought to be responsible for the production of molecular hydrogen in the early universe[18] through the reaction $H^- + H \longrightarrow H_2 + e^-$.

[18]Now, it is nearly entirely produced at the surface of dust grains, as it was thoroughly reviewed in Wakelam et al. (2017a)

2.4 Grain-surface processes

The importance of dust grains in the context of Astrochemistry has been emphasized several times since the beginning of this work. We saw in Section 2.3.2 that one of the main properties of dust grains is its catalytic role during a three-body chemical reaction[19]. The adsorbed species will encounter and react onto the grain surface, and the grain will just take away the excess of energy, allowing for the stabilization of the product. Dust grains are thus indispensable in the context of this work since they will allow to **climb the molecular complexity ladder**, i.e. to build more and more complex species, which would be impossible to achieve with pure gas-phase reactions due to the low densities and temperatures. When talking about such processes, two main mechanisms can be considered which are the **Langmuir-Hinshelwood mechanism** and the **Eley-Rideal mechanism**[20].

2.4.1 Langmuir-Hinshelwood mechanism

Let us begin with the Langmuir-Hinshelwood mechanism. Such a process, which is illustrated in Figure 2.2, may be decomposed into four steps that will be described in the following subsection (inspired from Potapov and McCoustra 2021 and De Becker 2013): (i) **Accretion** (ii) **Migration** (iii) **Reaction** (iv) **Desorption**.

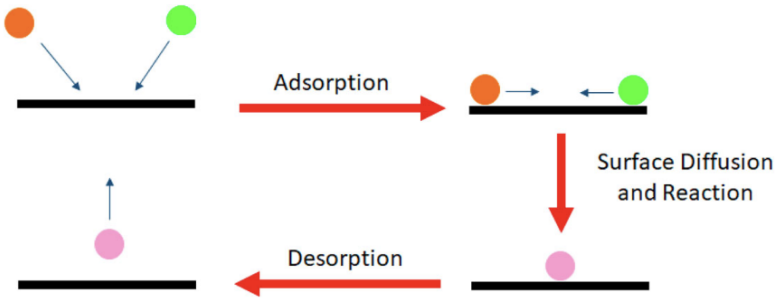

Figure 2.2: Schematic view of the Langmuir-Hinshelwood mechanism. Taken from Potapov and McCoustra (2021).

Accretion

The first step of the process is **accretion**, during which an atom or a molecule from the gas phase will be adsorbed onto the surface. Two types of adsorption may be considered depending on the nature of the interaction: (i) **Physisorption**, in which case the interaction is a weak attraction caused by Van der Waals forces or (ii) **Chemisorption**, where the interaction is much stronger than the previous case since a chemical bond is created with the surface. The binding energy of the adsorption will depend on the composition of the dust grain as well as the presence of some adsorbates on the surface.

[19] We may also note that, in a medium depleted in dust, Polycyclic Aromatic Hydrocarbon (PAH) molecules may play this catalytic role (Tielens, 2008).

[20] A third mechanism may be considered, namely the Kasemo-Harris mechanism. It follows roughly the same steps as the Langmuir-Hinshelwood mechanism, but involves a so-called hot atom, i.e. an adsorbed species that did not have the time to thermalize (Harris and Kasemo, 1981).

Concerning the kinetic constant of the adsorption process, it is expressed as

$$k_{ad} = n_d \sigma_d v S \tag{2.5}$$

where n_d is the number density of dust grains, σ_d is the cross-section of the grains, v is the mean speed of the particles and S is the sticking factor, which express the probability of adsorption and is generally close to 1 (cf. ***Nautilus*** presented in Chapter 4).

Migration onto the surface

Once an atom or molecule has been adsorbed onto the dust surface, whether through chemisorption or physisorption, it may migrate from one site to another before desorbtion. The **mobility** of that species will be induced by two major effects: (i) **Temperature** and (ii) **Quantum tunneling**. Temperature will of course affect the mobility: the higher the temperature, the greater the thermal energy available to overcome migration barriers. Provided the temperature is high enough, a molecule may thus go to another adsorption site (we speak of **thermal hopping**). The energy required will of course depend on the adsorption site. As previously emphasized, it requires more energy to leave a chemisorbed site than a physisorbed one. In fact, when the temperature has dropped severely, migration from chemisorbed sites may be almost forbidden. In the latter case, the quantum tunneling effect[21] becomes non-negligible for very light species. Thanks to this process, molecules and atoms are still allowed to migrate even at low temperature. The **mass of the considered species has also a strong effect on migration**, light species being more mobile than heavier ones.

We may express the thermal migration time scale, i.e. the characteristic time needed for a molecule to acquire sufficient energy to migrate to another site, in the following way:

$$\tau_m = \nu_m^{-1} e^{E_m / k_B T_d} \tag{2.6}$$

where ν_m is the vibrational frequency of the adsorbed species, E_m is the energy barrier against migration, k_B is still the Boltzmann constant and T_d is the dust temperature. Through Equation 2.6, **one clearly sees the relationship with temperature** since the higher T_d, the lower τ_m. For molecular clouds, we may thus expect that the mobility of the species will be strongly reduced due to the low temperatures (10 to 20 K).

Reaction

During their random migration process, adsorbates may encounter onto the surface and interact (formation/destruction of chemical bonds), leading potentially to new chemical species. In the case of reactions involving radicals, the adsorbates will directly interact without any further formality, but it is more complex when energetic barriers are involved. Indeed, while they are nearly completely inhibited in gas phase, the time spent onto the grain will increase the chance of interaction. As stated in Tielens (2005), the probability that a reaction takes place before evaporation (i.e. the probability to cross the activation barrier) is given by:

$$\mathbb{P}_{reaction} \propto \tau_d \, \theta_r \, p \tag{2.7}$$

[21] Quantum tunneling is a phenomenon where particles pass through a potential barrier that they classically should not be able to overcome due to insufficient energy. This occurs because, in quantum mechanics, particles have wave-like properties, and their position is described by a probability wave. If the barrier is thin enough, the wave function can extend beyond it, allowing the particle to "tunnel" through, even if its energy is lower than the barrier's height.

where τ_d is the residence time of the species (Equation 2.8), θ_r is the surface coverage and p expresses the probability to overcome the migration barrier.

Desorption

Finally, the newly formed species may desorb from the surface and return to the gas phase to participate to its chemistry. We define the **residence time** of a chemical species with the following formula:

$$\tau_d = \nu_d^{-1} e^{E_b/k_B T_d} \tag{2.8}$$

where ν_d is the vibrational frequency of the species on the grain surface and E_b is the binding energy of the species (greater than the migration barrier). Through Equation 2.8, the strong influence of the temperature is again emphasized. However, temperature is not the only parameter. We can consider other influencing factors such as (i) **the action of UV radiation**, which provides the necessary energy for ejection, (ii) **the action of X-rays**, which have the same role as UV photons but also play a role in the heating of the grain, (iii) **the action of cosmic rays**, which may directly eject an adsorbate or deposit some of its energy allowing thus the desorption and (iv) **hydrodynamic shocks**, through the heating of the grains or their sputtering.

2.4.2 Eley-Rideal mechanism

The Eley-Rideal mechanism, illustrated in Figure 2.3, was in fact the first to be introduced (Eley and Rideal, 1940).

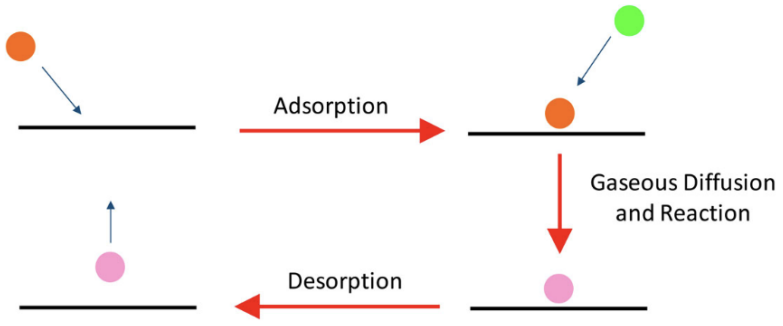

Figure 2.3: Schematic view of the Eley-Rideal mechanism. Taken from Potapov and McCoustra (2021).

It is a process which is taking place only in conditions of **high surface coverage**. In such conditions, the adsorbed species arrives onto a surface which is already highly populated. The migration step that is part of the Langmuir-Hinshelwood mechanism is thus not required. Formulated differently, the surface coverage is high and the newly adsorbed specie directly reacts with an already adsorbed specie to form a new compound. Then, depending on the residence time, the new species will finally desorb to return to the gas phase. **This mechanism will not be considered in our models**.

2.4.3 Bulk-ice chemistry

In Section 2.2.2, it was mentioned that in cold environments dust grains could be surrounded but icy mantles. When the thickness of this mantle becomes high enough (at

least a few monolayers), it becomes important to differentiate between the reactions taking place at the surface of the grains (like the ones presented just before) and the reactions taking place **within** the mantle. Below the few top monolayers involved in surface processes, the species are considered to be "trapped" in the ice, i.e. they are fully surrounded by neighboring molecules and thus tightly bound. But this does not mean that nothing is happening. Indeed, recent experiments and calculations like the ones in Andersson and van Dishoeck (2008) and Öberg et al. (2009b) have shown that sub-surface processes should be at work in interstellar dust grains. Even if the temperature is low and the species strongly bound, diffusion may be at work within icy mantles. As done in the implementation of ***Nautilus*** (cf. Chapter 4), it will be assumed that the bulk diffusion is driven by the diffusion of H_2O within the ice (Ruaud et al., 2016). Depending on the activation barrier, some reactions between compounds may be allowed as well as recombination reactions. Photo-reactions may also take place depending on the density of the environment as well as photo-reactions induced by cosmic rays. Moreover, there are interactions between the ice core and surface. Molecules formed within the core may diffuse towards the surface and vice-versa, but we could also envisage a swapping between the two as done in the ***Nautilus*** model.

Let us go a little bit into the details of the formation and chemistry of such mantles, following Shingledecker et al. (2024). The more abundant molecule in interstellar ices is H_2O which can be formed, **depending on the environment**, through a hydrogenation reaction[22] with O, O_2 or O_3 (Tielens and Hagen 1986, Cuppen and Herbst 2007), H being the more mobile specie at such low temperatures. These H_2O molecules will form a metastable phase known as **amorphous solid water**, which acts as an icy matrix where other atoms and molecules can adsorb and further react and where energy can be dissipated. Within such H_2O-OH matrix, other species such as CH_3OH, NH_3 and CH_4 can be formed. We thus have at our disposal several simple species, which can themselves be involved into other chemical reactions leading to more and more complex, potentially organic (Öberg, 2016), species. Indeed, several laboratory and modeling works, like the ones presented in Garrod et al. (2008) and Woon (2002), have shown that complex organic molecules, including some biologically significant compounds like glycine, can be formed during late stages of stellar formation through energetic processing of ices (UV photons, cosmic rays, electrons, X-rays, and thermal effects). Other works have even shown that complex molecules can be formed through **non-energetic processes**, during much earlier stages of stellar formation than previously thought (i.e. at the state of interstellar clouds). Ioppolo et al. (2021) for example have shown that glycine could be formed in icy mantles at temperatures as low as 10 K through the reaction between radicals and molecules which were formed in the vicinity of one another (more about this paper in Chapter 3). It is interesting to note that, if prebiotic molecules can indeed be formed at such early stages, they could very well be **preserved in the ice** (assuming that it did not suffer from a strong alteration) which could allow a further detection in the future. This discussion partly illustrates the complexity of the chemistry that might take place in this so-called **polar ice layer**.

Moreover, in dense ($n \gtrsim 10^4$ cm^{-3}) and dark interstellar environments ($A_v > 9$ mag and $T < 20$ K, Qasim et al. 2018), the phenomenon which is called **catastrophic condensation of CO** might happen, forming an additional layer called the **apolar ice layer**. This addition of CO opens a new doorway towards a more complex chemistry, as described

[22] A successive hydrogen addition.

for example in Shingledecker et al. (2024) and references therein. The structure of an icy mantle is illustrated in Figure 2.4.

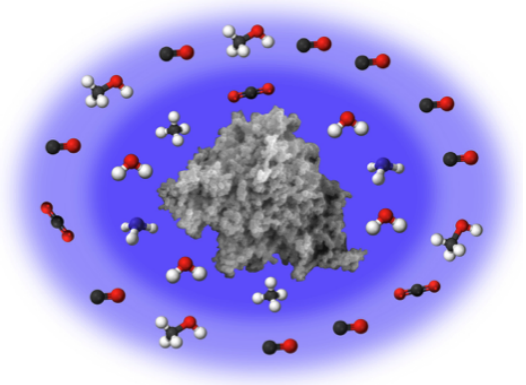

Figure 2.4: Schematic view of the icy mantle that may form in the right conditions around dust grains. The innermost layer is the one called polar layer, the other being the apolar layer. Taken from Shingledecker et al. (2024).

In conclusion of this section, one can see that, on the contrary to the naive assumption that dust particle surfaces and mantles are inert, the reality is quite opposite.

2.5 Molecular clouds and the crucial interplay between gas and surface processes

Now that we introduced all those astrochemical considerations, let us come back to molecular clouds in order to summarize once and for all everything that will enter into consideration in order to explain the chemical processes at work within such environments. One may find a summary of the following discussion in Figure 2.5.

Molecular clouds are dense and cold regions of the ISM primarily composed of molecular hydrogen H_2, though they also contain heavier and more complex molecules like carbon monoxide CO, as well as dust grains (surrounded by icy mantles). These clouds have typical temperatures of 10 to 20 K and densities ranging from a few 10^3 to 10^6 particles per cm^3. Due to their low temperatures, **the gas is predominantly found in molecular form rather than ionized or atomic**. Molecular clouds serve as the birthplaces of stars, as gravitational collapse within these regions can lead to the formation of protostars and planetary systems.

Before discussing the chemistry, let us define the concept of what will be called the **reaction time-scale**. It is the time after which the abundance of reactant A has dropped by a factor e during the considered elementary process. The expression depends on the molecularity. For a unimolecular reaction we have $\tau_{reac} \propto 1/k$ and for a bimolecular reaction we have $\tau_{reac} \propto 1/(k\, n(B))$. It is relevant in our context to confront this reaction time-scale with another time-scale called **dynamical time-scale** τ_{dyn}, which is the time during which the physical properties of the medium may be considered as constants. The dynamical time-scale of a molecular cloud is found between 10^6 and 10^8 years. The comparison between both time-scales leads to an important question: *Does a chemical reaction*

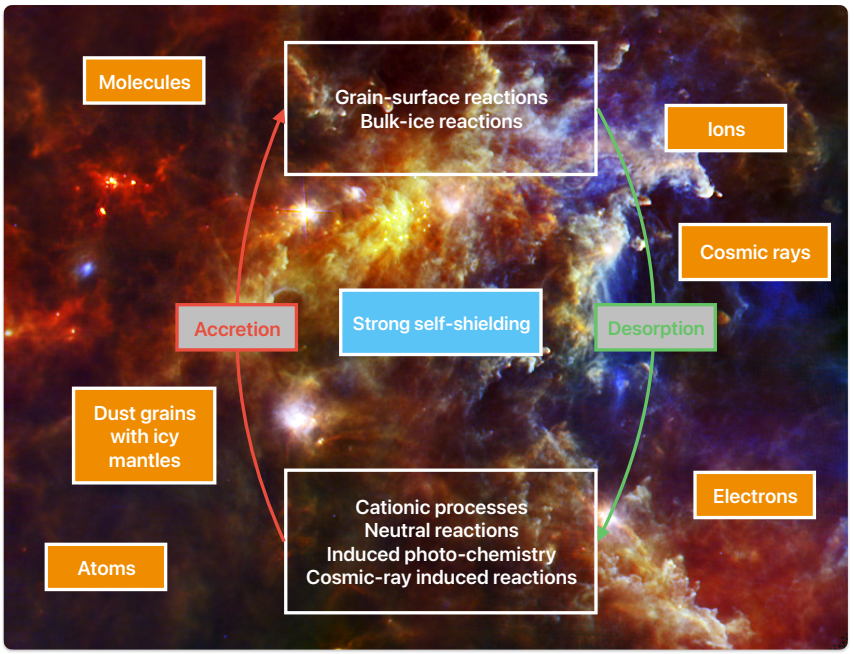

Figure 2.5: Summary of the chemistry taking place within a molecular cloud. The image of the Rosette molecular cloud (in IR), is taken from the ESA website (`https://www.esa.int/ESA_Multimedia/Images/2010/04/The_Rosette_molecular_cloud_seen_by_Herschel`).

have the time to occur significantly before changes in the properties of the medium? Yes, but at the condition that $\tau_{reac} << \tau_{dyn}$. For molecular clouds, considering the low densities and temperatures, **the chemistry will usually take a long time**, sometimes larger than the dynamical time of the cloud.

In contrast to diffuse clouds, which have much lower densities, extinction is very strong within molecular clouds. Atoms and molecules at the borders of those objects will absorb a lot of the external UV radiation emitted by nearby stars, preventing it to reach the core of the cloud and preserving thus its molecular content. In other words, the lack of penetration of external UV photons prevents photo-reactions to be active in dense clouds, especially in their inner parts. Another concept to introduce is **isotopic fractionation** that arises from the mass differences between isotopes, affecting their reactivity, especially at low temperature. Heavier isotopes form more stable molecules, making them less prone to dissociation and leading to an **enrichment in heavier isotopes** in cold environments like molecular clouds. This effect is especially seen in hydrogenated species, where the enrichment in deuterium in some abundant organic compounds such as H_2CO and CH_3OH is quite high (Charnley et al., 1997). This is also seen in the carbon and oxygen content of various species. This is linked to **self-shielding**, which depends on the specific absorption frequencies of each isotopologue. In the case of CO, the most abundant species ($^{12}C^{16}O$) primarily shields itself, leaving rarer isotopologues ($^{13}C^{16}O$, $^{12}C^{17}O$) more exposed to photo-dissociation. This selective shielding enhances the availability of less abundant isotopes for further chemical reactions, allowing them to be well incorporated in other compounds. For a detailed discussion, see Visser et al. (2009) or Colzi et al. (2020).

Now that we clarified some of the properties of molecular clouds, let us emphasize what are the important chemical processes at work. Concerning the gas-phase processes, we already established that photo-reactions are inhibited. However, as discussed in Section 2.3.2, energetic cosmic rays have the capability to enter molecular clouds and to reach the deepest regions. They will then interact with the content of the cloud, typically with H_2, that may generate some UV photons, and these photons will then be involved in photo-chemical reactions. Cosmic rays themselves also interact with the content of the cloud, leading to dissociation reactions as well as ionization reactions. What is important to remember is that, since external UV photons are severely attenuated by extinction, **cosmic rays are a relevant agent bringing energy within molecular clouds**. Such very energetic particles allow to break molecules and to create ions. Thanks to cosmic rays, we thus have some ions that may be involved in ion-molecule reactions as the one described in Section 2.3.2. Since such reactions are usually not inhibited by activation barriers and therefore do not suffer from a temperature dependence, the low temperature of molecular clouds is not a problem. Neutral-neutral reactions on the other hand are quite inhibited [23] in such cold environment, making the ion-molecule reactions the dominant ones. On top of that, we have to note that thanks to the low temperatures, atoms and molecules stay easily onto dust grains, favoring surface and bulk-ice reactions as the ones described in Section 2.4. The molecules produced may then desorb, thanks to the action of cosmic rays for example, and return to the gas phase to be involved in some gas-phase reactions.

Important remark:
In the context of this work, molecular clouds possess thus a huge potential, since they contain a rich molecular diversity allowing interesting chemical reactions to take place. Within such environments, we have seen throughout this theoretical section that both gas and surface processes are at work, and even that there is a **crucial interplay between gas-phase, grain-surface and bulk-ice processes**.

2.6 Amino acids and the building blocks of life

We finally arrive at the end of this theoretical chapter, but before diving into the practical part of the work we still have one more thing to discuss. It concerns the core molecules of interest in this master thesis, i.e. **amino acids**. In this section will be presented the nature and structure of amino acids, their role and importance in our biochemistry as well as their current detection status within the ISM and more generally celestial objects.

2.6.1 The building blocks of proteins: amino acids

We have discussed about Astrophysics, we have discussed about Chemistry, and now it is time to discuss (shortly) about Biology and Biochemistry.

First of all, *why are we so interested in amino acids*? Because they are **essential building blocks of life as we know it**, since they are the monomers used to build proteins which are macromolecules having a central role in our biochemistry. Proteins play indeed a wide variety of essential roles in living organisms. Structural proteins such as collagen and keratin provide strength and structure to connective tissues, skin, hair,

[23] That does not mean that some are not taking place, everything depends on the activation barrier.

and nails. Enzymatic proteins, including DNA polymerase and amylase, act as catalysts in processes such as DNA replication and digestion. Transport proteins like hemoglobin and albumin are responsible for transporting oxygen and other substances throughout the body, while aquaporins facilitate water transport across cell membranes. Defensive proteins, such as antibodies and fibrinogen, play key roles in the immune system by identifying pathogens and aiding in blood clotting (coagulation). Signaling proteins, including insulin and growth hormones, regulate biological processes, while receptors detect signals like hormones and neurotransmitters. Storage proteins like ferritin and casein store essential molecules such as iron and amino acids, respectively. Additionally, contractile and motor proteins like myosin and dynein are involved in muscle movement and intracellular transport. These are just some examples that illustrate the importance of the role played by proteins in our bodies. The 3D structure of proteins is of great importance, as it determines their biological function. Without its proper conformation or with different sequences of amino acids, a given protein would not be able to carry out its function.

Now that the importance of proteins have been highlighted (more information can be found for example in Whitford 2013), let us get a bit deeper into the nature and structure of their building blocks that are amino acids. Natural amino acids, which are part of the α-H-amino-acids[24], are organic molecules. They are all based on the following skeleton:

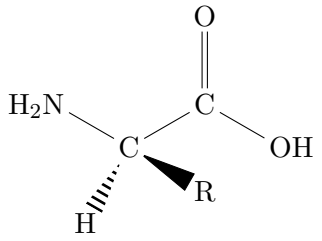

where the constitutive parts are as follows:

- A stereogenic center (except for glycine), which is the carbon at the α position with respect to the carboxylic acid functional group
- An amine functional group NH_2
- A carboxylic acid functional group COOH
- A hydrogen atom
- A radical R, which is the part unique to each amino acid. Each natural amino acid possesses a different radical, the simplest one corresponding to a single H atom included in the amino acid glycine.

In order to build proteins, amino acids will react between each others forming **peptidic bonds**. More specifically, what happens is that the amine group from one will react with the carboxylic acid group from another (through what is called a **nucleophilic substitution**) forming an **amide group** linking both amino acids and releasing one water molecule at the end of the process. Successive additions lead to larger and larger molecules called polypeptides, which will ultimately lead to proteins.

[24]Other kinds of amino acids exists do exist, like α-CH_3-amino-acids, β-amino-acids with the amine group at the β position with respect to the carboxylic group or diamino acids, but we do not take them into consideration here since we are interested in the ones found in proteins.

Important remark:
Proteins are, of course, not the only essential macromolecules in our organism. **Sugars** (or carbohydrates) play a crucial role, not only as an energy source but also in the structure of DNA and RNA. These **nucleic acids** are fundamental for genetic information storage, transmission, and expression, making them indispensable for life. Another essential class of biomolecules is **lipids**, which contribute to cell membrane integrity, energy storage, and cellular signaling.

2.6.2 Amino acids detection in astrophysical environments

After this small biological parenthesis, let us come back to Astrochemistry and discuss about what we know of amino acids in abiotic environments. Their different formation processes will be addressed in depth in Chapter 3.

The question that has fascinated (and still does) scientists for decades is the one of the **origin of life**. In our context we should even be a little bit more specific: *From where do the molecules required for the emergence of life come from*? As for now, we do not have the answer, but two approaches may be followed to tackle this problem: the **endogenous** and **exogenous** origins. The first one, assuming that molecules were synthesized in-situ on Earth, will not be considered in this work. Complementary readings related to this approach are the following papers: Miller (1953), Miller and Urey (1959) and Bada (2013). On the other hand, the exogenous origin is exactly what is studied in this master thesis. In this approach, we are looking at the possibility that molecules required for the appearance of life have been delivered to Earth, typically through cometary or asteroid bombardment. As an example, an instructive discussion about the possibility of nucleobases formation during the era of the **Late Heavy Bombardment** can be found in Ferus et al. (2014). In order to be delivered to Earth, molecules must thus have been formed in some astrophysical environment and successfully stored in a reservoir such as cometary ices or asteroids.

Interstellar medium

As already emphasized before, a lot of molecules could be of interest to us in order to study the emergence of life. In this work, it has been chosen to study different pathways towards the building blocks of proteins which are amino acids. We will further explore some chemical pathways taking place in the ISM, more precisely in molecular clouds, that may lead to the simplest of all amino acids that is glycine (more about that in Chapter 3). Studies such as Ioppolo et al. (2021) suggest that glycine formation could occur in cold environments like molecular clouds, while others, like Garrod (2013), indicate that this amino acid may form in warmer regions such as hot molecular cores. This naturally leads to the question: *Has glycine been detected in the ISM*? The answer remains no, **glycine has yet to be confirmed in any region of the ISM**. Although Kuan et al. (2003) initially reported its detection in the hot molecular cores Sgr B2(N-LMH), Orion KL, and W51 e1/e2, these claims were later refuted by multiple studies, including Snyder et al. (2005). Nonetheless, though the detection of glycine remains elusive, the detection of one of its isomers ($NH_2C(O)CH_2OH$, Rivilla et al. 2023) reinforced the confidence in its detection in the future.

Asteroids and comets

Though glycine has not been detected in the ISM, it does not mean that it has not been identified at all out of the Earth. Indeed, assuming that glycine has been formed in regions typical of stellar formation (as it is now more and more believed), one may wonder if this glycine could have been preserved in some way (like within icy mantles surrounding dust grains), thus surviving the stellar formation process. This will probably depend on the position of those molecules within the protoplanetary disk. Considering that glycine has been formed on dust particles, and stored within their mantles, only the ones far from the central star will avoid a strong energetic processing. Such grains, if not incorporated in planets, might very well be included in the small bodies of the solar system, i.e. **comets** and **asteroids**. Such bodies are quite representative of the pristine conditions of the young solar system epoch, and represent thus legitimate environments for glycine detection.

And indeed, astrochemists detected not so long ago the simplest natural amino acid not at the surface but within the coma (thus in gas-phase) of 67P/Churyumov-Gerasimenko. The Rosetta spacecraft/Philae lander mission from ESA[25], through measurements made by the ROSINA instrument, led to the first **unambiguous detection** of the amino acid glycine in gaseous state, of some of its possible precursors (methylamine NH_2CH_3 and ethylamine $CH_3CH_2NH_2$), as well as phosphorus[26] within the coma of 67P/Churyumov-Gerasimenko (Altwegg et al., 2016). This was the first valid detection of glycine in a cometary environment, since the detection of extraterrestrial glycine made at the epoch of the Stardust mission (NASA[27]) was tainted by some perturbations. Even if a contamination by terrestrial glycine was completely ruled out through isotopic ratio measurements (Elsila et al., 2007), the origin of this glycine was still questionable (Sandford et al., 2006). Indeed, **it may have resulted from the chemical alteration of other cometary compounds during the collection process**. The results presented by Altwegg et al. (2016) were thus needed to firmly establish that glycine can be found in cometary environments. One question still remains though, which is the one concerning the **origin** of this glycine. *What is formed onto the cometary body*? *What is formed previously in cold protoplanetary disk's regions or even before within the molecular cloud itself*? We may also wonder by which mechanism glycine was released in the coma of comet 67P/Churyumov-Gerasimenko. Actually, this last question was discussed by Hadraoui et al. (2019), in which three emission mechanisms of glycine were discussed as illustrated in Figure 2.6. The conclusion that is achieved according to their model is that mechanism (c), where glycine is first embedded in an icy mantle and then released through sublimation of the ice, seems to explain the observed distribution. Further studies are needed to conclude that this possible explanation is fully valid.

Asteroids have also been studied thanks to the Hayabusa 2 mission (JAXA[28]), which successively collected and brought back to Earth samples taken on the C-type asteroid Ryugu. As discussed in Naraoka et al. (2023), 15 amino acids, including glycine, were discovered in the studied samples along with many other organic molecules. However, as already noted in Naraoka et al. (2023) and further discussed in Potiszil et al. (2023), **aqueous alteration is expected to influence the amino acid content of a body**, primarily through Strecker synthesis (see Chapter 3). This does not imply that amino acids

[25] `https://www.esa.int/Science_Exploration/Space_Science/Rosetta_overview`
[26] Which has an important role in the DNA structure.
[27] `https://science.nasa.gov/mission/stardust/`
[28] `https://www.isas.jaxa.jp/en/missions/spacecraft/current/hayabusa2.html`

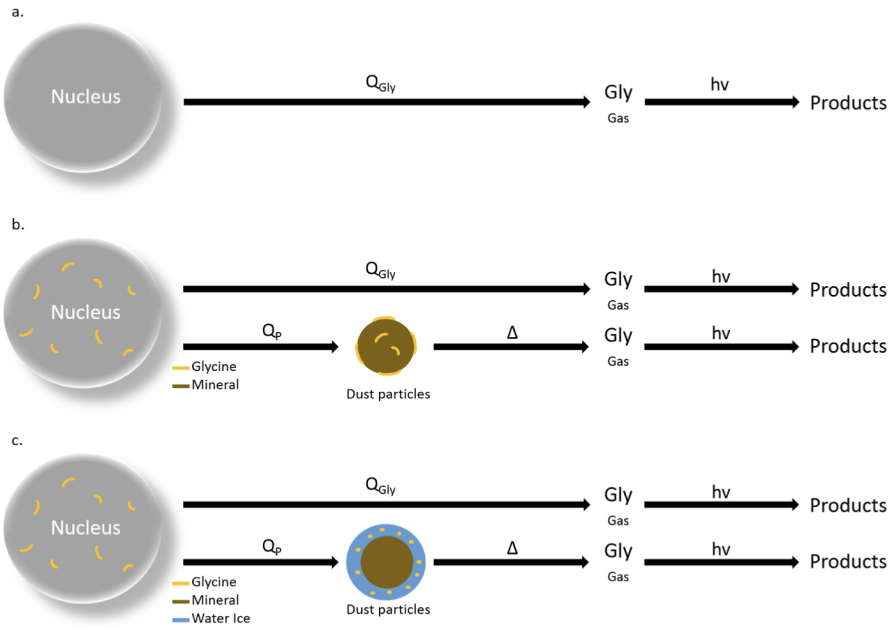

Figure 2.6: Mechanisms proposed in Hadraoui et al. (2019) to explain the desorption of glycine from the cometary nucleus. It does not mean that other mechanisms could not be at work. Panel (a): Glycine sublimates directly and exclusively from the comet's nucleus. Panel (b): Dust particles, carrying solid-state glycine adsorbed on their surfaces, are first ejected from the comet. Subsequently, this adsorbed glycine undergoes desorption, releasing it into the gas phase. Panel (c): Dust particles with icy mantles, containing glycine embedded in the ice, are first ejected from the nucleus. Then, as glycine diffuses within the ice and the ice mantle sublimates, glycine is released into the coma.

were absent before the collapse of the molecular cloud or during the next parts of stellar evolution. Rather, it remains possible that they were already present, and the findings of Potiszil et al. (2023) simply suggest that aqueous alteration leads to an increase in amino acid abundance within a parent body.

Meteorites

When a comet or an asteroid enters the Earth's atmosphere and survives the ground impact, we speak of a **meteorite**[29]. In that case, *could the initial glycine survive the impact*? Before answering this question, let us emphasize directly that glycine has been discovered in meteorites. Indeed, detailed analysis performed on a few meteorites have allowed to study their composition, revealing their rich organic molecular content, including several kinds of amino acids (natural and other ones). One detailed example would be the case of the Murchison meteorite[30] (see Figure 2.7). The study performed by Kvenvolden et al. (1970) unequivocally established the presence of 5 natural amino acids (glycine, valine, alanine, proline and glutamic acid) along with other non-proteic amino acids. Since this

[29] Meteorites are pieces of celestial small bodies such as asteroids and comets which were trapped in the Earth's gravitational field and survived both the entry in the atmosphere and the impact on the ground. They are of various kinds but in our context, the carbonaceous chondrites (CCs) are the most interesting regarding their high carbonaceous ($> 5\%$) and water ($> 20\%$) contents.

[30] One of the CM type, which impacted the Earth and subsequently exploded into fragments over the Australian town of Murchison on September, 28 1969.

study, more amino acids (even some exotic ones) have been discovered in the same meteorite, as reported by Koga and Naraoka (2017) or Lawless (1973). Even though this is still a matter of debate, some clues are pointing towards an extraterrestrial origin for this organic material. Indeed, in the previous finding for other meteorites, human contamination could not have been ruled out due to the high abundance of serine, which is the principal amino acid found in fingerprints. In the case of the Murchison meteorite, as described in Kvenvolden et al. (1970), the total abundance of serine was about one order of magnitude lower than glycine, which could not be explained by human contamination. Isotopic fractionation, which was introduced in Section 2.5, consists also of a strong clue towards an interstellar origin. Indeed, we have seen that cold environments such as molecular clouds tend to favor an enrichment in heavier isotopes (such as D, ^{15}N, ^{13}C) with respect to cosmic standards. Other papers clearly show that the amino acids found on the Murchison meteorite are quite enriched with such heavier isotopes (Cronin and Chang 1993 and Pizzarello et al. 1991).

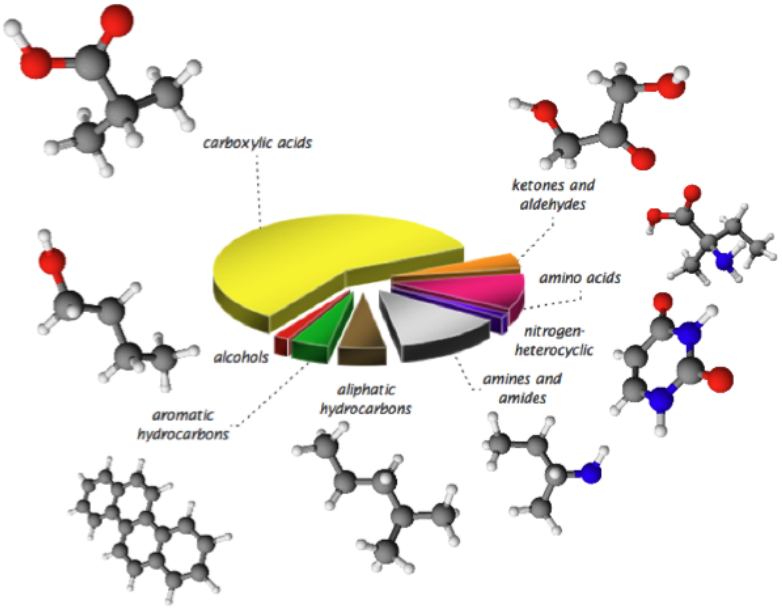

Figure 2.7: Relative abundances of organic compounds found in the Murchison meteorite. From Remusat (2014).

Important remark:

Amino acids are not the only biologically interesting molecules that were discovered on the Murchison meteorite. Nucleobases such as uracil have been found (Martins et al., 2008) but also sugars such as ribose (Furukawa et al., 2019). Both are building blocks of RNA, which could be a support regarding the RNA world hypothesis (Ayukawa et al., 2019).

To conclude this section, we must address one remaining question: *What is the true origin of the glycine molecules*? While we have discussed evidences supporting an extraterrestrial origin, the possibility of material alteration cannot be entirely ruled out. Carbonaceous chondrites, such as Murchison, are known to contain significant amounts of

water, which could modify the pristine material (Le Guillou et al., 2014). Additionally, catalytic reactions on clay minerals, as proposed by Garvie and Buseck (2007), as well as thermal alterations during atmospheric entry and impact, could further affect the molecular composition. As a result, **the original molecular content may have undergone significant changes, potentially influencing isotopic ratios**. However, a study by Busemann et al. (2006) demonstrated that meteorites can effectively preserve primitive organic compounds and their isotopic signatures, much like interplanetary dust grains, which are often regarded as the most pristine material from the early Solar System. This suggests that meteorites are capable of storing, preserving, and transporting primordial material, delivering it to Earth largely intact. It is also important to note that even if glycine can be preserved from a time predating the solar system, this does not exclude the possibility of its formation within the parent body, such as an asteroid or comet. Distinguishing between glycine formed before the parent body's formation and that produced in situ remains a considerable challenge (Aponte et al., 2017).

We now have a better understanding of the current status of glycine detection in space, but **its origin remains only partially explored**. Key questions such as "*How is glycine synthesized*?" and "*Which precursors contribute to its formation*?" are crucial for gaining deeper insight into its origins. Addressing these questions is challenging, as no straightforward answers exist. In the next Chapter 3, we will provide an overview of the various proposed mechanisms for glycine formation.

Chapter 3

Glycine synthesis in abiotic environments

In this chapter, different formation mechanisms of our molecule of interest, i.e. glycine, are reviewed. The chosen glycine precursors analyzed in this study will also be presented based on the various proposed formation pathways.

3.1 Formation mechanisms of glycine in the ISM

In order to perform this work, it was necessary to have a global view about the different chemical processes that may lead to the amino acid glycine. One can find in the literature several proposed routes toward this molecule, but not with the same relevance. Some are indeed more probable than others, and moreover some have been much more theoretically studied. Therefore, the discussion will be **restricted to the pathways that are the most promising based on a deep bibliographic investigation**. This has already been done a couple of years ago in the thorough study performed by Groyne (2023), which will therefore be the reference work that allowed the writing of this chapter.

As stated in the latter work, glycine formation mechanisms are usually studied within the framework of a specific phase, i.e. considering reactions taking place within dust grain's icy mantles or in the gas phase, the interplay between them being not accounted for. That is what was done in the work of Groyne (2023), where different glycine precursors were studied in gas-phase, but this master thesis aims at pushing further that work by considering all those glycine precursors within a set of reactions taking place **both in gas-phase and solid-phase**.

3.1.1 Strecker-like formation mechanism

The first mechanism, and maybe the best known, that will be addressed is the **Strecker-like mechanism**. The chemical reactions composing this mechanism take place within the water-based icy mantle of dust grains. We speak of "Strecker-like", since a pure Strecker mechanism involves the reaction of an aldehyde R−COH or ketone R−CO−R with an amine R−NH_2 and a CN bearing species in a **water liquid solvent** under acidic conditions. However, water in its liquid state does not exist in the ISM. A modified mechanism may nonetheless be invoked where reactions take place within an icy water matrix such as the icy mantles around dust grains. For the synthesis of glycine, the

simplest precursors of the compounds cited above are as follows: H_2CO, NH_3, HCN and H_2O. All the chemical reactions participating in this mechanism are illustrated below.

Formation Route A

$$H_2CO + NH_3 \rightleftharpoons NH_2CH_2OH$$
$$NH_2CH_2OH \rightleftharpoons CH_2NH + H_2O$$
$$CH_2NH + HCN \rightleftharpoons NH_2CH_2CN$$
$$NH_2CH_2CN + H_2O \rightleftharpoons NH_2CH_2COOH + NH_3$$

Formation Route B

$$H_2CO + HCN \rightleftharpoons CH_2(OH)CN$$

Then, two subroutes may be envisaged:

Subroute B1

$$CH_2(OH)CN + NH_3 \rightleftharpoons NH_2CH_2OH$$
$$NH_2CH_2OH \rightleftharpoons CH_2NH + H_2O$$
$$CH_2NH + HCN \rightleftharpoons NH_2CH_2CN$$
$$NH_2CH_2CN + H_2O \rightleftharpoons NH_2CH_2COOH + NH_3$$

Subroute B2

$$CH_2(OH)CN + NH_3 \rightleftharpoons NH_2CH_2CN + H_2O$$
$$NH_2CH_2CN + H_2O \rightleftharpoons NH_2CH_2COOH + NH_3$$

In this mechanism, **the presence of ammonia is indispensable** in order to lead to the formation of amino acids. Indeed, depending on the relative abundance of ammonia and hydrogen cyanide, two formation routes can be considered: route A and route B. The first one is based on the classical Strecker synthesis. We first have a reaction between ammonia and formaldehyde, leading to an unstable aminomethanol which dissociates directly to form an imine CH_2NH molecule. This step is followed by a nucleophilic attack of an hydrogen cyanide molecule on the imine, forming an aminoacetonitrile NH_2CH_2CN. The final step consists of the hydrolysis of this last compound, which finally forms the glycine molecule, NH_2CH_2COOH.

When the NH_3 abundance becomes negligible compared to HCN, the second formation route B may dominate. In that case, we start with a nucleophilic attack of the formaldehyde molecule by HCN forming a cyanohydrin molecule $CH_2(OH)CN$. Then, an other nucleophilic attack by an ammonia molecule follows, the results of which will depend on the leaving side group[1]. Subroute B1 and Subroute B2 must thus be considered, in which we will come back to route A at some point **provided ammonia is present in the environment**. Indeed, without this important molecule, the production of cyanohydrin in route B will be followed by an hydrolysis of the cyano group on this molecule, resulting in **the production of an hydroxy-acid** ($CH_2(OH)COOH$). In the absence of NH_3, the Strecker-like mechanism thus leads to the production of hydroxy-acids instead of amino acids. Both NH_3 and HCN are thus required to produce glycine through this mechanism.

[1]During a usual experiment in a lab at room temperature, one relies on acidity constant values to determine the leaving group which in usual conditions would be the $-CN$. Such values are however only tabulated at usual temperature values, therefore not for extreme conditions such as the ones within molecular clouds. In our context, it is thus required to consider the loss of both side groups (Groyne, 2023).

It is legitimate to ask ourselves whether or not this process is able to produce glycine in a significant manner in environments such as molecular clouds. First, not only the simplest precursors of glycine in this mechanism, i.e. NH_3 (Cheung et al., 1968), H_2CO (Snyder et al., 1969), HCN (Snyder and Buhl, 1971) and of course H_2O (Cheung et al., 1969), have been firmly identified in the ISM but also its direct precursor aminoacetonitrile NH_2CH_2CN (Belloche et al., 2008). An hydrolysis is then simply required to form glycine. Moreover, the computational study performed by Rimola et al. (2010) showed that **all reactions are thermodynamically favorable**, provided that they occur on their water-modeled surface, and that they are catalyzed by the icy-matrix.

This mechanism seems thus quite promising, nonetheless it has a main flaw. Indeed, despite the catalytic role played by the icy-matrix, the kinetics of this set of reactions is quite low due to the **high activation energy barriers** (especially for the final hydrolysis supposed to lead to glycine). This is due to the cryogenic conditions typical of molecular clouds, that inhibit neutral-neutral reactions as seen in Chapter 2. Although alternative reactions were investigated, such as in Kayanuma et al. (2017) where the reaction between NH_2CH_2CN and CO_2 was studied, energetic barriers are still too high to be overcome **without an external energy source** such as UV irradiation or shock heating. In order to circumvent the previous limitations, one may directly think about reactions involving ions. Indeed, we have seen that such reactions are not highly dependent on the temperature. In fact, one way to create ions would be the **external processing of the water-based icy mantles**, which has been neglected until now. Several studies, including the one of Bernstein et al. (2002), have shown that interstellar ice analogues under UV photolysis conditions may lead to the production of several amino acid precursors. A direct question would then be, *where could these UV photons originate from*? We have seen that molecular clouds are quite well shielded against external UV radiation. The answer comes from the discussion in Section 2.5, where it was said that cosmic rays are able to act as an energy source within molecular clouds leading notably to the **production of radicals and ions**. Regarding the typical composition of dust grain's mantles (more than 50% water), the radicals H and OH and the cations H^+ and H_3O^+ are expected to be the most abundant.

Studies by Walch et al. (2001) and Walch and Bakes (2001) have shown that substituting ions (CH_2OH^+, $CH_2NH_2{}^+$ and $NH_2CH_2CNH^+$) in the Strecker-like mechanism's route A activates the reactions. This provides us low or inexistent-barrier processes that are more plausible to take place in cryogenic conditions. This will be called the **activated Strecker-like mechanism** in the subsequent chapters.

3.1.2 Radical-radical pathways

A first radical-radical pathway which is quite interesting is the one referred to as the **Woon's mechanism**. It is based on the work of Woon (2002), where the viability of various glycine formation routes in UV irradiated water-ices were studied.

This mechanism is characterized by the following barrierless reactions:

Formation of the carboxylic acid radical

$$OH + CO \longrightarrow COOH \longrightarrow CO_2 + H$$

Formation of the aminomethyl radical

$$\begin{aligned} \mathrm{HCN} + \mathrm{H} &\longrightarrow (\mathrm{CH_2N}, \mathrm{HCNH}) \\ (\mathrm{CH_2N}, \mathrm{HCNH}) + \mathrm{H} &\longrightarrow \mathrm{CH_2NH} \\ \mathrm{CH_2NH} + \mathrm{H} &\longrightarrow (\mathrm{CH_3NH}, \mathrm{CH_2NH_2}) \\ (\mathrm{CH_3NH}, \mathrm{CH_2NH_2}) + \mathrm{H} &\longrightarrow \mathrm{CH_3NH_2} \end{aligned}$$

Final step towards glycine

$$\mathrm{CH_2NH_2} + \mathrm{COOH} \longrightarrow \mathrm{NH_2CH_2COOH}$$

In this route, one can notice the presence of an imine, as in the Strecker-like synthesis, emphasizing a potential interconnection between the two mechanisms. Moreover, unlike the Strecker-like pathway, **no ammonia is required**. As remarked in Groyne (2023), this might be linked to the work of Elsila et al. (2007), which highlighted that the major glycine formation pathway in UV irradiated ices is achieved without NH_3.

Important remark:
Woon (2002) emphasized that irradiated ices contain significantly more available energy than icy mantles completely shielded from UV radiation. Photolysis products, primarily radicals, exhibit a substantial excess of internal energy. This energy excess can help overcome activation barriers in subsequent reactions, a process that also applies to cationic species generated through cosmic-ray interactions. Furthermore, the barrierless recombination of radicals releases additional energy. However, in the cryogenic conditions of dense molecular clouds, most radicals, except hydrogen, lack the mobility to diffuse through the ice and encounter reaction partners. As a result, **heavier radicals primarily react with hydrogen or nearby species**, significantly restricting the range of possible chemical interactions.

Before moving on to the next mechanism, it is worth noting that the simplest molecules involved in this pathway have already been detected in the interstellar medium: OH (Weinreb et al., 1963), CO (Wilson et al., 1970), and CH_2NH (Godfrey et al., 1973). While their direct precursors, COOH and CH_2NH_2, have yet to be observed, some closely related species, such as formic acid HCOOH (Zuckerman et al., 1971) and methylamine CH_3NH_2 (Kaifu et al., 1974), have been successfully detected. The formation of the missing precursors could thus be achieved through a simple hydrogen ablation process.

The next formation mechanism that might be relevant is the one studied in the paper from Rimola et al. (2012). In that work, a pathway involving **both radicals and cations** is considered, taking thus the kinetic advantages of both types of compounds. The entire process is illustrated by the following reactions[2]:

$$\begin{aligned} \mathrm{CO_{incoming}} + \mathrm{OH^\bullet} &\longrightarrow \mathrm{COOH^\bullet} \\ \mathrm{COOH^\bullet} + \mathrm{CH_2NH_2}^+ &\longrightarrow \mathrm{NH_2CH_2COOH}^{+\bullet} \\ \mathrm{NH_2CH_2COOH}^{+\bullet} &\longrightarrow \mathrm{NH_2CHC(OH)_2}^{+\bullet} \\ \mathrm{NH_2CHC(OH)_2}^{+\bullet} - \mathrm{H}^+ &\longrightarrow \mathrm{NH_2CHCOOH^\bullet} \\ \mathrm{NH_2CHCOOH^\bullet} + \mathrm{H^\bullet} &\longrightarrow \mathrm{NH_2CH_2COOH} \end{aligned}$$

[2]The "•" symbol stands for a radical species.

It is worth noting that the hydrogen involved in the final radical addition step could be substituted by other radical species, potentially leading to the formation of different amino acids than glycine. Additionally, the "$-H^{\bullet}$" shown in the penultimate reaction is included to highlight the proton transfer between $NH_2CHC(OH)_2{}^{+\bullet}$ and the ice surface. While all these reactions are, in principle, thermodynamically favorable[3], it is important to emphasize that rate constants calculation indicate these processes are **unlikely to occur efficiently on astronomical time scales in cold and quiescent molecular clouds**. They are more typical of warm environments such as hot cores or shocked-regions.

The mechanisms discussed above represent only a fraction of the numerous pathways proposed in the literature for solid-phase astrochemistry in interstellar molecular clouds, with **several alternative routes likely to exist**. In this context, Garrod (2013) developed an astrochemical network to simulate coupled gas-phase, grain-surface, and bulk-ice chemistry in hot cores (built on earlier models). It was extended by including various formation and destruction reactions involving glycine and related species such as glycinal (H_2NCH_2CHO), propionic acid (CH_3CH_2COOH), propanal (CH_3CH_2CHO), and their precursors. Most of these new reactions follow radical-radical synthesis pathways through thermal diffusion, including the mechanism proposed by Woon (2002). A gas-phase formation route proposed by Blagojevic et al. (2003) was also included but showed negligible contribution to glycine formation. To implement this network, the ***MAGICKAL*** model, a three-phase astrochemical kinetic model (as the model used in this work, ***Nautilus***) which is unfortunately not open source, was developed. This model was applied to simulate hot core environments with a warm-up phase from 8 K to 400 K, starting from the collapse of a molecular cloud. The results highlighted several interesting points, among which the most important ones are summarized here:

- Four radical-radical recombination pathways leading to glycine were included in the network. Glycine is mainly formed on the surface and within icy mantles of dust grains between $\sim$ 40 K and 120 K, with no single pathway dominating the total contribution after sublimation.

$$\begin{aligned} H^{\bullet} + NHCH_2COOH^{\bullet} &\rightleftharpoons NH_2CH_2COOH \\ NH_2{}^{\bullet} + CH_2COOH^{\bullet} &\rightleftharpoons NH_2CH_2COOH \\ NH_2CH_2{}^{\bullet} + COOH^{\bullet} &\rightleftharpoons NH_2CH_2COOH \\ NH_2CH_2CO^{\bullet} + OH^{\bullet} &\rightleftharpoons NH_2CH_2COOH \end{aligned}$$

- The influence of each glycine formation pathway may vary slightly depending on the temperature and the warming timescale of the physical model. This was discussed, for example, in Sato et al. (2018).

The last glycine formation mechanism that can be discussed is the one proposed by Ioppolo et al. (2021), which is illustrated in Figure 3.1.

In contrast to previous studies, Ioppolo et al. (2021) explored glycine formation in dark clouds by considering a non-diffusive mechanism within icy matrices, occurring at an earlier stage of star formation than previously thought (see the bottom of Figure 3.1).

[3]Since the arrival of an imine molecule from the gas phase followed by its reaction with $COOH^{\bullet}$ has been shown to face a high energy barrier, an alternative pathway involving proton transfer from a surface H_3O^+ to the imine—forming $CH_2NH_2{}^+$—has been proposed as shown in the second reaction (Rimola et al., 2012).

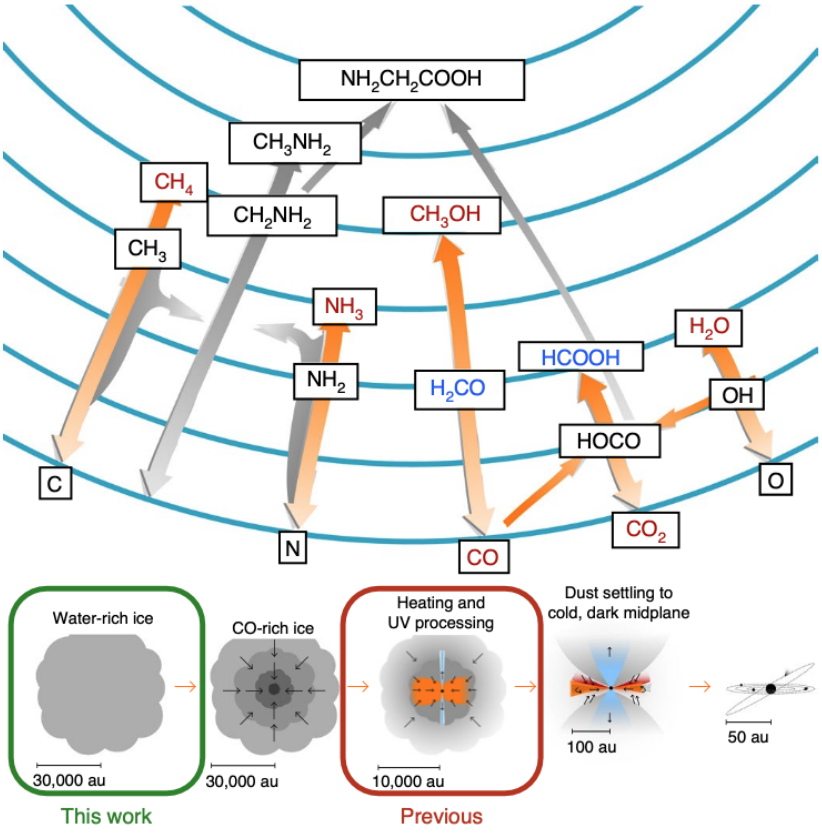

Figure 3.1: Schematic representation of surface reaction pathways leading to glycine formation in a water-rich ice during the early stages of low-mass stellar evolution. The reaction network shown has been taken from Ioppolo et al. (2021). Each blue ring represents an additional hydrogenation step. Hydrogenation–addition reactions are indicated by upward arrows, while downward arrows denote hydrogenation–abstraction reactions. Radical–radical recombination reactions are represented by horizontal or diagonal arrows. Non-energetic surface reaction routes tested under laboratory conditions are shown with orange arrows, whereas reactions examined in Ioppolo et al. (2021) are marked with grey arrows. In a water-rich ice environment, H and OH initiated surface reactions lead to the formation of stable species, such as H_2O, CH_4, NH_3, and CO_2, along with intermediate radicals like HOCO, CH, CH_2, CH_3, NH, and NH_2. Further radical–radical recombination enables the formation of the NH_2CH_2 radical and methylamine (NH_2CH_3). Glycine ultimately forms through the recombination of the HOCO complex with the NH_2CH_2 radical. Species unambiguously detected in ices are highlighted in red, while tentatively detected species (which have been now detected since the publication of that paper) are shown in blue. All other species involved in the reaction network are represented in black.

While many studies, such as the previous paper of Garrod (2013), have focused on glycine formation under higher temperature conditions, including simulations in hot cores, Ioppolo et al. (2021) showed that glycine can form in such dense cloud environments (around 15 K) via a primordial formation pathway that **does not require energetic irradiation** from stellar UV photons, cosmic rays, or cosmic-ray-induced UV photons. One may note that the final step towards glycine is reminiscent of the work performed by Woon (2002).

Regarding gas-phase processes, previous mechanisms are basically considered unchanged. As rightfully discussed in Groyne (2023), one may however wonder if such mechanisms should not be modified. Indeed, as discussed previously, light molecules are usually subject to dissociation when formed in gas-phase since no external agent is able to take away the excess of energy as the dust grain would. Moreover, icy mantles are noted here to play a catalytic role, allowing the reduction of some activation barriers. However, when the gas-phase is taken into account, **these mechanisms are usually considered unchanged in the literature** for the sake of comparison (Groyne, 2023). Moreover, the proposed mechanisms are not exhaustive. Many others exist in the literature, but considering all of them would be impractical. Therefore, a selection was made based on their **scientific relevance**. The main criteria included the availability of detailed studies, such as quantum calculations and kinetic simulations, as well as the number of references supporting each mechanism with minimal kinetic or thermodynamic limitations (Groyne, 2023).

As a conclusion to this section, it is important to understand that, even if those mechanisms are usually considered in each phase separately, their might more than probably be **interconnections between the phases**. Indeed, a particular glycine precursor may form through an initial gas-phase mechanism, then be adsorbed onto the dust-grain surface, diffuse into the bulk of the ice, and become incorporated into a solid-phase process, potentially leading to glycine formation. These connections have to be taken into account if one intends to make a comprehensive glycine formation study. For this reason, it has been chosen to work with the three-phase astrochemical code ***Nautilus***, which will be deeply introduced in Chapter 4.

3.2 Which glycine precursors are to be selected?

Before diving into generalities about astrochemical modeling in the next chapter, it is important to select which pathways, and thus which glycine precursors, will be studied in this work. As detailed previously, this work can be seen as a continuity of the one performed by Groyne (2023). The species studied in that work will thus also be studied here[4] (see Table 3.1). One may note that only simple species have been considered, for reasons related to the limited complexity of the code's chemical network, as detailed in Chapter 4.

Mechanism	Precursors
Classical Strecker-like mechanism	H_2O, HCN/HNC, NH_3, H_2CO
Activated Strecker-like mechanism	H_2CO^+, $NH_3{}^+$, H_2COH^+
Woon's mechanism	CO, CO_2, H_2O, OH, HCOOH, HCN, CH_2NH, HOCO, CH_2NH_2

Table 3.1: Glycine precursors studied in this work, according to the various formation mechanisms discussed in this chapter and already studied in Groyne (2023).

[4]Those species are shortly presented in Appendix D.

Chapter 4

Astrochemical modeling with *Nautilus*

In this chapter, the bases for astrochemical kinetic modeling, i.e. the modeling tool used in this master thesis, are presented in a general way. Furthermore, we describe in details the model that has been used, ***Nautilus***, as well as its various inputs and outputs.

4.1 Generalities about astrochemical modeling

Numerical astrochemical modeling is an indispensable tool in Astrochemistry. It allows scientists to explore the chemistry taking place in various astrophysical environments, such as the ones interesting to us: molecular clouds. As we have seen, those clouds are characterized by very low temperatures and densities, which are quite difficult to reproduce on Earth. Moreover, as a result of such unusual conditions, **astrochemical timescales are usually quite long**, which means that the chemical content evolves slowly at least within the gas-phase. Chemical equilibrium is therefore slowly reached, resulting in out-of-equilibrium chemistry for most of the cloud lifetime. For that purpose, **full time-dependent kinetics** should be resolved to grasp every aspect of the chemistry within the cloud. We have seen that in the framework of this concept, in order to study the abundance evolution of a certain compound over time, **rate equations have to be solved** (chemical kinetics). The problem is that, in the context of Astrochemistry in general, the equations that are to be solved are extremely complex (even more so for dynamical objects). On the contrary to laboratory experiments, it is impossible to isolate and study one particular reaction. All the reactions are coupled with each other, resulting in a complex system of hundreds of **Ordinary Differential Equations** (ODEs) that are analytically unsolvable. Numerical methods[1] are thus needed, and that is why **astrochemical models** were implemented. An additional major challenge lies in the fact that astrochemical systems are often **stiff**, meaning that they contain reactions evolving on very different timescales—from fractions of a second to millions of years. This stiffness can render standard integration schemes numerically unstable or prohibitively slow. To overcome this, most astrochemical models make use of **implicit numerical solvers** such as Backward Differentiation Formula (BDF) methods, which are specifically designed to handle stiff systems. The stiffness is usually evaluated from the system's Jacobian matrix and the derivatives dn_i/dt, reflecting the fast and slow chemical pathways present. While

[1]The interested reader is invited to consult Reynolds (2024), where several numerical algorithms are described.

robust, BDF methods are significantly more **computationally demanding**, adding to the complexity of solving astrochemical kinetics. The rate equation approach is not the only one that may be implemented in astrochemical codes. Other methods such as kinetic Monte-Carlo may be used (cf. Section 4.3), but one has to keep in mind that these methods, though sometimes indispensable to include more complexity in the grain modeling, are also much more CPU demanding (as discussed in Cuppen et al. 2013, 2017 and references therein). The advantage to use the rate equation approach is its convenience and rather quick numerical performances.

It should be noted that several kinds of astrochemical models exist. Some are proprietary while others are public (open-source). Moreover, the models may be further subdivided into categories depending on their applicability. We have pure gas-phase models (such as ***Astrochem***, Maret and Bergin 2015), 2-phase gas-grain surface models which consider the mantle and its surface as a single entity, and 3-phase models which make the difference between the grain surface and its mantle (such as ***Nautilus***, Ruaud et al. 2016, the one used in this work). It is important to understand that **different models are not exactly equivalent**. It means that, if you provide two models with the same parameters and networks, **they will not yield inevitably the same results**. "*There are always code-level differences (k parametrization, approximations made, solver tolerance, ...) that one cannot detect and correct without direct access to the codes being compared*" (Sipilä and Ruaud, 2024). Sometimes the benchmarking of the results between two chemical networks (i.e. files regrouping all the chemical reactions) can thus be complicated, especially if you are trying to compare your network with a private one. Nonetheless, it does not mean that results cannot be equivalent between two models.

4.1.1 Requirements for astrochemical models

Astrochemical models require two principal ingredients, which are the **set of parameters** characterizing the environment and a **chemical network**.

First of all, let us talk about the **required parameters**. There are four main parameters which dictate the chemistry taking place: the density n, the temperature T, the cosmic-ray ionization rate ξ and the visual extinction A_v. It is mandatory to specify those[2] in your model. At this point, it is important to recall the discussion in Section 2.5 regarding the timescales. In what follows, we will consider that τ_{chem} is below τ_{dyn}, meaning that the chemistry taking place will happen before a significant evolution (change of the physical parameters) of the considered medium. In other words, assuming an homogeneous medium, **the values of the previous parameters will be considered as constant with time in every region of the molecular cloud**. If we considered $\tau_{chem} > \tau_{dyn}$, it would mean that the medium has the time to evolve significantly before the chemistry modifies the molecular content. We would thus have an important and continuous change in the physical parameters describing the environment, which would require much powerful simulation tools[3].

These are not the only parameters, since the model may also take various parameters describing the solid-phase (dust temperature, grain density, dust-to-gas mass ratio,

[2]Depending on the model type, you may choose to differentiate the gas and grain temperatures (`grain_temperature_type`). In what follows, we will assume $T_{gas} = T_{dust}$.

[3]Let us note that with ***Nautilus***, it is possible to implement a **discrete** temporal evolution of the environment as described later.

sticking coefficient, grain radius, ...). Other specifications should also be given, such as the duration of the study period. One is referred to the documentation of his favorite astrochemical code for more information concerning its own specificities.

The second important requirement for an astrochemical model is the **chemical network**. We have seen that in our context thousands of reactions involving hundreds of compounds are all interconnected, occurring all simultaneously and making impossible the task to isolate one particular reaction and thus the involved chemical species. Chemical networks are provided in the form of **files including all the chemical reactions that are considered**. An example of graphical illustration of a chemical network is shown in Figure 4.1, which is an easy way to visualize the interconnection between all the compounds. It is obvious that networks that are of use in astrochemical models are much richer than the one illustrated in this figure, as they actually involve much more reactions.

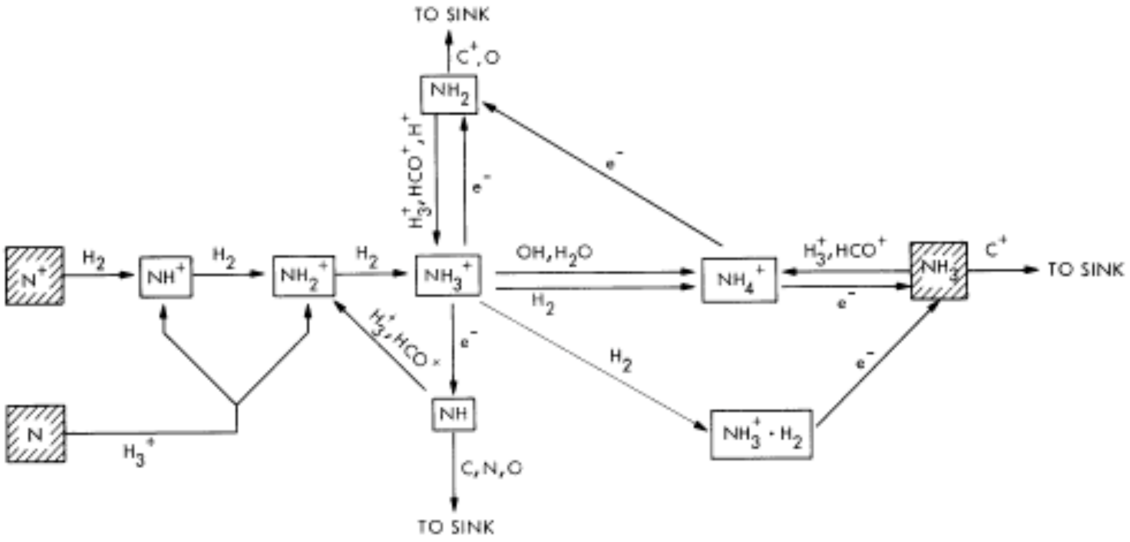

Figure 4.1: Simplified gas-phase chemical network showing the principal formation routes towards ammonia NH_3 in dense clouds. From Prasad and Huntress (1980b).

In a practical way, chemical networks are simply text files composed of several columns. Each line of such files contains the information concerning one particular reaction, such as the reactants, the products, the kinetic parameters (used to compute the expression of the rate constant k and which can be found in relevant databases) and the index of the formula used to compute k[4] (the ID of the reaction, i.e. its number in the file, can also be found as it is the case for ***Nautilus***). In order to build such networks, we are thus in need of **kinetic data** specific to each reaction. These can be found in astrochemical databases. The most used ones are the NIST chemical kinetics database[5], the UMIST database for astrochemistry[6] (Woodall et al., 2007) and KIDA[7] (Wakelam, 2009). The last two databases are constantly updated. Databases are built upon laboratory experiments and chemical quantum computations, and in that sense are thus limited. Indeed, it is very time demanding to determine the parameters for each molecule and each reaction,

[4]Depending on the used database, k can be parametrized with different mathematical expressions.
[5]`https://kinetics.nist.gov/kinetics/`
[6]`http://udfa.ajmarkwick.net/index.php`
[7]`https://kida.astrochem-tools.org`

and that sometimes limits the extent of an astrochemist's study[8].

Some concepts are still needed to fully characterize an astrochemical network, as thoroughly discussed in Groyne (2023). Firstly, it is important to ensure the model is able to infer the most accurate abundance evolutions possible. It is therefore necessary to include as many formation and destruction pathways[9] as you can in your network. This requirement refers to what is called the **completeness of a chemical network**. This concept refers to the extent to which a network includes all relevant chemical species and reactions necessary to accurately describe the chemistry of a given astrophysical environment. A complete network should account for gas-phase, grain-surface, bulk-ice and photo-chemical reactions, as well as interactions driven by cosmic rays and thermal processes. However, achieving full completeness is challenging due to the huge number of possible reactions and the limited availability of experimental or theoretical data for many rate coefficients. As a result, astrochemical models often rely on continuously updated reaction databases, such as the ones presented above, to improve their accuracy. Secondly, what will be called the **complexity limit** has to be taken into account. The latter can be seen as the highest molecular complexity (cf. Chapter 1) achievable in the astrochemical network. The higher this complexity limit, the more complex the astrophysical environments that can be studied (Groyne, 2023).

Balance between completeness, complexity and computational feasibility is also crucial to ensure that the network remains both representative and manageable in numerical simulations. Indeed, the more reactions and molecules are included in the network, the more CPU will be needed to solve the ODEs system. For 0D and 1D-simulations[10], this is usually not a problem, but for 3D-simulations it is required to work with a tailored network in order to reduce the computing time (Sipilä and Ruaud, 2024).

From all this discussion, it results that **the best astrochemical network should combine both a high completeness and complexity**. However, as we saw previously, we are limited in what can be achieved in terms of parameter computations. As for now, the complexity limit achievable is not very high (for example, in the ***Nautilus*** network

[8]Moreover, the rate coefficients of chemical reactions always carry some degree of uncertainty. For gas-phase reactions, they are typically known with a precision factor of about 2–3 at a given temperature, though this uncertainty may vary with temperature. Similarly, grain-surface reaction rates are subject to **much higher** uncertainties. Even small variations in key reaction rates can significantly impact simulation outcomes. Despite this, most astrochemical models do not account for these uncertainties. Addressing this issue requires varying the rate coefficients of all uncertain reactions using random distributions and running hundreds or even thousands of simulations to obtain a range of possible abundances rather than a single time-dependent solution. However, such an approach is computationally impractical for most modeling studies. More about this topic can be found in Sipilä and Ruaud (2024) and references therein.

[9]The **closure** of an astrochemical network is another fundamental characteristic. Each species in the network must possess both formation and destruction routes, or it would lead to so-called **sink-species** which could cause serious problems since some compounds could just disappear (Sipilä and Ruaud, 2024).

[10]In astrochemical modeling, 0D, 1D and 3D simulations refer to the spatial dimensionality of the models used to study chemical and physical processes in astrophysical environments. 0D simulations assume a uniform value of the physical parameters across the entire environment. In that case, a molecular cloud would be considered as a unique cell of uniform density and temperature. 1D simulations assume variations occur along a single axis, making them computationally efficient for studying time-dependent chemistry in molecular cloud cores, protoplanetary disks, or shock fronts. In contrast, 3D simulations capture the full spatial complexity of turbulent, magnetized, and evolving structures, such as star-forming regions or protoplanetary disks with gaps and spiral arms. While 0D and 1D models provide fundamental insights with simpler assumptions, 3D models are essential for realistically simulating complex gas dynamics, magnetic fields, and turbulence, though they require significantly more computational resources.

described in Section 4.2, the simplest amino acid, glycine, is currently not included). What is great is that those networks are constantly evolving, including more and more complex species while **keeping quite high completeness at each step**, which is the most important to insure sufficient confidence in the obtained results.

Important remark:
Another characteristic that has to be emphasized is the nomenclature of the different species. As emphasized in Sipilä and Ruaud (2024), astrochemical networks do not necessarily have the same nomenclature for the same species (as an example, H_3CO^+ in ***Astrochem*** but H_2COH^+ in ***Nautilus***).

4.2 Presentation of the 3-phase gas-grain code *Nautilus*

This section aims at providing the reader with a basic overview of the capabilities of ***Nautilus***, but one is referred to the official documentation for more in depth presentation of the software.

In this work, it has been chosen to use the ***Nautilus*** astrochemical code. A legitimate question would be: "*Why* ***Nautilus*** *and not another chemical network*?" This master thesis aims at going one step further than the thorough work done by Groyne (2023) focusing on the gas phase. We need therefore a code that includes the solid-phase chemistry, allowing us to describe in more depth the dust grain component. Private networks such as ***MAGICKAL*** (Garrod, 2013) were of course out of reach. Other 3-phase codes do exist, such as ***Chempl*** (Fujun, 2021) or ***Uclchem*** (Holdship et al., 2017), but it was chosen to use ***Nautilus*** for its reliability (i.e. the code has been reworked several times[11], minimizing bugs) and ease of use. This astrochemical code is quite sufficient for the extent intended in this work. ***Nautilus*** (Ruaud et al., 2016) is a 3-phase gas-grain code, meaning that in addition to the gas-phase chemistry, the solid-phase chemistry is taken into account by not only including the reactions at the grain surfaces but also the complex chemistry taking place in icy mantles surrounding dust grains in cold environments such as molecular clouds. The code and all the documentation can be downloaded from the dedicated webpage[12].

Model description

Nautilus is an astrochemical model written in FORTRAN and based on the KIDA database. It can be used to study various astrophysical environments, such as hot molecular cores, protostellar envelopes, protoplanetary disks and of course molecular clouds. These various environments may be simulated thanks to a large set of tunable parameters which will be described later.

As explained in Ruaud et al. (2016), it has been assumed in the network implementation that **accretion and desorption processes only occur from the surface of the mantle**, i.e. the first two monolayers, and the gas phase[13]. As already emphasized,

[11] The last updates of the code were implemented in March 2022, as described in the documentation.
[12] `https://forge.oasu.u-bordeaux.fr/LAB/astrochem-tools/pnautilus`
[13] This does not mean that the species found deeper in the mantle are trapped forever. Some diffusion or swapping mechanisms are at work, allowing species to move within the icy mantle.

chemical reactions are allowed within the mantle, but with a slower diffusion rate of the species in comparison with the ones on the surface.

In order to illustrate the complexity of the ODEs to be solved, the following equations have been reproduced[14] from Ruaud et al. (2016), where more details about the calculation of the various terms can be found:

$$\left.\frac{dn(i)}{dt}\right|_{\rm tot} = \sum_l \sum_j k_{lj} n(l) n(j) + \sum_j k_{\rm UV-CR}(j) n(j) + k_{\rm des}(i) n_s(i) - k_{\rm acc}(i) n(i) - k_{\rm UV-CR}(i) n(i) - n(i) \sum_l k_{ij} n(j), \tag{4.1}$$

$$\begin{aligned}\left.\frac{dn_s(i)}{dt}\right|_{\rm tot} = & \sum_l \sum_j k^s_{lj} n_s(l) n_s(j) + \sum_j k^s_{\rm UV-CR}(j) n_s(j) + k_{\rm acc}(i) n(i) \\ & + k^m_{\rm swap}(i) n_m(i) + \left.\frac{dn_m(i)}{dt}\right|_{\rm m\rightarrow s} \\ & - n_s(i) \sum_j k^s_{ij} n_s(j) - k_{\rm des}(i) n_s(i) - k^s_{\rm UV-CR}(i) n_s(i) \\ & - k^s_{\rm swap}(i) n_s(i) - \left.\frac{dn_s(i)}{dt}\right|_{\rm s\rightarrow m},\end{aligned} \tag{4.2}$$

$$\begin{aligned}\left.\frac{dn_m(i)}{dt}\right|_{\rm tot} = & \sum_l \sum_j k^m_{lj} n_m(l) n_m(j) + \sum_j k^m_{\rm UV-CR}(j) n_m(j) \\ & + k^m_{\rm swap}(i) n_s(i) + \left.\frac{dn_s(i)}{dt}\right|_{\rm s\rightarrow m} \\ & - n_m(i) \sum_j k^m_{ij} n_m(j) - k^m_{\rm UV-CR}(i) n_m(i) \\ & - k^m_{\rm swap}(i) n_m(i) - \left.\frac{dn_m(i)}{dt}\right|_{\rm m\rightarrow s}.\end{aligned} \tag{4.3}$$

Those equations describe the evolution of the abundance (represented by the number densities) of a given chemical specie i for the 3 phases considered in the code: the gas ($n(i)$), the surface ($n_s(i)$) and the mantle ($n_m(i)$). In these equations, various terms describe all the processes that may take place. The rate coefficients k_{ij}, k^s_{ij}, and k^m_{ij} [$\rm cm^3 s^{-1}$] correspond to reactions between species i and j occurring in the gas phase, on the grain surface, and within the mantle, respectively. The coefficients $k_{\rm acc}$ and $k_{\rm des}$ [$\rm s^{-1}$] represent the accretion and desorption rates of individual species onto and from the grain surface. In this model, $k_{\rm des}$ can account for both thermal and non-thermal processes. The dissociation rate coefficient, $k_{\rm UV\text{-}CR}$ [$\rm s^{-1}$], encompasses contributions from (1) direct cosmic-ray interactions, (2) secondary UV photons induced by cosmic rays, and (3) standard interstellar UV photons. The coefficients $k^s_{\rm swap}$ and $k^m_{\rm swap}$ [$\rm s^{-1}$] express

[14] These equations have been slightly modified after some thoughts on the matter. A sum have been added in front of the terms $k_{\rm UV-CR}(j)n(j)$, $k^s_{\rm UV-CR}(j)n_s(j)$ and $k^m_{\rm UV-CR}(j)n_m(j)$ since not only one given species "j" could be dissociated to produce the species "i". You have to sum over all the species that could produce it, as it is implemented in the code. Moreover, the notation used in Ruaud et al. (2016), i.e. $k_{\rm diss}$, has been replaced by $k_{\rm UV-CR}$ in this work for the sake of clarity.

the swapping rates between the surface and the mantle, in both directions. The terms $\frac{dn_s(i)}{dt}\Big|_{s\to m}$ and $\frac{dn_m(i)}{dt}\Big|_{m\to s}$ describe the individual transfer rates of species i from the surface to the mantle and vice versa.

Inputs of the *Nautilus* model

The entire collection of parameters available for modification is described in Appendix B, for which the file name must be `parameters.in`, which is the name recognized by the ***Nautilus*** code. The most important parameters have already been described in Section 4.1, we will thus not come back to them. Nevertheless, other parameters must be presented in order to understand all the possibilities that can be explored with this modeling tool.

Besides the grain and gas parameters, several switches are available. The code may be used in multiple modes. It can either work as a 2-phase or 3-phase model (switch `is_3_phase`), or as a pure gas-phase model by setting the parameter `is_grain_reactions` to 0. A discrete temporal evolution can be implemented if `is_structure_evolution` is set to 1. This functionality will not be used, and one is referred to the documentation for further details. A last possibility to be discussed is the **dimensionality of the simulation**. 0D simulations will be performed during this work, i.e. an homogeneous medium with the same mean parameters everywhere will be assumed. But the ***Nautilus*** software allows also the user to work with 1D simulations, i.e. a radial evolution of the physical quantities. In that case, the switch `structure_type` has to be set to `1D_no_diff`. The parameters alone are of course not sufficient to run the model. The initial abundances[15] for chosen chemical compounds must be given through the input file `abundances.in`, cf. Table 4.1. When not specified, a default value is used by the code which can be set with the parameter `minimum_initial_abundance`. The file `elements.in` lists all the elements which are included in your medium. The files `surface_parameters.in` and `activation_energies.in` contain the information related respectively to the parameters of some species on the surface (mass, binding energies, ...) and on the activation energies values for some species. And finally, we still have to specify the molecular compounds that we are considering as inputs. This is done thanks to the files `gas_species.in` and `grain_species.in`, where species populating the gas phase and the solid phase have to be specified separately even if interactions between the phases do exist.

The last files to be given are of course the astrochemical networks. Since we are considering both solid and gas phases in this model, networks compiling reactions for each phase have to be provided. We thus have two different networks to give to the software which are stored in files `gas_reactions.in` and `grain_reactions.in`. The only important parameters are: the reactants, the products, the kinetic parameters (A, B, C)[16], the temperature range of validity of the parameters, the formula used to compute the reaction rate (label of the reaction type) as based on the KIDA database and the reaction ID (i.e. its number in the file). The gas-phase network contains 8275 reactions, involving 567 **unique** species and the solid-phase network contains 4837 reactions involving 511 species. Let us emphasize that those networks are the ones found in the folder `example_simulation`, that

[15] For the electron initial abundance, it is chosen in the code to ensure global charge neutrality.

[16] Reaction rates are often expressed using formulas as Equation 2.4, but not always depending of the model. In a general way, the factors A, B and C describe the values that have to be injected in the kinetic constant's parametrization depending on the reaction type. One is referred to `https://kida.astrochem-tools.org/help` for details about the rate constant parametrization.

Species	Abundance
He	9.000000E-02
N	6.200000E-05
O	2.400000E-04
H	0.000000E+00
H_2	0.500000E+00
C^+	1.700000E-04
S^+	8.000000E-08
Si^+	8.000000E-09
Fe^+	3.000000E-09
Na^+	2.000000E-09
Mg^+	7.000000E-09
P^+	2.000000E-10
Cl^+	1.000000E-09
F	6.680000E-09

Table 4.1: Initial elemental abundances relative to Hydrogen.

can be found when downloading ***Nautilus***, and are the most up to date (i.e., 2023, as described on the ***Nautilus*** webpage). Actually, the 2024 version of the KIDA network has been released (Wakelam et al., 2024) but all the necessary files are not made available (only gas-phase network).

Outputs of the *Nautilus* model

We have introduced in details the inputs of our astrochemical model, but *what about the results provided by the code, i.e.* ***the outputs***? Well, as for the inputs, all the output files are described in the ***Nautilus*** documentation. The important output files are as follows: `species.out`, `elemental_abundances.out`, `abundances.out` and `rates.out`. `species.out` provides the information concerning the species found at the end of the simulation. Basically, it is just a file consisting of a list of molecules. `elemental_abundances.out` contains the information about the final elemental abundances (which is not supposed to have changed since elements should be conserved all along the simulation). In the files `abundances.out` and `rates.out`, one finds the information about the molecular abundances and the reaction rates, respectively, **for each of the considered time-steps**. They are thus as many `abundances.out` and `rates.out` files as the number of steps chosen in the simulation. Those two files will be used to generate the plots for our analysis in the following chapters. Note that the last two files are in binary format. They will thus need further formatting to be used in the different routines of the ***Nautilus*** software.

Not only the astrochemical code can be obtained when downloading the software, but also some routines and Python scripts that allow the user to exploit the output files. It is possible to plot abundances of some chosen species within a given time interval. The user may also choose to compare the abundance evolutions between two or more simulations. Finally, it is possible to plot the time evolution of the main formation and destruction pathways of a given species. Once again, the reader is referred to the documentation for further understanding concerning the code usage.

Important remark:

The plotting scripts have been adapted to improve readability and interpretation of the figures presented in Chapter 6. This modification particularly concerns the graphical representation of formation and destruction pathways. In the original code, all reactions deemed non-negligible by the software were plotted, often resulting in an overwhelming number of reactions and unreadable graphs. To address this issue, a selection criterion was introduced: only reactions contributing to at least 5% of the total integrated production/destruction fraction were retained. Additionally, reactions that, at any time, accounted for more than 50% of the fraction were also included to ensure that important contributors were not omitted. It is important to note, however, that **other reactions may still play a role**, even if their contributions are smaller.

As a summary of this section, Figure 4.2 illustrates the basic working principle of the ***Nautilus*** code.

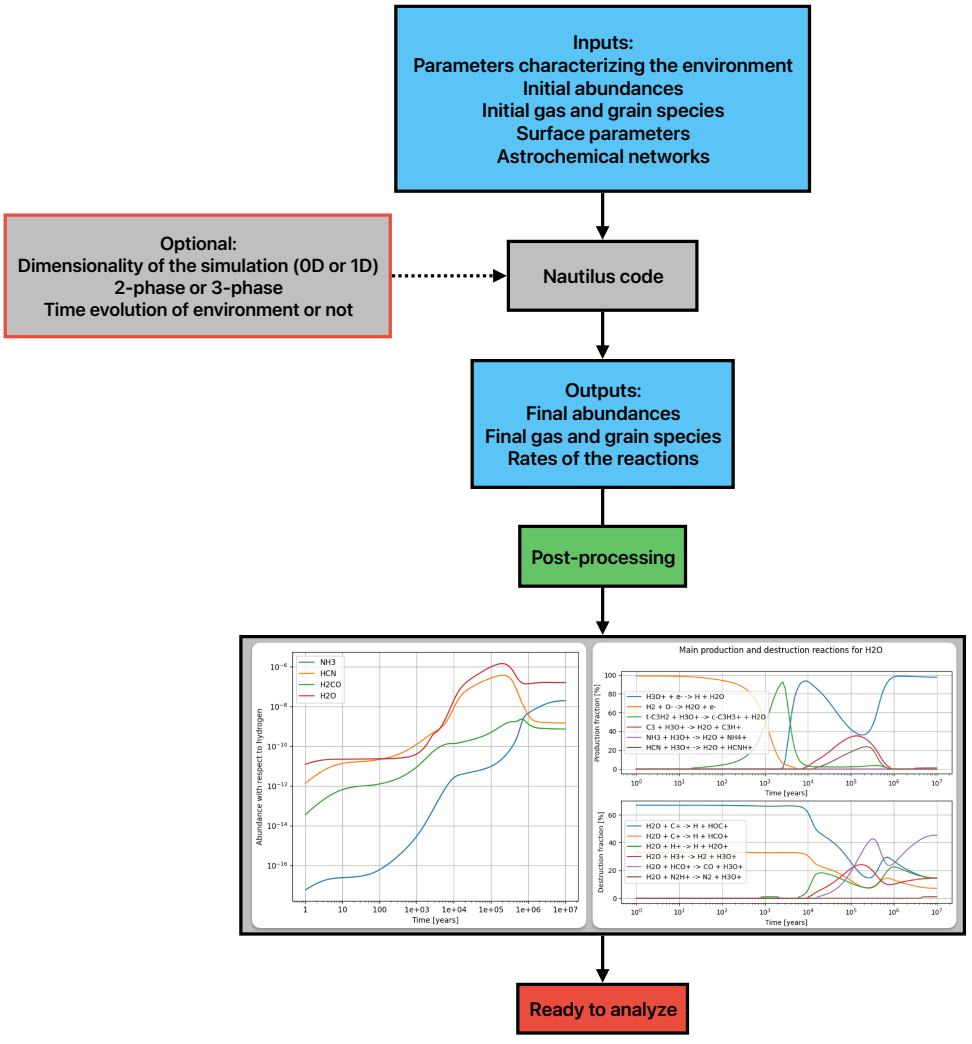

Figure 4.2: Schematization of the working principle of the ***Nautilus*** astrochemical model.

4.3 Limitations of the *Nautilus* model

While traditional rate-equation models such as ***Nautilus*** are widely used in astrochemical simulations due to their ability to handle large chemical networks in terms of computational requirements, it is crucial to acknowledge the limitations of this approach—**particularly regarding its treatment of grain-surface chemistry and ice mantle formation**.

One significant limitation lies in the treatment of surface binding sites. Standard rate-equation models typically assume a single type of binding site, characterized by a single value of binding energy for each species. This oversimplification is problematic because, in reality, interstellar grain surfaces are heterogeneous, featuring a distribution of binding site energies (Ferrero et al., 2020; Duflot et al., 2021; Tinacci et al., 2022; Groyne et al., 2025). As shown in Furuya (2024), the outputs of astrochemical models significantly vary if a distribution is used instead of a single value for the binding energy of species. Since this value is fixed in rate-equation models, the results are heavily dependent on an arbitrary or poorly constrained parameter, reducing the predictive reliability of such simulations.

Another critical aspect concerns the formalism adopted for desorption processes. Various desorption mechanisms, such as thermal desorption, photo-desorption, and reactive desorption, can be treated differently depending on the model. For example, Wakelam et al. (2017b) compared the formalism introduced by Garrod et al. (2007) with that of Minissale et al. (2016), showing that the assumptions made in these formalisms can lead to notably different outcomes. This sensitivity to the choice of desorption model further amplifies the dependency of rate-equation simulations on the specific parameter set and assumptions employed. Binding energy values themselves again play a central role here, reinforcing the previous concern.

Furthermore, as in all astrochemical modeling tools, chemical networks used in these models may omit key reactions due to incomplete kinetic data, especially for grain-surface and bulk-ice processes. The lack of well-characterized rate coefficients for certain reactions can result in inaccurate modeling of the formation and destruction pathways of key molecules. This limitation reflects both the incompleteness of current reaction networks and the inherent difficulty in quantifying surface reaction rates under interstellar conditions.

A major limitation of the ***Nautilus*** model lies in its use of the rate equation approach to simulate surface and mantle chemistry. The following is based on the review from Cuppen et al. (2013), and one is referred to it for further details. In astrochemical modeling — particularly for grain-surface and ice-mantle chemistry — two fundamentally different approaches are used: the rate equation (RE) method, which is deterministic, and a class of stochastic approaches that include the master equation formalism and kinetic Monte Carlo (KMC) methods. These approaches differ significantly in terms of physical realism, computational complexity, and suitability for modeling processes under interstellar conditions. Unlike deterministic rate equations, which have been proven to be inaccurate to simulate chemistry on dust grains (Vasyunin et al., 2009), KMC methods provide a more detailed treatment of grain-surface chemistry. In contrast to the deterministic nature of rate equations, which solve coupled stiff ordinary differential equations based on average concentrations, **KMC methods simulate the stochastic evolution of individual chemical events** — such as accretion, diffusion, reaction, and desorption —

using event-based time stepping. This inherently probabilistic approach is based on the chemical master equation[17], and it allows for a more accurate modeling of processes that occur with low surface populations or when discrete effects become important. There are two main variants of KMC methods: macroscopic and microscopic. While both include similar reaction types and physical processes, microscopic KMC simulations offer several key advantages. In these models, **each species is tracked individually**, including its exact location on the grain surface. Diffusion is modeled as discrete hops between binding sites, and species may revisit the same site multiple times - a process known as back diffusion. While this effect can be introduced approximately in rate equations, microscopic KMC accounts for it naturally and explicitly. Moreover, reactions in microscopic KMC occur only when species occupy the same or adjacent binding sites, meaning the reaction order is not imposed a priori and may deviate from classical second-order kinetics depending on the local surface environment. Another important feature of microscopic KMC is its ability to incorporate complex surface structures. Binding sites can differ in energy, allowing the model to represent heterogeneous grain surfaces, such as amorphous silicates or ices with topographical features like steps and pores. This spatial heterogeneity directly affects diffusion and desorption rates, which is site-specific. As a result, the reaction-diffusion competition - i.e. whether a particle reacts before desorbing or diffusing away - is automatically captured by the simulation rather than manually imposed via corrective factors as in rate-equation models. Microscopic KMC also naturally simulates ice mantle growth. As the mantle thickens, molecules can become buried in lower layers, where their mobility is reduced. These buried species may no longer participate in surface chemistry or desorb efficiently, a phenomenon difficult to model using rate equations, which typically lack positional information. Thus, the stratification of ices and chemical inhomogeneities within the mantle is inherently taken into account in microscopic KMC simulations. While these benefits make microscopic KMC highly realistic and powerful for studying surface chemistry in cold interstellar environments, they come at the cost of significantly increased computational expense. This limits their application to smaller chemical networks and shorter simulation times compared to rate-equation models, which are computationally more tractable but necessarily involve simplifying assumptions.

In conclusion, rate-equation models offer a computationally cheap yet simplified framework for exploring large-scale chemical evolution in astrophysical environments. However, due to assumptions such as single binding energy per species, different desorption schemes, and deterministic treatment of inherently stochastic processes, caution must be exercised in interpreting their predictions—particularly for surface and bulk-ice chemistry. Acknowledging these limitations and comparing results with more detailed probabilistic approaches like KMC is essential for a more robust understanding of interstellar chemistry. Therefore, the treatment that will be presented in Chapters 5, 6 and 7 must be considered within that limited framework. Nonetheless, the results will greatly help to obtain first insights into the behavior of the glycine precursors, and will open the doors to more detailed studies as proposed in Chapter 9.

[17]The chemical master equation (CME) is a probabilistic framework that describes the time evolution of the probability distribution of a system's chemical states, accounting for the stochastic nature of individual reaction events. Unlike deterministic rate equations, the CME tracks how likely the system is to be in each possible state, making it well-suited for systems with small numbers of reactants or discrete events. More information can be found in Section 2 of Cuppen et al. (2013) and references therein.

Chapter 5

Comparison between *Astrochem* and *Nautilus*

The first step of the practical aspect of the work was a comparison between the astrochemical codes ***Nautilus*** and ***Astrochem***. If this work intends to be a continuation of the one performed in Groyne (2023), it is primordial to be sure that the gas-phase results presented in that work can be reproduced using ***Nautilus***, allowing us to start on a concordant basis.

5.1 Comparison between the gas-phase networks

First of all, it was required to compare the gas-phase chemical networks of both models to be sure that the molecules we want to study can be found in our model's network.

In order to perform that comparison, several **Python functions** have been written. The first (and longest) function[1] was built in order to read the text files in which the networks were contained and to store the relevant information into Python arrays that will subsequently be used in the various codes for comparison. Practically, what this first function does is decompose the text file into its different columns of interest for each network and to store each column as elements of the array. We thus have at the output of the function two Python arrays (one for each network), the columns of which are (i) the list of reactants ("0") (ii) the list of products ("1") (iii) the list of kinetic parameters ("2") (iv) the label of the reaction type ("3"), cf. KIDA database. The principal result that emerges from this comparison is that the ***Nautilus*** gas-phase network has a **higher completeness** (8275 vs. 6046 reactions) in absolute terms (some redundancy must be considered) and a **higher complexity** (567 vs 469 unique reactants). All the glycine precursors studied in Groyne (2023) (Table 3.1) can be found in the gas-phase network from ***Nautilus***. Moreover, each of these precursors is involved in more formation/destruction pathways in the network from ***Nautilus*** than in the one from ***Astrochem*** (one exception being HCOOH, which is involved in one less formation route than in ***Astrochem***).

From this comparison, it seems that ***Nautilus*** can be used to reproduce some of the results obtained in the work of Groyne (2023), as shown in the next section.

[1]This function has been written with the help of Maria Groyne, a PhD student at the University of Liège, whom I thank for the help.

5.2 Reproduction of the results

In this section, the main results of Groyne (2023) will be reproduced using ***Nautilus*** in order to push further the comparison. **We are thus still focusing here on pure gas-phase chemistry**.

To reproduce the results, only two of the files required modifications: `abundances.in` and `parameters.in`. The abundances in elements were set to the same values as those used in Groyne (2023) (Table 4.1) and the parameters and switches were set to consider an homogeneous molecular cloud, where only gas-phase reactions are taken into account (`is_grain_reactions` = 0). In those conditions, only the gas initial density and temperature as well as the visual extinction and cosmic-ray ionization rate required modifications.

Important remark:
In order to compute the initial gas density n_H, one must be aware that **all the hydrogen is assumed to be in its molecular form** H_2. According to the ***Nautilus*** documentation, the initial gas density is calculated using the following formula: $n_H = n(H) + 2n(H_2)$. The previous comment means that $n_H = 2n(H_2)$ and that $n(H_2)/n_H = 0.5$ in the `abundances.in` file (see Table 4.1).

In the following, we will use the different models from Groyne (2023) to study the glycine precursors presented earlier. The different physical conditions considered are described in Table 5.1.

	n_H (cm^{-3})	T_{gas} (K)	A_v (mag)	ξ (s^{-1})	F_{UV} (ref. units)
Model 1a	10^4	10	20	10^{-17}	1
Model 2a	10^6	10	20	10^{-17}	1
Model 3a	10^4	20	20	10^{-17}	1
Model b	10^5	50	20	10^{-17}	1

Table 5.1: Models with various gas-phase conditions describing an homogeneous stable through time molecular cloud. Reproduced from Groyne (2023).

This section does not aim at performing a deep analysis of the various glycine precursors. This has been done thoroughly in Groyne (2023) for the gas phase and it would be pointless to just rewrite that discussion. A pure comparison will thus be performed and in this chapter we will only emphasize the differences that may be encountered between the two astrochemical codes. The reader is referred to Appendix E for a detailed discussion of both similarities and discrepancies, along with some relevant figures. However, a thorough analysis of the results including the solid-phase chemistry will be performed in Chapter 6.

5.2.1 Strecker-like synthesis - Neutral pathway

This pathway towards glycine involves the following simple precursors: H_2O, NH_3, H_2CO and HCN, as previously specified in Chapter 3. In Table 5.2, one can find the equilibrium[2]

[2]Readers unfamiliar with the equilibrium formalism are invited to consult Appendix C.

abundances from both the present work and the one of Groyne (2023).

Groyne (2023)	H_2O	HCN/HNC	NH_3	H_2CO
Model 1a	$2.5\ 10^{-7}$	$8.5\ 10^{-10}$	$2\ 10^{-8}$	$6.3\ 10^{-10}$
Model 2a	$1.2\ 10^{-7}$	$2.1\ 10^{-10}$	$1\ 10^{-8}$	$1.8\ 10^{-10}$
Model 3a	$3\ 10^{-7}$	$1.13\ 10^{-9}$	$4.2\ 10^{-8}$	$5.7\ 10^{-10}$
This work	H_2O	HCN/HNC	NH_3	H_2CO
Model 1a	$1.65\ 10^{-7}$	$1.53\ 10^{-9}$	$2.02\ 10^{-8}$	$7.59\ 10^{-10}$
Model 2a	$4.43\ 10^{-8}$	$1.47\ 10^{-10}$	$5.69\ 10^{-9}$	$1.40\ 10^{-10}$
Model 3a	$1.92\ 10^{-7}$	$1.36\ 10^{-9}$	$2.05\ 10^{-8}$	$7.28\ 10^{-10}$

Table 5.2: Equilibrium abundances with respect to hydrogen for the four precursors studied in the framework of the neutral Strecker-like mechanism.

What can be seen from Table 5.2, looking first at model 1a, is that results from ***Astrochem*** and ***Nautilus*** converge quite well. Indeed, the equilibrium concentrations are remarkably similar. As in Groyne (2023), H_2O remains the dominant species throughout most of the simulation. This indicates that, at first sight, ***Astrochem*** and ***Nautilus*** give consistent gas-phase abundances. The chemical equilibrium is reached after approximately 10^6 years, which aligns with the discussion in Groyne (2023). However, **notable differences arise before equilibrium**. For instance, in the ***Nautilus*** simulation, HCN is the second most abundant molecule, whereas in Groyne (2023) it is surpassed by H_2CO after roughly 10^3 years except at the very end. This discrepancy may be attributed to the greater completeness of ***Nautilus***, which incorporates more reaction pathways - for example, HCN has more than twice the number of formation routes in ***Nautilus*** as compared to ***Astrochem*** - but also to differences in the kinetic parameters used in the two models. Indeed, on top of the fact that both codes are based onto two different databases (OSU versus KIDA), kinetic parameters are continuously refined across the years. Discrepancies in the parameters are thus expected. Those hypotheses can be checked with the main formation/destruction pathways over time and their rates, as discussed hereafter.

Important remark:
It must be pointed out that the Y-axis of the figures shown in Appendix E, which displays the chemical routes, is not the same between the results of the two codes (rates versus production/destruction fraction). Therefore, only qualitative comparisons are allowed, i.e. we may only discuss about the dominant reactions taking place and their relative importance, respective to each code outputs.

Starting with H_2O, a comparison with Groyne (2023) shows that the overall conclusions remain consistent, although some differences should be noted. While four of the six main formation reactions are shared between both models, discrepancies appear primarily in the early chemistry (before $\sim 10^3$ years). Beyond 10^3 years, the **dominant reactions are nearly identical**, except for the absence of the reaction involving SiO in our work. Groyne (2023) previously identified missing contributors to water formation in the early

stages (i.e. the reaction involving molecular hydrogen). This was corrected by considering a higher density that permitted additional reactions to take place (model 2a). Interestingly, this issue does not arise in this study. One may have thought that the kinetic parameters are different, however they are exactly identical in both networks. It is therefore probably linked to code differences, emphasizing the fact that providing two codes with the same parameters for a given reaction does not ensure that the results will be identical (cf. Chapter 4). Moreover, it must not be forgotten that everything is interconnected, meaning that changes in kinetic parameters for other reactions could have an impact on reactions involving water precursors. For the destruction pathways, the ***Nautilus*** model accounts for the same reactions as the one used in Groyne (2023). Overall, the results remain highly similar. One slight difference is that, at the end, the reaction involving HCO^+ dominates clearly whereas in Groyne (2023), there were nearly equal contributions of HCO^+ and $H_3{}^+$, with a slight dominance of the latter. On top of those considerations, one may note the nearly identical equilibrium abundance of water. Despite ***Nautilus*** including additional reaction routes involving water compared to ***Astrochem***, this does not significantly affect its final abundance. This suggests that the newly introduced pathways contribute only marginally to the overall balance of water formation and destruction.

Important remark:
It is important to keep in mind that more reactions included in a network does not necessarily mean a higher completeness. Indeed, although ***Nautilus*** includes dozens more reactions than ***Astrochem***, **these may have little impact at the low temperature considered (they would be deactivated)**. This reason might also explain, at least partially, the similarity between the results of the two codes.

Having a look at the formaldehyde formation pathways, it is striking to note that the results are quite similar to those of Groyne (2023), though two reactions from ***Astrochem*** are not found in the results of ***Nautilus***. For the formaldehyde destruction pathways, we still have clear similarities but also deviations. Between 10^3 and 10^6 years, a reaction involving atomic carbon clearly dominates destruction (Figure E.3), which is clearly different from the results presented in Groyne (2023). This can be explained by the simple fact that the latter reaction is not included in the network from ***Astrochem***.

For hydrogen cyanide HCN (Figure E.4), even if final abundances are not strongly affected, one directly notices the differences between both modeling approaches. If we look at the formation pathways, the chemistry until $\sim 10^4$ years is dominated by the reaction $N + CH_2 \longrightarrow HCN + H$ in ***Nautilus*** whereas in ***Astrochem*** the reaction $HCNH^+ + e^- \longrightarrow HCN + H$ must also be taken into account. Looking closer at the networks, the kinetic parameter A between the networks is not the same (9.622×10^{-8} in ***Nautilus*** versus 1.85×10^{-7} in ***Astrochem***). In the work of Groyne (2023), the last reaction therefore has a higher kinetic, which could explain the difference from our results. Out of the 6 main reactions in Groyne (2023), only three are found in this work. While the reaction $H^+ + HNC \longrightarrow H^+ + HCN$ is not included in the network of ***Nautilus***, the two other reactions are present with the same kinetic parameters as in ***Astrochem***. Regarding the destruction routes, the only main difference is that in our results, the importance of the contribution of the reaction involving C^+ is comparable (even higher) to the ones involving H^+, H_3O^+ and $H_3{}^+$, whereas in Groyne (2023) it is completely negligible. As previously, that may probably be explained by differences in the kinetic parameters. Indeed, the values of all

the parameters have been changed between the networks ($A = 4.75 \times 10^{-9}$, $B = -5 \times 10^{-1}$ and $C = 0$ in ***Astrochem*** becomes $A = 1$, $B = 1.28 \times 10^{-9}$ and $C = 6.61$ in ***Nautilus***). Nonetheless, it is important to keep in mind that there are **important differences in the kinetic constant parametrization between the two codes**, meaning that the comparison between the parameters might be in this case irrelevant. Whereas an Arrhenius like parametrization is assumed in the OSU database on which is based ***Astrochem***, ion-neutral[3] reactions are computed using the Su-Chesnavich capture approach. The detailed comparison of those approaches goes beyond the scope of this master thesis and one is referred to the following document (and references therein) if in need of further details: `https://kida.astrochem-tools.org/uploads/documents/ionpol_notice.pdf`.

It is now interesting to compare the results concerning the abundances of HCN and HNC. In Groyne (2023), the abundance ratio remained close to unity throughout the simulation, a result consistent with Graninger et al. (2014), where this ratio was found to be stable in cryogenic environments such as molecular clouds. However, in this work, we observe a divergence of about two orders of magnitude between 10^4 and 10^5 years. Interestingly, a closer look at Graninger et al. (2014) (Figure 5, using parameters similar to ours) reveals a similar feature: a temporary bump in the same time range, where HCN becomes more abundant than HNC. Despite this temporary difference, the abundances of both species eventually converge at equilibrium, reaching values comparable to those reported in Groyne (2023). This transient enhancement in HCN abundance could be attributed to its slightly higher stability compared to its isomer, HNC. Since both molecules share the same dominant reaction pathways (except during a short time between 10^4 and 10^5 years), HNC may be preferentially destroyed, as confirmed by the slightly higher kinetics of the reactions involving hydrogen isocyanide.

Finally, let us analyze the results concerning the ammonia molecule (see Figure E.6). Ammonia being mainly produced through a cationic chain starting with nitrogen and its cation, finally ending through the dissociative recombination of the ammonium cation, the similarity with Groyne (2023) was expected. For the destruction pathways, the main differences are the involvement of the reaction involving atomic carbon and the importance at equilibrium of one of the reactions ($NH_3 + C^+ \longrightarrow H + HCNH^+$) involving C^+, which were already discussed previously.

The first results are thus similar in both work. One main deviation is the involvement of C^+ in the late destruction equilibrium chemistry, which was completely negligible in Groyne (2023). Verifying in the networks, the values of the kinetic parameters of the reactions are different (both codes are not built on the same database and the kinetic constant parametrization for some ion-neutral reactions is different). We may also note that the destruction equilibrium chemistry is, in this work, dominated by HCO^+ (see Appendix E for more details), whereas in the previous work of Groyne (2023) there is a slight dominance of $H_3{}^+$. Once again, the parametrization is not the same between the codes. If the physical parametrization is not the same, one could have expected such differences and a comparison of the parameters cannot be performed since their role in the formulas are not the same. On top of that, everything is interconnected, and changes in parametrization and parameter values of various reactions could lead to significant changes in the chemical modeling results.

[3]The following is valid for ion-neutral reactions in which the neutral molecule has a dipole moment.

Important remark:
All these studied precursors are expected to be involved in pathways leading to more and more complex species, themselves being probably involved in a plethora of other processes. Our astrochemical code has nonetheless a limited complexity and these first results are coming from purely gas-phase chemistry treatment, without any source of sink terms from the solid-phase. The expected synergy of the results with a more complete network and a solid-phase linked treatment should therefore be kept in mind when interpreting these results, without drawing hasty conclusions.

Now that differences in the results from model 1a have been compared, let us have a look at model 2a where the overall density of the cloud is enhanced by two orders of magnitude. From Table 5.2, we reach easily the same conclusions as Groyne (2023), the abundances at chemical equilibrium being very close between models 1a and 2a despite the hundredfold increase in initial hydrogen density. As discussed in Groyne (2023), it can be noted that the time required to reach equilibrium does not depend on the initial hydrogen density, as shown in Appendix E. Looking at the main formation/destruction pathways, results are close from the ones of Groyne (2023) though discrepancies exist in the involved reactions between the two models, as already emphasized in the case of model 1a.

We will conclude by the results obtained with model 3a, in which T has been increased from 10 K to 20 K compared to model 1a. The abundances at equilibrium and even their temporal evolution remain pretty similar, which is in perfect agreement with the results obtained by Groyne (2023). Indeed, as discussed in that work, a small temperature increase is not sufficient in such cryogenic conditions to enhance sufficiently the chemistry. In other words, **reactions that were inhibited at** 10 **K will remain inhibited at** 20 **K**. To notice sufficient differences, one would have to raise the temperature to a higher level, but that would mean leaving the physical conditions of a **quiescent** molecular cloud.

What can be said in conclusion of this first comparison is that although the time-dependent chemistry varies between the results, **the equilibrium chemistry obtained with both codes is always similar**.

5.2.2 Strecker-like synthesis - Activated pathways

As discussed in Groyne (2023) and in Chapter 3, in order to activate the kinetics (lower the activation barriers) of the Strecker-like formation route, ions can be substituted in the reactions to give the **activated Strecker-like mechanism**. In that context, the following precursors will be considered: H_2CO^+, H_2CO, HCN, NH_3, H_2COH^+ and $NH_3{}^+$. Table 5.3 includes a summary of the equilibrium abundances of this work and that of Groyne (2023).

Let us begin to study the results obtained from model 1a for those precursors. As discussed in the previous section, even though the time-dependent chemistry varies slightly in comparison with the results from Groyne (2023), the equilibrium results are quite similar. The abundances of the cationic/protonated species are about 2 to 3 orders of magnitude lower than the neutral ones, as expected in environments such as molecular clouds, fewer ions being created. Despite their low abundances, ion-involved reactions remain relevant to our study because of their significantly lower activation barriers, which make them much more reactive and thus compensate for their scarcity.

Groyne (2023)	H_2COH^+	H_2CO^+	NH_3^+
Model 1a	$1.65\ 10^{-12}$	$1.57\ 10^{-13}$	$2.13\ 10^{-12}$
Model 2a	$3.44\ 10^{-14}$	$1.08\ 10^{-15}$	$1.87\ 10^{-14}$
Model 3a	$1.49\ 10^{-12}$	$1.31\ 10^{-13}$	$8.13\ 10^{-12}$
This work	H_2COH^+	H_2CO^+	NH_3^+
Model 1a	$1.48\ 10^{-12}$	$2.66\ 10^{-13}$	$5.23\ 10^{-12}$
Model 2a	$1.05\ 10^{-13}$	$4.23\ 10^{-15}$	$4.27\ 10^{-14}$
Model 3a	$1.69\ 10^{-12}$	$3.30\ 10^{-13}$	$2.55\ 10^{-11}$

Table 5.3: Equilibrium abundances with respect to hydrogen for the three supplementary precursors of the Strecker-like synthesis. Adapted from Groyne (2023).

Considering model 2a, the conclusions made with the neutral species are no longer valid and one finds an agreement with the results of Groyne (2023). Quantitatively, we notice that the equilibrium abundances are very similar to those found in the latter work. This agreement might be explained by the **close similarity in terms of the number of pathways in which these precursors are involved in both networks**. Nonetheless, one must not forget the effect of the kinetic parameters on the results as well as the different parametrization for ion-neutral reactions. Looking in more detail at those of the dominant formation/destruction pathways plotted by ***Nautilus***, when the parametrization is the same, the parameter values are not always identical; when the parametrization is not the same then the comparison is not really relevant. One has to keep in mind that it is those kinetic parameters and the parametrization of the reaction rates in which they are involved that dictate the chemistry. The fact that they differ, even slightly, between the codes adds a complexity layer on top of this comparison.

The curves obtained for model 3a are this time also pretty similar to those obtained with model 1a as in Groyne (2023). This is further illustrated in Table 5.3, where the abundances from both models are nearly the same except for $NH_3{}^+$ which has an equilibrium abundance enhancement of nearly one order of magnitude. This increase in abundance has already been observed in Groyne (2023), though with a lower amplitude. Looking closer at the networks, the dominant destruction of that species ($H_2 + NH_3{}^+ \longrightarrow H + NH_4{}^+$) is included only one time in ***Astrochem***, but 3 times in ***Nautilus***, each time with different values of the kinetic parameters but also ranges of temperature validity. For the relevant temperature range (10 to 20 K), though the A parameter is the same, in ***Nautilus*** the B has decreased and C has increased. Differences in the kinetic parameters and the complex interconnection between various reactions may explain the slight difference in the equilibrium abundance value.

5.2.3 Precursors for Woon's mechanism and its variants

Concerning the so-called Woon's mechanism, based on the work carried out by Woon (2002) and discussed in detail in Chapter 3, some details have to be pointed out that differentiate this work from the one of Groyne (2023). First of all, since that work only

focuses on gas-phase chemistry, the initial Woon's mechanism (based on reactions taking place within interstellar ice analogues) had to be modified to **take into account the fragment losses** that may take place in gas-phase, dust grains being absent to take away the excess of energy. In the context of this work, the mechanism will not require any modification since we are considering both grains and their icy mantles. Nonetheless, this modified pathway will have to be taken into account in order to reproduce the results. The interested reader is referred to the original work of Groyne (2023) for the discussion, but a summary of the processes considered can be found in Figure 5.1.

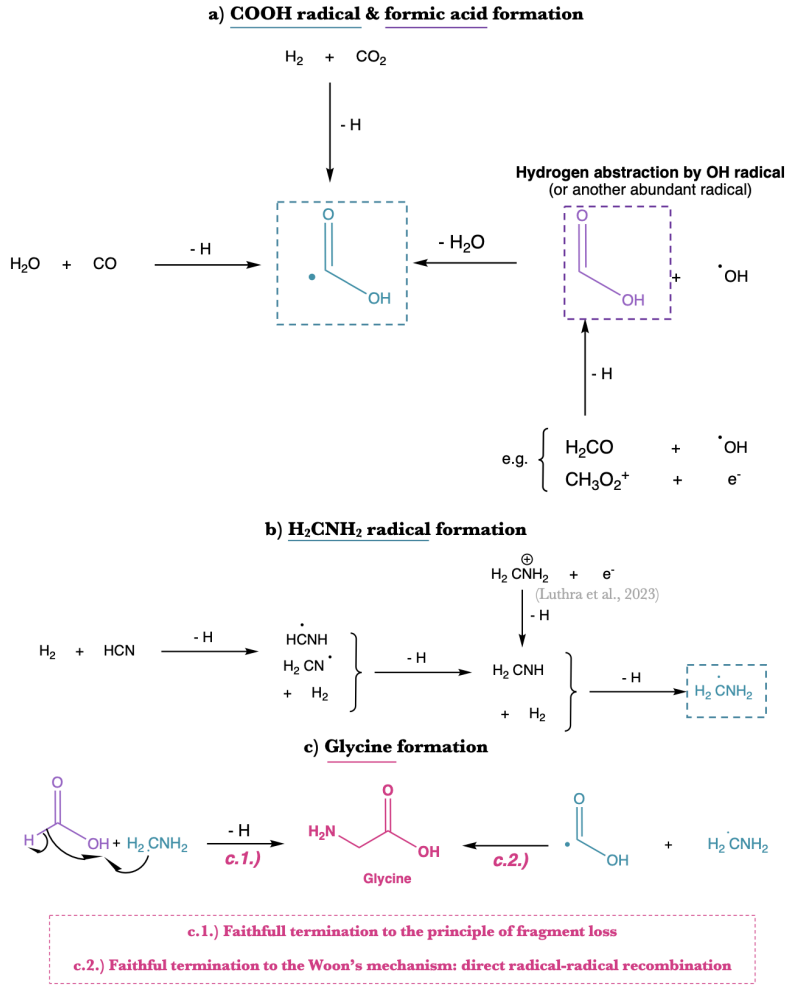

Figure 5.1: Modified Woon's mechanism, taking into account the fact that when considering gas-phase, fragment losses cannot be excluded. From Groyne (2023).

Moreover, it was acknowledged in that work that the targeted direct precursors of glycine NH_2CH_2COOH, i.e. COOH and H_2CNH_2, were not included in the ***Astrochem*** genuine network. Within the ***Nautilus*** gas-phase network, both of those species are included (named respectively HOCO and CH_2NH_2). The presence of these precursors could then allow their direct (radical-radical) recombination to form glycine, following the mechanism proposed by Woon (2002). We will come back in the next chapter at the solid-phase study of this mechanism, but as for now let us focus on the gas-phase synthesis.

The results obtained thanks to model 1a for both steps of Woon's mechanism are presented in Table 5.4.

Groyne (2023)	CO_2	H_2O	CO	OH	CH_2O_2
Model 1a	$2.75\ 10^{-7}$	$2.5\ 10^{-7}$	$6.15\ 10^{-5}$	$1.35\ 10^{-7}$	$2.72\ 10^{-10}$
Model 2a	$1.2\ 10^{-7}$	$1.2\ 10^{-7}$	$6.53\ 10^{-5}$	$2.28\ 10^{-9}$	$4.21\ 10^{-10}$
Model 3a	$3\ 10^{-7}$	$3\ 10^{-7}$	$6.15\ 10^{-5}$	$1.39\ 10^{-7}$	$2.01\ 10^{-10}$
Groyne (2023)	HCN	CH_3N	CH_4N^+	CH_5N^+	CH_6N^+
Model 1a	$8.5\ 10^{-10}$	$3.04\ 10^{-12}$	$1.07\ 10^{-14}$	$7.65\ 10^{-16}$	$2.30\ 10^{-14}$
Model 2a	$2.1\ 10^{-10}$	$7.10\ 10^{-13}$	$1.81\ 10^{-16}$	$8.09\ 10^{-18}$	$3.71\ 10^{-16}$
Model 3a	$1.13\ 10^{-9}$	$4.13\ 10^{-12}$	$1.64\ 10^{-14}$	$8.94\ 10^{-16}$	$3.02\ 10^{-14}$
This work	CO_2	H_2O	CO	OH	HCOOH
Model 1a	$2.33\ 10^{-7}$	$1.65\ 10^{-7}$	$1.70\ 10^{-4}$	$4.70\ 10^{-8}$	$4.94\ 10^{-10}$
Model 2a	$3.55\ 10^{-7}$	$4.43\ 10^{-8}$	$1.69\ 10^{-4}$	$6.00\ 10^{-10}$	$1.10\ 10^{-9}$
Model 3a	$2.18\ 10^{-7}$	$1.92\ 10^{-7}$	$1.70\ 10^{-4}$	$5.21\ 10^{-8}$	$3.14\ 10^{-10}$
This work	HCN	CH_2NH	$CH_2NH_2^+$	$CH_3NH_2^+$	$CH_3NH_3^+$
Model 1a	$1.53\ 10^{-9}$	$4.19\ 10^{-11}$	$1.04\ 10^{-13}$	$2.79\ 10^{-14}$	$2.32\ 10^{-13}$
Model 2a	$1.47\ 10^{-10}$	$7.14\ 10^{-12}$	$4.89\ 10^{-15}$	$3.73\ 10^{-16}$	$1.04\ 10^{-14}$
Model 3a	$1.36\ 10^{-9}$	$4.49\ 10^{-11}$	$1.35\ 10^{-13}$	$2.58\ 10^{-14}$	$2.52\ 10^{-13}$

Table 5.4: Equilibrium abundances with respect to hydrogen for the precursors of the Woon's mechanism. Adapted from Groyne (2023).

The equilibrium abundances values are quite consistent between both works, as can be seen in Table 5.4. However, there are some discrepancies, like in the case of carbon monoxide and the hydroxyl radical. The abundance of CO is slightly higher by almost an order of magnitude in this work, while OH is lower by a similar factor. This difference is likely due to the greater completeness of the gas-phase reaction network in ***Nautilus***, where both species participate in more than twice as many reactions compared to ***Astrochem***. That could also be related to variations in the kinetic parameters and related parametrization (for example, the main way to destroy CO is parametrized differently in both codes), as already discussed previously. It is not surprising that CO dominates, since it is the second most abundant molecule in the galaxy due to its high stability (and the high relative abundances of C and O). The case of formic acid deserves more comments. In the gas-phase network of ***Nautilus***, HCOOH is only involved in **one formation route**, while it was involved in two routes in the work of Groyne (2023). As in that work, some completeness issues may arise concerning this species, and that will have to be kept in mind. Moreover, even though it has a higher complexity than the other compounds, it is still found in an appreciable amount, which is beneficial with regard to Woon's mechanism.

Using model 2a, the results once again align well with those presented in Groyne (2023). However, a notable and somewhat unexpected difference arises in the relative abundances

of formic acid and the OH radical. Contrary to expectations—since OH is typically more abundant—the results show formic acid as the most prevalent species. This discrepancy likely stems from differences in the dominant reaction networks implemented in the two chemical codes. In the case of ***Nautilus***, the main formation pathway for OH under model 2a conditions is the reaction $O + HC_3O \longrightarrow OH + C_3O$, which is absent from ***Astrochem***. Although OH also participates in a greater number of destruction reactions in ***Nautilus***, its primary destruction pathway, $O + OH \longrightarrow H + O_2$, exhibits similar, but not equal, kinetic parameters in both models. As for formic acid, its main destruction route in ***Nautilus*** involves ion-neutral chemistry, and differences in reaction parametrization between the codes likely contribute to the observed variation. Furthermore, the higher density used in model 2a compared to model 1a favors the reactivity of transient radicals such as OH, leading to a more efficient depletion than for more stable species like HCOOH. Another discrepancy in the results arises when looking at the abundance of $CH_3NH_2^+$. Indeed, differences close to two orders of magnitude can be observed. As discussed in Groyne (2023), which is also valid in this case, this is a quite complex species and its completeness in the network is not really high. The results obtained here are therefore questionable.

For model 3a, the same curves as for model 1a are obtained, aligning once again on the conclusion of Groyne (2023).

5.2.4 Comparison to previous results and observational data

To conclude, we will compare the results obtained thanks to the ***Nautilus*** code with those of Groyne (2023) and results previously published in Prasad and Huntress (1980a,b). In order to complete this last step, model b proposed in Groyne (2023) has been used, which aims to mimic the conditions used in the two previously cited papers. The results from the different works are summarized in Table 5.5.

Our results match quite well those obtained both in Groyne (2023) and in Prasad and Huntress (1980a,b). The maximum deviation being limited to less than one order of magnitude. Since we are considering quite low complexity species, this is not unexpected, knowing that all the works are based on quite complete networks regarding those molecules. The exception arises when looking at the most complex species of this table, i.e. H_2CO^+, H_2COH^+ and $CH_2NH_2^+$, which have abundances well above those of Prasad and Huntress (1980a,b). This was already encountered in Groyne (2023), and was related to the much lower completeness of the network used in Prasad and Huntress (1980a,b) than the one from ***Astrochem***. This argument is also valid for this work, as we know that the completeness of the network from ***Nautilus*** is even higher than in ***Astrochem***. Regarding the comparison with observational data, one must first bear in mind that **in a real molecular cloud there is a crucial interplay between the gas-phase and solid-phase chemistry**. Therefore, perfectly matching results are not expected since a pure gas-phase model is used.

5.2.5 Conclusions from this comparison

As a first step in this work, we performed a detailed comparison with the results from Groyne (2023), focusing on the gas-phase precursors of glycine. The aim of this master thesis is to build upon that foundation by incorporating grain-surface and bulk-ice chemistry, thereby enabling a more realistic and complete modeling of molecular clouds and the complex chemistry occurring within them. At the end of this comparison, we

Species	Groyne (2023)	This work	Prasad and Huntress (1980a; 1980b)	Obs. data
H_2O	$1.11\ 10^{-7}$	$6.39\ 10^{-8}$	$5.04\ 10^{-6}$	$< 7\ 10^{-8}$ [a]
HCN	$7.62\ 10^{-11}$	$1.89\ 10^{-10}$	$8.01\ 10^{-10}$	$\sim 2\ 10^{-10}$ [b]
H_2CO	$3.15\ 10^{-10}$	$5.73\ 10^{-11}$	$9.93\ 10^{-10}$	$4 - 8\ 10^{-9}$ [c]
NH_3	$1.03\ 10^{-8}$	$9.73\ 10^{-9}$	$1.25\ 10^{-8}$	$\sim 10^{-8}, 2\ 10^{-8}$ [e]
CO	$7.11\ 10^{-5}$	$1.70\ 10^{-4}$	$1.44\ 10^{-4}$	$\sim 4\ 10^{-5}$ [f], $8\ 10^{-5}$ [g]
CO_2	$7.92\ 10^{-8}$	$1.92\ 10^{-7}$	$2.09\ 10^{-6}$	-
OH	$5.87\ 10^{-9}$	$1.54\ 10^{-9}$	$6.01\ 10^{-9}$	-
C^+	$2.46\ 10^{-11}$	$7.24\ 10^{-11}$	$2.39\ 10^{-11}$	-
NH_3^+	$4.53\ 10^{-13}$	$7.40\ 10^{-13}$	$8.15\ 10^{-13}$	-
H_2CO^+	$4.59\ 10^{-15}$	$1.12\ 10^{-14}$	$2.23\ 10^{-16}$	-
H_3CO^+	$2.29\ 10^{-13}$	$1.00\ 10^{-13}$	$6.23\ 10^{-16}$	-
CH_4N^+	$9.95\ 10^{-16}$	$1.51\ 10^{-14}$	$1.63\ 10^{-18}$	-

[a] Roberts and Herbst (2002).
[b] Gottlieb et al. (1975)
[c] Evans and Kutner (1976)
[d] Morris et al. (1973)
[e] Ohishi and Kaifu (1998)
[f] Liszt et al. (1974)
[g] Ohishi et al. (1992)

Table 5.5: Comparison of the precursor abundances that were studied in this work, Groyne (2023) and both Prasad and Huntress (1980a,b), with some observational data towards the Orion A molecular cloud **when available**. Adapted from Groyne (2023).

can conclude that the results of Groyne (2023) were successfully reproduced to a large extent. Those results were not unexpected because the scientific community largely agrees on the way to compute gas-phase chemical evolution. While some discrepancies were observed—particularly in the temporal evolution of molecular abundances—the equilibrium abundances we obtained were systematically similar. Although not all contributing reactions were identical, most of the key pathways for formation and destruction were consistent between the two studies. These differences are expected, given that ***Nautilus*** is not only a different code from ***Astrochem***, but also one that allows for a higher level of completeness and complexity. Interestingly, despite differences in the implementation, the reference kinetic parameters and their related parametrization as well as the ODE solvers used in both codes, the results remain remarkably consistent. As a result, many of the conclusions drawn in Groyne (2023) remain valid here as well. Thanks to this reproducibility, ***Nautilus*** will be used to perform a more comprehensive description of the chemistry in molecular clouds. The reader is referred to Appendix E for a summary of both similarities and discrepancies in the results from both codes.

The logical next step is to increase the model's complexity by including the chemistry occurring on dust grains. This is the focus of Chapter 6, where all glycine precursors are examined in greater detail.

Chapter 6

Three-phase chemical modeling of glycine precursors

In this chapter, we will revisit all the glycine precursors examined in Chapter 5, but this time within an extended model that includes solid-phase chemistry. Rather than relying solely on a gas-phase approach, we will now use a comprehensive 3-phase model that accounts for gas-phase reactions as well as grain-surface and bulk-ice processes to carry out a more complete study of glycine precursor formation.

6.1 Model modifications to include dust grains

6.1.1 Solid-phase astrochemical network

As we have seen in Chapter 4, when considering solid-phase reactions with the ***Nautilus*** code, a second astrochemical network (`grain_reactions.in` file) has to be considered. To analyze this network with care, the Python functions used for the comparison in Chapter 5 have been slightly modified.

A key observation when examining the solid-phase network is the **complete absence of charged species (both cations and anions) in surface reactions**. Only neutral species are considered. Moreover, the default values for the sticking coefficients of anions and cations are considered equal to 0, which means that **charged species do not accrete on the surface of dust grains**. The ***Nautilus*** documentation states that *"We do not consider ions on the surfaces because grains are usually negatively charged so that any cation produced on the surface would recombine quickly"*. Having a closer look at the astrochemical network `gas_reactions.in`, we can see that grains with a negative charge can be produced in only one way, which is the capture of free electrons. Although some neutralization processes through collisions (but not accretion) with cations are present, the production of negatively charged grains is characterized by such a high kinetic constant ($\sim 10^{-3}$) that a neutral grain would quickly capture a new free electron. One must understand that grain charging mechanisms are not simple processes, and are functions of various parameters such as the grain sizes, their composition, the ISM environment considered, the local radiation field strength, the temperature, and the electron number density. For instance, Draine and Sutin (1987) have shown that, assuming an MRN power law (cf. Section 2.2.2) extended down to a minimum grain size a_{min} of approximately

$3\mathring{A}$[1], **charged dust grains can carry a significant fraction of free electrons**[2] in cold clouds with very low fractional ionizations ($n_e/n_H < 4 \times 10^{-7}$). Consequently, in all reactions of the solid-phase network in ***Nautilus***, **dust grains are assumed to be negatively charged** and only neutral species are considered. As a result of this absence of cations on dust grains, surface processes analogous to gas-phase photo-ionization would occur at similar rates but ultimately yield the neutral products expected from electronic recombination rather than sustaining ionic species.

However, one may wonder about the origin of these considerations. Concerning the anions, assuming negatively charged dust grains, this can simply be explained by the classic Coulomb interaction, causing negative species to just be repelled by the grains. For the cations, it deserves a more in depth exploration. Calling again the Coulomb interaction, positively charged species should on the contrary be attracted by the grain, which should reinforce the sticking coefficient, making it very close to 1. However, as assumed in the ***Nautilus*** code, the sticking coefficient of ions, both anionic or cationic, is equal to 0. This can be arguably explained by the following considerations:

1. A cationic adsorption reaction such has $C^+ + \text{grain}^- \longrightarrow JC + \text{grain}$ has both a high speed and very high exothermic nature. This energy excess is principally found in form of translational energy rather than in the ro-vibrational levels, which are discrete and limited. Moreover, through momentum conservation, the initial momentum of the cation will be conserved due to the fact that the grain is way more massive than the cation. Therefore, such reactions would be dissociative, and cations would not stay on the grain. One may nonetheless wonder if the grain could not take away the energy excess as in the case of classical surface reactions. This is unfortunately not that simple, since in that case the grain does not have a third body passive role. Some studies (Fredon et al. 2021a,b, Cuppen et al. 2022) have shown that the dissipation of kinetic energy from translational towards ro-vibrational levels of grains is quite slow and may be even slower than the recombination kinetics.

2. Adsorbed species are considered to be physisorbed in the implementation of ***Nautilus***. No chemical bond is thus created[3]. This weak interaction between the species and the grain allows the situation to be simply parametrized by sticking coefficients. However, when considering the adsorption of a cation on a negatively charged grain, the interaction is much stronger (notably, through Coulomb interaction at long range). This simple treatment would then be less justified than for neutral species.

3. Cations are very reactive species that might directly react with the ice and its components (water, ammonia, methane, ...). Those interactions could then potentially lead to chemisorption, which would enter in contradiction with the adsorption model intrinsically based on physisorption.

What we see through those proposed hypotheses is that, in light of the direct desorption caused by the high exothermic nature of such processes, the approximation of considering only neutral species in solid-phase is valid in first approximation.

[1] At the time of the publication of Draine and Sutin (1987), little was known about the real size distribution and abundances of very small grains. This minimum size was chosen for the sake of illustration, acknowledging that interstellar clouds are likely to have higher abundances of very small grains.

[2] To be perfectly correct, that is not so easy. Studies like the one performed by Ivlev et al. (2015) have shown that cosmic rays may have an impact on grain charging in dense molecular clouds.

[3] ***Nautilus*** and other astrochemical codes do not consider **direct chemisorption**.

Important remark:
The ***Nautilus*** solid-phase network involves 763 species and 4837 reactions. But something important to emphasize is that within that network (`grain_reactions.in`), a same species can be considered in three phases. It can either be found in gas-phase, adsorbed on the surface and within the icy mantle. Therefore, when it is said that 763 species are involved, several species are in fact counted three times. **In both solid phases,** 255 **unique species (all found also in gas-phase) have to be considered**. In agreement with the conventions adopted in ***Nautilus***, species adsorbed on the grain surface will be affected by the letter "J" in front of the molecule formula and species within the mantle with the letter "K". Neither of those means that the species is in gas-phase.

On a final note, all the **neutral precursors** studied in the previous chapter are also present in the solid-phase network, both in the mantle and on the surface. That will therefore allow us to perform our 3-phase analysis of glycine precursor formation pathways, which will be described in the following sections.

6.1.2 Parameters from *Nautilus*

It is in this chapter that the full capacity of ***Nautilus*** will be used based on the conditions summarized in Table 6.1.

Gas	n_H (cm^{-3})	T_{gas} (K)	A_v (mag)	ξ (s^{-1})
Model 1a	10^4	10	20	8.79 10^{-18}
Model 2a	10^6	10	20	8.79 10^{-18}
Model 3a	10^4	20	20	8.79 10^{-18}
Grain	m_{dust}/m_{gas}	T_{dust} (K)	radius (cm)	$S_{neutral}$
Model 1a	1/100	10	10^{-5}	1
Model 2a	1/100	10	10^{-5}	1
Model 3a	1/100	20	10^{-5}	1

Table 6.1: Summary of the three models that will be considered in this chapter to perform a study of glycine formation both in gas-phase and solid-phase. Those models are adapted from Groyne (2023). Note that, as before, no temporal evolution will be considered.

The `parameters.in` file had of course to be modified. First of all, the switch `is_3_phase` had to be set to 1, in order to allow the model to **take into account, the gas-phase and grain surface reactions, along with the bulk-ice component**. Moreover, by putting the switch `is_grain_reactions` to 1, the existence of dust grains as well as the chemical reactions taking place on them are acknowledged. In terms of grain parameters, the initial temperature was kept fixed throughout the simulations (see Table 6.1), at the same value as the gas component (`grain_temperature` = `gas`). The quantity of dust with respect to the gaseous component, described in terms of a ratio (`dust_to_grain_mass_ratio`), was set using the usual considered value for the galactic dust content, i.e. 1/100. Moreover, the sticking coefficient S is considered to be equal to 1 for all the neutral species, which

means that if a gas-phase species encounters a dust grain, it will be adsorbed on it. For the charged species, it is equal to zero as discussed above. The other parameters, described in Appendix B, were kept to their default values.

For the following analyses, we use the models defined by Groyne (2023) (see Table 5.1) to maintain consistency with that previous work, though they are slightly adapted as shown in Table 6.1. In addition, previous considerations will also still be valid. Hydrogen is still entirely found in its molecular form, and we keep considering a **homogeneous, steady in time molecular cloud**. However, the cosmic-ray ionization rate is now computed from an extinction-based formula from Wakelam et al. (2021) thanks to the switch `is_compute_zeta` (see value in Table 6.1). Indeed, the cosmic-ray ionization rate has been observed to depend on the extinction of the cloud for $A_v > 0.5$ mag (Neufeld and Wolfire, 2017). In the work performed in this chapter, we thus have an extended set of parameters to take into account. Concerning the energy barriers and desorption energy, values were not modified (cf. `surface_parameters.in` or default values).

6.2 Results from the *Nautilus* model

We will now begin the 3-phase study of the precursors entering in glycine formation, by considering the main pathways described in details in Chapter 3. The Strecker-like synthesis (neutral and activated) will be addressed first, before an in depth exploration of the radical-radical pathway presented in Woon (2002) as well as its variants.

6.2.1 Strecker-like mechanism - Neutral pathway

For the study of the Strecker-like synthesis, the modified model 1a (Table 6.1) has first been used. In Figure 6.1, one may see the temporal evolution of the abundances of the four previous glycine precursors (H_2O, NH_3, H_2CO and HCN) in each phase. Having a look at Figure E.1, one clearly notices the similarity between the curve obtained for the gas-phase and the previous one from the pure gas-phase model, the more affected curve being that of formaldehyde. Moreover, the final abundances (in gas-phase) are similar to the previous ones, except once again for H_2CO whose final abundance raises by 2 orders of magnitude with respect to the pure gas-phase. The curves of the three other molecules have only been subject to minor changes. The dominance of water and ammonia in the solid-phase for the last 10 million years is expected, knowing that they are among the major species composing icy mantles (cf. Chapter 2). Whereas H_2CO is more abundant in gas-phase, it does not seem to be abundant in ices regarding the other molecules of interest. In order to study in more detail the abundance evolutions, we will now (as we did in Chapter 5) look at the formation and destruction routes of each molecule.

Starting with H_2O, we notice in Figure 6.2 that most of the dominant gas-phase chemistry is similar to the one of the pure gas-phase model. The same dominant formation routes in the gas-phase are found at the same time as before, whereas this is a bit different for the destruction pathways. The destruction until 10^4 years is still dominated by reaction with C^+, but afterwards the dominance of the reaction involving HCO^+, followed by the one with $H_3{}^+$, are this time clear. New formation (such as the production on the surface and direct desorption) and destruction (like accretion on the surface) routes have appeared, but with small contributions. For the solid-phase chemistry, only one reaction dominates in each case (with fractions higher than 99%). The main formation route of

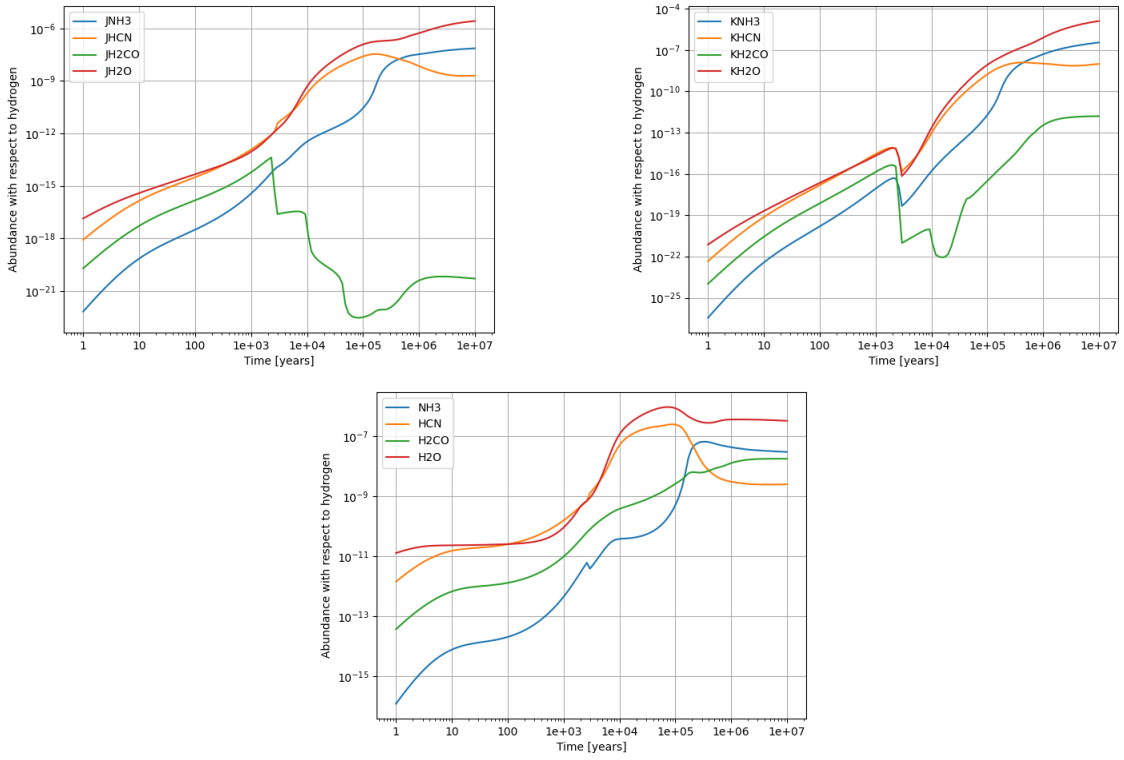

Figure 6.1: Temporal evolution of glycine precursors from model 1a via neutral Strecker-like synthesis, shown separately by phase: Surface (top left), Mantle (top right), Gas (bottom).

surface water JH_2O is a swapping with one mantle water molecule KH_2O throughout the simulation and its main destruction pathway is a swapping from the surface to the mantle. For mantle water KH_2O, it is the exact reverse case. We thus see that **water in the solid-phase seems to stay preferentially on the grain**.

For HCN, the dominant gas-phase formation and destruction pathways closely resemble those from Chapter 5, though some differences are worth highlighting. In terms of formation, the reaction $HCNH^+ + e^- \longrightarrow H + HCN$ becomes dominant earlier in the simulation than it does in the pure gas-phase model. Additionally, new surface reactions—such as $JH + JCN \longrightarrow HCN$, i.e. reaction on the grain followed by direct chemical desorption—have emerged. Regarding destruction, the most notable change is the diminished role of the reaction with C^+ at the end of the simulation. Instead, the final destruction is now driven mainly by reactions with HCO^+, followed by those with $H_3{}^+$ and H_3O^+. As for solid-phase chemistry, the relevant reactions are identical to those observed for the water molecule.

It is important to note that, although the gas-phase abundances remain comparable, the abundances of the isomeric couple HCN/HNC on the surface and in the mantle are less similar (Figure 6.4). We have close evolutions during the first 10^3 years, then deviations are observed. At the end of the simulation, there is maximum 1 order of magnitude of difference for the surface and mantle abundances of HCN and HNC. Even if those differences are not huge, they are nevertheless more significant than in the framework of

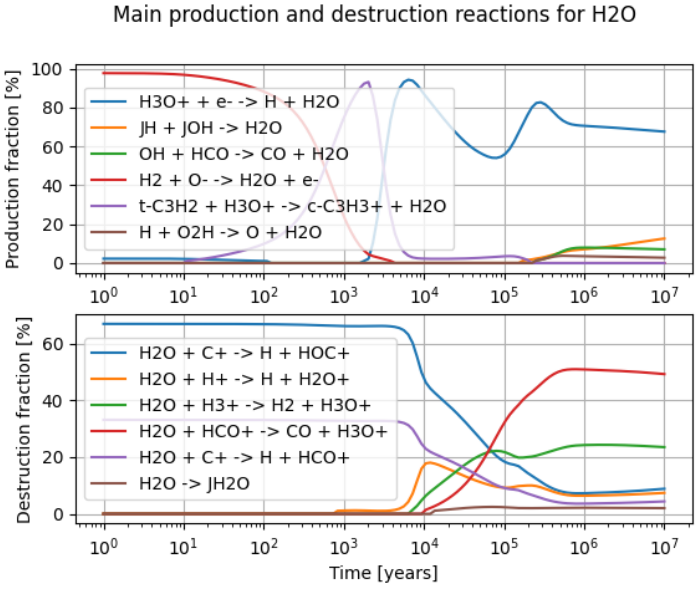

Figure 6.2: Main formation/destruction routes obtained with model 1a for H_2O.

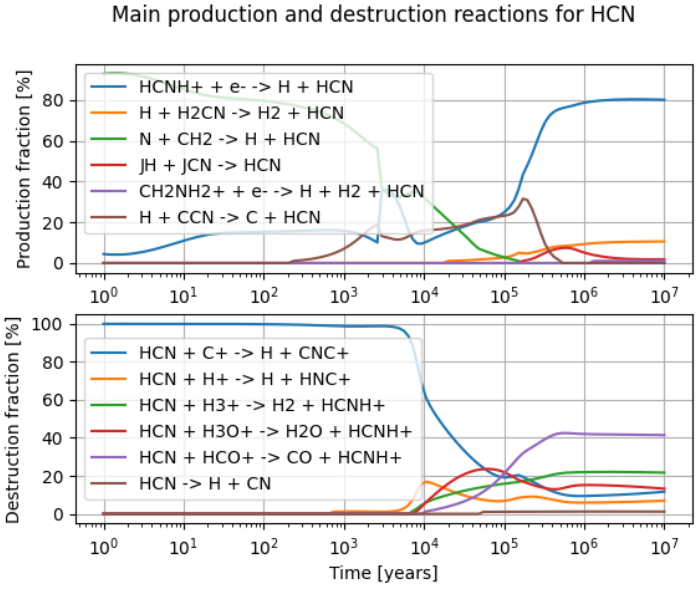

Figure 6.3: Main formation/destruction routes obtained with model 1a for HCN.

a pure gas-phase model. However, the equivalence between both abundances will still be assumed in each phase.

With regard to the ammonia molecule, the gas-phase formation/destruction routes (Figure 6.5) are again extremely similar to those presented in Figure E.6. A new surface chemistry-related formation reaction appears ($JH + JNH_2 \longrightarrow NH_3$), but with only a small contribution at the end of the simulation. For the destruction routes, what is changing is the negligible contribution of C^+ at the end of the simulation, where, as in the case of HCN, reactions with HCO^+, $H_3{}^+$ and H_3O^+ dominate. For solid-phase chemistry, swapping reactions between the surface and the mantle once again dominate.

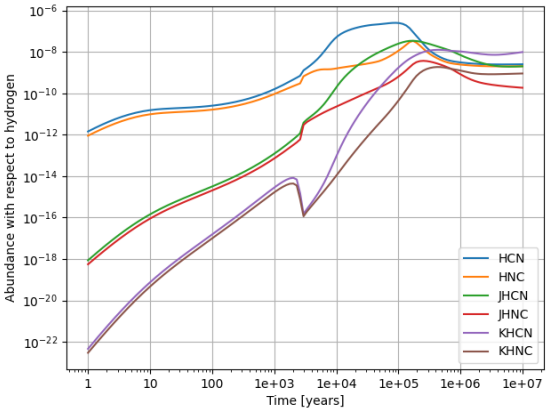

Figure 6.4: Temporal evolution of the abundances in the 3 phases of HCN and HNC.

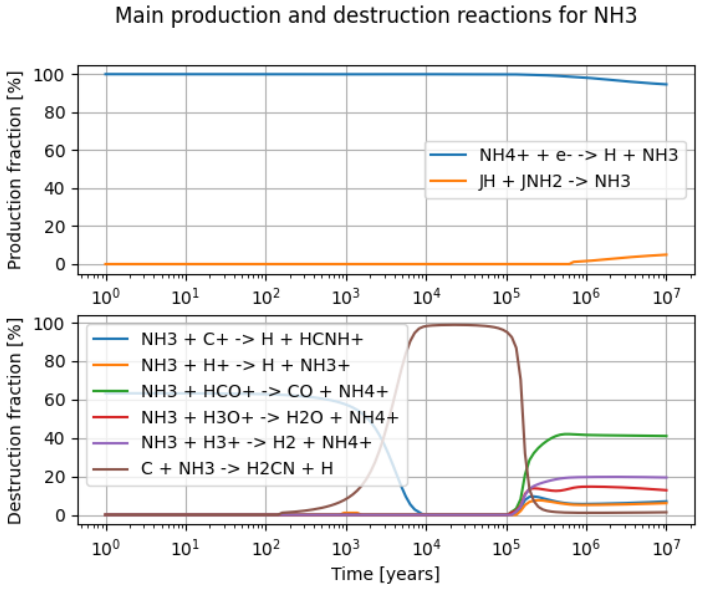

Figure 6.5: Main formation/destruction routes obtained with model 1a for NH_3.

One may wonder about the clear dominance of swapping reactions in the simulation. Such reactions involve an exchange of species between the surface phase (the first two monolayers) and the mantle phase. But in the case of the rate-equation approach implemented in ***Nautilus***, the code has no consideration for the fact that species in the mantle have to be found at the interface between the surface and the mantle for such reactions to take place (rate-equation approach threats this as an average process). This constitutes, in fact, another limitation of the rate-equation approach and the ***Nautilus*** model. As emphasized in Section 4.3, other modeling approaches as microscopic KMC methods allow for fully taking into account positioning considerations as well as the layering of icy mantles. Unfortunately, as previously discussed, such an approach would require much more CPU power than the one at our disposal. Following this discussion, one may wonder about the origin and physical justification of the dominance of those swapping reactions. First of all, if the code does not consider the depth of the species in the mantle for swapping to hap-

pen, the mobility of deeply buried species will be overvalued. This is therefore expected to influence non-negligibly the simulation results, and the impact is expected to be greater along the time evolution of our cloud in static physical conditions. Indeed, the mantle is modeled as a homogeneous phase with no internal structure or spatial dimension. All species in the bulk are treated as physically equivalent, as if uniformly distributed in a hypothetical collection from which molecules can be randomly selected for a swapping event, regardless of whether they are near the surface interface or deeply embedded. This is analogous to representing the mantle as a bag of marbles where each marble has equal access to the surface, despite the physical unlikelihood of such behavior. Similarly, the surface is also represented as a constant-sized bag of marbles once the ice and its top two layers are formed. In contrast to the surface, however, the number of species in the mantle increases as the ice grows, especially under the low-temperature static conditions considered in this study. Consequently, as time evolves, the mantle becomes increasingly populated, and the RE assumption of equal access leads to a growing bias - overestimating the frequency of swapping processes. This likely explains the dominance of such reactions toward the end of the simulations for certain species. This dominance, however, is non-physical, resulting from a modeling artifact rather than a true chemical behavior. It suggests an **unrealistic over-mixing of the ice**, the implications of which cannot be reliably quantified without resorting to a more physically detailed micro-physical model - an approach beyond the scope and computational capacity of this work.

We still have one molecule to study, that is, formaldehyde, for which we might suspect some effects of the solid phase on the increase in the final abundance in the gas phase (Table 6.2). For the gaseous chemistry in Figure 6.6, nothing seems to have changed much compared to the pure gas phase. In terms of formation routes, the reaction $O + CH_3 \longrightarrow H + H_2CO$ still dominates completely. A new non-negligible surface reaction followed by direct chemical desorption ($JH + JHCO \longrightarrow H_2CO$) have appeared at the end, that may be partially responsible for the density increase observed in gas-phase compared to the results in Chapter 5. The destruction routes are very similar to the ones of ammonia, though a new reaction involving OH becomes as dominant as the one involving H_3^+ at the end. The early destruction chemistry is on the other end still dominated by the reaction with C^+. *What about the solid-phase chemistry*? Figure 6.7 reveals a notable contrast with the three previously discussed molecules, for which gas–solid interactions played only a minor role. In the case of H_2CO, such interactions are much more significant. For the formation routes of surface formaldehyde, we have an alternation between adsorption and swapping with the mantle during the simulation, with swapping being dominant at the end. It is even more interesting for the destruction, since one can see that, after 10^3 years, the main sink terms of JH_2CO are $JH + JH_2CO \longrightarrow HCO + H_2$ and $JH + JH_2CO \longrightarrow CH_3O$. In each case, we have a surface reaction and direct chemical desorption, rejecting therefore the products of the reaction in gas-phase. For the mantle population, the formation is dominated after 10^4 years by the reaction $KH + KHCO \longrightarrow KH_2CO$, and after more or less the same time the destruction is dominated with an equal destruction fraction by the two same reactions as for the surface formaldehyde. In the case of this simple organic molecule, **the solid-phase chemistry seems thus to be way more active than for the three previous compounds**.

Returning to the evolution of the abundance of H_2CO, we can now try to explain what is happening. The decrease of surface/mantle formaldehyde after 10^3 years results probably from its destruction and the subsequent release in gas-phase of the two main products,

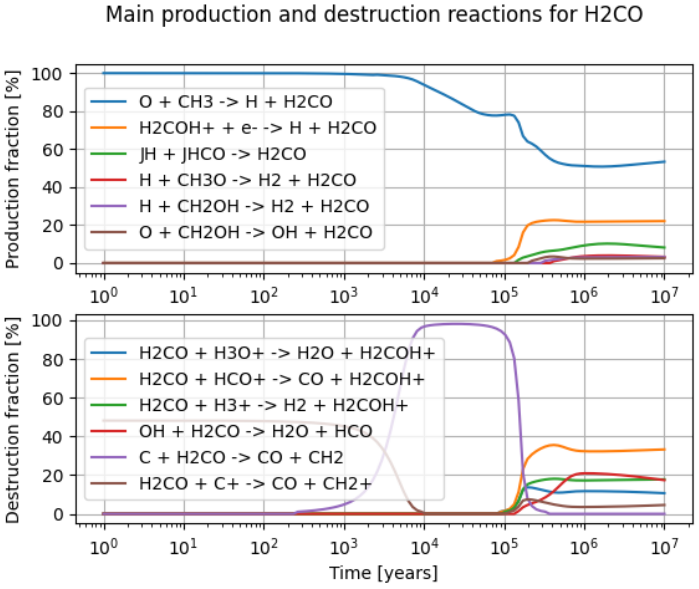

Figure 6.6: Main formation/destruction routes obtained with model 1a for H_2CO.

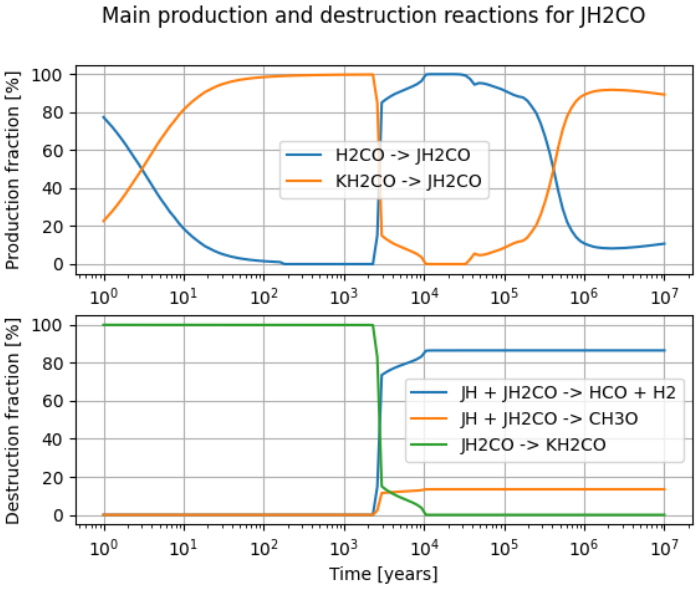

Figure 6.7: Main formation/destruction routes obtained with model 1a for JH_2CO.

i.e. HCO and CH_3O. The increase in gas-phase abundance in comparison with the pure gas-phase model may then be explained by the fact that more dominant reactions have to be considered, in which some species originate mainly from the dust surface like CH_2OH, isomer of CH_3O. The main destruction path after 10^5 years of that species is the reaction $H + CH_2OH \longrightarrow CH_3 + OH$, the product of which may then be involved in the formation of gas-phase formaldehyde. In that case, there is a bigger interplay between the phases.

Important remark:

There **does not seem to be any real global chemical equilibrium for any phase**, unless maybe at the very end. In fact, no perfect horizontal line can be observed. This may probably be related to the fact that, in contrast to a pure gas-phase model, the abundance evolutions of the species are linked to what happens on dust grains. Knowing that reactions on and within the grains are usually slower (limited by diffusion) than in gas-phase, especially at such a low temperature, the chemistry will be slower and **equilibrium may not be reached within the lifetime of the cloud**. As will be seen throughout the remainder of the chapter, **everything will depend on the species considered**.

Now that model 1a has been studied in detail, let us use model 2a and see if the arguments that were used in the context of the pure gas-phase model are still valid now. The evolution of the abundances is reproduced in Figure 6.8.

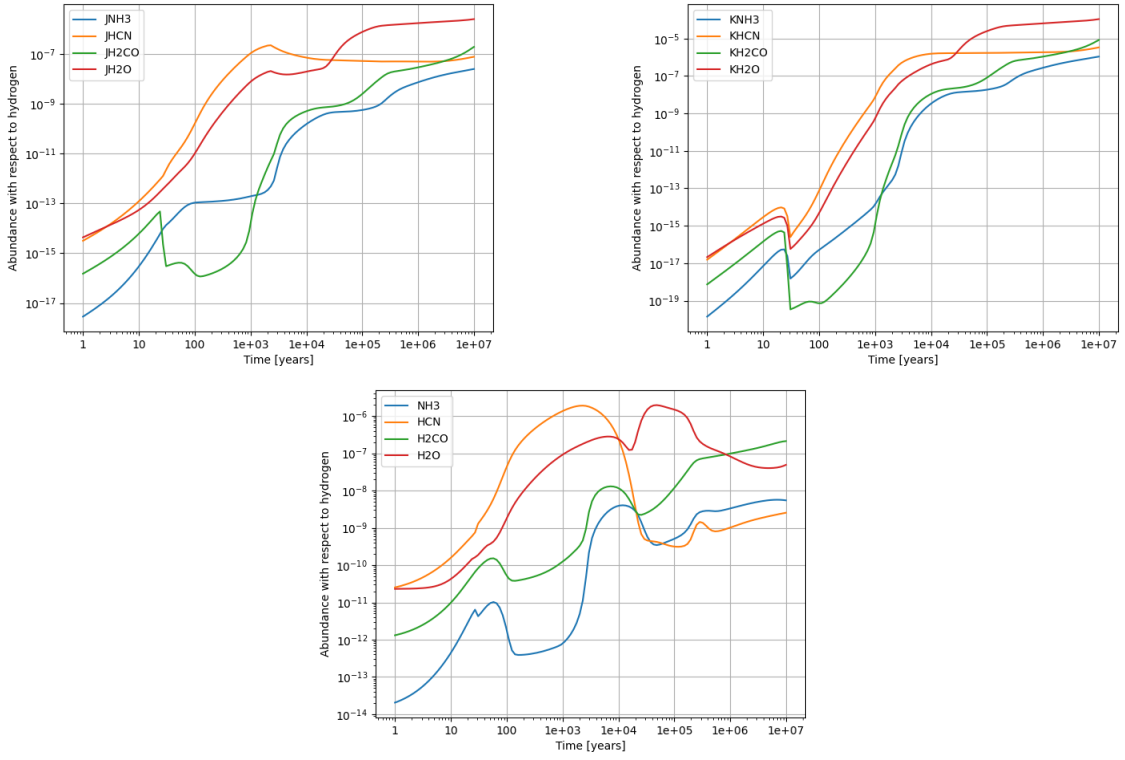

Figure 6.8: Temporal evolution of glycine precursors from model 2a via neutral Strecker-like synthesis, shown separately by phase: Surface (top left), Mantle (top right), Gas (bottom).

The curves here are clearly different from those obtained with model 1a (Figure 6.1). Some similarities still exist, but what has been said for the case of the pure gas-phase model (i.e. a rise in density will not change the gas-phase abundances) is no longer valid here for the solid-phases. Indeed, one may see in Table 6.2 that the abundances in gas-phase for the two models are pretty much the same, except for some variations limited to the order of magnitude. Abundances on the surface have also remained at similar levels,

with the exception of H_2CO, whose fraction has increased dramatically. For the mantle, the abundances of H_2O and NH_3 did not change much, whereas those of hydrogen cyanide and formaldehyde have increased significantly. Since model 2a considers an increase in density, we know from Chapter 2 that **accretion should be favored**. In order to understand the chemistry at work, let us have a look at the formation and destruction pathways.

First, the solid-phase chemistry of H_2O has not been modified. The swapping reactions from the surface to the mantle and vice versa are still completely dominant. By comparing Figures 6.9 and 6.2, it can be seen that the formation chemistry in gas-phase has been affected by the increase in density. At the end of the simulation, it is now the reaction $H_2CO + H_3O^+ \longrightarrow H_2O + H_2COH^+$ that dominates, followed by $OH + H_2CO \longrightarrow H_2O +$ HCO and $H_3O^+ + e^- \longrightarrow H + H_2O$. This can be explained by the huge increase in the abundance of formaldehyde, which will be involved in more reactions. The destruction chemistry has also changed. We now have a **clear dominance of the adsorption of water on the dust surface between** 100 **and** 10^5 **years**. Even afterward, it remains the second dominant process after destruction through the reaction with H_3^+. However, this change in the chemistry at work does not seem to strongly affect the final water abundance, although it could explain the small decrease in the abundance of gaseous water.

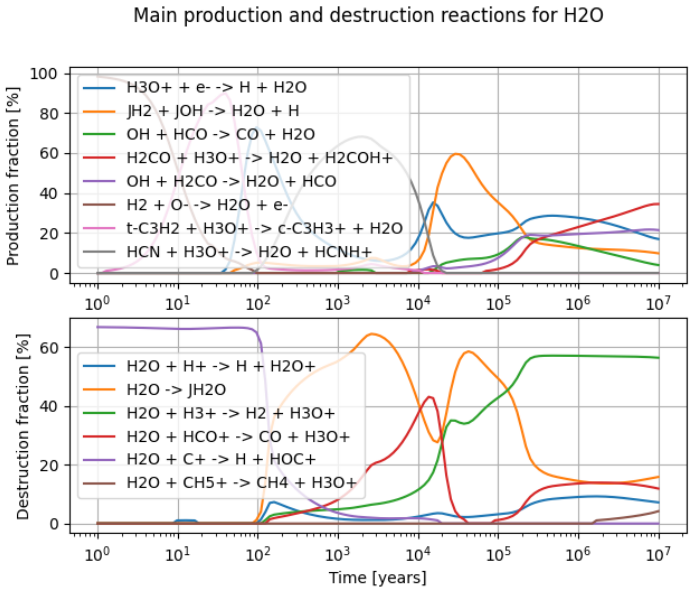

Figure 6.9: Main formation/destruction routes obtained with model 2a for H_2O.

In the case of HCN in Figure 6.10, we also observe some differences. Although it is still the dominant formation route during most of the simulation, the production fraction by dissociative electronic recombination of $HCNH^+$ is surpassed at the end of the simulation by the reaction $H_2CO + HCNH^+ \longrightarrow HCN + H_2COH^+$. The third reaction which is of importance is, as before, the surface reaction $JH_2 + JCN \longrightarrow HCN + H$. In terms of destruction chemistry, only the late chemistry has been subject to some changes. What we observe is that, in the end, the reaction involving H_3^+ is completely dominant. The other dominant processes in the end are adsorption on the surface and destruction through reactions with H^+ and HCO^+. Once again, the solid-phase chemistry has not been modified by the increase in density. The rise in solid-phase abundances might then be related

to the increase in formaldehyde, the newly formed HCN would then simply have to be adsorbed on the surface, before being transferred to the mantles by swapping reactions.

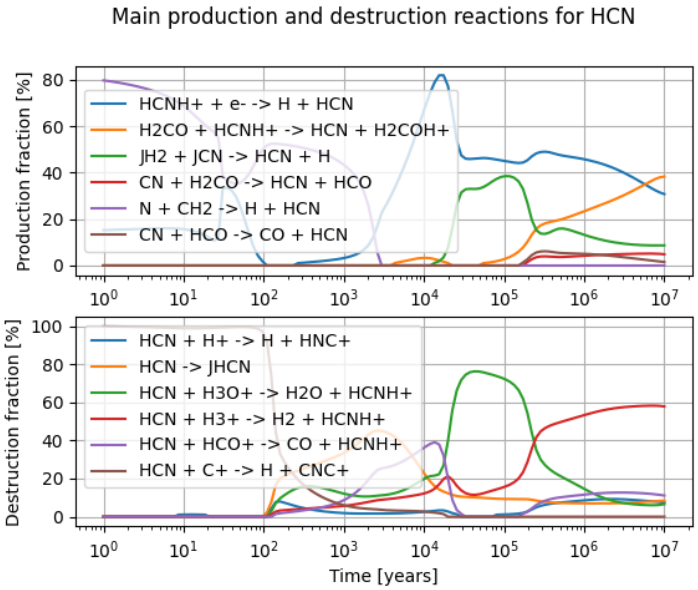

Figure 6.10: Main formation/destruction routes obtained with model 2a for HCN.

For the ammonia molecule (Figure 6.11), we observe the same formation chemistry as in Figure 6.5. For destruction chemistry, some similarities to hydrogen cyanide may be observed. Indeed, we again observe the rise of the dominance of the destruction reaction involving H_3^+. After that, it is the reaction involving H_2COH^+ that dominates followed closely by adsorption on the grain. No changes in the solid-phase chemistry were observed.

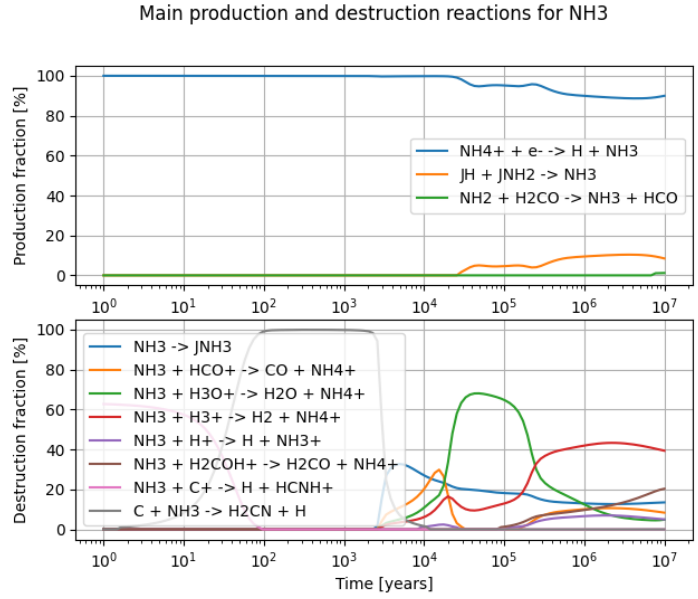

Figure 6.11: Main formation/destruction routes obtained with model 2a for NH_3.

Finally, let us study the formaldehyde routes illustrated in Figure 6.12. In that case,

the chemistry was significantly affected by the increase in density. First, the formation after 10^4 years is now completely dominated by the surface reaction $JH + JHCO \longrightarrow H_2CO$. That may be related to the dramatic increase of CO on dust surfaces (therefore, of its hydrogenated form), discussed later in this chapter. The destruction caused by the reaction with C^+ at the beginning has now disappeared. In fact, as for the previous ones, the displacement towards the left of the curves is observed, and the reaction involving atomic carbon begins now much earlier. In addition, the previously dominant reaction, that is, the one involving HCO^+, drops now at the end to be surpassed by the reaction involving $H_3{}^+$. Moreover, adsorption on the surface is now the third dominant destruction route, after reactions with HCO^+, at the end of the simulation, while it did not even appear before. Turning to the solid-phase chemistry, it is notable that the reactions involving surface species are now almost entirely dominated by swapping processes; other surface reactions have minimal influence, except around 100 years. In light of the earlier discussion regarding the increasing bias introduced by the rate-equation treatment of swapping reactions, a rise in density - as in model 2a - would accelerate the growth of the icy mantle, thereby exacerbating this bias. The rise in abundances in both solid phases may therefore be directly linked to the enhanced efficiency of adsorption under higher density conditions.

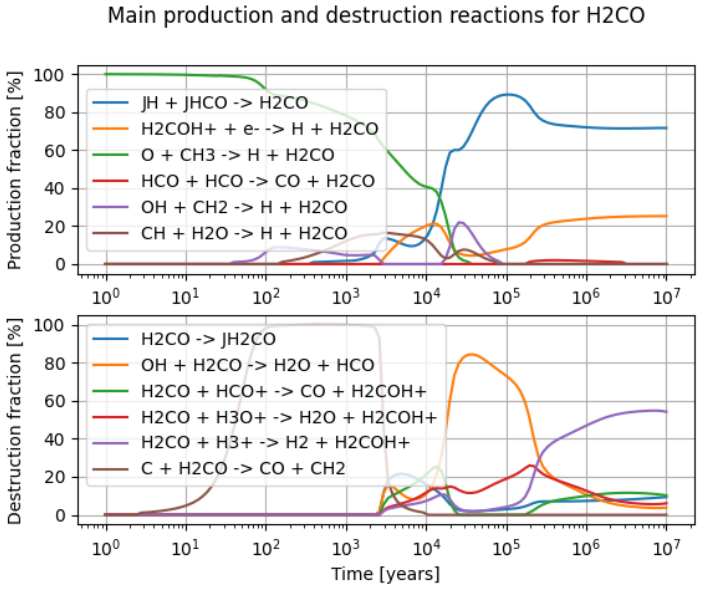

Figure 6.12: Main formation/destruction routes obtained with model 2a for H_2CO.

In conclusion, the results from model 2a show that **not all species have been affected in the same way by the density increase**. Indeed, while the abundances of water and ammonia did not change by more than one order of magnitude, formaldehyde has seen its abundance in both solid phases increase significantly allowing also to increase the HCN abundance in the solid-phase. As will be seen when discussing the Woon's mechanism, at high densities CO, direct precursor to HCO, tends to condense significantly on dust grains forming the so-called apolar layer, which will allow to increase significantly the production of formaldehyde. Moreover, we have seen that for each molecule in its gaseous state, the destruction fraction through adsorption has increased significantly which might probably explain the abundance increase in the surface phase, but also in the mantle phase knowing that swapping reactions between the surface and the mantle are completely domi-

nating. Therefore, we see that simple adsorption is not the answer to everything, and that one has to consider the specificities of each molecule before drawing any hasty conclusion.

Finally, the neutral Strecker-like synthesis precursors will be studied by means of model 3a. Table 6.2 shows that the final abundances have remained almost at values similar to those of model 1a, the deviations being kept below one order of magnitude, with the exception of surface formaldehyde and mantle water. As discussed in the next subsection about the Woon's mechanism, we will see that the abundance of solid-phase CO has reached a quite high value compared to model 1a, probably explaining the important difference in the abundances of surface formaldehyde between models 1a and 3a. In the same section, we will also see that the decrease in the abundance of mantle water might be related to the fact that less OH will be affected to its formation. Moreover, the evolutionary curves in Figure 6.13 and Figure 6.1 look quite similar (except again for surface formaldehyde and mantle water). We find clear similarities with what has been done in the case of the pure gas-phase model for the gas-phase, but **for some species** the solid phases seem to have been more affected by the temperature increase.

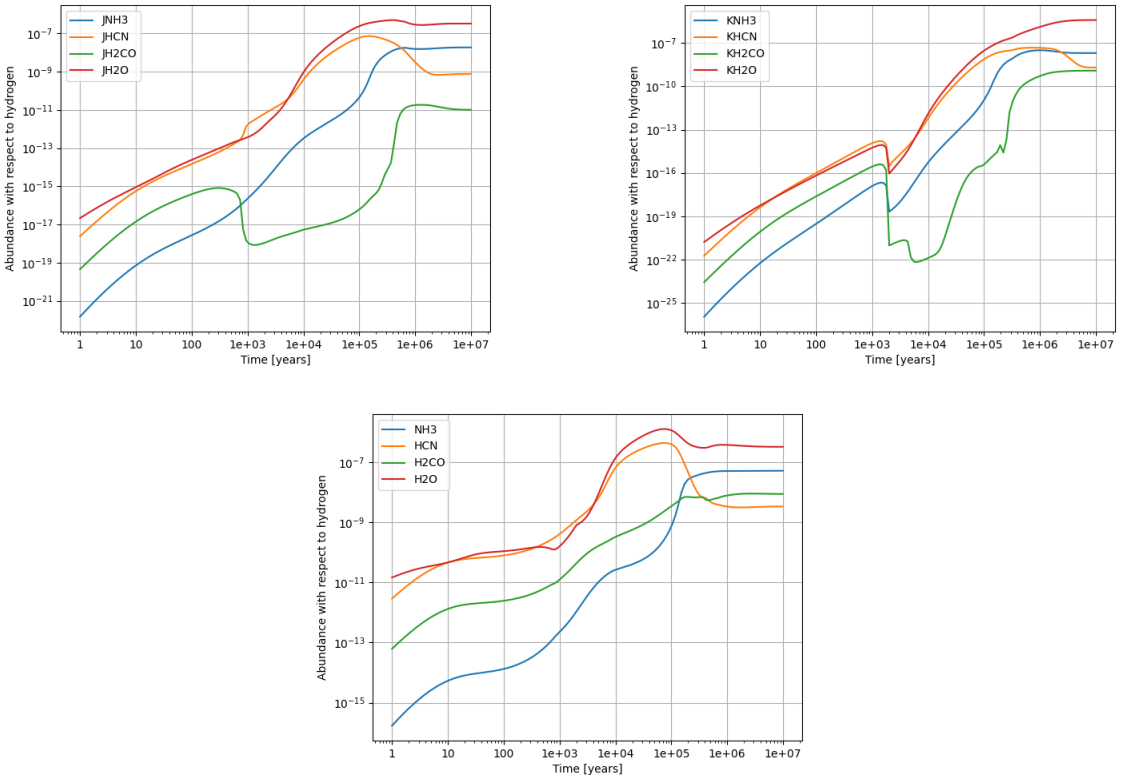

Figure 6.13: Temporal evolution of glycine precursors from model 3a via neutral Strecker-like synthesis, shown separately by phase: Surface (top left), Mantle (top right), Gas (bottom).

It is still interesting to consider the formation and destruction routes of the molecules, notably to try to explain what is happening with formaldehyde. We notice that the same dominant reactions as model 1a have to be considered for all phases, although some minor changes can be noticed in the gas phase. Therefore, despite slight changes in the fractions of the formation and destruction routes of the precursors, the chemistry between model 1a

and 3a is closely similar. For H_2CO, this is no longer the case. Although destruction has not been subject to significant changes, formation is now completely dominated by surface reaction $JH + JHCO \longrightarrow H_2CO$, hence the previous link regarding the increase in surface CO. Moreover, the solid-phase chemistry has also been affected, since now swapping reactions dominate, except between 10^3 and 3×10^5 years for the surface population where the previous reactions from model 1a dominate. In contrast to a pure gas-phase model, the solid-phase chemistry can thus be affected by such a slight increase in temperature. Indeed, in the case of surface formaldehyde, we see that the previously cited reaction has been activated, though the amount of surface atomic hydrogen has decreased significantly, hydrogen being a weakly bound species. The case of mantle water is also interesting because it has seen its abundance decrease significantly by two orders of magnitude. As will be seen later, this can partially be explained by the changing chemistry of the OH radical.

Gas-phase	H_2O	HCN	NH_3	H_2CO
Model 1a	$3.30\ 10^{-7}$	$2.53\ 10^{-9}$	$3.04\ 10^{-8}$	$1.79\ 10^{-8}$
Model 2a	$4.92\ 10^{-8}$	$2.55\ 10^{-9}$	$5.48\ 10^{-9}$	$2.13\ 10^{-7}$
Model 3a	$3.30\ 10^{-7}$	$3.39\ 10^{-9}$	$5.25\ 10^{-8}$	$8.87\ 10^{-9}$
Surface	JH_2O	JHCN	JNH_3	JH_2CO
Model 1a	$2.62\ 10^{-6}$	$2.00\ 10^{-9}$	$7.25\ 10^{-8}$	$5.17\ 10^{-21}$
Model 2a	$2.46\ 10^{-6}$	$7.61\ 10^{-8}$	$2.46\ 10^{-8}$	$1.90\ 10^{-7}$
Model 3a	$3.25\ 10^{-7}$	$7.50\ 10^{-10}$	$1.85\ 10^{-8}$	$1.01\ 10^{-11}$
Mantle	KH_2O	KHCN	KNH_3	KH_2CO
Model 1a	$1.28\ 10^{-5}$	$9.80\ 10^{-9}$	$3.55\ 10^{-7}$	$1.58\ 10^{-12}$
Model 2a	$1.09\ 10^{-4}$	$3.38\ 10^{-6}$	$1.09\ 10^{-6}$	$8.43\ 10^{-6}$
Model 3a	$7.63\ 10^{-7}$	$1.76\ 10^{-9}$	$4.34\ 10^{-8}$	$2.36\ 10^{-11}$

Table 6.2: Final abundances with respect to hydrogen of the four precursors studied in the framework of the Strecker-like neutral mechanism for the three phases.

6.2.2 Strecker-like mechanism - Activated pathway

Now that we have explored the neutral Strecker-like precursors, let us study the activated ones. Before going further, let us recall what has been said in Section 6.1. Cations, such as those used in the activated Strecker-like mechanism, are not included in solid-phase reactions. Nevertheless, it is interesting to study whether including the surface and mantle chemistry has an impact on the gas-phase chemistry or not.

We will begin this study within the framework of model 1a, as reproduced in Figure 6.14. Having a look at Table 6.3, and comparing with the results in Table 5.3, we notice that the final abundances are not the same. Indeed, the abundances of H_2COH^+ and H_2CO^+ have increased significantly compared to the pure gas-phase model, while the final abundance of $NH_3{}^+$ remains at a similar value. In order to understand this abundance

increase, one may be interested in looking at the main processes of formation and destruction of those species.

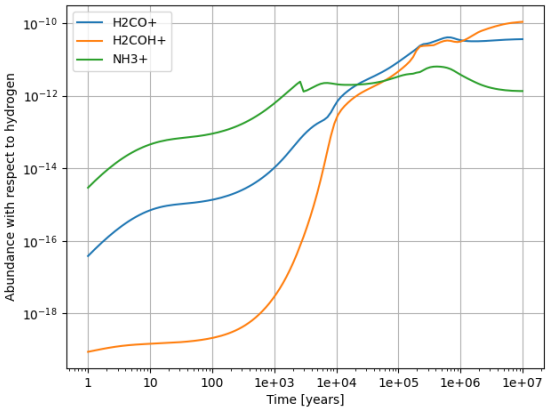

Figure 6.14: Temporal evolution of glycine precursors from model 1a via activated Strecker-like synthesis, **only in the gas-phase**.

Concerning protonated formaldehyde, we see in Figure 6.15 that its 3 main formation routes involve neutral formaldehyde. As we have seen in the previous subsection when analyzing the neutral Strecker-like mechanism, the gas-phase abundance of formaldehyde has increased by two orders of magnitude compared with the pure gas-phase model. Thus, if more formaldehyde is available in gas-phase, more of it may be involved in reactions with H_3O^+, H_3^+ or HCO^+ to produce its protonated form.

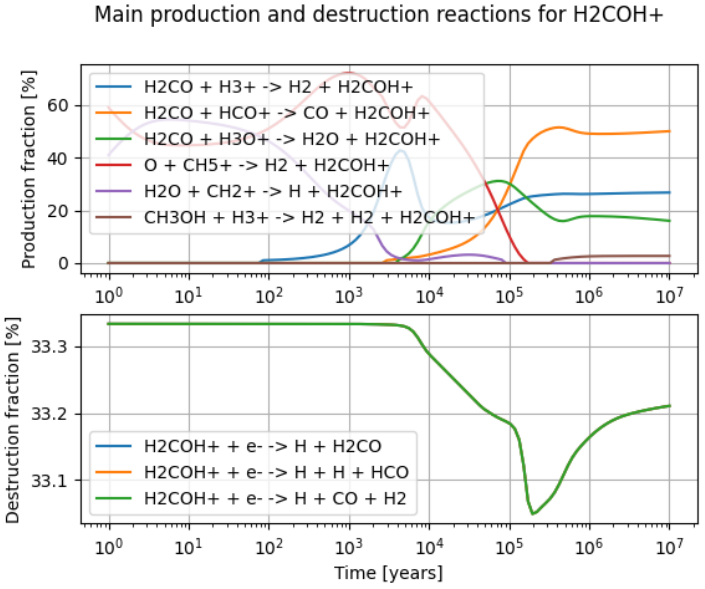

Figure 6.15: Main formation/destruction routes obtained with model 1a for H_2COH^+.

Concerning cationic formaldehyde, it is less direct. Having a look at its main formation and destruction routes (Figure 6.16), one may see that it is mainly produced through reaction involving HCO with HCO^+ or H_3^+. Therefore, it was necessary to go a bit deeper

and look at the abundance as well as the formation/destruction routes of HCO. The gas-phase abundance of HCO has increased by four orders of magnitude compared to the pure gas-phase model. Moreover, looking at the main formation routes of the same molecule, the completely dominant pathway ($\sim 100\%$) to produce it after approximately 10^3 years is the surface reaction followed by direct chemical desorption $JH + JCO \longrightarrow HCO$ even if in the case of model 1a, the surface abundance of carbon monoxide is quite low. **Although cations may not accrete onto the grains, the surface chemistry still has an indirect effect on their abundances**, at least for some of them. Indeed, for NH_3^+, the abundance has not really evolved compared to pure gas-phase. It is predominantly produced during the entire simulation by the reaction $H_2 + NH_2^+ \longrightarrow H + NH_3^+$, as in Chapter 5. No effect of the solid-phase seems thus to be detectable.

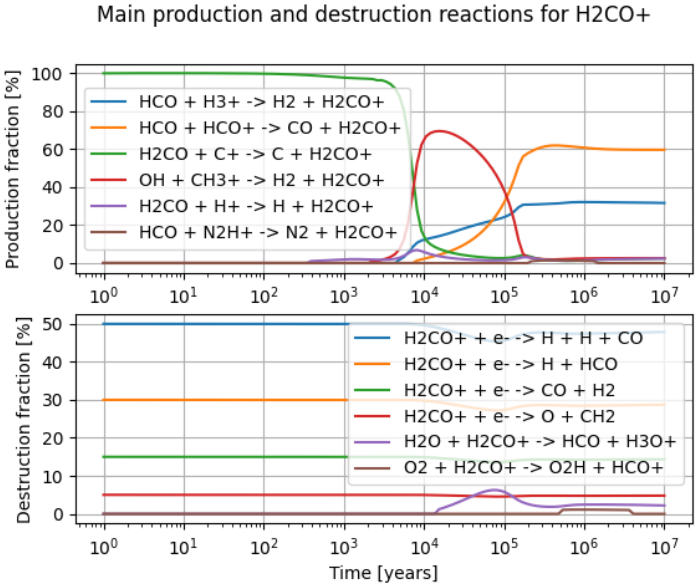

Figure 6.16: Main formation/destruction routes obtained with model 1a for H_2CO^+.

Results obtained with the modified model 2a (Figure 6.17) will now be presented. It is surprising because one would have expected the abundances of H_2COH^+ and H_2CO^+ to drop as for NH_3^+, as observed in the pure gas-phase model. In contrast, the abundances of H_2COH^+ increased and the one of H_2CO^+ remained nearly at the same level as for model 1a (Table 6.3). To explain the abundances of both cations, let us again come back to their formation mechanisms. One may directly suspect some effect of the solid-phase chemistry. Indeed, as seen in the previous case, the surface chemistry has a noticeable effect on the abundances of both ions, while its effect on NH_3^+ is negligible. For this last molecule, we thus have a decrease of the abundance when a density increase is considered, as already noticed in the case of the pure gas-phase model. An increase in density enhances the reactivity (more collisions) of this cation, and thus its destruction. Considering the main chemical reactions, they have not really changed, except that the chemistry involving H_3^+ is now dominant. This had already been pointed out when looking at the destruction reactions of the neutral Strecker-like mechanism, and is linked to the fact that the other dominant cation, i.e. HCO^+, which is predominantly formed from gas-phase CO, is decreasing when the density increases, knowing that CO preferentially condenses on dust grains at high densities. Moreover, less CO would be available to participate in

the destruction of H_3^+.

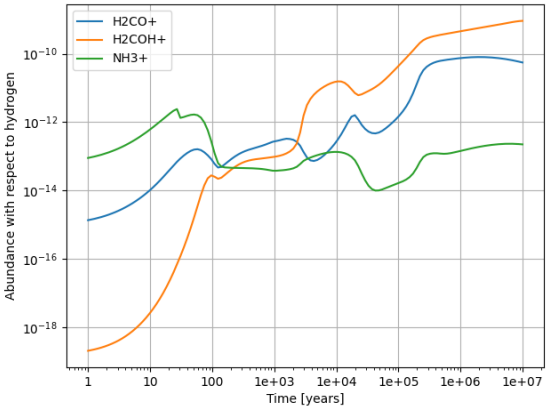

Figure 6.17: Temporal evolution of glycine precursors from model 2a via activated Strecker-like synthesis, **only in gas-phase**.

For H_2COH^+, we know that it is mainly formed from formaldehyde. In Table 6.2, one sees that although the gas-phase abundance of formaldehyde remained almost the same, its surface abundance has increased dramatically. Surface formaldehyde would then simply have to desorb and participate in gas-phase reactions producing its protonated form. For H_2CO^+, we know that it is formed primarily through reactions that involve hydrogenated CO. In addition, CO is known to heavily condense on dust grains in dense and cold mediums (cf. Section 2.4.3). More HCO might therefore be formed on the surface and then released in gas-phase to participate in the formation of H_2CO^+, potentially maintaining its abundance at similar values as before.

The conclusions previously drawn remain valid for the results of model 3a. In the gas phase, the chemistry is not altered significantly enough to meaningfully impact the overall chemical processes.

Gas-phase	H_2COH^+	H_2CO^+	NH_3^+
Model 1a	$5.68\ 10^{-11}$	$5.93\ 10^{-11}$	$9.66\ 10^{-12}$
Model 2a	$9.16\ 10^{-10}$	$5.55\ 10^{-11}$	$2.24\ 10^{-13}$
Model 3a	$2.89\ 10^{-11}$	$1.12\ 10^{-10}$	$7.89\ 10^{-11}$

Table 6.3: Final abundances with respect to hydrogen of the three cationic precursors studied in the framework of the activated Strecker-like mechanism for the gas-phase only, since cations are not considered in the solid-phase.

Some elements of interpretation have been proposed, but it is critical to understand that any **treatment of cations in the framework of *Nautilus* must be carried out with extreme caution**. Cations are not considered in the solid-phase. Unfortunately, these considerations raise numerous questions about the exact chemistry that is taking place and uncertainty remains about the exact scientific validity of the results obtained in this context. Thus, great care must be taken when analyzing the results, even if potential

explanations have been provided at the beginning of the chapter to justify the absence of cations on grains.

6.2.3 Precursors for Woon's mechanism and its variants

As already emphasized in Chapter 5, both the original Woon's mechanism and the modified version proposed by Groyne (2023) will now be investigated.

Step a of the Woon's mechanism

As a reminder, the simple precursors linked to this mechanism are the following: CO_2, CO, H_2O, OH and HCOOH. The results obtained with model 1a, are first shown in Figure 6.18 and Table 6.4.

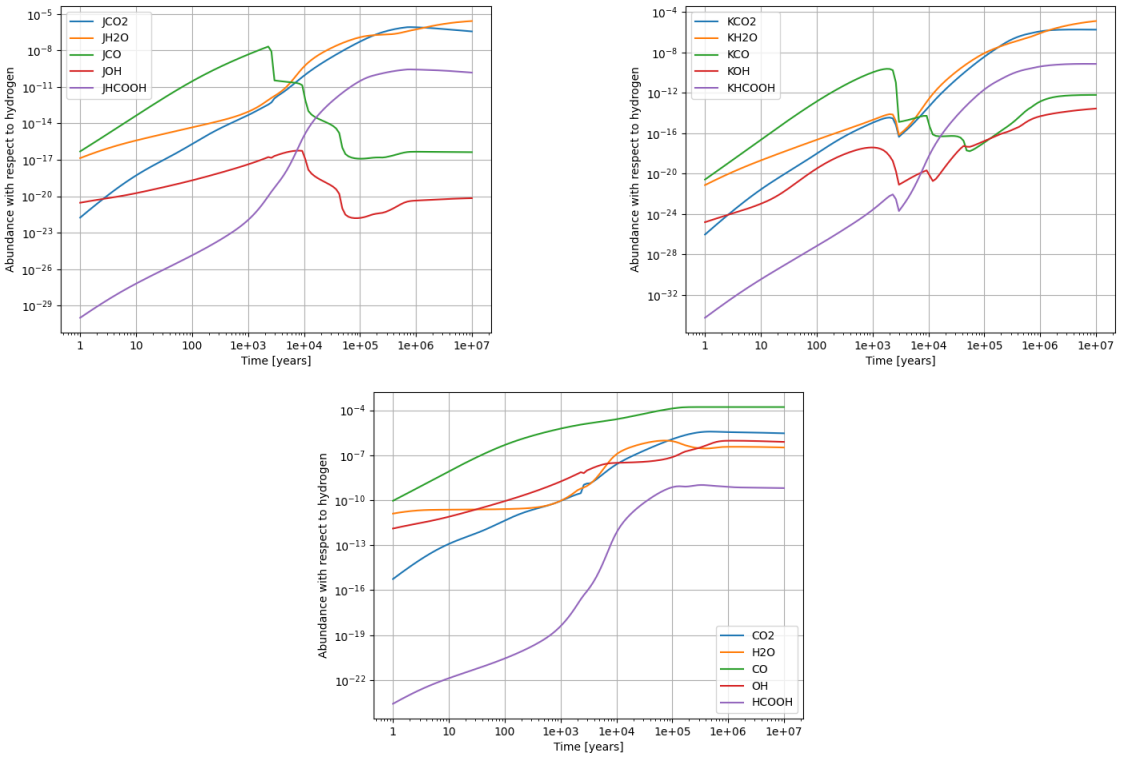

Figure 6.18: Temporal evolution of glycine precursors from model 1a via step a of Woon's mechanism, shown separately by phase: Surface (top left), Mantle (top right), Gas (bottom).

CO dominates the gas-phase by at least two orders of magnitude, as one may have expected, knowing it is the second more abundant molecule after molecular hydrogen. On the other hand, the solid phases are completely dominated by water, which is logical knowing it is the dominant component of interstellar ices. Something surprising is the low abundance of CO on the grains. Indeed, as seen in Chapter 2, under dark clouds conditions (i.e, $A_v > 9$ mag, $T < 20$ K and $n_H > 10^4$ cm^{-3}), carbon monoxide is expected to enter its dramatic freeze-out regime, in which a huge fraction of it is expected to be found on the grains. The solid-phase results could be explained here in the case of an important destruction of that molecule, as discussed shortly after. As one is now used to,

we will study the formation/destruction pathways to try to explain what is observed.

For the routes of carbon monoxide, we can see in Figure 6.19 that its main direct precursors in gas-phase are HCO, along with its cationic form HCO^+. Moreover, its main destruction pathway throughout the simulation is its reaction with $H_3{}^+$, followed by the adsorption on dust surfaces. We thus see that solid-phase chemistry seems to have a significant effect on the gas-phase abundance of CO, since adsorption is the second main sink of this species as expected, knowing the freeze-out phenomenon. For surface chemistry, the swapping reactions with the mantle dominates until 1000 years, before adsorption takes over and completely dominates the formation of JCO. The destruction chemistry is dominated after the same time by the reaction $JH + JCO \longrightarrow HCO$, releasing HCO in gas-phase. For mantle chemistry, swapping reactions dominate until 10^4 years, the time when the formation of KCO is dominated by $KCO_2 \longrightarrow KCO + KO$ and its destruction by $KH + KCO \longrightarrow KHCO$. Returning to what has been said on the abundances, the results obtained here would mean that hydrogenation reactions in the solid phases seem to be able to destroy JCO and KCO significantly, decreasing their abundances by an important amount.

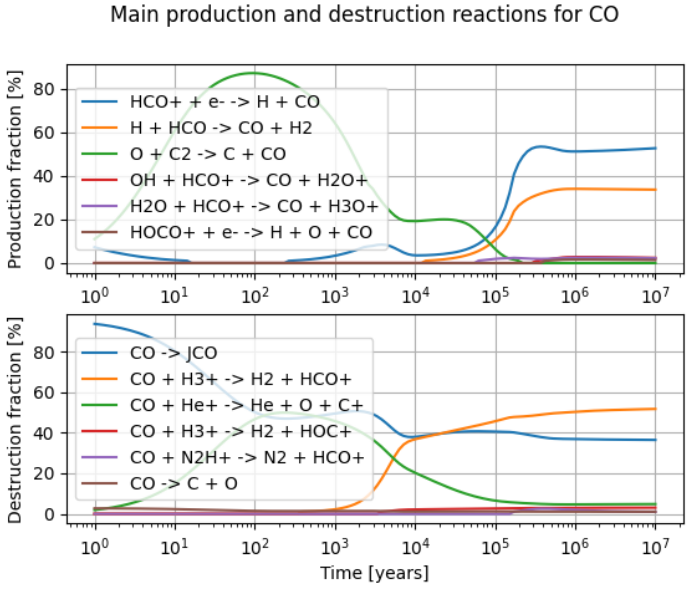

Figure 6.19: Main formation/destruction routes obtained with model 1a for CO.

The formation and destruction pathways of CO_2 are illustrated in Figure 6.20. Up to around 10^6 years, the dominant formation route is the reaction $O + HCO \rightarrow H + CO_2$, with a brief exception during which $O + HC_3O \rightarrow CCH + CO_2$ temporarily takes over. Toward the end of the simulation, the formation is mainly driven by a gas-phase reaction involving CO and $HOCO^+$, alongside the previous reaction, highlighting the central role of carbon monoxide and its protonated form as key precursors of carbon dioxide. As for the destruction processes, initially, destruction is dominated by the reaction with C^+, as also seen in Strecker-like synthesis routes. However, beyond 10^5 years, the reaction involving $H_3{}^+$ becomes the primary sink, soon followed by adsorption onto dust grains. These results once again underline the significant impact of solid-phase chemistry on the gas-phase abundance of this molecule. Regarding the evolution of CO_2 in the solid-phase, both surface and mantle populations are governed mainly by swapping reactions.

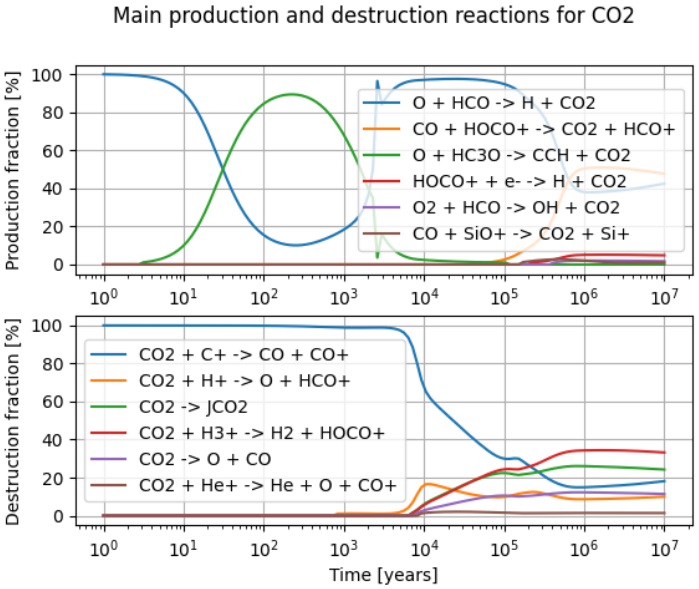

Figure 6.20: Main formation/destruction routes obtained with model 1a for CO_2.

For the OH radical (Figure 6.21), H_3O^+ remains the primary precursors at late times. However, during the first 10^6 years, OH is predominantly produced through the surface reaction $JH + JO \rightarrow JOH$. Regarding destruction pathways in the early stages, OH is primarily destroyed by reactions with C^+ and then with atomic carbon. In the later stages, destruction is mainly driven by reactions with atomic oxygen.

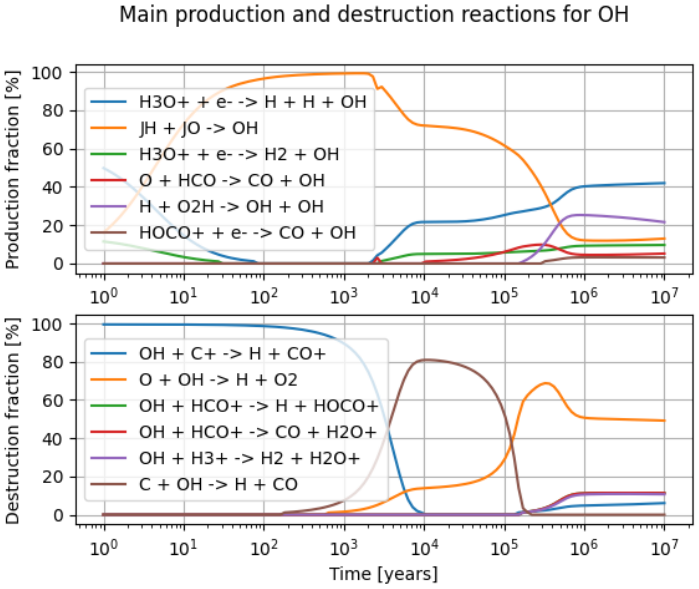

Figure 6.21: Main formation/destruction routes obtained with model 1a for OH.

The surface chemistry of OH presents an interesting deviation from the typical behavior observed for other species. As shown in Figure 6.22, this is the first case in our study where swapping reactions do not appear at all in the dominant pathways. Instead,

the main pathway for surface formation JOH is the direct adsorption of the gas-phase OH, except at later times where water dissociation dominates. Its destruction is primarily due to reaction with surface H_2, before reaction with surface atomic hydrogen. The mantle chemistry is also more nuanced than in previous cases. Although swapping with the surface is dominant during certain periods, after 10^5 years two main reactions have to be considered, water dissociation and the simple addition of KH and KO. In terms of destruction, swapping reactions prevail for most of the simulation, but around 10^5 years, reaction with molecular hydrogen of the mantle becomes the main destruction pathway.

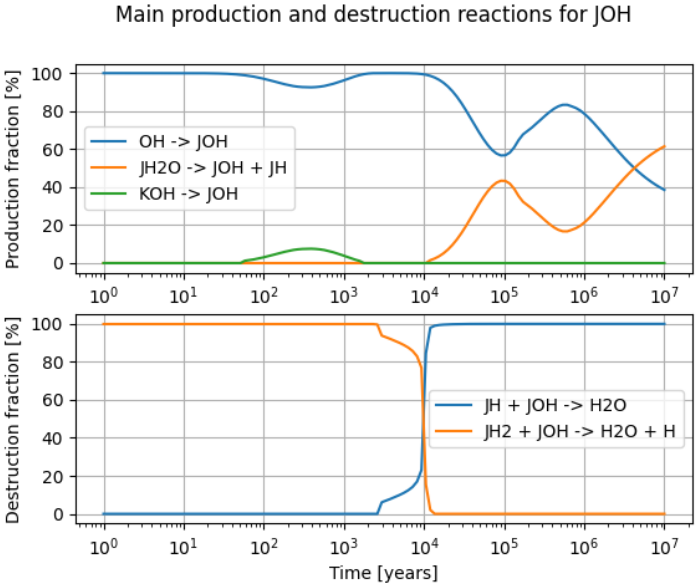

Figure 6.22: Main formation/destruction routes obtained with model 1a for JOH.

Finally, for gas-phase formic acid (Figure 6.23), only one formation route appears, which is logical knowing that the ***Nautilus*** gas-phase network contains only one formation reaction linked to that species. The destruction chemistry is dominated after 10^4 years by a reaction involving HCO^+ followed by reactions involving $H_3{}^+$. For solid-phase chemistry, only swapping reactions between surface and mantle have to be considered.

Details in the context of model 1a have been given. Let us now turn to model 2a. In Figure 6.24 and Table 6.4, the most notable changes are the ones linked to CO and CO_2. Remembering what has been said in Chapter 2 and previous discussions, we know that density is an important factor in the freezing-out process. If, as in model 2a, we increase the density by two orders of magnitude, then the freezing-out process will be reinforced, decreasing the gas-phase abundances of CO. Concerning CO_2, as we will see just after, the adsorption will be strongly reinforced due to the increase in density.

Although the gas-phase chemistry of carbon monoxide formation has not been much affected by the density increase, the same cannot be said about its destruction. Indeed, now the entire simulation is dominated by the adsorption onto dust grains, as one may have expected. For CO_2, the formation is now completely dominated by the surface reaction $JO + JCO \longrightarrow CO_2$, while its destruction is dominated by adsorption on grains as for CO. However, in contrast to carbon monoxide, we do not observe an increase in abundance in

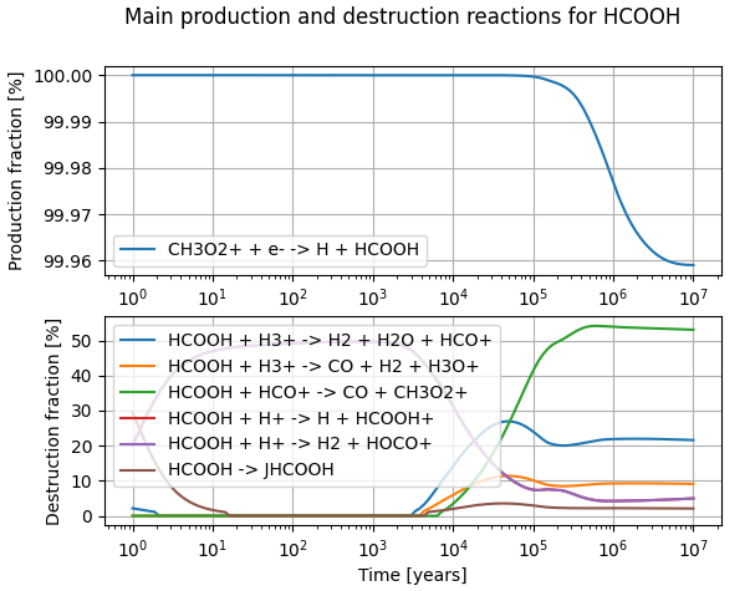

Figure 6.23: Main formation/destruction routes obtained with model 1a for HCOOH.

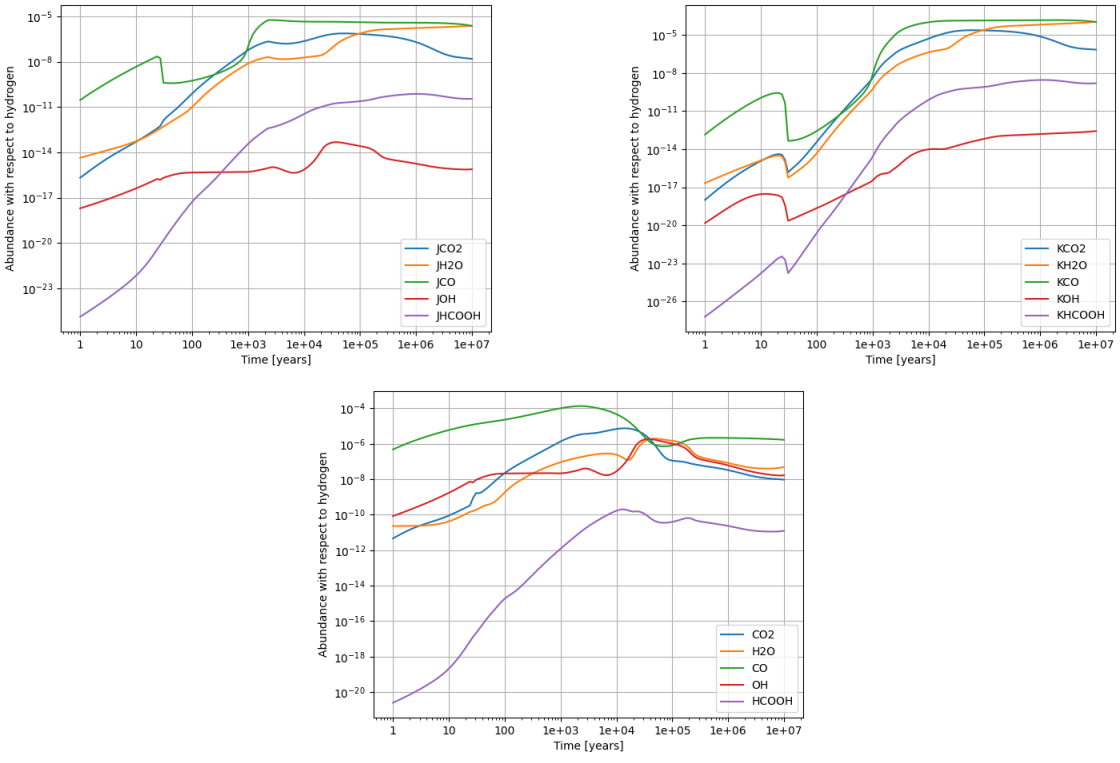

Figure 6.24: Temporal evolution of glycine precursors from model 2a via step a of Woon's mechanism, shown separately by phase: Surface (top left), Mantle (top right), Gas (bottom).

the solid phases; we even notice a decrease. Unfortunately, no noticeable changes were observed in the solid-phase chemistry. That could mean that some processes at work destroy the CO_2 (or even some of its indirect precursors), decreasing its solid-phase abundance.

These results allow us to emphasize the fact that **interstellar chemistry is not always intuitive or easy to study**. When trying to understand in detail what is happening in the context of a full 3-phase model, one should take into account all the specificities of each molecular compound as well as its tendency to react. Moreover, as discussed in Chapter 7, one has to keep in mind that **a static model such as the one used here is not the most representative of reality** (Clément et al., 2023). It is interesting to note that the solid-phase chemistry of CO has been affected, and swapping reactions now dominate everything. Concerning the results related to the OH radical, one may notice that adsorption on grains dominates the simulation between 10^4 and 10^5 years, probably explaining the increase on the surface and mantle since the solid-phase chemistry has not been strongly affected. For formic acid, similar discussions to those described previously might be made.

Gas-phase	CO_2	H_2O	CO	OH	HCOOH
Model 1a	$2.93\ 10^{-6}$	$3.30\ 10^{-7}$	$1.65\ 10^{-4}$	$7.80\ 10^{-7}$	$6.48\ 10^{-10}$
Model 2a	$9.49\ 10^{-9}$	$4.92\ 10^{-8}$	$1.69\ 10^{-6}$	$1.68\ 10^{-8}$	$1.24\ 10^{-11}$
Model 3a	$1.11\ 10^{-5}$	$3.30\ 10^{-7}$	$1.41\ 10^{-4}$	$8.54\ 10^{-7}$	$2.16\ 10^{-9}$
Surface	JCO_2	JH_2O	JCO	JOH	JHCOOH
Model 1a	$3.68\ 10^{-7}$	$2.62\ 10^{-6}$	$4.30\ 10^{-17}$	$7.05\ 10^{-21}$	$1.50\ 10^{-10}$
Model 2a	$1.57\ 10^{-8}$	$2.46\ 10^{-6}$	$2.33\ 10^{-6}$	$7.56\ 10^{-16}$	$3.54\ 10^{-11}$
Model 3a	$3.57\ 10^{-6}$	$3.25\ 10^{-7}$	$1.54\ 10^{-6}$	$4.49\ 10^{-20}$	$1.24\ 10^{-9}$
Mantle	KCO_2	KH_2O	KCO	KOH	KHCOOH
Model 1a	$1.80\ 10^{-6}$	$1.28\ 10^{-5}$	$6.22\ 10^{-13}$	$2.79\ 10^{-14}$	$7.36\ 10^{-10}$
Model 2a	$6.97\ 10^{-7}$	$1.09\ 10^{-4}$	$1.03\ 10^{-4}$	$2.66\ 10^{-13}$	$1.57\ 10^{-9}$
Model 3a	$8.39\ 10^{-6}$	$7.63\ 10^{-7}$	$3.62\ 10^{-6}$	$3.33\ 10^{-12}$	$2.90\ 10^{-9}$

Table 6.4: Final abundances with respect to hydrogen of the five precursors studied in the framework of step a of the Woon's mechanism for the three phases.

Finally, let us look at the model 3a, whose results seem to be consistent with previous discussions for most compounds. The increase in temperature to 20 K is not enough to strongly affect the abundances in the gas phase, but the chemistry in the solid phase could still be affected, especially reactive species such as OH. Indeed, for KOH, i.e. an increase by two orders of magnitude, it might probably be explained by the fact that the chemistry has been significantly modified. Now, after 10^4 years, the dissociation of water dominates completely the formation, whereas destruction is dominated by swapping reactions. Moreover, the case of mantle water has already been emphasized, and it may be linked to the behavior of surface OH. The water formation reaction no longer dominates, less OH will thus be affected to its formation, and surface CO_2 formation takes over, which could explain the observed increase in its surface abundance compared to model 1a. Other strange results are those related to surface and mantle carbon monoxide. Indeed, solid-phase abundances are at expected values, in a catastrophic freeze-out regime. Obviously, something must have changed in the chemistry of surface carbon monoxide

to notice such an important difference between models 1a and 3a, while until now both models produced quite similar results. After checking the dominant formation/destruction routes, the only notable important change is that, after 10^5 years, the hydrogenation of the surface CO falls to negligible contributions and the swapping reactions dominate completely. Since swapping also dominate the mantle, it would mean that CO in the solid-phase is no longer destroyed, but instead accumulates in the mantle. *How to explain these chemical differences with a small temperature increase*? Knowing that hydrogen has such a small desorption energy, most of it just probably desorbs directly and returns to the gas phase. One may, however, wonder if the only effect of one reaction is sufficient to cause such abundance differences, and the answer is probably no. Other phenomena, unnoticeable and probably linked to the entanglement of the chemistry, might be at work. Having said this, knowing the real complexity of interstellar chemistry, things might sometimes be counterintuitive, especially when using an (over)simplified model. In fact, in the simulations (using ***Nautilus***) from Clément et al. (2023), it is clearly acknowledged that static models such as those used in this work have a difficult time accurately reproducing the abundances of ices. Another key result from the same paper is that the dust grain temperature is an important ingredient for solid-phase chemistry. Considering that the dust temperature is at the same value as the gas might have a significant effect on the abundances.

Step b and final step of Woon's mechanism

For step b of the mechanism, three precursors must be considered: HCN, CH_2NH, and $CH_2NH_2^+$. In the final step, the direct precursors HOCO and CH_2NH_2 are also involved. As with other complex species discussed in this thesis, it is important to note that - aside from HCN - these molecules participate in relatively few reactions. Consequently, some important chemical processes related to these species might be omitted, and this will have to be considered when analyzing the results.

Looking at model 1a (Figure 6.25), the abundances of CH_2NH and $CH_2NH_2^+$ closely match those in the pure gas-phase model. The strong correlation between their gas-phase curves, as noted in Appendix E, also holds in the 3-phase model. In contrast, the abundances of more complex organic molecules in the solid phases - especially HOCO - are notably low. This is expected to some extent: HOCO is **highly reactive** and its chemical network (like that of CH_2NH_2) possesses a very low completeness. These limitations mean that the results must be interpreted with caution, as key reactions may be missing from the model. Additionally, as discussed below, the only gas-phase production route for HOCO is the reaction JOH + JCO $\longrightarrow$ HOCO. Given that surface CO is scarce under the conditions of model 1a, the low abundance of HOCO is more or less consistent with expectations, even if such a low abundance seems at first sight surprising. To better understand the underlying chemistry, we now turn to the analysis of the specific reactions involved.

Looking at the formation/destruction routes of methanimine in Figure 6.26, we see that, after 10^3 years, the most dominant reactions are the dissociative electronic recombination of iminium and $CH_3NH_3^+$, respectively. Its destruction is dominated in the first 10^4 years by a reaction involving C^+, and after that by reactions involving HCO^+ and H_3^+. The main formation routes from the pure gas-phase model are thus recovered, except the dissociative electronic recombination of $CH_3NH_2^+$ which no longer appears. Looking at the solid phase chemistry, surface methanimine production is dominated by

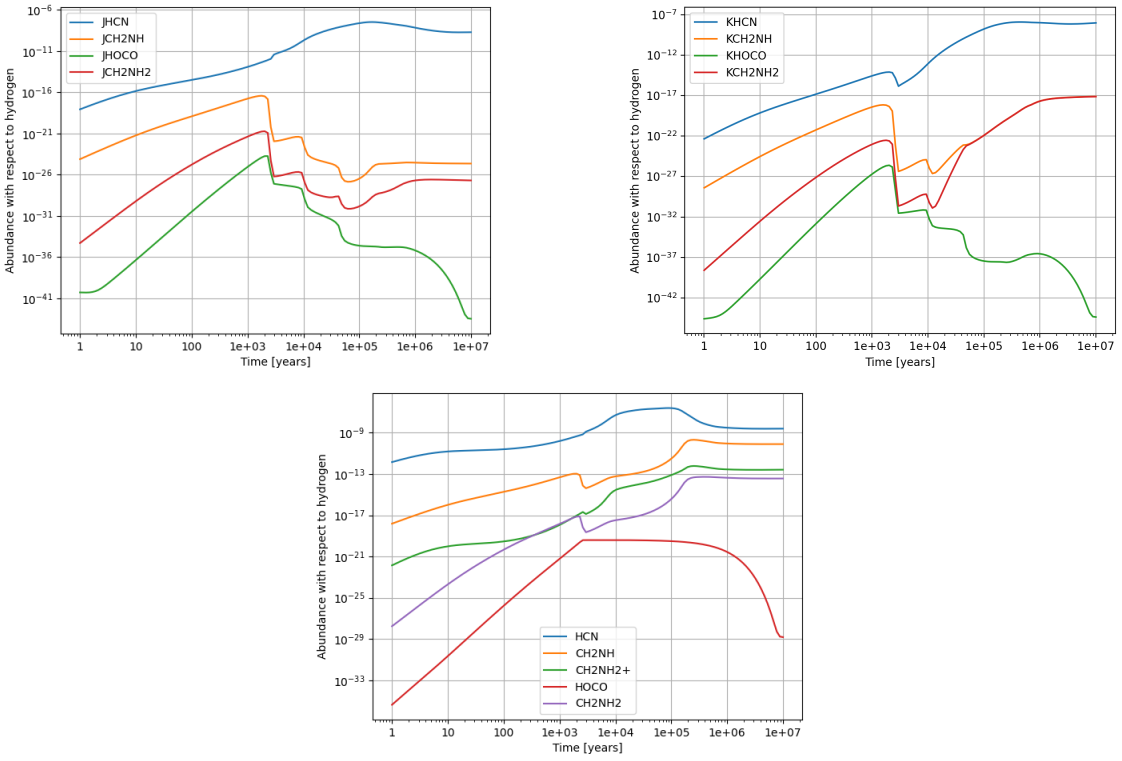

Figure 6.25: Temporal evolution of glycine precursors from model 1a via step b and final step of Woon's mechanism, shown separately by phase: Surface (top left), Mantle (top right), Gas (bottom).

adsorption on the grains after 10^3 years. For the destruction of JCH_2NH, it is the reaction $JH + JCH_2NH \longrightarrow CH_2NH_2$ that dominates after 10^3 years. This reaction is quite important, as it allows the production of one of the direct precursors of glycine, i.e. CH_2NH_2. For mantle chemistry, the reactions $KCH_3NH_2 \longrightarrow KCH_2NH + KH_2$ and $KH + KCH_2NH_2 \longrightarrow KCH_2NH + KH_2$ dominate the formation, whereas the reaction $KH + KCH_2NH \longrightarrow KCH_2NH_2$ dominates the destruction.

Concerning the routes of the iminium cation (Figure 6.27), the early chemistry is dominated by a reaction involving NH_2 and CH_3^+ whereas the late chemistry is dominated by the reactions $CH_2NH + HCO^+ \longrightarrow CO + CH_2NH_2^+$ and $NH_3 + CH_3^+ \longrightarrow H_2 + CH_2NH_2^+$. The destruction is, on the other hand, always dominated by the dissociative electronic recombination of the cation.

Looking at HOCO, it is completely dominantly formed in gas-phase by the surface reaction $JOH + JCO \longrightarrow HOCO$. Nevertheless, one must understand that, in addition to desorption reactions from the surface, it is its only gas-phase formation reaction included in the network. What is interesting **is that it is the exact reaction taking place in the Woon's mechanism**. We also see the interplay between the phases, since it is considered that the newly formed HOCO is ejected towards the gas-phase (chemical desorption). Concerning its destruction, it is dominated all along the simulation by the dissociation into its constituents with a perfectly constant destruction fraction. Then, with a slightly lesser fraction, is the adsorption on the grain. Looking at the chemistry of

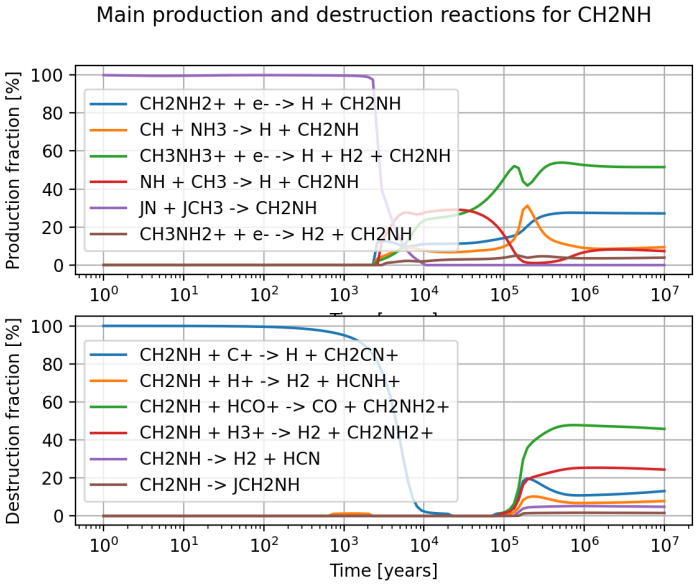

Figure 6.26: Main formation/destruction routes obtained with model 1a for CH_2NH.

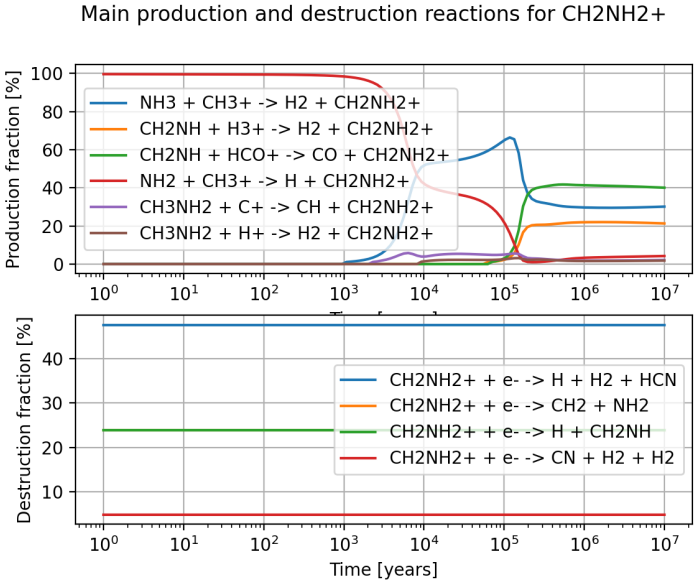

Figure 6.27: Main formation/destruction routes obtained with model 1a for $CH_2NH_2^+$.

the surface species, it is the swapping with the mantle that dominates the formation until 10^3 years, after which adsorption dominates. The same is true for destruction, except that after 10^3 years it is the reaction JH + JHOCO $\longrightarrow$ JH_2 + JCO_2 that dominates. The mantle formation chemistry is completely dominated by swapping reactions with the surface, while the destruction is dominated by reactions that involve KH after 10^4 years.

For CH_2NH_2, its gas-phase formation is completely dominated by the surface reaction JH + JCH_2NH $\longrightarrow$ CH_2NH_2, which is once again important for Woon's mechanism. However, in addition to desorption, **it is the only formation pathway that is considered in the network**. Its destruction is dominated by reaction with atomic hydrogen.

Looking at its surface chemistry, we may see that for the formation of JCH_2NH_2, we have an alternation of adsorption and swapping all long the simulation, with swapping finally dominating after 10^5 years. Its destruction is dominated by the reaction $JH + JCH_2NH_2 \longrightarrow JCH_2NH + JH_2$ after 10^3 years. Concerning mantle chemistry, the reaction $KH + KCH_2NH \longrightarrow KCH_2NH_2$ is the dominant one after 10^4 years, meaning that the production in the mantle may be non-negligible. For destruction, the same reaction as for the surface may be considered, but this time in the mantle.

Looking now at Table 6.5 and Figure 6.28, we see that the increase in density from model 2a has induced an increase in the final abundances in both solid phases, as one may expect in higher density conditions. The gas-phase abundances have remained at similar values, except for the hydrocarboxyl radical. For the ionic compound, previous arguments might be referred to. Indeed, knowing the limitations of the code we are using, analyzing the results of cations is quite difficult.

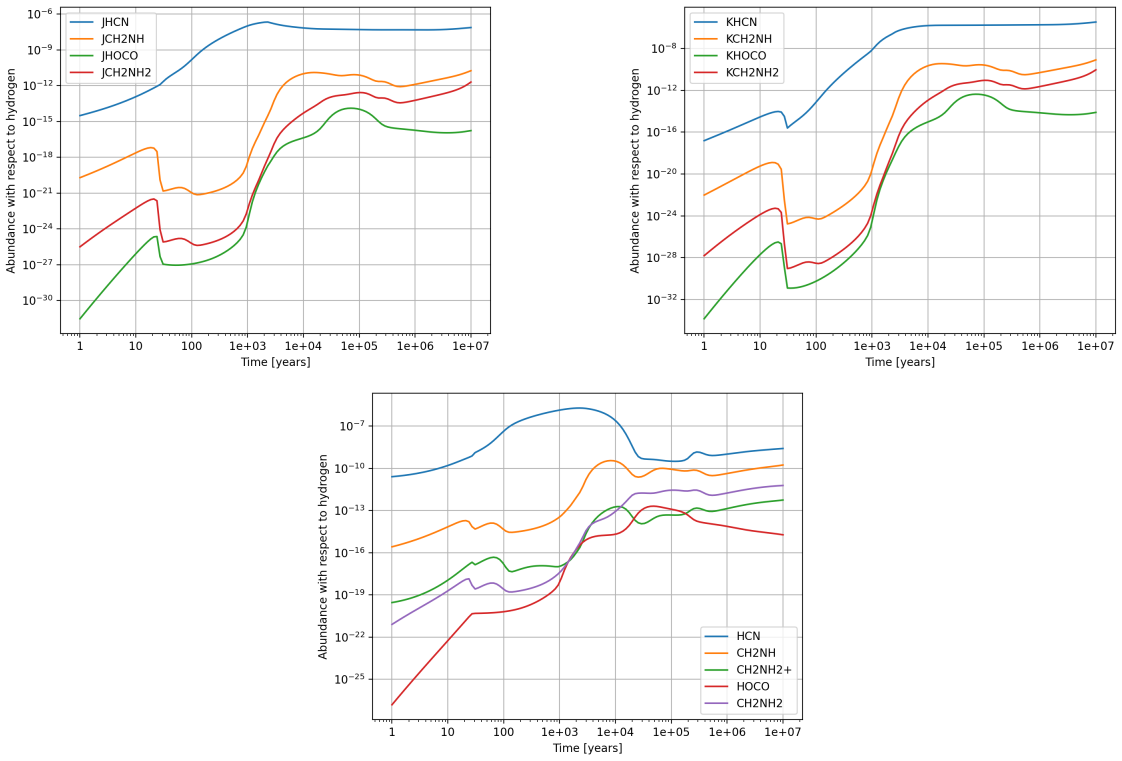

Figure 6.28: Temporal evolution of glycine precursors from model 2a via step b and final step of Woon's mechanism, shown separately by phase: Surface (top left), Mantle (top right), Gas (bottom).

Due to this density increase, the surface formation through the reaction $JN + JCH_3 \longrightarrow CH_2NH$ becomes the main formation pathway of CH_2NH throughout the simulation. The electronic dissociative recombination of $CH_2NH_2^+$ and the reaction $CH + NH_3 \longrightarrow H + CH_2NH$ remain key contributors. Regarding destruction processes, the most significant change is the emergence of adsorption on dust grains, which has become the second most important destruction pathway after reaction with H_3^+. As seen previously, the increase in environmental density appears to enhance adsorption efficiency. As for the solid-phase

chemistry, it is now dominated by swapping reactions. As for $CH_2NH_2^+$, its chemistry remains mostly unchanged, except that its formation through the reaction $CH_2NH + H_3^+ \longrightarrow H_2 + CH_2NH_2^+$ now dominates overwhelmingly by the end of the simulation. In the case of HOCO, while its gas-phase formation has remained unchanged, the destruction is now fully dominated by its adsorption on the grain, as expected with respect to the increase in density. The huge increase in abundance originates from the increase in abundance in the surface CO. Swapping reactions also dominate the chemistry in this case. Finally, for CH_2NH_2, the gas-phase chemistry has remained similar to the previous case. As for the surface and mantle chemistry, swapping reactions dominate.

Gas-phase	HCN	CH_2NH	$CH_2NH_2^+$	HOCO	CH_2NH_2
Model 1a	$2.53\ 10^{-9}$	$7.99\ 10^{-11}$	$2.62\ 10^{-13}$	$1.49\ 10^{-29}$	$3.69\ 10^{-14}$
Model 2a	$2.55\ 10^{-9}$	$1.71\ 10^{-10}$	$5.55\ 10^{-13}$	$1.88\ 10^{-15}$	$5.98\ 10^{-12}$
Model 3a	$3.38\ 10^{-9}$	$1.24\ 10^{-10}$	$4.36\ 10^{-13}$	$5.59\ 10^{-7}$	$1.23\ 10^{-13}$
Surface	JHCN	JCH_2NH	$JCH_2NH_2^+$	JHOCO	JCH_2NH_2
Model 1a	$2.00\ 10^{-9}$	$2.23\ 10^{-25}$	/	$3.20\ 10^{-44}$	$2.01\ 10^{-27}$
Model 2a	$7.61\ 10^{-8}$	$1.84\ 10^{-11}$	/	$1.75\ 10^{-16}$	$2.07\ 10^{-12}$
Model 3a	$7.50\ 10^{-10}$	$3.50\ 10^{-16}$	/	$7.78\ 10^{-13}$	$3.07\ 10^{-19}$
Mantle	KHCN	KCH_2NH	$KCH_2NH_2^+$	KHOCO	KCH_2NH_2
Model 1a	$9.80\ 10^{-9}$	$7.88\ 10^{-18}$	/	$4.42\ 10^{-45}$	$7.67\ 10^{-18}$
Model 2a	$3.38\ 10^{-6}$	$8.19\ 10^{-10}$	/	$7.77\ 10^{-15}$	$9.20\ 10^{-11}$
Model 3a	$1.76\ 10^{-9}$	$9.42\ 10^{-16}$	/	$1.83\ 10^{-12}$	$7.45\ 10^{-19}$

Table 6.5: Final abundances with respect to hydrogen of precursors studied in the framework of both step b and final step of Woon's mechanism for the three phases (except $CH_2NH_2^+$).

To conclude this chapter and this study, let us analyze the results from model 3a. As one can see in Table 6.5, gas-abundances has remained similar to the ones from model 1a, except in the case of HOCO in which the abundance is even higher than in model 2a, surpassing even hydrogen cyanide. This is surprising, because as seen when discussing step a of Woon's mechanism the surface CO abundance, though much higher than in model 1a, was not higher than in model 2a. Moreover, the abundances in the solid phases have all increased, especially those at the surface. This illustrates once again the fact that **a small increase in temperature is sufficient to enhance and modify surface chemistry**. In order to try to find an explanation to those, the formation/destruction routes have been studied one last time. First of all, though some slight differences can be noticed, the gas-phase chemistry of the species has remained similar to the case of model 1a. Notably, for CH_2NH, the surface formation pathway $JN + JCH_3 \longrightarrow CH_2NH$ is dominant for a longer time, even if at the end the two previous formation routes are back. For HOCO, one may notice that the destruction is now dominated by its adsorption throughout the simulation, which is also the main formation route of JHOCO. The destruction reaction with JH still dominates, although the swapping has now a high destruction fraction. Moreover,

swapping dominates now in the mantle, both for formation and destruction. For CH_2NH_2, the surface chemistry has been affected, since now adsorption dominates the formation at the end, whereas destruction is dominated by swapping reactions. Together, these changes in chemistry could explain the differences with model 1a, especially at such low abundances that a small chemical change could cause an important increase in terms of order of magnitude. Moreover, **one must absolutely keep in mind the small completeness of those species**, such that results obtained here should not be considered as robust, but more indicative. A more complete network will be more than welcome in the near future to generate results with much higher confidence. However, this section allowed us to show the effect of a change in temperature on the surface chemistry, where the last parameter was identified as a key to unlocking some reactions, contrary to the effect on the gas-phase discussed in Groyne (2023).

6.2.4 Main conclusions from this chapter

In this chapter, several precursors of the glycine molecule (see Figure 1.3), identified from the formation pathways proposed in Chapter 3, have been studied using a 3-phase astrochemical model. We examined their abundance evolution over time along with their main formation and destruction routes. One key takeaway is that the use of a comprehensive 3-phase model such as ***Nautilus*** can make the interpretation of the results quite complex. A complete understanding of the chemistry at play requires considering all the interconnections between chemical species and reaction pathways, something that can quickly become overwhelming. As observed throughout this chapter, intuitive reasoning is often insufficient to fully grasp the behavior of the system; see e.g., the case of carbon monoxide. Another limitation encountered is the absence of cationic species in solid-phase reactions, even if justifications for these considerations have been proposed at the beginning of the chapter. This limitation should be kept in mind when interpreting results related to ionic species. It is likely an aspect that could be improved with a more chemically inclusive modeling code, but adding electrostatic considerations on top of a microscopic KMC simulation would be very complicated, not to mention the high CPU requirements. Additionally, the rate-equation approach used in ***Nautilus*** introduces certain non-physical biases, notably in the treatment of swapping reactions. This limitation hampers the accurate modeling of the icy mantle structure. Last but not least, we have seen that contrary to the work of Groyne (2023), a small temperature increase is sufficient to activate or at least enhance some solid-phase reactions, changing the chemistry between models 1a and 3a.

Finally, although direct routes of glycine formation (NH_2CH_2COOH) were not explored - due to their absence in current astrochemical networks, which remain limited in terms of complexity and completeness - this study provides a broader understanding of its key precursors and how they behave under simulated conditions representative of molecular clouds. As discussed in Chapter 4, these results must be considered in the limited framework of the model that is used, being fully aware of its limitations. One must not take these results for granted and is invited to test their robustness by comparing them to the literature/observation data, as done in Chapter 7.

Chapter 7

Confrontation with observations

As a concluding note to this work, we will now compare the abundance values obtained in Chapter 6 with observational values from the literature. The gas-phase will first be addressed before moving to the icy mantles.

7.1 Gas-phase observations of molecular clouds

Gas-phase molecules in the interstellar medium are primarily detected through their rotational transitions, which emit and absorb radiation in the **microwave and radio domains of the electromagnetic spectrum**. These transitions arise because of changes in the rotational energy levels of polar molecules (the presence of a dipole moment is a strict requirement). Moreover, these transitions are very specific to molecular compounds, making them a useful tool for precise molecular identification. Facilities such as the Atacama Large Millimeter/submillimeter Array (ALMA), the IRAM 30 m telescope, and the Green Bank Telescope have played key roles in identifying and characterizing a wide variety of molecular species in cold interstellar clouds.

Referring to Appendix D, in our group of interest, only H_2O, NH_3, HCN, H_2CO, H_2COH^+, CO, OH, HCOOH and CH_2NH have been firmly detected in gas-phase in the ISM. In order to confront our theoretical values obtained thanks to ***Nautilus*** with observational results from the literature, a bibliographic investigation has been undertaken to make an assessment of the available interstellar abundance values towards dark clouds. The comparison can be found in Table 7.1, where the abundances are compared with observations towards two extensively studied dark clouds, TMC-1 and L134N[1] (data from the review paper of Agúndez and Wakelam 2013). According to Pratap et al. (1997), the TMC-1 cloud seems to have along its ridge a temperature close to 10 K and a density value of about 6×10^4 cm^{-3}. Swade (1989) derived for the L134N molecular core a kinetic temperature of about 12 K and a peak molecular hydrogen density of about 3×10^4 cm^{-3}. Therefore, new models, respectively called Model T and Model L for TMC-1 and L134N were built to adapt to those cloud conditions.

[1]One has to be aware that the study carried out by Ruaud et al. (2016) contains also a comparison between the results from ***Nautilus*** and the observational values in both cold cores. However, this is not a comparison as intended in this work. Whereas it their work confidence levels with observations are sought **for the entire molecular population identified in those clouds** (according to Agúndez and Wakelam 2013), we are here looking for specific abundance values for the precursors of interest.

Molecule	Model T	TMC-1 dark cloud	Model L	L134N dark cloud
H_2O	$3.26\ 10^{-6}$	$< 7\ 10^{-8}$ [a]	$1.93\ 10^{-7}$	$< 3\ 10^{-7}$ [a]
NH_3	$1.36\ 10^{-8}$	$2.45\ 10^{-8}$ [c]	$2.98\ 10^{-8}$	$5.9\ 10^{-8}$ [d]
HCN	$6.37\ 10^{-10}$	$1.1\ 10^{-8}$ [c]	$1.31\ 10^{-8}$	$7.3\ 10^{-9}$ [d]
H_2CO	$5.89\ 10^{-9}$	$5\ 10^{-8}$ [e]	$7.60\ 10^{-9}$	$2\ 10^{-8}$ [b]
H_2COH^+	$1.48\ 10^{-11}$	/	$1.82\ 10^{-11}$	/
CO	$5.71\ 10^{-5}$	$1.7\ 10^{-4}$ [c]	$1.26\ 10^{-4}$	$8.7\ 10^{-5}$ [d]
OH	$5.06\ 10^{-6}$	$3\ 10^{-7}$ [b]	$3.13\ 10^{-7}$	$7.5\ 10^{-8}$ [b]
HCOOH	$1.84\ 10^{-9}$	/	$5.51\ 10^{-10}$	$3\ 10^{-10}$ [b]
CH_2NH [g]	$3.39\ 10^{-10}$	$< 6.5\ 10^{-11}$ [f]	$1.52\ 10^{-8}$	$< 7\ 10^{-11}$ [f]

[a] Snell et al. (2000)
[b] Ohishi et al. (1992)
[c] Pratap et al. (1997)
[d] Dickens et al. (2000)
[e] Ohishi and Kaifu (1998)
[f] Luthra et al. (2023)
[g] Not firmly detected in TMC-1 and L134N, but upper limits have been proposed in terms of column densities by Dickens et al. (1997), converted into abundances by Luthra et al. (2023) (relative to H) assuming an H column density of 2×10^{22} cm^{-3}.

Table 7.1: Table comparing the abundances (at 1.956×10^5 years) in gas-phase from this work to the ones from observations towards the TMC-1 and L134N dark clouds **when available**. Note that the molecular abundances from Agúndez and Wakelam (2013) in these clouds are expressed relative to the H_2 abundance. Knowing that in this work, **all the hydrogen is assumed to be found in the form of H_2**, we are indeed able to compare the abundances.

Important remark:
Ruaud et al. (2016), using the 3-phase astrochemical code ***Nautilus***, have **constrained the age of both dark clouds to be of the order of a few 10^5 years**. To be as close as possible to reality, the abundance values shown in Table 7.1 are those found at 1.956×10^5 years in our simulations.

In the results presented in Table 7.1, one can see that the modeled abundances generally fall within a one order of magnitude range of the observed values for all species. In the case of TMC-1, the modeled abundance of water is however overpredicted by two orders of magnitude whereas the one of hydrogen cyanide is underpredicted by the same amount. Regarding L134N, the main exception concerns CH_2NH, which is clearly overpredicted in regards of the upper limit determined by Luthra et al. (2023).

These results suggest that our model is capable of predicting gas-phase abundances not too far from the measured values reported in the literature. However, it is important to recognize that we are working with a simplified model[2], and these simplifications inevitably affect the accuracy of the predicted values. In fact, the close matches observed for certain species may be coincidental rather than indicative of true predictive power, an aspect

[2]For example, we consider only a single cell with constant density, temperature, cosmic-ray ionization rate and visual extinction, as well as the inherent approximations to the rate-equation approach.

that could be better assessed using more sophisticated models, as discussed in Chapter 9. As already highlighted in the work of Ruaud et al. (2016), "*such comparisons must be approached with caution, since these sources possess complex internal structures and may have undergone different physical histories*". It is therefore not surprising that comparisons between different molecular clouds lead to slightly different results, as reflected in Table 7.1. Moreover, as will be seen in the next section, results concerning the solid-phase are subject to strong uncertainties. As seen throughout this work, for several species the interaction between the phases is strong; therefore, the uncertainty related to the results in solid-phase will more than probably be propagated to the gas-phase.

7.2 Solid-phase observations of molecular clouds

In contrast to gas-phase molecules, which are typically detected via their rotational transitions in the microwave and radio domains, molecules embedded in interstellar ices are primarily observed through their vibrational transitions in the infrared. Within the dense and cold environments of molecular clouds, many volatile species rapidly accrete onto the surfaces of dust grains, forming icy mantles. Once trapped in this solid matrix, **these molecules are no longer free to rotate**, and thus their rotational spectra become inaccessible. However, their vibrational modes—such as stretching and bending motions—remain active and can be excited by background radiation, leading to absorption features at characteristic wavelengths in the near- and mid-infrared. Instruments aboard space telescopes like ISO, Spitzer, and more recently JWST (NIRCam, NIRSpec, MIRI) have revealed rich ice absorption spectra.

As described in Appendix D, much less species have been firmly identified in interstellar ices. In this case, only H_2O, NH_3, CO, CO_2, H_2CO and HCOOH have to be considered for comparison. For the last two organic molecules, no reliable data were found in the literature. Those will thus not be studied in the rest of this chapter.

Important remark:
Abundances within interstellar ices are usually expressed as percentages compared to water. The ratio between the abundances of a given and that of water will thus be taken. Moreover, the abundances on the surface and in the mantle will be summed for each species.

Comparison with observational results will be made with some results from the ICE AGE[3] JWST observation program (McClure et al., 2023). In that paper, JWST instruments are used to explore the pristine ice composition towards two background stars (NIR38 and J110621) in the Chamaeleon I molecular cloud. As we did for the results in the gas phase, the literature was explored in order to find some information describing the physical conditions towards those background stars on top of the visual extinction/column densities already provided in McClure et al. (2023). In that context, it is interesting to consider the paper by Jiménez-Serra et al. (2025). That paper aims at modeling the ice chemistry in the Chamaeleon I cloud, based on the observations of McClure et al. (2023), in order to establish the dominant formation processes of ice compounds, principally methanol CH_3OH. This is achieved using various astrochemical models, including

[3]The ICE AGE program (`https://jwst-iceage.org`) was part of JWST's observation Cycle 1, which aimed (observations ended in 2023) at tracing the building blocks of life in ices.

Nautilus and KMC simulations, which allow for a benchmarking of various codes. Their simulations aim at studying the free-fall collapse following a translucent phase, the parameters of which start as a base for the free-fall collapse simulations (varying density with time). Thanks to that paper, we found that the densities that can be assumed lie somewhere between 10^5 and 10^6 cm^{-3}, according to Belloche et al. (2011) and Väisälä et al. (2014). Therefore, in the following, a constant density of about 4×10^5 cm^{-3} will be assumed. In addition, according to the Herschel-based dust temperature maps of Väisälä et al. (2014), a dust temperature (assumed equal to the gas temperature) of 14 K for NIR38 and 12 K for J110621 can be assumed. We also collected information concerning the visual extinction in these clouds. Indeed, McClure et al. (2023) used pre-flight estimates of 60 mag and 95 mag for NIR38 and J110621 respectively, which were also the values used in Jiménez-Serra et al. (2025). As explained in the latter paper, Dartois et al. (2024) revised those values, dividing them by a factor close to 2. Therefore, the values of 34 mag and 47 mag for NIR38 and J110621 will be used respectively. The new models will be called "Model N" and "Model J" based on the names of the background stars. Let us keep in mind that the dust temperature has an important effect on chemistry (cf. Clément et al. 2023). Therefore, a small temperature modification could have a significant impact. As seen before, it is assumed in our models that the dust temperature is kept at a constant value equal to the gas temperature, and that is expected to have an impact on the simulations.

A strong limitation that affects this comparison is the age of the considered clouds, on top of their different physical conditions and histories. Indeed, as we have seen throughout Chapter 6, the abundance of the various species varies continuously over time, stabilizing only at the end. Therefore, the **composition of a molecular cloud will be a function of its age** and the final abundance values of this work put in Table 7.2 might not be the relevant ones for the comparison. Note that this comment is also valid for the previous section, even if the ages of TMC-1 and L134N have been more or less constrained.

Molecule	Model N	NIR38 [a]	Model J	J110621 [a]
H_2O	100	100	100	100
NH_3	~ 1	~ 4	~ 1	~ 5
CO	~ 283	~ 40	~ 217	~ 30
CO_2	~ 41	~ 20	~ 22	~ 15

[a] McClure et al. (2023)

Table 7.2: Table comparing the final abundances (**expressed as percentages with respect to water**) in icy mantles (both "J-" and "K-" species) from this work to the ones from observations. Here, we are looking at dark clouds towards background stars (NIR38 and J110621, McClure et al. 2023). Note that other ice components, such as methanol CH_3OH, are not accounted for. Moreover, error bars are not indicated.

The results provided in Table 7.2 show that the predictions by ***Nautilus*** are not in good agreement with the observations. Indeed, while the abundances of NH_3 and CO_2 seem to be approximately close to the observations, this could very well be a coincidence regarding the huge differences with observations for the abundance of CO. We already

mentioned in Chapters 4 and 6 that the rate-equation approach to model the solid-phase might not be the best to reproduce observations, but we may also come back to some of the previous hypotheses to have a better understanding of the results.

We have seen in Chapter 6 that the mantle water abundance obtained with model 3a seems quite low compared to those obtained with previous model 1a, even if an increase in dust temperature is expected to affect chemistry. Therefore, even if new models were built in this section, one may wonder if the ***Nautilus*** code is truly reliable in terms of calculating the H_2O abundance. Indeed, some major formation routes might have been omitted, owing to a lack of kinetic data, for example. As described by Grieco et al. (2024), two main solid-phase pathways[4] are expected to dominate water formation on dust grain:

Pathway 1:

$$O + H \longrightarrow OH$$
$$OH + H \longrightarrow H_2O$$

or

$$OH + H_2 \longrightarrow H_2O + H$$

Pathway 2:

$$O_2 + H \longrightarrow HO_2$$
$$HO_2 + H \longrightarrow H_2O_2$$
$$H_2O_2 + H \longrightarrow H_2O + OH$$

After checking in the chemical network, it appears that **both pathways are included in both solid phases** (mantle and surface). Therefore, it seems that the main pathways of solid water formation are taken into account. As proposed in Chapter 6, the decrease in the mantle should thus probably be related to the fact that less OH is affected to water formation and is instead used in the formation of CO_2, therefore adding an argument to the overabundance of CO_2 with respect to H_2O when using model 3a.

Let us now come back to the CO freeze-out hypothesis that was assumed at the beginning of Chapter 6. Indeed, in order to explain the abundances of carbon monoxide between the models, it was assumed that, regardless of the model, the conditions for the freeze-out presented in Chapter 2 are met[5]. Knowing the environments considered, this is not a bad approximation and the differences observed in the framework of the ***Nautilus*** model might be reasonably explained by the chemistry presented in the previous chapter. One must nonetheless understand that the freeze-out process as well as the ice composition still require much more studies and observations to be fully understood. As an example, the study presented in Penteado et al. (2015) discusses the fact that observations towards young stellar objects are better reproduced using a CO:CH_3OH ice mixture rather than the generally assumed CO:H_2O. Another very interesting paper is the one by Smith et al. (2025), in which a new mapping of H_2O with CO_2 and CO within the Chamaeleon I molecular cloud is presented. What is new in that publication is that the same molecular cloud is observed from numerous lines of sight (44) towards background stars thanks to JWST, whereas in previous publications various clouds with different physical histories

[4]Note that hydrogenation starting from ozone O_3 has also been proposed as one of the dominant formation pathways towards water.

[5]Even if the freeze-out process is reinforced when using higher density conditions, as shown when using model 2a instead of model 1a.

were averaged. That study, in addition to highlighting the role that JWST will play in the future, showed that within a same environment variations in column densities (thus, in the freeze-out of CO) can be observed, as **real molecular clouds are not at all uniform astrophysical environments**. Additionally, the layered icy-mantle formation model presented in Chapter 2 might not be the only one. Indeed, considering the accretion, formation, and diffusion rates of the relevant species, as well as the wettability[6] of the surface, Kouchi et al. (2021a,b) recently proposed an alternative mechanism for icy mantle formation illustrated in Figure 7.1. In their model, (a) an amorphous solid water (ASW) matrix forms around the grain core, with nano-crystals of CO_2 (produced in situ through the exothermic reaction between CO and OH) and amorphous CO_2 embedded in its upper layers, and (b) a single α-CO crystal island develops atop the ASW surface via efficient Ostwald ripening[7]. This structure is supported by their experimental results showing that α-CO wets the ASW surface poorly, which explains why the α-CO crystal forms above, rather than within, the amorphous water ice. Furthermore, compared to a classical layered structure, thin crystalline layers are less stable (due to their higher surface energy) than small spherical aggregates of the same volume, lending additional credibility to the model proposed by Kouchi et al. (2021a,b). One thus sees that interstellar dust grains can be more complicated than initially thought, suggesting that models should be adapted to take into account this alternative structure.

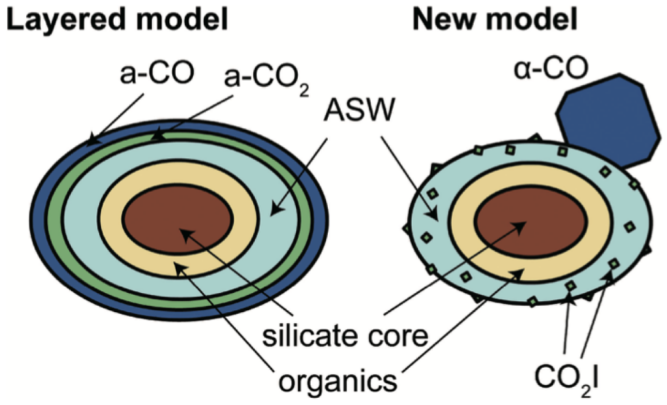

Figure 7.1: Comparison between the usual layered model and the new model proposed by Kouchi et al. (2021a,b), from Tsuge and Watanabe (2023). Note the 'a-' refers to amorphous phase, while 'α-' means crystalline component.

When trying to make this comparison, the interesting paper by Clément et al. (2023) deserves to be considered. In their work, the 3-phase gas-grain code ***Nautilus*** was used to predict the ice abundances of the dominant species in order to compare these predictions with the observed abundances. Two types of simulations were ran in their work: one with

[6]Wettability refers to the ability of a solid dust grain surface to allow the spreading and adhesion of gas-phase species that condense into ices under cold interstellar conditions, such as carbon monoxide and carbon dioxide. A highly wettable surface promotes the uniform growth of ices, leading to more extended coverage of the grain. Conversely, low wettability may result in patchy, non-uniform coverage or the preferential formation of molecular clusters or islands.

[7]Ostwald ripening is a process that can occur in solids or liquids, involving the gradual redistribution of material and the evolution of an initially inhomogeneous structure over time. In solids, it leads to the dissolution of smaller crystals and their re-deposition onto larger ones, as larger particles are energetically favored compared to smaller ones. In the context of our study, this process is facilitated by the high diffusion coefficient of CO on amorphous solid water (ASW).

static conditions (similar to this work) and one accounting for the full 3D dynamic structure of the clouds. However, in their static simulation, the physical conditions (density, dust temperature, extinction) as measured by the Herschel telescope were used. As this does not consider a unique value for each of the physical quantities, but rather several fixed values depending on the point considered, **the comparison with our results may thus not be fully relevant**. One of their conclusions is that the model using static conditions - corresponding to a snapshot of the physical conditions as observed by Hershel - does not reproduce the observed trends in interstellar ices, as one could see in their Figure 1.

Important remark:

Another major limitation in interpreting the results lies, as previously emphasized, in the choice of binding parameters. As discussed in Sections 5 and 7 of the review by Minissale et al. (2022), which focuses on the thermal desorption properties of species, the simplified approach from Hasegawa and Herbst (1992) — used in the ***Nautilus*** code — may not be the most accurate for describing desorption processes. In particular, the treatment of the pre-exponential factor ν in the desorption rate is often oversimplified: many astrochemical models typically encode this factor as a fixed, arbitrary value (typically, around 10^{12} to 10^{13} s^{-1}) regardless of the species or process involved. However, **such an approximation is not physically justified**. A more rigorous alternative would be to derive these factors using Transition State Theory (TST), as discussed in Minissale et al. (2022) and references therein, which allows one to compute pre-exponential factors specific to each process. **This modeling uncertainty can have drastic consequences on the calculated abundances**. Notably, this uncertainty in modeling thermal desorption could also affect the reliability of the gas-phase results, as desorption rates play a critical role in determining the availability of species across phases.

As a concluding note, the full discussion presented in this chapter **must be considered in the framework of the *Nautilus* model**. As emphasized in Section 4.3, the rate-equation method applied to solid-phase chemistry is subject to heavy uncertainties. The results coming from the code must thus be considered uniquely in this limited framework, and it is important not to draw any hasty conclusion. Nevertheless, this work provided us with a first insight into the behavior of these glycine precursors in a 3-phase context and moreover allowed us to have a better understanding of both theoretical and observed composition and structure of interstellar ices. It also allowed a critical assessment about the veracity and the extent of the results that were obtained, demonstrating the limitations of the ***Nautilus*** astrochemical model. A key takeaway from this chapter is that the structure, composition, and properties of icy mantles are highly complex. Future advancements in ice modeling, along with new observational data, will be essential to better constrain our understanding of these features.

Chapter 8

Conclusion

The question of the origin of life has always been one of the most dominant and intriguing questions among the scientific community. In this master thesis, it has been chosen to contribute to the exploration of the **exogenous origin of life's building blocks**, i.e. the possibility that the molecules essential for the development of terrestrial life may have originated from space. The emphasis was placed on molecular clouds, which are the coldest and densest phase of the interstellar medium. The focus has been set on natural amino acids, essential biomolecules in living organisms (cf. Chapter 2), and more particularly on the simplest one known as glycine, NH_2CH_2COOH.

This work intends to be the continuation of the work presented in Groyne (2023), extending the pure gas-phase study of various glycine precursors to a full 3-phase study accounting for both surface and mantle of interstellar dust grains. In order to fulfill the objective of this study, an astrochemical kinetic modeling tool has been used, as described in Chapter 4. In this work, the astrochemical code ***Nautilus*** (Ruaud et al., 2016) was used and allowed us to conduct a study of various **potential glycine precursors**, according to the dominant mechanisms proposed in the literature (Chapter 3), i.e. Strecker-like and Woon's (Woon, 2002) mechanisms.

The first part of the practical work in this master thesis consisted of a comparison with the pure gas-phase results obtained using ***Astrochem***, as presented in Groyne (2023), and discussed in Chapter 5. In general, this comparison demonstrates that we successfully reproduced the main results presented in Groyne (2023). Although some discrepancies were observed, particularly in regard to the temporal evolution of certain species, **the equilibrium abundances are, in most cases, remarkably similar**. Although not all contributing reactions were identified identically, **the dominant formation and destruction pathways largely overlap in both models**. These differences are expected, given that ***Nautilus*** and ***Astrochem*** are distinct chemical codes, developed with different implementations, the former being more complete and complex than the latter (cf. Section 4.2). This reinforces the robustness of the findings presented by Groyne (2023), many of which remain valid in the extended framework explored in this work.

Following this comparison and the intermediate conclusion that ***Nautilus*** constitutes a valuable tool to perform a more elaborate analysis of glycine precursors, the full 3-phase study (gas, surface and mantle phases) was carried out and described in Chapter 6. This study allowed us to see the behavior of the chemistry of all those various molecules. A detailed summary of those results can be found in Table 8.1.

Important remark:
The values of the final abundances in Table 8.1 have all been rounded to keep only orders of magnitude for easier visualization. Moreover, the last columns, i.e. formation and destruction, regroup all the dominant species involved in those processes. To be representative, the agents found in those columns are only those whose fraction is higher than 20% after 10^5 years.

Looking first at the neutral Strecker-like synthesis, in which the precursors H_2O, NH_3, HCN and H_2CO were considered, we observed that the species are not affected in the same way by the surface chemistry. Indeed, while for the first three compounds, they do not seem to have a strong interaction between the gas-phase and the surface, making the final gas-phase abundances quite similar with those of the pure gas-phase model, this was not the case for formaldehyde. This last molecule was strongly affected by the solid-phase, and was in fact mainly produced on the surface of grains before being released to gas-phase. Moreover, the apparent dominance of swapping reactions between the surface and mantle was found to result from a non-physical bias inherent to the rate-equation approach. Nonetheless, in some cases the chemistry is more active than simple swapping reactions. When increasing the density using model 2a (Table 6.1), we found intuitive results, since the phases that have been the most affected are the surface and mantle phases due to an increased accretion rate. Finally, we observed that a small increase of 10 K (model 3a) in temperature is not enough to significantly enhance the gas-phase chemistry, as already noted in Groyne (2023), but that it is no longer valid for the surface and the mantle. In that case, **the solid-phase chemistry for some species can be significantly affected by a small increase in temperature**, as in the case of formaldehyde.

As a next step, attention was paid to the activated Strecker-like synthesis, in which cationic and protonated species are considered (H_2CO^+, H_2COH^+ and $NH_3{}^+$). The study of charged species allowed us to realize that they are not considered in the solid-phase network of ***Nautilus***. This was justified at the beginning of Chapter 6, and would in fact be difficult to implement as discussed in Chapter 9. However, it was seen that though they are not considered in solid-phase reactions, **surface chemistry may have an indirect impact on their abundances** through the effect on the neutral precursors of these ions (or not, depending on the species considered). When increasing the density, we saw that the effect for H_2CO^+ and H_2COH^+ was opposite to a pure gas-phase model, their abundances being either increased or kept constant. Through this first surprising result, we noted that **the interconnection between species is important**, and that the abundance variations of other compounds have to be taken into account to find a plausible explanation. When using the ***Nautilus*** code, it is mandatory to be careful when analyzing results related to the study of ions.

As a last step of the 3-phase study, the precursors involved in the glycine formation mechanism proposed by Woon (2002) (CO, CO_2, OH, HCOOH, CH_2NH, $CH_2NH_2{}^+$) were studied. The study of those precursors, especially the results related to CO and CO_2, showed that the results may sometimes be counter-intuitive. Being aware of the CO freeze-out phenomenon, we found that the abundance differences between models 1a and 3a were huge and unexpected. Looking closer at the chemical pathways, this was linked to a lack of destruction of JCO, but these discrepancies must be considered in the framework of the limited model that is used, as discussed in Chapter 4. For the Woon's mechanism, the work could even go a bit further than in Groyne (2023), since the network of ***Nautilus*** contains some information about the two direct precursors of glycine which are HOCO and

CH_2NH_2. However, great care must be taken when analyzing the results, knowing that the completeness of the network regarding these species is quite low.

In chapter 7, a comparison with observations was carried out. Even though the results from the gas phase were more or less in agreement with observations, it was not really the case for the solid phase. Potential explanations were proposed for the discrepancies, emphasizing the limitations of the ***Nautilus*** model. According to the work of Clément et al. (2023), we saw that a static model might not be the more relevant to reproduce interstellar ice observations. The use of a full time dependent 3D model might thus be a huge step forward to continue this work, as proposed in Chapter 9.

As a final remark, this study provided a detailed preliminary 3-phase investigation of the chemistry of several glycine precursors under simulated molecular cloud conditions, focusing on the most promising pathways identified in the literature. It highlighted that 3-phase modeling is inherently complex and results can sometimes be counter-intuitive, particularly when using a simplified framework such as the one in this thesis. Consequently, any interpretation of the results must carefully consider multiple factors: the unique properties and reactivity of each molecule, their chemical interconnections within the network, and, crucially, the limitations of the model itself. Only by acknowledging these aspects can we avoid over-interpreting the findings.

Water H_2O				
Model	Phase	Final Ab.	Formation	Destruction
Model 1a	Gas	$\sim 10^{-7}$	H_3O^+, e^-	HCO^+, H_3^+
	Surface	$\sim 10^{-6}$	swap.	swap.
	Mantle	$\sim 10^{-5}$	swap.	swap.
Model 2a	Gas	$\sim 5 \times 10^{-8}$	H_2CO, H_3O^+, e^-, JH_2, JOH	ad., H_3^+
	Surface	$\sim 10^{-6}$	swap.	swap.
	Mantle	$\sim 10^{-4}$	swap.	swap.
Model 3a	Gas	$\sim 10^{-7}$	H_3O^+, e^-	HCO^+, H_3^+
	Surface	$\sim 10^{-7}$	swap.	swap.
	Mantle	$\sim 10^{-6}$	swap.	swap.
Protonated formaldehyde H_2COH^+				
Model	Phase	Final Ab.	Formation	Destruction
Model 1a	Gas	$\sim 10^{-10}$	H_2CO, H_3^+, HCO^+, H_3O^+	e^-
Model 2a	Gas	$\sim 10^{-9}$	H_2CO, H_3^+, H_3O^+	e^-
Model 3a	Gas	$\sim 10^{-11}$	H_2CO, H_3^+, HCO^+, H_3O^+	e^-

Table 8.1: Summary of the results obtained in Chapter 6 for glycine precursors involved in the mechanisms considered in this work. *Note*: "ad." stands for adsorption, "diss." for the dissociation of the molecule and "swap." for swapping reactions.

Ammonia NH_3				
Model	Phase	Final Ab.	Formation	Destruction
Model 1a	Gas	$\sim 10^{-8}$	NH_4^+, e^-	C, HCO^+, H_3^+
	Surface	$\sim 10^{-7}$	swap.	swap.
	Mantle	$\sim 10^{-7}$	swap.	swap.
Model 2a	Gas	$\sim 10^{-8}$	NH_4^+, e^-	HCO^+, H_3^+
	Surface	$\sim 10^{-8}$	swap.	swap.
	Mantle	$\sim 10^{-6}$	swap.	swap.
Model 3a	Gas	$\sim 10^{-7}$	NH_4^+, e^-	HCO^+
	Surface	$\sim 10^{-8}$	swap.	swap.
	Mantle	$\sim 10^{-8}$	swap.	swap.
Hydrogen cyanide HCN				
Model	Phase	Final Ab.	Formation	Destruction
Model 1a	Gas	$\sim 10^{-9}$	$HCNH^+$, e^-, H, CCN, H_2CO	H_3^+, HCO^+
	Surface	$\sim 10^{-9}$	swap.	swap.
	Mantle	$\sim 10^{-8}$	swap.	swap.
Model 2a	Gas	$\sim 10^{-9}$	$HCNH^+$, e^-, JH_2, JCN, H_2CO	H_3^+, H_3O^+
	Surface	$\sim 10^{-7}$	swap.	swap.
	Mantle	$\sim 10^{-6}$	swap.	swap.
Model 3a	Gas	$\sim 10^{-9}$	$HCNH^+$, e^-	HCO^+, H_3^+
	Surface	$\sim 10^{-9}$	swap.	swap.
	Mantle	$\sim 10^{-9}$	swap.	swap.
Formaldehyde H_2CO				
Model	Phase	Final Ab.	Formation	Destruction
Model 1a	Gas	$\sim 10^{-8}$	O, CH_3, H_2COH^+, e^-,	HCO^+
	Surface	$\sim 10^{-20}$	ad., swap.	JH
	Mantle	$\sim 10^{-12}$	KH, KHCO	KH
Model 2a	Gas	$\sim 10^{-7}$	JH, JHCO, H_2COH^+, e^-	OH, H_3^+, H_3O^+
	Surface	$\sim 10^{-5}$	swap.	swap.
	Mantle	$\sim 10^{-5}$	swap.	swap.
Model 3a	Gas	$\sim 10^{-8}$	JH, JHCO, O, CH_3, H_2COH^+, e^-	OH, HCO^+
	Surface	$\sim 10^{-11}$	ad., swap.	swap., JH
	Mantle	$\sim 10^{-11}$	KH, KHCO, swap.	swap.

Table 8.1: (continued from previous page).

Cationic ammonia NH_3^+				
Model	Phase	Final Ab.	Formation	Destruction
Model 1a	Gas	$\sim 10^{-11}$	NH_2^+, H_2	H_2
Model 2a	Gas	$\sim 10^{-13}$	NH_2^+, H_2, NH_2, H_3^+	H_2
Model 3a	Gas	$\sim 10^{-10}$	NH_2^+, H_2	H_2
Cationic formaldehyde H_2CO^+				
Model	Phase	Final Ab.	Formation	Destruction
Model 1a	Gas	$\sim 10^{-10}$	HCO, H_3^+, HCO^+	e^-
Model 2a	Gas	$\sim 10^{-9}$	HCO, H_3^+, H_2CO, H^+	e^-, H_2O
Model 3a	Gas	$\sim 10^{-11}$	HCO, H_3^+, HCO^+	e^-
Protonated methanimine $CH_2NH_2^+$				
Model	Phase	Final Ab.	Formation	Destruction
Model 1a	Gas	$\sim 10^{-13}$	NH_3, CH_3^+, CH_2NH, HCO^+, H_3^+	e^-
Model 2a	Gas	$\sim 10^{-12}$	CH_3^+, CH_2NH	e^-
Model 3a	Gas	$\sim 10^{-13}$	NH_3, CH_3^+, CH_2NH, HCO^+, H_3^+	e^-
Carbon dioxide CO_2				
Model	Phase	Final Ab.	Formation	Destruction
Model 1a	Gas	$\sim 10^{-6}$	O, HCO, CO, $HOCO^+$	ad., H_3^+
	Surface	$\sim 10^{-7}$	swap.	swap.
	Mantle	$\sim 10^{-6}$	swap.	swap.
Model 2a	Gas	$\sim 10^{-8}$	JO, JCO, O, HCO	ad., H_3^+
	Surface	$\sim 10^{-8}$	swap.	swap.
	Mantle	$\sim 10^{-6}$	swap.	swap.
Model 3a	Gas	$\sim 10^{-5}$	O, HCO, JO, JCO, CO, $HOCO^+$	ad., H_3^+
	Surface	$\sim 10^{-6}$	swap.	swap.
	Mantle	$\sim 10^{-5}$	swap.	swap.

Table 8.1: (continued from previous page).

Carbon monoxide CO				
Model	Phase	Final Ab.	Formation	Destruction
Model 1a	Gas	$\sim 10^{-4}$	H, HCO, HCO^+, e^-	ad., $H_3{}^+$
	Surface	$\sim 10^{-17}$	ad.	JH
	Mantle	$\sim 10^{-12}$	KCO_2	KH
Model 2a	Gas	$\sim 10^{-6}$	H, HCO, HCO^+, e^-	ad., $H_3{}^+$
	Surface	$\sim 10^{-6}$	swap.	swap.
	Mantle	$\sim 10^{-4}$	swap.	swap.
Model 3a	Gas	$\sim 10^{-4}$	H, HCO, HCO^+, e^-	ad., $H_3{}^+$
	Surface	$\sim 10^{-6}$	ad., swap.	JH, swap.
	Mantle	$\sim 10^{-6}$	swap.	swap.
Hydroxyl radical OH				
Model	Phase	Final Ab.	Formation	Destruction
Model 1a	Gas	$\sim 10^{-6}$	H_3O^+, e^-, JH JO, H, O_2H	O
	Surface	$\sim 10^{-20}$	ad., JH_2O	JH
	Mantle	$\sim 10^{-14}$	KH_2O, KH, KO swap.	KH_2, KH
Model 2a	Gas	$\sim 10^{-8}$	H_3O^+, e^-	H_2CO, $H_3{}^+$, ad.
	Surface	$\sim 10^{-15}$	ad., JH_2O	JH_2
	Mantle	$\sim 10^{-13}$	KH_2O	KH_2
Model 3a	Gas	$\sim 10^{-6}$	H_3O^+, e^-, JH, H, JO, O_2H	O
	Surface	$\sim 10^{-20}$	ad., swap., JH_2O	JCO, JCH_4
	Mantle	$\sim 10^{-12}$	KH_2O	swap.
Formic acid HCOOH				
Model	Phase	Final Ab.	Formation	Destruction
Model 1a	Gas	$\sim 10^{-9}$	CH_3O_2, e^-	HCO^+, $H_3{}^+$
	Surface	$\sim 10^{-10}$	swap.	swap.
	Mantle	$\sim 10^{-9}$	swap.	swap.
Model 2a	Gas	$\sim 10^{-11}$	CH_3O_2, e^-	ad., $H_3{}^+$
	Surface	$\sim 10^{-11}$	swap.	swap.
	Mantle	$\sim 10^{-9}$	swap.	swap.
Model 3a	Gas	$\sim 10^{-9}$	CH_3O_2, e^-, JH, JHOCO	HCO^+, $H_3{}^+$
	Surface	$\sim 10^{-9}$	swap.	swap.
	Mantle	$\sim 10^{-9}$	swap.	swap.

Table 8.1: (continued from previous page).

Methanimine CH_2NH				
Model	Phase	Final Ab.	Formation	Destruction
Model 1a	Gas	$\sim 10^{-10}$	$CH_2NH_2^+$, $CH_3NH_3^+$, e^-	H_3^+, HCO^+
	Surface	$\sim 10^{-25}$	ad.	JH
	Mantle	$\sim 10^{-17}$	KCH_3NH_2, KH, KCH_2NH_2	KH
Model 2a	Gas	$\sim 10^{-10}$	JN, JCH_3, $CH_2NH_2^+$, e^-	ad., H_3^+
	Surface	$\sim 10^{-11}$	swap.	swap.
	Mantle	$\sim 10^{-9}$	swap.	swap.
Model 3a	Gas	$\sim 10^{-10}$	JN, JCH_3, $CH_2NH_2^+$, $CH_3NH_3^+$, e^-	H_3^+, HCO^+
	Surface	$\sim 10^{-16}$	ad., swap.	JH, swap.
	Mantle	$\sim 10^{-15}$	KCH_3NH_2, swap.	swap.
Hydrocarboxyl radical HOCO				
Model	Phase	Final Ab.	Formation	Destruction
Model 1a	Gas	$\sim 10^{-29}$	JOH, JCO	ad., diss.
	Surface	$\sim 10^{-44}$	ad.	JH, swap.
	Mantle	$\sim 10^{-45}$	swap.	KH
Model 2a	Gas	$\sim 10^{-15}$	JOH, JCO	ad.
	Surface	$\sim 10^{-16}$	swap.	swap.
	Mantle	$\sim 10^{-14}$	swap.	swap.
Model 3a	Gas	$\sim 10^{-6}$	JOH, JCO	ad., diss.
	Surface	$\sim 10^{-12}$	ad., swap.	JH, JN, swap.
	Mantle	$\sim 10^{-12}$	swap.	swap.
Aminomethyl radical CH_2NH_2				
Model	Phase	Final Ab.	Formation	Destruction
Model 1a	Gas	$\sim 10^{-14}$	JH, JCH_2NH	H, O
	Surface	$\sim 10^{-27}$	swap., ad.	JH
	Mantle	$\sim 10^{-17}$	KH, KCH_2NH	KH
Model 2a	Gas	$\sim 10^{-11}$	JH, JCH_2NH	H
	Surface	$\sim 10^{-12}$	swap.	swap.
	Mantle	$\sim 10^{-10}$	swap.	swap.
Model 3a	Gas	$\sim 10^{-13}$	JH, JCH_2NH	H, O
	Surface	$\sim 10^{-19}$	swap., ad.	swap., JH
	Mantle	$\sim 10^{-18}$	swap., KH, KCH_2NH, KNH_2CH_2OH	swap.

Table 8.1: (continued from previous page).

Chapter 9

Future perspectives

The final part of this master thesis presents some perspectives for future research based on the work carried out.

9.1 Towards more comprehensive astrochemical models

Several avenues can be explored to enhance the fidelity and scope of astrochemical models in future work. As underlined throughout this work, particularly in Chapter 7, rate equation models such as ***Nautilus*** are limited in their ability to capture the detailed behavior of grain surface chemistry and the structure of icy mantles. These models rely on mean-field approximations and are unable to represent effects such as site heterogeneity, back diffusion, or trapping of species in deeper layers of the ice. Kinetic Monte Carlo methods, especially microscopic variants, are better suited for this task because they allow for spatial resolution of surface processes and naturally account for stochasticity and site-specific dynamics. However, they are computationally intensive and have historically been restricted to smaller chemical networks. The increasing availability of high-performance computing resources and ongoing developments in efficient algorithms could make us hope that in the future, KMC models could realistically incorporate more complex networks and become a standard tool in astrochemical modeling, allowing for a better understanding of (organic) solid-phase chemistry. However, this is not sure at all regarding the complexity of such simulations. One type of improvement that seems to be very promising would be the inclusion of binding energy distributions such as proposed in Furuya (2024). Although such methods still require improvements, the work presented in the latter paper paves the way towards a method halfway between the rate-equation and KMC approaches, being computationally cheaper than KMC and at the same time more comprehensive than the rate-equation approach in capturing the complex microphysics describing grain surfaces.

One could also consider to modify ***Nautilus*** or adopting an alternative modeling tool capable of handling the chemistry of charged species, particularly cations, on grain surfaces. Indeed, current implementations typically focus on neutral species and neglect the role of electrostatic interactions and surface charge effects, which may be crucial in accurately modeling surface reactions in cold cores. However, the hypotheses presented at the beginning of Chapter 6 justify the fact that cationic species are not considered in solid-phase reactions. The most important is to capture the complexity of the microphysics at work on grain surfaces and the stochasticity of the mechanisms, with several binding sites and binding energies for each species. Adding on top of that electrostatic interactions between ions would be computationally complicated, if not unfeasible.

Finally, significant progress in the construction of chemical networks will depend on continued laboratory experiments and quantum chemical simulations. These efforts are crucial in better constraining fundamental parameters such as kinetic parameters, binding energies, activation barriers, and reaction rates under interstellar conditions. By incorporating these new data into models, it will be possible to build more realistic and comprehensive descriptions of interstellar chemistry, from the gas phase to complex grain surface and ice mantle processes.

9.2 Towards a real molecular cloud, and beyond

To improve the realism and applicability of astrochemical modeling, future efforts could aim at better reflecting the physical structure and dynamical complexity of molecular clouds. One promising direction would be to implement ***Nautilus*** in a one-dimensional (1D) configuration, allowing for spatially varying physical parameters such as temperature and density as a function of the radial distance within a cloud. Even more ambitious would be the use of fully three-dimensional (3D) models that integrate hydrodynamics or magnetohydrodynamics with chemistry. Although ***Nautilus*** in its current form does not support such 3D modeling, these more advanced frameworks would enable a more complete representation of cloud evolution, including collapse, turbulence, and heterogeneous chemical environments. These are key features in accurately reproducing observed chemical structures and abundances in molecular clouds.

Another natural extension of this work would be to go beyond cold molecular clouds and apply similar modeling strategies to more evolved or active environments, such as hot cores or protoplanetary disks. These regions present different physical conditions, including higher temperatures, UV irradiation, and denser, more complex structures. These changes profoundly impact the chemical composition, especially the formation and survival of complex organic molecules such as glycine, which was the focal point of the present study. Although such environments fall outside the scope of this work, they represent an exciting continuation of astrochemical modeling that could help trace molecular complexity from the earliest stages of star formation to planet-forming disks.

9.3 Towards more biologically relevant molecules

Finally, another possible extension of this work would be to expand the focus to include additional molecules of prebiotic interest, like other natural amino-acids. Indeed, though glycine is the most simple one, there are 19 other amino-acids playing a role in our biochemistry. Glycine is not the only one that could potentially form under some astrophysical conditions. Others, such as serine and alanine, have been firmly identified to be of extraterrestrial origins owing to studies performed on samples from the Ryugu asteroid (cf. Chapter 2). The study of Potiszil et al. (2023) has even shown that these two last amino acids can be found in an appreciable amount. Therefore, even if they have not been detected in molecular clouds, the study could extend to such simple amino acids.

In that case, one may wonder about their formation mechanisms. Regarding the Woon's mechanism, both serine and alanine could be formed in the continuity of glycine. In fact, as discussed in Woon (2002), when CH_2NH_2 and COOH recombine, the internal energy accumulated could cause the newly formed glycine to dissociate. An H atom

would be ejected, leaving the radical $NH_2CHCOOH$ behind. That radical could then simply react with CH_3, forming alanine, or with CH_2OH, forming in that case serine. One may note that both last reactants can originate from methanol photo-dissociation (Woon, 2002), making their presence highly likely in interstellar ices. Regarding the Strecker-like mechanism, one may note that, as illustrated in Figure 9.1, since the radicals R and R' are not changed by the process, **everything will depend on the nature of the initial carbonyl compound**.

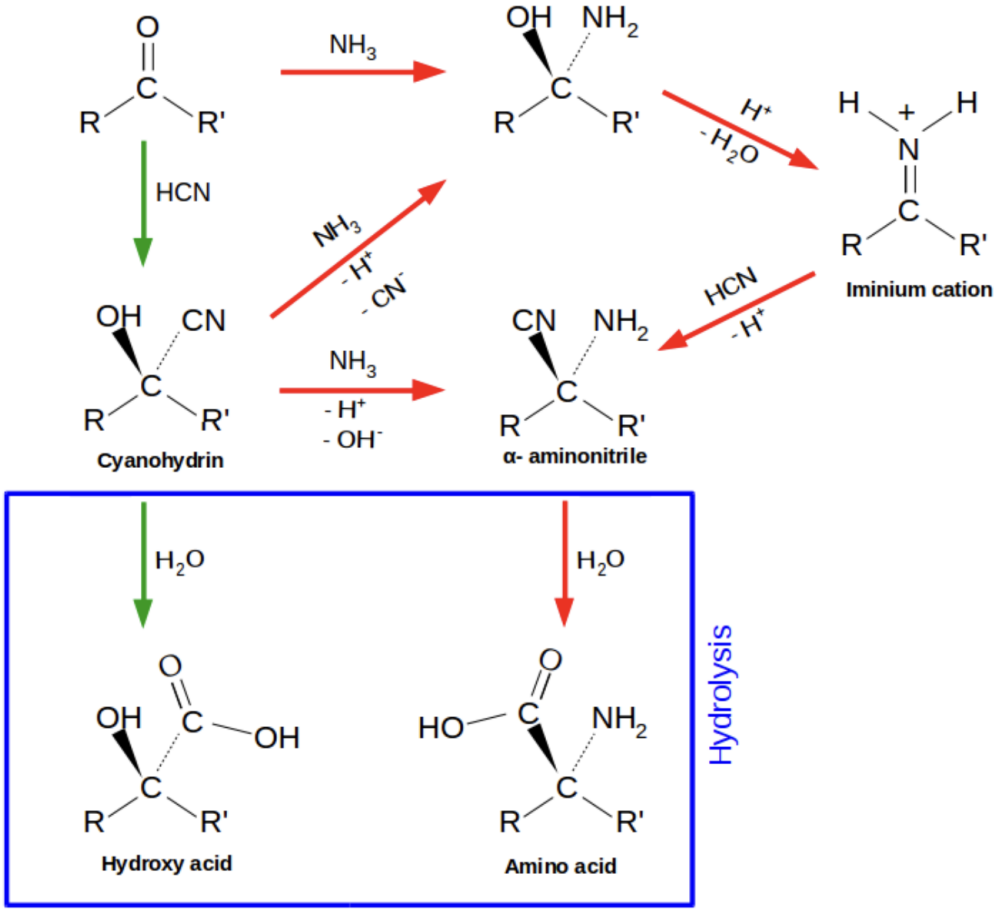

Figure 9.1: General view at the Strecker-like mechanism. From De Becker (2023-2024).

In this work, we started with the simplest precursor, i.e. formaldehyde, where R and R' are simply H atoms. However, starting with acetaldehyde (R = CH_3 and R' = H) or glycolaldehyde (R = CH_2OH and R' = H) would produce alanine and serine, respectively. Note that both CH_3 and CH_2OH have been discovered in the ISM (Gottlieb, 1973; Hollis et al., 2000). Therefore, we see that considering other precursors, being aware of the given complexity limit of our model, could constitute a promising extent for this work.

Bibliography

M. Agúndez and V. Wakelam. Chemistry of dark clouds: Databases, networks, and models. *Chemical Reviews*, 113:8710–8737, 2013.

K. Altwegg, H. Balsiger, A. Bar-Nun, J.-J. Berthelier, A. Bieler, P. Bochsler, C. Briois, U. Calmonte, M. R. Combi, H. Cottin, J. D. Keyser, F. Dhooghe, B. Fiethe, S. A. Fuselier, S. Gasc, T. I. Gombosi, K. C. Hansen, M. Haessig, A. Jäckel, E. Kopp, A. Korth, L. L. Roy, U. Mall, B. Marty, O. Mousis, T. Owen, H. Rème, M. Rubin, T. Sémon, C.-Y. Tzou, J. H. Waite, and P. Wurz. Prebiotic chemicals - amino acid and phosphorus - in the coma of comet 67P/Churyumov-Gerasimenko. *Science Advances*, 2:e1600285, 2016.

S. Andersson and E. F. van Dishoeck. Photodesorption of water ice : A molecular dynamics study. *Astronomy and Astrophysics*, 491(3):907–916, 2008.

J. C. Aponte, J. E. Elsila, D. P. Glavin, S. N. Milam, S. B. Charnley, and J. P. Dworkin. Pathways to meteoritic glycine and methylamine. *ACS Earth and Space Chemistry*, 1: 3–13, 2017.

M. Asplund, N. Grevesse, A. J. Sauval, and P. Scott. The chemical composition of the Sun. *Annual Review of Astronomy and Astrophysics*, 47:481–522, 2009.

S. Ayukawa, T. Enomoto, and D. Kiga. Chapter 6 - RNA world. In *Astrobiology: From the Origins of Life to the Search for Extraterrestrial Intelligence*, pages 77–90. Springer Singapore, 2019.

J. Babb. Chapter 1 - Gas-phase chemistry. In *Astrochemical Modeling*, pages 9–11. Elsevier, 2024.

J. L. Bada. New insights into prebiotic chemistry from Stanley Miller's spark discharge experiments. *Chemical Society reviews*, 42:2186–2196, 2013.

E. E. Barnard. On a nebulous groundwork in the constellation Taurus. *The Astrophysical Journal*, 25:218–225, 1907.

E. E. Barnard. On a great nebulous region and the question of absorbing matter in space and the transparency of the nebulae. *The Astrophysical Journal*, 31:8–14, 1910.

A. Belloche, K. M. Menten, C. Comito, H. S. P. Müller, P. Schilke, J. Ott, S. Thorwirth, and C. Hieret. Detection of amino acetonitrile in Sgr B2(N). *Astronomy and Astrophysics*, 482:179–196, 2008.

A. Belloche, F. F. Schuller, B. Parise, P. André, J. Hatchell, J. K. Jørgensen, S. Bontemps, A. Weib, K. M. Menten, and D. Muders. The end of star formation in Chamaeleon I? A LABOCA census of starless and protostellar cores. *Astronomy and Astrophysics*, 527: A145, 2011.

M. P. Bernstein, J. P. Dworkin, S. A. Sandford, G. W. Cooper, and L. J. Allamandola. Racemic amino acids from the ultraviolet photolysis of interstellar ice analogues. *Nature*, 416:401–403, 2002.

V. Blagojevic, S. Petrie, and D. K. Bohme. Microwave detection of interstellar formic acid. *Monthly Notices of the Royal Astronomical Society*, 339:L7–L11, 2003.

A. C. A. Boogert, P. A. Gerakines, and D. C. B. Whittet. Observations of the icy universe. *Annual review of astronomy and astrophysics*, 53:541–581, 2015.

H. Busemann, A. F. Young, H. Alexander, C. M. O'D. Hoppe, S. Mukhopadhyay, and L. R. Nittler. Interstellar chemistry recorded in organic matter from primitive meteorites. *Science*, 312:727–730, 2006.

J. A. Cardelli, J. S. Mathis, D. C. Ebbets, and B. D. Savage. Abundance of interstellar carbon toward ζ Ophiuchi. *The Astrophysical Journal*, 402:L17–L20, 1993.

J. A. Cardelli, U. J. Sofia, B. D. Savage, F. P. Keenan, and P. L. Dufton. Interstellar detection of the intersystem line Si II lambda 2335 toward ζ Ophiuchi. *The Astrophysical journal*, 420:L29–L32, 1994.

C. Cerf and A. Jorissen. Is amino-acid homochirality due to assymetric photolysis in space? *Space Science Reviews*, 92:603–612, 2000.

S. B. Charnley, A. G. G. M. Tielens, and S. D. Rodgers. Deuterated methanol in the Orion compact ridge. *The Astrophysical Journal*, 482(2):L203–L206, June 1997.

A. C. Cheung, D. M. Rank, C. H. Townes, D. D. Thornton, and W. J. Welch. Detection of NH_3 molecules in the interstellar medium by their microwave emission. *Physical Review Letters*, 21:1701–1705, 1968.

A. C. Cheung, D. M. Rank, C. H. Townes, D. D. Thornton, and W. J. Welch. Detection of water in interstellar regions by its microwave radiation. *Nature*, 221:626–628, 1969.

A. Clément, A. Taillard, V. Wakelam, P. Gratier, J.-C. Loison, E. Dartois, F. Dulieu, J. A. Noble, and M. Chabot. Astrochemical models of interstellar ices: History matters. *Astronomy and Astrophysics*, 675:A165, 2023.

L. Colzi, O. Sipilä, E. Roueff, P. Caselli, and F. Fontani. Carbon isotopic fractionation in molecular clouds. *Astronomy and Astrophysics*, 640:A51, 2020.

G. Crinklaw, S. R. Federman, and C. L. Joseph. The depletion of calcium in the interstellar medium. *The Astrophysical Journal*, 424:748–753, 1994.

J. R. Cronin and S. Chang. Organic matter in meteorites: Molecular and isotopic analyses of the Murchison meteorite. In *The Chemistry of Life's Origins*, pages 209–258. Springer Netherlands, 1993.

H. Cuppen, C. Walsh, T. Lamberts, D. Semenov, R. T. Garrod, E. M. Penteado, and S. Ioppolo. Grain surface models and data for astrochemistry. *Space Science Reviews*, 212:1–58, 2017.

H. M. Cuppen and E. Herbst. Simulation of the formation and morphology of ice mantles on interstellar grains. *The Astrophysical Journal*, 668(1):294–309, 2007.

H. M. Cuppen, L. J. Karssemeijer, and T. Lamberts. The kinetic Monte Carlo method as a way to solve the master equation for interstellar grain chemistry. *Chemical Reviews*, 113:8840–8871, 2013.

H. M. Cuppen, J. A. Noble, S. Coussan, B. Redlich, and S. Ioppolo. Energy transfer and restructuring in amorphous solid water upon consecutive irradiation. *Journal of Physical Chemistry*, 126:8859–8870, 2022.

E. Dartois, J. A. Noble, P. Caselli, H. J. Fraser, I. Jiménez-Serra, B. Maté, M. K. McClure, G. J. Melnick, Y. J. Pendleton, T. Shimonishi, Z. L. Smith, J. A. Sturm, A. Taillard, V. Wakelam, A. C. A. Boogert, M. N. Drozdovskaya, J. Erkal, D. Harsono, V. J. Herrero, S. Ioppolo, H. Linnartz, B. A. McGuire, G. Perotti, D. Qasim, and W. R. M. Rocha. Spectroscopic sizing of interstellar icy grains with JWST. *Nature Astronomy*, 8:359–367, 2024.

M. De Becker. Astrochemistry: The issue of molecular complexity in astrochemical environments. *Bulletin de la Société Royale des Sciences de Liège*, 82:33–94, 2013.

M. De Becker. *Astrochemistry, Lecture Notes*. University of Liège, 2023-2024.

L. B. D'Hendecourt and M. Jourdain de Muizon. The discovery of interstellar carbon dioxide. *Astronomy and Astrophysics*, 223:L5–L8, 1989.

J. E. Dickens, W. M. Irvine, C. H. DeVries, and M. Ohishi. Hydrogenation of interstellar molecules: A survey for methylenimine (CH_2NH). *The Astrophysical Journal*, 479(1): 307, 1997.

J. E. Dickens, W. M. Irvine, R. L. Snell, E. A. Bergin, F. P. Schloerb, P. Pratap, and M. P. Miralles. A study of the physics and chemistry of L134N. *The Astrophysical Journal*, 542(2):870, 2000.

B. T. Draine. *Physics Of The Interstellar And Intergalactic Medium*. Princeton University press, 2011.

B. T. Draine and B. Sutin. Collisional charging of interstellar grains. *The Astrophysical Journal*, 320:803–817, 1987.

D. Duflot, C. Toubin, and M. Monerville. Theoretical determination of binding energies of small molecules on interstellar ice surfaces. *Frontiers in Astronomy and Space Sciences*, 8, 2021.

D. D. Eley and E. K. Rideal. Parahydrogen conversion on tungsten. *Nature*, 146:401–402, 1940.

J. E. Elsila, D. P. Glavin, and J. P. Dworkin. Cometary glycine detected in samples returned by Stardust. *Cometary and Planetary Science*, 44:1323–1330, 2007.

N. J. Evans and M. L. Kutner. H_2CO emission at 2 millimeters in dark clouds. *The Astrophysical Journal*, 204:L131–L134, 1976.

S. R. Federman, Y. Sheffer, D. L. Lambert, and R. L. Gilliland. Detection of boron, cobalt, and other weak interstellar lines toward ζ Ophiuchi. *The Astrophysical Journal*, 413: L51–L54, 1993.

S. Ferrero, L. Zamirri, C. Ceccarelli, A. Witzel, A. Rimola, and P. Ugliengo. Binding energies of interstellar molecules on crystalline and amorphous models of water ice by ab initio calculations. *The Astrophysical Journal*, 904:11, 2020.

M. Ferus, D. Nesvorny, J. Sponer, P. Kubelik, R. Michalcikova, V. Shestivska, J. E. Sponer, and S. Cvis. High-energy chemistry of formamide: A unified mechanism of nucleobase formation. *Proceedings of the National Academy of Sciences*, 112(3):657–662, 2014.

A. Fredon, G. C. Groenenboom, and H. M. Cuppen. Molecular dynamics simulations of energy dissipation on amorphous solid water: Testing the validity of equipartition. *ACS Earth and Space Chemistry*, 5:2032–2041, 2021a.

A. Fredon, A. K. Radchenko, and H. M. Cuppen. Quantification of the role of chemical desorption in molecular clouds. *Accounts of Chemical Research*, 54:745–753, 2021b.

N. Fujii. D-amino acids in living higher organisms. *Origins of life and evolution of the biosphere*, 32:103–127, 2002.

D. Fujun. Chempl: a playable package for modeling interstellar chemistry. *Research in Astronomy and Astrophysics*, 21(3):77, 2021.

Y. Furukawa, Y. Chikaraishi, N. Ohkouchi, N. Ogawa, D. Glavin, J. Dworkin, C. Abe, and T. Nakamura. Extraterrestrial ribose and other sugars in primitive meteorites. *Proceedings of the National Academy of Sciences*, 116(49):24440–24445, 2019.

K. Furuya. A framework for incorporating binding energy distribution in gas-ice astrochemical models. *The Astrophysical Journal*, 974:115–136, 2024.

R. T. Garrod. A three-phase chemical model of hot cores: The formation of glycine. *The Astrophysical Journal*, 765:60, 2013.

R. T. Garrod, V. Wakelama, and E. Herbst. Non-thermal desorption from interstellar dust grains via exothermic surface reactions. *Astronomy and Astrophysics*, 467:1103–1115, 2007.

R. T. Garrod, S. L. Widicius Weaver, and E. Herbst. Complex chemistry in star-forming regions: An expanded gas-grain warm-up chemical model. *The Astrophysical Journal*, 682:283–302, 2008.

L. A. J. Garvie and P. R. Buseck. Prebiotic carbon in clays from Orgueil and Ivuna (CI), and Tagish lake (C2 ungrouped) meteorites. *Meteoritics and Planetary Science*, 42(12): 2111–2117, 2007.

G. Genchi. An overview on D-amino acids. *Amino Acids*, 49:1521–1533, 2017.

W. Gilbert. Origin of life: The RNA world. *Nature*, 319:618, 1986.

F. C. Gillett and W. J. Forrest. Spectra of the Becklin-Neugebauer point source and the Kleinmann-Low nebula from 2.8 to 13.5 microns. *The Astrophysical Journal*, 179:483, 1973.

P. D. Godfrey, R. D. Brown, B. J. Robinson, and M. W. Sinclair. Discovery of interstellar methanimine (formaldimine). *Astrophysical Letters*, 13:119, 1973.

C. A. Gottlieb. Detection of Acetaldehyde in Sagittarius. In M. A. Gordon and L. E. Snyder, editors, *Molecules in the Galactic Environment*, page 181, 1973.

C. A. Gottlieb, C. J. Lada, E. W. Gottlieb, A. E. Lilley, and M. M. Litvak. Observations of millimeter-wave HCN in four prototype clouds. *The Astrophysical Journal*, 202:655–672, 1975.

D. M. Graninger, E. Herbst, K. I. Öberg, and A. I. Vasyunin. The HNC/HCN ratio in star-forming regions. *The Astrophysical Journal*, 787:74, 2014.

F. Grieco, F. Dulieu, I. De Looze, and S. Baouche. Experimental H_2O formation on carbonaceous dust grains at temperatures up to 85 K. *Monthly Notices of the Royal Astronomical Society*, 527:10604–10614, 2024.

M. Groyne. Astrochemical pathways for the synthesis of amino-acids in interstellar clouds. Master's thesis, University of Liège, 2023.

M. Groyne, B. Champagne, C. Baijot, and M. De Becker. Robust binding energy distribution sampling on amorphous solid water models. method testing and validation with NH_3, CO and CH_4. 2025.

K. Hadraoui, H. Cottin, S. L. Ivanovski, P. Zapf, K. Altwegg, Y. Benilan, N. Biver, V. Della Corte, N. Fray, J. Lasue, S. Merouane, A. Rotundi, and V. Zakharov. Distributed glycine in comet 67P/Churyumov-Gerasimenko. *Astronomy and Astrophysics*, 630:A32, 2019.

J. S. Hall. Observations of the polarized light from stars. *Science*, 109:166–167, 1949.

J. Harris and B. Kasemo. On precursor mechanisms for surface reactions. *Surface Science*, 105:L281–L287, 1981.

T. I. Hasegawa and E. Herbst. Models of gas-grain chemistry in dense interstellar clouds with complex organic molecules. *The Astrophysical Journal Supplement Series (ISSN 0067-0049)*, 82(1):167–195, 1992.

E. Herbst and W. Klemperer. The formation and depletion of molecules in dense interstellar clouds. *The Astrophysical Journal*, 185:505–534, 1973.

J. Holdship, S. Viti, I. Jiménez-Serra, A. Makrymallis, and F. Priestley. UCLCHEM: A gas-grain chemical code for clouds, cores, and C-shocks. *The Astrophysical Journal*, 154 (1):38, 2017.

J. M. Hollis, F. J. Lovas, and P. R. Jewell. Interstellar glycolaldehyde: The first sugar. *The Astrophysical Journal*, 540(2):L107–L110, 2000.

E. Iglesias. The chemical evolution of molecular clouds. *The Astrophysical Journal*, 218: 697–715, 1977.

N. Indriolo and B. J. McCall. Cosmic-ray astrochemistry. *Chemical Society Reviews*, 42: 7763–7773, 2013.

S. Ioppolo, G. Fedoseev, K.-J. Chuang, H. M. Cuppen, A. R. Clements, M. Jin, R. T. Garrod, D. Quasim, V. Kofman, E. F. van Dishoeck, and H. Linnartz. A non-energetic mechanism for glycine formation in the interstellar medium. *Nature Astronomy*, 5: 197–205, 2021.

A. V. Ivlev, M. Padovani, D. Galli, and P. Caselli. Interstellar dust charging in dense molecular clouds: Cosmic ray effects. *The Astrophysical Journal*, 812(2):135, 2015.

E. B. Jenkins. A unified representation of gas-phase elements depletions in the interstellar medium. *The Astrophysical Journal*, 700:1299–1348, 2009.

I. Jiménez-Serra, A. Megías, J. Salaris, H. Cuppen, A. Taillard, M. Jin, V. Wakelam, A. I. Vasyunin, P. Caselli, Y. J. Pendleton, E. Dartois, J. A. Noble, S. Viti, K. Borshcheva, R. T. Garrod, T. Lamberts, H. Fraser, G. Melnick, M. McClure, W. Rocha, M. N. Drozdovskaya, and D. C. Lis. Modelling methanol and hydride formation in the JWST Ice Age era. *Astronomy and Astrophysics*, 695:A247, 2025.

A. Jorissen and C. Cerf. Asymmetric photoreactions as the origin of biomolecular homochirality: A critical review. *Origins of Life and Evolution of the Biosphere*, 32:129–142, 2002.

N. Kaifu, M. Morimoto, K. Nagane, K. Akabane, T. Iguchi, and K. Takagi. Detection of interstellar methylamine. *The Astrophysical Journal*, 191:L135–L137, 1974.

M. Kayanuma, K. Kidachi, M. Shoji, Y. Komatsu, A. Sato, Y. Shigeta, Y. Aikawa, and M. Umemura. A theoretical study of the formation of glycine via hydantoin intermediate in outer space environment. *Chemical Physics Letters*, 687:178–183, 2017.

T. Koga and H. Naraoka. A new family of extraterrestrial amino acids in the Murchison meteorite. *Scientific reports*, 7:636, 2017.

A. Kouchi, M. Tsuge, T. Hama, H. Niinomi, N. Nakatani, T. Shimonishi, Y. Oba, Y. Kimura, S.-I. Sirono, S. Okuzumi, M. Momose, K. Furuya, and N. Watanabe. Formation of chiral CO polyhedral crystals on icy interstellar grains. *Monthly Notices of the Royal Astronomical Society*, 505:1530–1542, 2021a.

A. Kouchi, M. Tsuge, T. Hama, Y. Oba, S. Okuzumi, S.-I. Sirono, M. Momose, N. Nakatani, K. Furuya, T. Shimonishi, T. Yamazaki, H. Hidaka, Y. Kimura, K.-I. Murata, K. Fujita, S. Nakatsubo, S. Tachibana, and N. Watanabe. Transmission electron microscopy study of the morphology of ices composed of H_2O, CO_2, and CO on refractory grains. *The Astrophysical Journal*, 918(2):45, 2021b.

Y.-J. Kuan, S. B. Charnley, H.-C. Huang, W.-L. Tseng, and Z. Kisiel. Interstellar glycine. *The Astrophysical Journal*, 593(2):848–867, 2003.

K. Kvenvolden, J. Lawless, K. Pering, E. Peterson, J. Flores, C. Ponnamperuma, K. I. R., and C. Moore. Evidence ofr extraterrestrial amino-acids and hydrocarbons in the Murchison meteorite. *Nature*, 228:923–926, 1970.

J. H. Lacy, H. Faraji, S. A. Sandford, and L. J. Allamandola. Unraveling the 10 micron 'silicate' feature of protostars: The detection of frozen interstellar ammonia. *The Astrophysical Journal*, 501:L105–L109, 1998.

J. G. Lawless. Amino acids in the Murchison meteorite. *Geochimica et Cosmochimica Acta*, 37(9):2207–2212, 1973.

C. Le Guillou, S. Bernad, and L. Brearley, A. et Remusat. Evolution of organic matter in Orgueil, Murchison and Renazzo during parent body aqueous alteration: *In situ* investigations. *Geochimica et Cosmochimica Acta*, 131:368–392, 2014.

H. S. Liszt, R. W. Wilson, A. A. Penzias, K. B. Jefferts, P. G. Wannier, and P. M. Solomon. CO and CS in the Orion nebula. *The Astrophysical Journal*, 190:557–564, 1974.

H. Luthra, V. Wakelam, M. K. Sharma, and S. Chandra. Predictions of gas-phase methanimine (CH_2NH) abundance in cold cores. *Monthly Notices of the Royal Astronomical Society*, 521:2181–2186, 2023.

S. Maret and E. A. Bergin. Astrochem: abundances of chemical species in the interstellar medium. *Astrophysics Source Code Library*, 2015.

Z. Martins, O. Botta, M. L. Fogel, M. A. Sephton, D. P. Glavin, J. S. Watson, J. P. Dworkin, A. W. Schwartz, and P. Ehrenfreund. Extraterrestrial nucleobases in the Murchison meteorite. *Earth and Planetary Science Letters*, 270:130–136, 2008.

J. S. Mathis, W. Rumpl, and K. H. Nordsieck. The size distribution of interstellar grains. *The Astrophysical Journal*, 217:425–433, 1977.

M. K. McClure, W. R. M. Rocha, K. M. Pontoppidan, N. Crouzet, L. E. U. Chu, E. Dartois, T. Lamberts, J. A. Noble, Y. J. Pendleton, G. Perotti, D. Qasim, M. G. Rachid, Z. L. Smith, F. Sun, T. L. Beck, A. C. A. Boogert, W. A. Brown, P. Caselli, S. B. Charnley, H. M. Cuppen, H. Dickinson, M. N. Drozdovskaya, E. Egami, J. Erkal, H. Fraser, R. T. Garrod, D. Harsono, S. Ioppolo, I. Jiménez-Serra, M. Jin, J. K. Jørgensen, L. E. Kristensen, D. C. Lis, M. R. S. McCoustra, B. A. McGuire, G. J. Melnick, K. I. Öberg, M. E. Palumbo, T. Shimonishi, J. A. Sturm, E. F. van Dishoeck, and H. Linnartz. An Ice Age JWST inventory of dense molecular cloud ices. *Nature Astronomy*, 7:431–443, 2023.

S. L. Miller. A production of amino acids under possible primitive Earth conditions. *Science*, 117:528–529, 1953.

S. L. Miller and H. C. Urey. Organic compound synthesis on the primitive Earth: Several questions about the origin of life have been answered, but much remains to be studied. *Science*, 130:245–251, 1959.

B. Mil'man. A complexity measure for chemical compounds. *Journal of Structural Chemistry*, 29:957–960, 1989.

M. Minissale, F. Dulieu, S. Cazaux, and S. Hocuk. Dust as interstellar catalyst I. quantifying the chemical desorption process. *Astronomy and Astrophysics*, 585:A24, 2016.

M. Minissale, Y. Aikawa, E. Bergin, M. Bertin, W. A. Brown, S. Cazaux, S. B. Charnley, A. Coutens, H. M. Cuppen, V. Guzman, H. Linnartz, M. R. S. McCoustra, A. Rimola, J. G. M. Schrauwen, C. Toubin, P. Ugliengo, N. Watanabe, V. Wakelam, and F. Dulieu. Thermal desorption of interstellar ices: A review on the controlling parameters and their implications from snowlines to chemical complexity. *ACS Earth and Space Chemistry*, 6(3):597–630, 2022.

M. Morris, B. Zuckerman, P. Palmer, and B. E. Turner. Interstellar ammonia. *The Astrophysical Journal*, 186:501–528, 1973.

D. C. Morton. Interstellar absorption lines in the spectrum of ζ Ophiuchi. *The Astrophysical Journal*, 197:85–115, 1975.

H. Naraoka, Y. Takano, J. P. Dworkin, Y. Oba, K. Hamase, A. Furusho, N. O. Ogawa, M. Hashiguchi, K. Fukushima, D. Aoki, P. Schmitt-Kopplin, J. C. Aponte, E. T. Parker, D. P. Glavin, H. L. McLain, J. E. Elsila, H. V. Graham, J. M. Eiler, F.-R. Orthous-Daunay, C. Wolters, J. Isa, V. Vuitton, R. Thissen, S. Sakai, T. Yoshimura, T. Koga, N. Ohkouchi, Y. Chikaraishi, H. Sugahara, H. Mita, Y. Furukawa, N. Hertkorn, A. Ruf, H. Yurimoto, T. Nakamura, T. Noguchi, R. Okazaki, H. Yabuta, K. Sakamoto, S. Tachibana, H. C. Connolly, D. S. Lauretta, M. Abe, T. Yada, M. Nishimura, K. Yogata, A. Nakato, M. Yoshitake, A. Suzuki, A. Miyazaki, S. Furuya, K. Hatakeda, H. Soejima, Y. Hitomi, K. Kumagai, T. Usui, T. Hayashi, D. Yamamoto, R. Fukai, K. Kitazato, S. Sugita, N. Namiki, M. Arakawa, H. Ikeda, M. Ishiguro, N. Hirata, K. Wada, Y. Ishihara, R. Noguchi, T. Morota, N. Sakatani, K. Matsumoto, H. Senshu, R. Honda, E. Tatsumi, Y. Yokota, C. Honda, T. Michikami, M. Matsuoka, A. Miura, H. Noda, T. Yamada, K. Yoshihara, K. Kawahara, M. Ozaki, Y. ichi Iijima, H. Yano, M. Hayakawa, T. Iwata, R. Tsukizaki, H. Sawada, S. Hosoda, K. Ogawa, C. Okamoto, N. Hirata, K. Shirai, Y. Shimaki, M. Yamada, T. Okada, Y. Yamamoto, H. Takeuchi, A. Fujii, Y. Takei, K. Yoshikawa, Y. Mimasu, G. Ono, N. Ogawa, S. Kikuchi, S. Nakazawa, F. Terui, S. Tanaka, T. Saiki, M. Yoshikawa, S. ichiro Watanabe, and Y. Tsuda. Soluble organic molecules in samples of the carbonaceous asteroid (162173) Ryugu. *Science*, 379(6634): eabn9033, 2023.

D. A. Neufeld and M. G. Wolfire. The cosmic-ray ionization rate in the galactic disk, as determined from observations of molecular ions. *The Astrophysical Journal*, 835:163, 2017.

M. Ohishi and N. Kaifu. Chemical and physical evolution of dark clouds molecular spectral line survey toward TMC-1. *Faraday Discussions*, 109:205–216, 1998.

M. Ohishi, S.-I. Ishikawa, T. Amano, H. Oka, W. M. Irvine, J. E. Dickens, L. M. Ziurys, and A. J. Apponi. Detection of a new interstellar molecular ion, H_2COH^+ (protonated formaldehyde). *The Astrophysical Journal Letters*, 471:L161, 1986.

M. Ohishi, W. M. Irvine, and N. Kaifu. Molecular abundance variations among and within cold, dark molecular clouds. *Symposium - International Astronomical Union*, 150, Astrochemistry of Cosmic Phenomena:171–178, 1992.

L. Pagani, J. Steinacker, A. Bacmann, A. Stutz, and T. Henning. The ubiquity of micrometer-sized dust grains in the dense interstellar medium. *Science*, 329:1622–1624, 2010.

E. M. Penteado, A. C. A. Boogert, K. M. Pontoppidan, S. Ioppolo, G. A. G. A. Blake, and H. M. Cuppen. Spectroscopic constraints on CH_3OH formation: CO mixed with CH_3OH ices towards young stellar objects. *Monthly Notices of the Royal Astronomical Society*, 454:531–540, 2015.

S. Pizzarello, R. Krishnamurthy, S. Epstein, and J. Cronin. Isotopic analyses of amino acids from the Murchison meteorite. *Geochimica et Cosmochimica Acta*, 55(3):905–910, 1991.

A. Potapov and M. McCoustra. Physics and chemistry on the surface of cosmic dust grains: A laboratory view. *International Reviews in Physical Chemistry*, 40:299–364, 2021.

C. Potiszil, T. Ota, M. Yamanaka, C. Sakaguchi, K. Kobayashi, R. Tanaka, T. Kunihiro, H. Kitagawa, M. Abe, A. Miyazaki, A. Nakato, S. Nakazawa, M. Nishimura, T. Okada, T. Saiki, S. Tanaka, F. Terui, Y. Tsuda, T. Usui, S.-I. Watanabe, T. Yada, K. Yogata, M. Yoshikawa, and E. Nakamura. Insights into the formation and evolution of extraterrestrial amino acids from the asteroid Ryugu. *Nature communications*, 15:1482, 2023.

S. S. Prasad and W. T. J. Huntress. A model for gas phase chemistry in interstellar clouds. I - The basic model, library of chemical reactions, and chemistry among C, N, and O compounds. *The Astrophysical Journal Supplement Series*, 43:1–35, 1980a.

S. S. Prasad and W. T. J. Huntress. A model for gas phase chemistry in interstellar clouds. II - Nonequilibrium effects and effects of temperature and activation energies. *The Astrophysical Journal*, 239:151–165, 1980b.

S. S. Prasad and S. P. Tarafdar. UV radiation field inside dense clouds - Its possible existence and chemical implications. *The Astrophysical Journal*, 267:603–609, 1983.

P. Pratap, J. E. Dickens, R. L. Snell, M. P. Miralles, E. A. Bergin, W. M. Irvine, and F. P. Schloerb. A study of the physics and chemistry of TMC-1. *The Astrophysical Journal*, 486(2):862, 1997.

D. Qasim, K.-J. Chuang, G. Fedoseev, S. Ioppolo, A. C. A. Boogert, and H. Linnartz. Formation of interstellar methanol ice prior to the heavy CO freeze-out stage. *Astronomy and Astrophysics*, 612:A83, 2018.

L. Remusat. Organic material in meteorites and the link to the origin of life. *BIO Web of Conferences*, 2:03001, 2014.

D. R. Reynolds. Chapter 3 - Time-dependent integration of chemical networks. In *Astrochemical Modeling*, pages 31–68. Elsevier, 2024.

A. Rimola, M. Sodupe, and P. Ugliengo. Deep-space glycine formation via Strecker-type reactions activated by ice water dust mantles. A computational approach. *Physical Chemistry Chemical Physics*, 12:5285–5294, 2010.

A. Rimola, M. Sodupe, and P. Ugliengo. Computational study of interstellar glycine formation occurring at radical surfaces of water-ice dust particles. *The Astrophysical Journal*, 741(1):24, 2012.

V. M. Rivilla, M. Sanz-Novo, I. Jiménez-Serra, J. Martín-Pintado, L. Colzi, S. Zeng, A. Megías, Á. López-Gallifa, A. Martínez-Henares, S. Massalkhi, B. Tercero, P. de Vicente, S. Martín, D. San Andrés, M. A. Requena-Torres, and J. L. Alonso. First glycine isomer detected in the interstellar medium: Glycolamide ($NH_2C(O)CH_2OH$). *Astrophysical Journal letters*, 953(2):L20, 2023.

H. Roberts and E. Herbst. The abundance of gaseous H2$OandO_2$ in cores of dense interstellar clouds. *Astronomy and Astrophysics*, 395:233–242, 2002.

W. R. M. Rocha, E. F. van Dishoeck, M. E. Ressler, M. L. van Gelder, K. Slavicinska, N. G. C. Brunken, H. Linnartz, T. P. Ray, H. Beuther, A. Caratti o Garatti, V. Geers, P. J. Kavanagh, P. D. Klaassen, K. Justtanont, Y. Chen, L. Francis, C. Gieser, G. Perotti, Ł. Tychoniec, M. Barsony, L. Majumdar, V. J. M. le Gouellec, L. E. U. Chu, B. W. P. Lew, T. Henning, and G. Wright. JWST observations of young protostars

(JOYS+): Detecting icy complex organic molecules and ions. I. CH_4, SO_2, $HCOO^-$, OCN^-, H_2CO, HCOOH, CH_3CH_2OH, CH_3CHO, CH_3OCHO, and CH_3COOH. *Astronomy and Astrophysics*, 683:A124, 2024.

M. Ruaud, V. Wakelam, and F. Hersant. Gas and grain chemical composition in cold cores as predicted by the Nautilus three-phase model. *Monthly Notices of the Royal Astronomical Society*, 459:3756–3767, 2016.

S. A. Sandford, J. Aléon, C. M. O. Alexander, T. Araki, S. Bajt, G. A. Baratta, J. Borg, J. P. Bradley, D. E. Brownlee, J. R. Brucato, M. J. Burchell, H. Busemann, A. Butterworth, S. J. Clemett, G. Cody, L. Colangeli, G. Cooper, L. D'Hendecourt, Z. Djouadi, J. P. Dworkin, G. Ferrini, H. Fleckenstein, G. J. Flynn, I. A. Franchi, M. Fries, M. K. Gilles, D. P. Glavin, M. Gounelle, F. Grossemy, C. Jacobsen, L. P. Keller, A. L. D. Kilcoyne, J. Leitner, G. Matrajt, A. Meibom, V. Mennella, S. Mostefaoui, L. R. Nittler, M. E. Palumbo, D. A. Papanastassiou, F. Robert, A. Rotundi, C. J. Snead, M. K. Spencer, F. J. Stadermann, A. Steele, T. Stephan, P. Tsou, T. Tyliszczak, A. J. Westphal, S. Wirick, B. Wopenka, H. Yabuta, R. N. Zare, and M. E. Zolensky. Organics captured from comet 81P/Wild 2 by the Stardust spacecraft. *Science*, 314(5806):1720–1724, 2006.

A. Sato, Y. Kitazawa, T. Ochi, M. Shoji, Y. Komatsu, M. Kayanuma, Y. Aikawa, M. Umemura, and Y. Shigeta. First-principles study of the formation of glycine-producing radicals from common interstellar species. *Molecular Astrophysics*, 10:11–19, 2018.

B. D. Savage, J. A. Cardelli, and U. J. Sofia. Ultraviolet observations of the gas phase abundances in the diffuse clouds toward ζ Ophiuchi at 3.5 kilometers per second resolution. *The Astrophysical Journal*, 401:706–723, 1992.

S. Seager, W. Bains, and R. Hu. A biomass-based model to estimate the plausibility of exoplanet biosignature gases. *The Astrophysical Journal*, 775(2):104–132, 2013.

S. Seager, W. Bains, and J. Petkowski. Toward a list of molecules as potential biosignature gases for the search for life on exoplanets and applications to terrestrial biochemistry. *Astrobiology*, 36(6):465–485, 2016.

C. N. Shingledecker, S. Vogt-Geisse, D. V. Mifsud, and S. Ioppolo. Chapter 4 - Chemistry on interstellar dust grains. In *Astrochemical Modeling*, pages 71–115. Elsevier, 2024.

O. Sipilä and M. Ruaud. Chapter 2 - Designing a gas-phase chemical network. In *Astrochemical Modeling*, pages 13–29. Elsevier, 2024.

Z. L. Smith, H. J. Dickinson, H. J. Fraser, M. K. McClure, J. A. Noble, A. C. A. Boogert, F. Sun, E. Egami, E. Dartois, J. Erkal, T. Shimonishi, T. L. Beck, J. B. Bergner, P. Caselli, S. B. Charnley, L. Chu, M. N. Drozdovskaya, R. Garrod, D. Harsono, S. Ioppolo, I. Jimenez-Serra, J. K. Jørgensen, G. J. Melnick, K. I. Öberg, M. E. Palumbo, Y. J. Pendleton, G. Perotti, K. M. Pontoppidan, D. Qasim, W. R. M. Rocha, J. A. Sturm, A. Taillard, U. R. G., and E. F. van Dishoeck. Cospatial ice mapping of H_2O with CO_2 and CO across a molecular cloud with JWST/NIRCam. *Nature astronomy*, 2025.

R. L. Snell, J. E. Howe, M. L. N. Ashby, E. A. Bergin, G. Chin, N. R. Erickson, P. F. Goldsmith, M. Harwit, S. C. Kleiner, D. G. Koch, D. A. Neufeld, B. M. Patten, R. Plume,

R. Schieder, J. R. Stauffer, V. Tolls, Z. Wang, G. Winnewisser, Y. F. Zhang, and G. J. Melnick. Water abundance in molecular cloud cores. *The Astrophysical Journal*, 539 (2):L101, 2000.

L. E. Snyder and D. Buhl. Observations of radio emission from interstellar hydrogen cyanide. *The Astrophysical Journal*, 163:L147, 1971.

L. E. Snyder and D. Buhl. Detection of several new interstellar molecules. *Annals of the New York Academy of Sciences*, 194:17–24, 1972.

L. E. Snyder, D. Buhl, B. Zuckerman, and P. Palmer. Microwave detection of interstellar formaldehyde. *Physical Review Letters*, 22:679–681, 1969.

L. E. Snyder, F. J. Lovas, J. M. Hollis, D. N. Friedel, P. R. Jewell, A. Remijan, V. V. Ilyushin, E. A. Alekseev, and S. F. Dyubko. A rigorous attempt to verify interstellar glycine. *The Astrophysical Journal*, 619:914–930, 2005.

D. A. Swade. The physics and chemistry of the L134N molecular core. *The Astrophysical Journal*, 345:828–852, 1989.

P. Swings and L. Rosenfeld. Considerations regarding interstellar molecules. *The Astrophysical Journal*, 86:483–486, 1937.

P. Thaddeus, M. Guelin, and R. A. Linke. Three new 'nonterrestrial' molecules. *The Astrophysical Journal, Part 2 - Letters to the Editor*, 246:L41–L45, 1981.

A. G. G. M. Tielens. *The Physics and Chemistry of the Interstellar Medium*. Cambridge University Press, 2005.

A. G. G. M. Tielens. Interstellar polycyclic aromatic hydrocarbon molecules. *The Annual Review of Astronomy and Astrophysics*, 46:289–337, 2008.

A. G. G. M. Tielens and W. Hagen. Model calculations of the molecular composition of interstellar grain mantles. *Astronomy and Astrophysics*, 114(2):245–260, 1986.

A. G. G. M. Tielens and D. Hollenbach. Photodissociation regions, I. Basic model. *The Astrophysical Journal*, 291:722–746, 1985a.

A. G. G. M. Tielens and D. Hollenbach. Photodissociation regions, II. A model for the Orion photodissociation region. *The Astrophysical Journal*, 291:747–754, 1985b.

L. Tinacci, A. Germain, S. Pantaleone, S. Ferrero, C. Ceccarelli, and P. Ugliengo. Theoretical distribution of the ammonia binding energy at interstellar icy grains: A new computational framework. *ACS Earth and Space Chemistry*, 6:1514–1526, 2022.

R. J. Trumpler. Absorption of light in the galactic system. *Publications of the Astronomical Society of the Pacific*, 42:214–227, 1930.

M. Tsuge and N. Watanabe. Radical reactions on interstellar icy dust grains: Experimental investigations of elementary processes. *Proceedings of the Japan Academy, Series B, Physical and Biological Sciences*, 99:103–130, 2023.

A. I. Vasyunin, D. A. Semenov, D. S. Wiebe, and T. Henning. A unified Monte Carlo treatment of gas–grain chemistry for large reaction networks. I. Testing validity of rate equations in molecular clouds. *The Astrophysical Journal*, 691:1459–1469, 2009.

R. Visser, E. F. van Dishoeck, and J. H. Black. The photodissociation and chemistry of CO isotopologues: Applications to interstellar clouds and circumstellar disks. *Astronomy and Astrophysics*, 503(2):323–343, 2009.

M. S. Väisälä, J. Harju, M. J. Mantere, O. Miettinen, R. S. Sault, C. M. Walmsley, and J. B. Whiteoak. High-resolution ammonia mapping of the very young protostellar core chamaeleon-MMS1. *Astronomy and Astrophysics*, 564:A99, 2014.

V. Wakelam. KIDA: A kinetic database for astrochemistry. *Bulletin of the American Astronomical Society*, 41:665, 2009.

V. Wakelam, E. Bron, S. Cazaux, F. Dulieu, C. Gry, P. Guillard, E. Habart, L. Hornekær, S. Morisset, G. Nyman, V. Pirronello, S. D. Price, V. Valdivia, G. Vidali, and N. Watanabe. H_2 formation on interstellar dust grains: The viewpoints of theory, experiments, models and observations. *Molecular Astrophysics*, 9:1–36, 2017a.

V. Wakelam, J. C. Loison, R. Mereau, and M. Ruaud. Binding energies: New values and impact on the efficiency of chemical desorption. *Molecular Astrophysics*, 6:22–35, 2017b.

V. Wakelam, E. Dartois, M. Chabot, S. Spezzano, D. Navarro-Almaida, J.-C. Loison, and A. Fuente. Efficiency of non-thermal desorptions in cold-core conditions. *Astronomy and Astrophysics*, 652:A53, 2021.

V. Wakelam, P. Gratier, J.-C. Loison, K. M. Hickson, J. Penguen, and A. Mechineau. The 2024 KIDA network for interstellar chemistry. *Astronomy and Astrophysics*, 689:A63, 2024.

S. P. Walch and E. L. O. Bakes. On the reaction CH_2NH_2+HCN/HNC$\longrightarrow NH_2CH_2CNH^+$. *Chemical Physics Letters*, 346:267–273, 2001.

S. P. Walch, C. W. Bauschlicher Jr., A. Ricca, and E. L. O. Bakes. On the reaction CH_2O+$NH_3\longrightarrow CH_2NH$+$H_2O$. *Chemical Physics Letters*, 333:6–11, 2001.

S. Weinreb, A. H. Barrett, M. L. Meeks, and J. C. Henry. Radio observations of OH in the interstellar medium. *Nature*, 200:829–831, 1963.

D. Whitford. *Proteins: Structure and Function*. John Wiley and Sons, 2013.

D. C. B. Whittet, A. J. Adamson, W. W. Duley, T. R. Geballe, and A. D. McFadzean. Infrared spectroscopy of dust in the Taurus dark clouds : Solid carbon monoxide. *Monthly Notices of the Royal Astronomical Society*, 241:707–720, 1989.

R. W. Wilson, K. B. Jefferts, and A. A. Penzias. Carbon monoxide in the Orion nebula. *The Astrophysical Journal*, 161:L43, 1970.

J. Woodall, M. Agúndez, A. J. Markwick-Kemper, and T. J. Millar. The UMIST database for astrochemistry 2006. *Astronomy and Astrophysics*, 466:1197–1204, 2007.

D. E. Woon. Pathways to glycine and other amino acids in ultraviolet-irradiated astrophysical ices determined via quantum chemical modeling. *The Astrophysical Journal*, 571:L177–L180, 2002.

B. Zuckerman, J. A. Ball, and C. A. Gottlieb. Microwave detection of interstellar formic acid. *The Astrophysical Journal*, 163:L41, 1971.

B. Zuckerman, M. Morris, P. Palmer, and B. E. Turner. Observations of CS, HCN, U89.2, and U90.7 in NGC 2264. *The Astrophysical Journal*, 173:L125, 1972.

K. I. Öberg. Photochemistry and astrochemistry: Photochemical pathways to interstellar complex organic molecules. *Chemical reviews*, 116:9631–9663, 2016.

K. I. Öberg, H. Linnartz, R. Visser, and E. F. van Dishoeck. Photodesorption of ices. II. H_2 and D_2. *The Astrophysical Journal*, 693(2):1209–1218, 2009b.

Appendix A

List of molecular compounds

1. H_2: Molecular hydrogen
2. H_3^+: Trihydrogen cation
3. O_2: Molecular oxygen
4. O_3: Ozone
5. OH: Hydroxyl radical
6. CO: Carbon monoxide
7. CO_2: Carbon dioxide
8. H_2O: Water
9. SiO: Silicon monoxyde
10. SiO_2: Silicon dioxyde
11. CH: Methylidyne radical
12. CH_2: Methylene radical
13. CH_3: Methyl radical
14. CH_4: Methane
15. C_2H: Ethynyl radical
16. C_2H_2: Acetylene
17. HCN: Hydrogen cyanide
18. HNC: Hydrogen isocyanide
19. $HCNH^+$: Protonated hydrogen cyanide
20. CH_3OH: Methanol
21. CH_2OH: Hydroxymethyl radical
22. H_2CO: Formaldehyde

23. HCOOH: Formic acid
24. HCO^+: Formyl cation
25. H_2CO^+: Formaldehyde cation
26. H_2COH^+: Protonated formaldehyde
27. NH: Imidogen
28. NH_2: Amine
29. NH_3: Ammonia
30. NH_3^+: Ammonium cation
31. CH_2NH: Methanimine
32. CH_2NH_2: Aminomethyl radical
33. $CH_2NH_2^+$: Iminium cation
34. NH_2CH_2CN: Aminoacetonytrile
35. $NH_2CH_2CNH^+$: Protonated aminoacetonytrile
36. $CH_3NH_2^+$: Methylamine cation
37. $CH_3NH_3^+$: Methylammonium
38. NH_2CH_3: Methylamine
39. $CH_2(OH)CN$: Cyanohydrin
40. $CH_3CH_2NH_2$: Ethylamine
41. H_2NCH_2CHO: Glycinal
42. CH_3CH_2COOH: Propionic acid
43. CH_3CH_2CHO: Propanal
44. NH_2CH_2COOH: Glycine
45. $NH_2CHCOOH$: Glycyl radical
46. $NH_2C(O)CH_2OH$: Syn-glycolamide, isomer of glycine
47. $Mg_xFe_{1-x}SiO_3$: Pyroxene, $0 < x < 1$
48. $Mg_2Fe_{2-2x}SiO_4$: Olivine, $0 < x < 1$
49. MgO: Magnesium oxyde
50. Fe_3O_4: Iron oxyde
51. HOCO: Hydrocarboxyl radical, that could react with a molecule and form a carboxylic acid functional group

Appendix B

All the parameters in *Nautilus*

Presentation of all the ***Nautilus*** parameters. It should be noted that several of those parameters remained set to their default values. The modified parameters are always specified throughout the thesis.

Listing B.1: All the parameters that can be modified when using the ***Nautilus*** astrochemical code.

```
!# -------------------------------------------------------
!# Parameter file for various properties of the disk.
!# -------------------------------------------------------
!# blanck line or with spaces will be skipped.
!# In fact, the only lines that matter are non commented lines with a
!# '=' character to distinguish the identificator and the value(s)
!# (each value must be separated with at least one space.
!# Line must not be longer than 80 character, but comments can be far
!# bigger than that, even on line with a parameter to read.

!*****************************
!*   Switch 2/3 phase model  *
!*****************************

is_3_phase = 0 ! 0: 2 phase, 1: 3 phase

!*****************************
!*          Switches         *
!*****************************

preliminary_test = 1 ! Will or will not do comprehensive tests before the
! simulation. Switch it off when lauching thousands or simulations
is_structure_evolution = 0 ! If 1, physical structure properties evolve
! with time, values come from structure_evolution.dat file that must exists
grain_temperature_type = fixed ! fixed, gas, table_evolv, table_1D,
! computed or computed_hocuk
! fixed: Tgrain = initial_dust_temperature. ;
! gas: Tgrain = Tgas ;
! table_evolv: Tgrain is interpolated from structure_evolution.dat data
! file (5th optional column) ;
```

```
! table_1D: Tgrain is read in the 1D_static.dat file (5th column) ;
! computed: calculated from uv_flux and visual extinction by radiative
! equilibrium
! computed_hocuk: computes the dust temperature using the approximation
! from Hocuk et al. (2017) (as a function of Av and UV_FLUX).
is_compute_zeta = 1 ! Computation of zeta using equations 6 and 7 of
! Wakelam et al. (2021) (1=activated)
is_dust_1D = 0 ! Reading the grain abundance and the NH/AV factor in the
! 1D_static.dat file (mostly for disks)
is_grain_reactions = 0 ! Accretion, grain surface reactions
is_h2_adhoc_form = 1 ! Ad hoc formation of H2 on grain surfaces (1=activated)
is_absorption_h2 = 1 ! H2 self-shielding from Lee & Herbst 1996 (1=activated)
is_absorption_co = 2 ! CO self-shielding (1: Lee & Herbst 1996,
! 2: Visser et al. 2009)
is_absorption_n2 = 1 ! N2 self-shielding from Li et al. 2013 (1=activated)
is_photodesorb = 1 ! Switch to turn on the photodesorption of ices
is_chem_des = 1 ! Flag for chemical desorption (0: Garrod 2007,1:
! Minissale et al. 2016)
is_er_cir = 0 ! Switch to turn on Eley-Rideal and Complex Induced
! Reaction mechanisms (default=0: desactivated)
grain_tunneling_diffusion = 2 ! 0=thermal; 1= QM for H and H2 only; 2=QM for
! all species depending on mass
conservation_type = 0 ! 0=only e- conserved;1=elem #1 conserved, etc

!*****************************
!*      1D and diffusion     *
!*****************************
!(diffusion is for species, not the structure)

structure_type = 0D ! 0D, 1D_no_diff
spatial_resolution = 1 ! If 1, we are in 0D, else, we are in 1D, with diffusion
! between gas boxes. Number of lines in 1D.

!*****************************
!*    Gas phase parameters   *
!*****************************

initial_gas_density =  1.000E+04 ! initial gas density [part/cm-3]
initial_gas_temperature =  1.000E+01 ! initial gas temperature [K]
initial_visual_extinction =  2.000E+01 ! initial visual extinction
initial_cr_ionisation_rate =  1.300E-17  ! cosmic ray ionisation rate [s-1]
! (standard=1.3e-17)
x_ionisation_rate =  0.000E+00 ! Ionisation rate due to X-rays [s-1]
uv_flux =  1.000E+00 ! Scale factor for the UV flux, in unit of the reference
! flux (1.=nominal)

!*****************************
!*      Grain parameters     *
!*****************************
```

```
initial_dust_temperature =  1.000E+01 ! initial dust temperature [K] when
! grain_temperature_type=fixed
initial_dtg_mass_ratio =  1.000E-02 ! dust-to-gas ratio by mass
sticking_coeff_neutral =  1.000E+00 ! sticking coeff for neutral species
sticking_coeff_positive =  0.000E+00 ! sticking coeff for positive species
sticking_coeff_negative =  0.000E+00 ! sticking coeff for negative species
grain_density =  3.000E+00 ! mass density of grain material
grain_radius =  1.000E-05 ! grain radius [cm]
diffusion_barrier_thickness =  2.500E-08 ! Barrier thickness [cm]
surface_site_density =  1.500E+15 ! site density on one grain [cm-2]
diff_binding_ratio_surf =  4.000E-01 ! Ratio used to compute the
! DIFFUSION_BARRIER from the BINDING_ENERGY if not known (surface species)
diff_binding_ratio_mant =  8.000E-01 ! Ratio used to compute the
! DIFFUSION_BARRIER from the BINDING_ENERGY if not known  (mantle species)
chemical_barrier_thickness =  1.000E-08 ! grain reaction activation energy
! barrier width. [cm]
cr_peak_grain_temp =  7.000E+01 ! peak grain temperature [K] (CR heating)
cr_peak_duration =  1.000E-05 ! duration [s] of peak grain temperature
Fe_ionisation_rate =  3.000E-14 ! (cosmic) Fe-ion grain
! encounter [s-1 grain-1]
!! (for 0.1 micron grain) For cosmic photo desorptions, only Fe-ions are
! efficient to heat grains.
vib_to_dissip_freq_ratio =  1.000E-02 ! [no unit] The ratio of the
! surface-molecule bond frequency to the frequency at
!! which energy is lost to the grain surface. Used for the RRK
! (Rice Ramsperger-Kessel) desorption mechanism
!! (see Garrod el al. 2007 for more). Assumed to be 1% by default.
ED_H2 =  2.300E+01 ! H2 binding energy over itself. Used for the desorption
! encounter mechanism. in K.

!****************************
!*  Integration and Outputs  *
!****************************

start_time =  1.000E+00 ! [yrs] first output time
stop_time =  1.000E+07 ! [yrs] last output time
nb_outputs = 128 ! Total number of outputs (used for linear and log
! spaced outputs)
output_type = log ! linear, log
! linear: Output times are linearly spaced
! log   : Outputs times are log-spaced
relative_tolerance =  1.000E-04 ! Relative tolerance of the solver
minimum_initial_abundance =  1.000E-40 ! default minimum initial abundance
```

Appendix C

Equilibrium chemistry

We have a chemical equilibrium when all the abundances (reactants and products) are steady, do not evolve anymore with time even though reactions are still occurring. We speak of a **dynamical equilibrium**. Such an equilibrium can only occur provided that the chemical processes have the time to complete compared to the changes within the environment (i.e. $\tau_{reac} < \tau_{dyn}$).

Let us consider that such an equilibrium exists. In that case, it is characterized by the following equations (the direct and inverse reactions), occurring simultaneously at two different rates to which the constants k_1 and k_2 are associated. In Equation C.1, a, b, c and d are the stoechiometric coefficients:

$$\mathrm{aA} + \mathrm{bB} \underset{\mathrm{k_2}}{\overset{\mathrm{k_1}}{\rightleftharpoons}} \mathrm{cC} + \mathrm{dD} \tag{C.1}$$

To this equilibrium, we can associate an **equilibrium constant** K defined through the following relationship:

$$K = \frac{n(C)^c n(D)^d}{n(A)^a n(B)^b} = \frac{k_1}{k_2} \tag{C.2}$$

This constant can be related to a thermodynamic quantity called the **Gibbs energy**, denoted G. Only in the case of an equilibrium, we have Equation C.3:

$$\Delta G = -RT \ln(K) \tag{C.3}$$

where R is the universal gas constant ($R = 8.314463 \times 10^7$ erg/mol K), T is the temperature and ΔG is the difference between the Gibbs energies of the products and the reactants ($\Delta G = \Sigma G_{products} - \Sigma G_{reactants}$). The ΔG values can be estimated base of the Gibbs free energy values which are tabulated in databases, such as the NIST-JANAF database[1].

In the case of a chemical equilibrium, the densities in reactants and products at equilibrium can be easily calculated. However, we usually deal with **non-equilibrium chemistry** in astrochemistry since the reaction time-scales of the processes taking place in the ISM are extremely long due to the low densities and low temperatures.

[1] `https://janaf.nist.gov`

Appendix D

Presentation of the studied glycine precursors

Water H_2O

Water (H_2O) is a small, polar molecule consisting of two hydrogen atoms covalently bonded to an oxygen atom. It plays a central role in astrochemistry due to its abundance and its participation in both gas-phase and solid-phase processes. Water ice constitutes a major fraction of the icy mantles covering interstellar dust grains and serves as a key environment for grain-surface reactions that can lead to the formation of complex organic molecules, including glycine precursors.

Water molecule

As seen in this work, water is formed in dense molecular clouds through several gas and solid pathways. Within such environments, water quickly freezes onto grains, making it the main constituent of icy mantles.

Moreover, water was firmly detected in the ISM a long time ago. Water vapor was first identified by Cheung et al. (1969) thanks to its microwave emission, before being discovered in interstellar ices by Gillett and Forrest (1973) thanks to absorption features in the infrared, around 3.1 μm.

Ammonia NH_3

Ammonia (NH_3) is a small, trigonal pyramidal molecule composed of a nitrogen atom bonded to three hydrogen atoms. It is a key nitrogen-bearing species in astrochemistry, known for its presence in both gas-phase and solid-phase reservoirs in interstellar environments. The lone pair[1] on the nitrogen atom contributes to its reactivity, especially in acid-base chemistry and hydrogen bonding.

[1]The lone pair on the nitrogen atom in ammonia (NH_3) refers to a pair of valence electrons that are not involved in bonding with hydrogen atoms. Nitrogen has indeed 5 valence electrons.

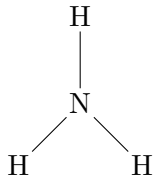

Ammonia molecule

In cold dense regions of the ISM, ammonia is primarily formed via a sequence of ion-molecule reactions (i.e. a cationic chain) followed by dissociative recombination. It can also be synthesized on the surface of dust grains through hydrogenation of nitrogen atoms or radicals. Ammonia contribute also significantly to the chemical composition of icy mantles.

Ammonia was one of the first polyatomic molecules detected in the interstellar medium, with its discovery dating back to the 1960s. Cheung et al. (1968) indeed detected NH_3 via its microwave emission in the direction of the galactic center. Moreover, it was also detected in interstellar ices by Lacy et al. (1998) thanks to its infrared spectra close to 10 microns.

Let us note that its cationic form, $NH_3{}^+$, has not yet been discovered in the ISM.

Hydrogen cyanide HCN and hydrogen isocyanide HNC

Hydrogen cyanide (HCN) and hydrogen isocyanide (HNC) are structural isomers, both consisting of one hydrogen, one carbon, and one nitrogen atom, but differing in the arrangement of these atoms. These two simple nitriles are of particular importance in astrochemistry due to their prevalence in the ISM and their participation in reaction networks leading to more complex nitrogen-bearing molecules, such as amino acids.

HCN (left) and HNC (right) molecules

HCN is generally more stable thermodynamically than HNC, but both are routinely observed in various astrophysical environments. In cold dense regions of the ISM, HNC can be nearly as abundant as HCN, due to the low temperature conditions that hinder isomerization (cf. close abundances of both in Chapter 6). As the temperature increases, however, the HNC/HCN abundance ratio tends to decrease, making this ratio a useful thermometer for cold molecular gas. In terms of astrochemical pathways, both isomers are notably formed via gas-phase reactions involving ions (but not only) such as $HCNH^+$, followed by dissociative recombination. They can also interact with grains through various processes.

Hydrogen cyanide was among the first molecules to be detected in space, first observed by Snyder and Buhl (1971) in gas-phase. Hydrogen isocyanide was also detected shortly thereafter simultaneously by Snyder and Buhl (1972) and Zuckerman et al. (1972). Unfortunately, they have **not yet been discovered** unambiguously in interstellar ices.

Formaldehyde H_2CO

Formaldehyde (H_2CO) is one of the simplest organic molecules and a fundamental species in interstellar chemistry. It consists of a central carbon atom double-bonded to an oxygen atom and single-bonded to two hydrogen atoms. Its relatively simple structure and high reactivity make it an important building block for more complex organic molecules, including amino acids such as glycine.

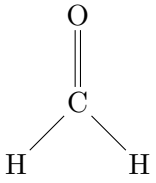

Formaldehyde molecule

In astrochemical environments, H_2CO is formed both in the gas phase and on the surface of interstellar dust grains. In grain mantles, it is typically produced through the hydrogenation of CO ice ($CO \longrightarrow HCO \longrightarrow H_2CO$), a key process in cold, dense molecular clouds as seen in Chapter 6.

Formaldehyde has been firmly detected in both the gas phase and solid phase (ices) of the interstellar medium. It was first identified in the gas phase by Snyder et al. (1969) via its microwave emission, and much later detected in ices by infrared spectroscopy through absorption features between 6.8 and 8.6 μm (Rocha et al., 2024).

Though its cationic form H_2CO^+ has not been discovered in the ISM, its protonated form H_2COH^+ was firmly detected in gas-phase (Ohishi et al., 1986).

Carbon Monoxide CO

Carbon monoxide (CO) is a simple, linear diatomic molecule composed of one carbon atom triple-bonded to an oxygen atom. It is one of the most abundant and widely observed molecules in the ISM, second only to molecular hydrogen (H_2). Due to its strong rotational transitions in the millimeter and submillimeter ranges, CO serves as a key tracer of H_2 molecular gas in cold interstellar clouds.

$$C{\equiv}O$$

Carbon monoxide molecule

In astrochemistry, CO plays a pivotal role in gas-phase and grain-surface processes. Its high abundance and chemical stability make it a **reservoir of carbon** in molecular clouds. CO also influences the chemistry of other species by acting as a precursor for more complex molecules such as formaldehyde.

Carbon monoxide was extensively detected both in the gas phase (Wilson et al., 1970) and in interstellar ices (Whittet et al., 1989).

Carbon Dioxide CO_2

Carbon dioxide (CO_2) is a linear, non-polar molecule consisting of one carbon atom double-bonded to two oxygen atoms. Although it lacks a permanent dipole moment and is therefore not observable through pure rotational transitions in the radio domain, it is readily detected in the infrared through its vibrational modes. In astrochemical environments, CO_2 is mainly observed in the solid phase, where it is an important constituent of interstellar ices. As with CO, it has indeed a tendency to condense at relatively high densities.

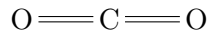

Carbon dioxide molecule

CO_2 is commonly found mixed with H_2O, CO, NH_3 and CH_3OH in icy mantles. It has been firmly detected in interstellar ices through its absorption band close to 15.2 microns (D'Hendecourt and Jourdain de Muizon, 1989), but on the contrary to previous molecules it **has not been discovered in gas-phase in cold environments**.

Hydroxyl radical OH

The hydroxyl radical (OH) is a diatomic molecule composed of one oxygen atom covalently bonded to a hydrogen atom. It is a highly reactive radical due to the presence of an unpaired electron and plays a crucial role in the oxygen-based chemistry of the interstellar medium, since it participates in various key reactions in both the gas and solid phases.

Hydroxyl radical

OH was one of the first molecules detected in the interstellar medium. It was discovered in the gas phase through its radio emission around 18 cm by Weinreb et al. (1963). Although **not directly observed in ices**, the presence of OH on grain surfaces is inferred from its fundamental role in the surface formation of various molecules. In this work, it has indeed been considered in solid-phase reactions.

Formic acid HCOOH

Formic acid (HCOOH) is the simplest carboxylic acid, consisting of a hydrogen atom and a carboxyl group attached to a central carbon. It is considered a key molecule in the chemistry leading toward complex organics and is often regarded as a possible glycine precursor (cf. Woon's mechanism) due to its functional group.

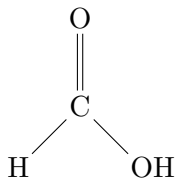

Formic acid molecule

HCOOH was firmly detected in both the gas phase and in interstellar ices. It was first observed in the gas phase towards the molecular cloud Sgr B2 (Zuckerman et al., 1971). Its presence in ices was confirmed through infrared absorption features, notably near 8.22 μm, as reported by Rocha et al. (2024).

Methanimine CH_2NH

Methanimine (CH_2NH) is a small imine molecule composed of a methylene group (CH_2) bonded to an imine group (NH). It is considered a prebiotic molecule of interest in astrochemistry, as it contains both carbon and nitrogen atoms and can serve as a building block for more complex organics, including amino acids such as glycine. Its relatively simple structure and reactivity make it a plausible intermediate in both gas-phase and grain-surface chemistry.

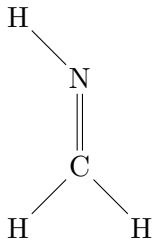

Methanimine molecule

CH_2NH was detected in gas-phase in the ISM towards Sgr B2 by Godfrey et al. (1973). It has **yet to be discovered in interstellar ices**. Because of its relevance to prebiotic chemistry and its role as a glycine precursor candidate, methanimine remains an important species in astrochemical modeling and observational studies.

Its protonated form, $CH_2NH_2^+$, had not been discovered in the ISM at the time of writing.

Hydrocarboxyl radical HOCO

The hydrocarboxyl radical (HOCO) is a highly reactive intermediate composed of a hydroxyl group (OH) bonded to a carbon center that also carries a carbonyl function. According to the mechanism proposed in Woon (2002), it is considered a key species in the formation of glycine since it acts as one of its direct precursors.

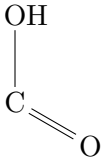

Hydrocarboxyl radical

Even though its cationic form was discovered decades ago (Thaddeus et al., 1981), the neutral form of this radical has yet to be discovered in the ISM.

Aminomethyl radical CH_2NH_2

The aminomethyl radical (CH_2NH_2) is a reactive species consisting of a methylene group (CH_2) bonded to an amino group (NH_2). It is a radical due to the presence of an unpaired electron on the carbon atom. This species is of significant interest in astrochemistry as a potential intermediate in the formation of more complex nitrogen-bearing organic molecules, including amino acids such as glycine.

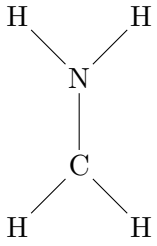

Aminomethyl radical

Its reactivity and role in radical-radical coupling pathways make it an important species to consider in models of prebiotic chemistry. Unfortunately, it has not yet been observed in the ISM, although closely related species such as methylamine CH_3NH_2 were discovered (Kaifu et al., 1974).

Appendix E

Detailed comparison between *Astrochem* and *Nautilus*

This appendix provides a more detailed comparison of the results obtained with the two astrochemical codes, serving as an extension of Chapter 5. It emphasizes the similarities between the codes' outputs and offers a concise overview of the findings reported by Groyne (2023). Some overlap with the content of Chapter 5 is to be expected.

Strecker-like synthesis - Neutral pathway

This pathway towards glycine involves the following simple precursors of glycine: H_2O, NH_3, H_2CO and HCN, as previously described in Chapter 3.

This appendix provides a more detailed comparison of the results obtained with the two astrochemical codes, serving as an extension of Chapter 5. It highlights the similarities between the results, and offers a concise summary of the findings presented in Groyne (2023). Some redundancy with previously discussed content may be noted.

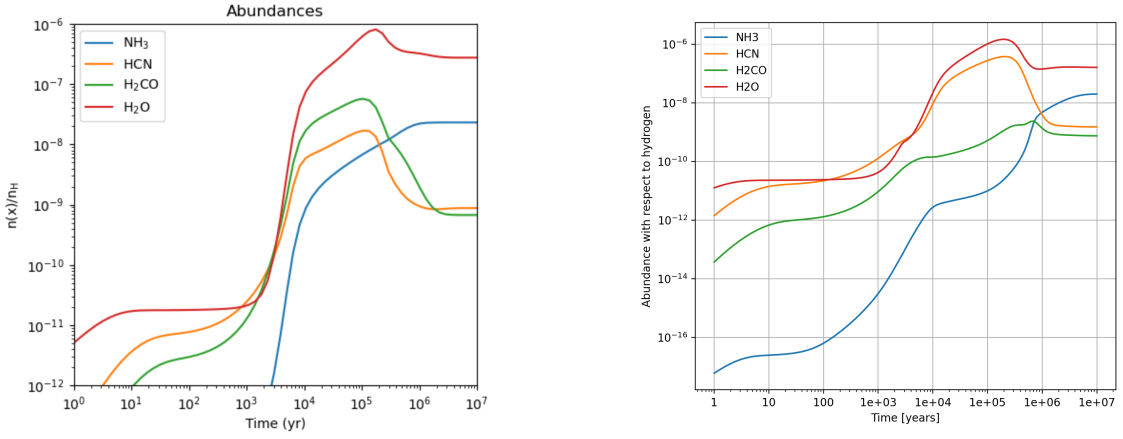

Figure E.1: Abundance temporal evolutions of the glycine precursors linked to the neutral Strecker-like pathway using model 1a. Left: Groyne (2023). Right: this work.

A first observation is that, while the time-dependent chemistry differs slightly, the equilibrium concentrations are remarkably similar (cf. Table 5.2). Indeed, as in Groyne (2023), H_2O remains the dominant species throughout most of the simulation, except for a brief period around 10^2–10^3 years. This indicates that, on first inspection, ***Astrochem***

and ***Nautilus*** give consistent gas-phase abundances. The chemical equilibrium is reached after approximately 10^6 years, which aligns with the discussion in Groyne (2023). However, **notable differences arise in the out-of-equilibrium phase**. For instance, in the ***Nautilus*** simulation, HCN is the second most abundant molecule, whereas in Groyne (2023), it is surpassed by H_2CO after roughly 10^3 years except at the very end. This discrepancy may be attributed to the greater completeness of ***Nautilus***, which incorporates more reaction pathways - for example, HCN has more than twice the number of formation routes in ***Nautilus*** as compared to ***Astrochem*** - but also to differences in the kinetic parameters used in the two models. Indeed, on top of the fact that both codes are based onto two different databases (OSU versus KIDA), kinetic parameters are continuously refined over the years. Discrepancies in the parameters are thus expected. Those hypothesis can be checked with the main formation/destruction pathways over time and their rates.

Let us begin with H_2O, as illustrated in Figure E.2. Two primary formation routes can be identified: $H_2 + O^- \longrightarrow H_2O + e^-$, which dominates during the first 10^3 years, and $H_3O^+ + e^- \longrightarrow H_2O + H$, which becomes dominant between 10^4 and 10^7 years. A third reaction, l-$C_3H_2 + H_3O^+ \longrightarrow$ c-$C_3H_3^+ + H_2O$[1], briefly plays a significant role around 10^3 years, while the three other reactions contribute only marginally. Beyond 10^3 years, the dissociative recombination of H_3O^+ becomes the dominant process, highlighting its crucial role in water formation. In fact, H_3O^+ is involved in five of the six major formation reactions, reinforcing the idea that gas-phase water formation in molecular clouds is driven primarily by ion-molecule reactions, as discussed in Chapter 2. When comparing with Groyne (2023), the overall conclusions remain consistent, although some differences must be noted. While four of the six main formation reactions are shared between both models, discrepancies appear primarily in the early chemistry (before $\sim 10^3$ years). Beyond 10^3 years, the **dominant** reactions are nearly identical, except for the absence of the SiO reaction in our work. Groyne (2023) previously identified missing contributors to water formation in the early stages (i.e. the reaction involving H_2), which were corrected by considering a higher density that permitted additional reactions to take place (model 2a). Interestingly, this issue does not arise in this study. One may have thought that the kinetic parameters are different, except that they are exactly the same between the two networks. It is therefore probably linked to code differences, emphasizing the fact that providing two codes with the same parameters for a given reaction does not ensure that the results will be identical. Moreover, it must not be forgotten that everything is interconnected, meaning that changes in kinetic parameters for other reactions could have an impact on other reactions involving water precursors. For the destruction pathways, this model accounts for the same reactions as the one obtained in Groyne (2023). Overall, the results remain highly similar. During the first 10^3 years, the chemistry is primarily governed by reactions with the C^+ cation, one of the most abundant ions at early times, as noted in Prasad and Huntress (1980b). As one of the first cations to form in molecular clouds, it is indeed expected to play a dominant role in the early chemistry (Prasad and Huntress, 1980b). However, beyond this point, the chemical processes become more complex and interconnected. It can be noted that the destruction chemistry is primarily influenced by a reaction with HCO^+, followed by reactions involving C^+, H_3^+ and H^+. In the work of Groyne (2023), there were nearly equal contributions of HCO^+ and H_3^+, with a slight dominance of the latter. On top of those considerations, one may note the nearly identical equilibrium abundance of water. Despite the fact that ***Nautilus*** includes additional reaction routes involving water compared to ***Astrochem***, this does not significantly

[1] "l-" standing for the linear form of the molecules and "c-" for the cyclic form.

affects its final abundance. This suggests that the newly introduced pathways contribute only marginally to the overall water formation and destruction balance.

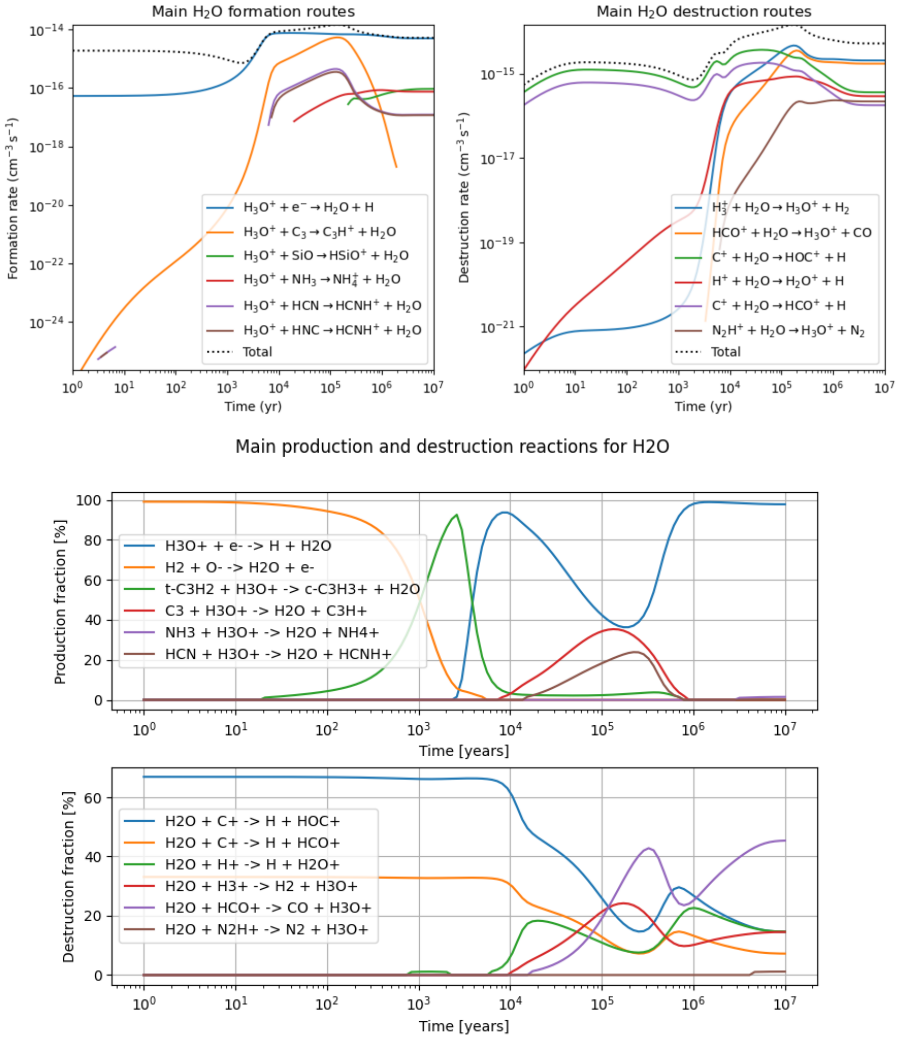

Figure E.2: Comparison between the different formation and destruction routes of H_2O using model 1a. Top: Groyne (2023). Bottom: this work.

Let us now consider formaldehyde H_2CO whose production and destruction fractions are reproduced in Figure E.3. Having a look at the formation pathways, it is striking to note that the results are quite similar to those of Groyne (2023). One reaction dominates clearly the chemistry all along the simulation, i.e. $O + CH_3 \longrightarrow H_2CO + H$. After about 10^6 years, the dissociative recombination reaction $H_2COH^+ + e^- \longrightarrow H_2CO + H$ becomes the second dominant reaction. This dominance was achieved earlier in Groyne (2023), but let us keep in mind that more reactions are considered in ***Nautilus*** and that the kinetic parameters/rate parametrization of various reactions may be different between the two networks, which may have an impact on the results. Even though the 2 other reactions in ***Nautilus*** are not found in Groyne (2023), there is still a clear similarity in the dominant formation chemistry taking place. For the destruction pathways of formaldehyde, there are still clear similarities, but also some deviations. The first 10^3 years are clearly

dominated by reactions with C^+ in both results, as we may expect regarding the previous discussion. Then, the destruction of H_2CO is clearly dominated by the reaction involving atomic carbon between 10^3 and 10^6 years, which is a clear deviation compared to the results presented in Groyne (2023). This can be explained by the simple fact that the reaction is not included in the ***Astrochem*** network. On the contrary, the equilibrium chemistry (after 10^6 years) is again clearly dominated by reaction with HCO^+ followed again by reactions involving H^+ and $H_3{}^+$. Contrary to what was encountered for the water molecule (for which it was not even found in the dominant reactions), the destruction of formaldehyde involving H_3O^+ has here to be taken into account, similarly to the work of Groyne (2023). As it was the case for water, the chemistry of formaldehyde is dominated by ionic reactions, i.e. barrierless reactions, as one may expect in cold environments.

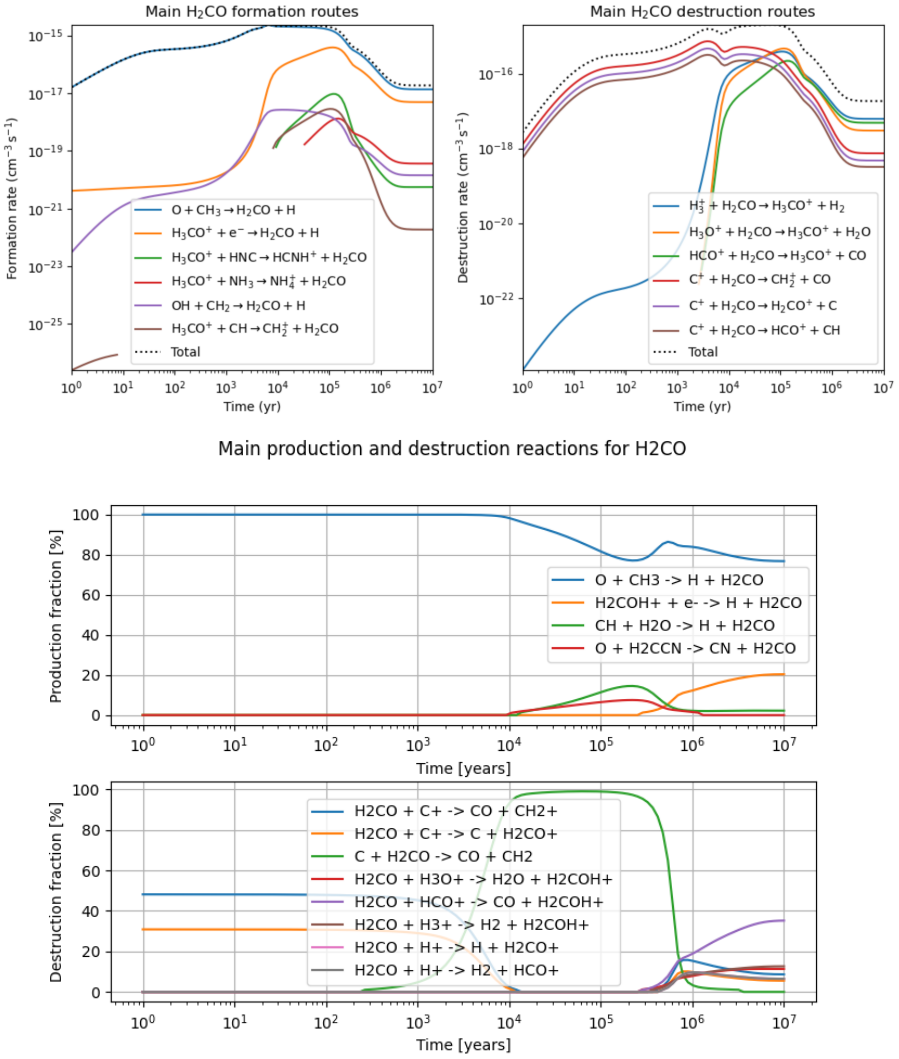

Figure E.3: Comparison between the different formation and destruction routes of H_2CO using model 1a. Top: Groyne (2023). Bottom: this work.

For hydrogen cyanide HCN (Figure E.4), one directly notices the differences between both modeling approaches.

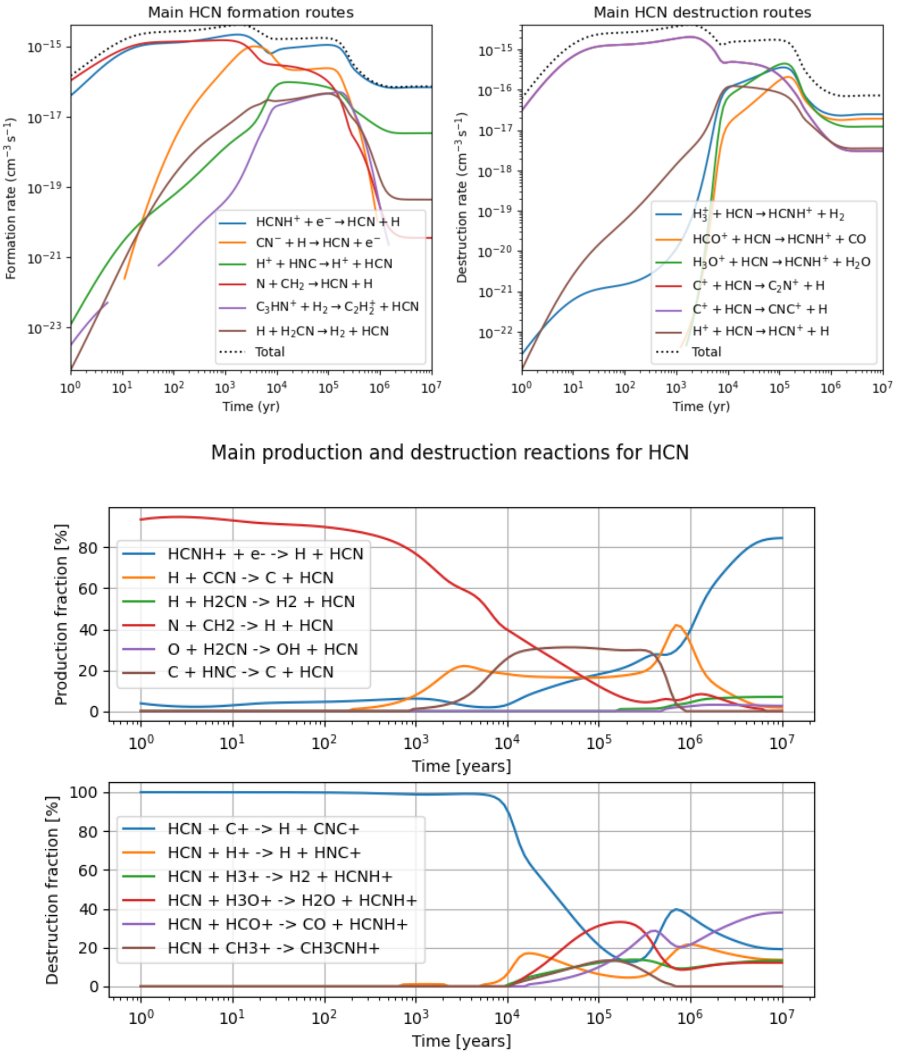

Figure E.4: Comparison between the different formation and destruction routes of HCN using model 1a. Top: Groyne (2023). Bottom: this work.

Concerning the formation pathways, the chemistry until $\sim 10^4$ years is dominated by the reaction $N + CH_2 \longrightarrow HCN + H$ in ***Nautilus*** whereas in ***Astrochem*** the reaction $HCNH^+ + e^- \longrightarrow HCN + H$ must also be taken into account. A closer look at the networks shows that the kinetic parameters A are not the same (9.622×10^{-8} in ***Nautilus*** versus 1.85×10^{-7} in ***Astrochem***). In the work of Groyne (2023), the reaction has thus a higher kinetic, which could explain the difference with our results. Out of the 6 main reactions in Groyne (2023), only three are found in this work. While the reaction $H^+ + HNC \longrightarrow H^+ + HCN$ is not included in the network of ***Nautilus***, the two other reactions are present with the same kinetic parameters as in ***Astrochem***. The equilibrium chemistry is the same, the dissociative recombination reaction of $HCNH^+$ being dominant in both results. Regarding the destruction routes, it is again the reaction with C^+ that unambiguously dominates the early chemistry in both results. Between 10^4 and 10^6 years, all reactions are intertwined (most reactions from Groyne (2023) being also found in this work). The equilibrium chemistry is again dominated in both results by a reaction involving HCO^+, followed by the reaction involving the carbon cation. The three same

molecules as before (i.e. H_3O^+, H_3^+ and H^+) follow, with the same destruction fraction. The only exception is that in our results, the importance of the contribution of the reaction involving C^+ is comparable (even higher) to the three others, whereas in Groyne (2023) it is completely negligible. As previously, that may probably be explained by differences in the kinetic parameters. Indeed, the values of all the parameters have been changed between the networks ($A = 4.75 \times 10^{-9}$, $B = -5 \times 10^{-1}$ and $C = 0$ in ***Astrochem*** becomes $A = 1$, $B = 1.28 \times 10^{-9}$ and $C = 6.61$ in ***Nautilus***). Nonetheless, it is important to keep in mind that there are **important differences in the kinetic constant parametrization between the two codes**, meaning that the comparison between the parameters might be in this case irrelevant. Whereas an Arrhenius-like parametrization is assumed in the OSU database on which is based ***Astrochem***, ion-neutral reactions in ***Nautilus*** are computed using the Su-Chesnavich capture approach. The detailed comparison of those approaches goes beyond the scope of this master thesis and one is referred to the following document (and references therein) if in need of further details: `https://kida.astrochem-tools.org/uploads/documents/ionpol_notice.pdf`.

It is now interesting to compare the results concerning the abundances of HCN and HNC (Figure E.5). In Groyne (2023), the abundance ratio remained close to unity throughout the simulation, a result consistent with Graninger et al. (2014), where this ratio was found to be stable in cryogenic environments such as molecular clouds. However, in this work, we observe a divergence of about two orders of magnitude between 10^4 and 10^5 years. Interestingly, a closer look at Graninger et al. (2014) (Figure 5, using parameters similar to ours) reveals a similar feature: a temporary bump in the same time range, where HCN becomes more abundant than HNC. Despite this temporary difference, the abundances of both species eventually converge at equilibrium, reaching values comparable to those reported in Groyne (2023). This transient enhancement in HCN abundance could be attributed to its slightly higher stability compared to its isomer, HNC. Since both molecules share the same dominant reaction pathways (except during a short time between 10^4 and 10^5 years), HNC may be preferentially destroyed, as confirmed by the slightly higher kinetics of the reactions involving hydrogen isocyanide.

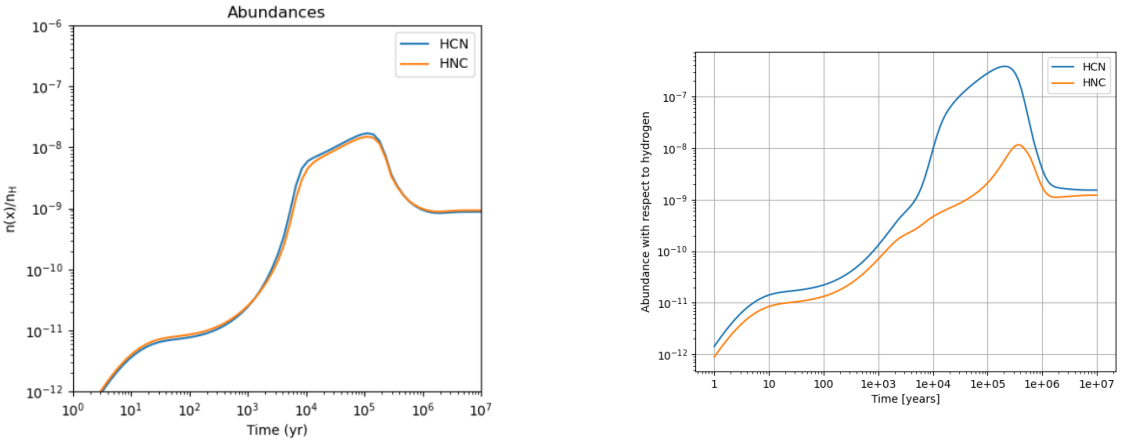

Figure E.5: Abundance temporal evolutions of the isomers HCN and HNC using model 1a. Left: Groyne (2023). Right: this work.

Finally, let us analyze the results concerning the ammonia molecule presented in Figure E.6. What is striking in the ***Nautilus*** results is that only one dominant formation

reaction of NH_3 occurs, which is the dissociative recombination of NH_4^+. That reaction is also found to be the dominant one in the results of Groyne (2023). Ammonia is in fact mainly produced through a cationic chain starting with nitrogen and its cation, finally ending through the dissociative recombination of the ammonium cation. For the destruction pathways, it is no surprise that the early chemistry until 10^3 years is dominated by reactions with C^+. Then, as it was the case for formaldehyde there is a clear dominance of reactions involving atomic carbon before completely dropping around 10^6 years. As for H_2CO, this did not appear in Groyne (2023) and is explained by the fact that the reaction is not included in the ***Astrochem*** network. Like the previous molecules, at equilibrium the destruction is dominated mainly by reaction with HCO^+, and then with less importance with H^+, H_3O^+, H_3^+ and C^+.

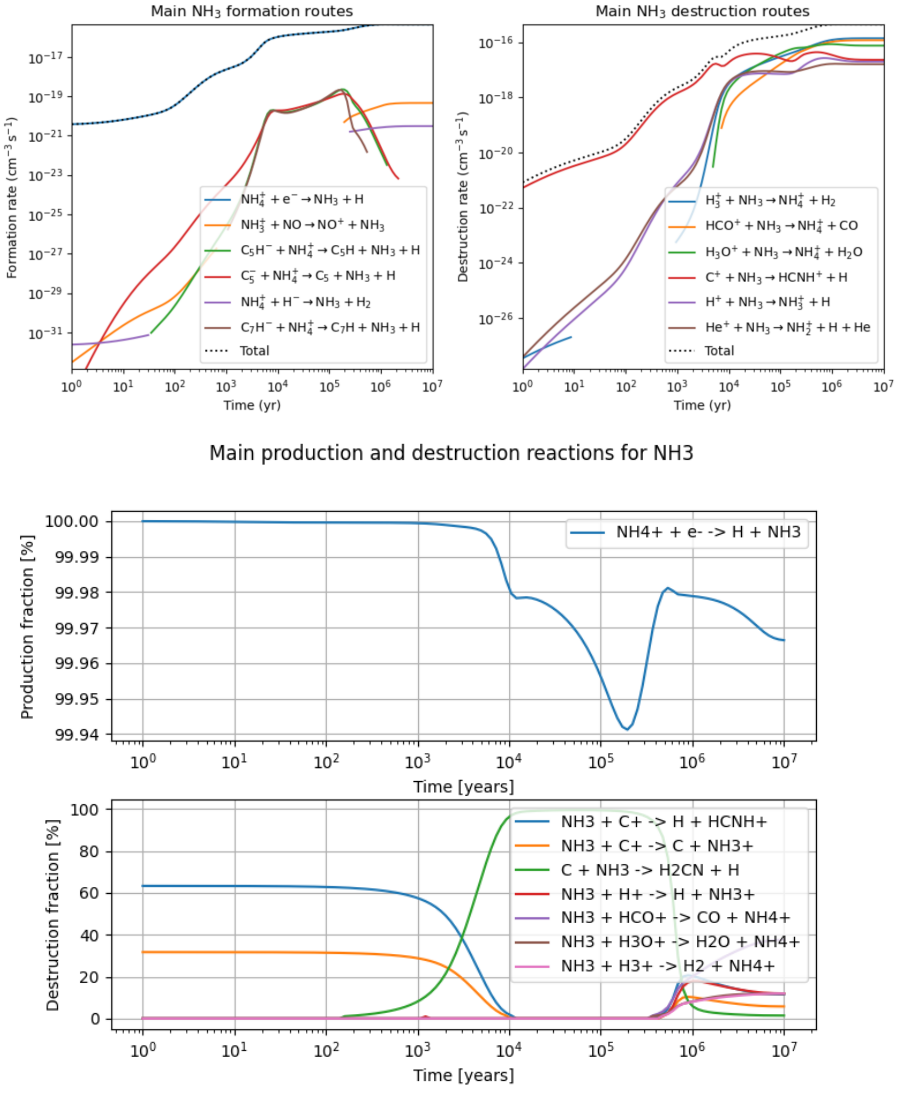

Figure E.6: Comparison between the different formation and destruction routes of NH_3 using model 1a. Top: Groyne (2023). Bottom: this work.

The first results are thus similar in both works. One main deviation is the involvement of C^+ in the late destruction equilibrium chemistry, which was completely negligible

in Groyne (2023). Verifying in the networks, the values of the kinetic parameters of the reactions are different (both codes are not built on the same database and the kinetic constant parametrization for some ion-neutral reactions is different). We may also note that the destruction equilibrium chemistry is, in this work, dominated by HCO^+, whereas in the previous work of Groyne (2023) there is a slight dominance of $H_3{}^+$. Once again, the parametrization is not the same between the codes. If the physical parametrization is not the same, one could have expected such differences and a comparison of the parameters cannot be performed since their role in the formulas are not the same. On top of that, everything is interconnected, and changes in parametrization and parameter values of various reactions could lead to significant changes in the chemical modeling results.

Now that results from model 1a have been compared in details, let us have a look at model 2a where the overall density of the cloud is enhanced by two orders of magnitude. Looking at the density profiles in Figure E.7, we reach easily the same conclusions as Groyne (2023). Again, even though the time-dependent chemistry is not the same between both works, we can notice that the abundances at chemical equilibrium are nearly the same.

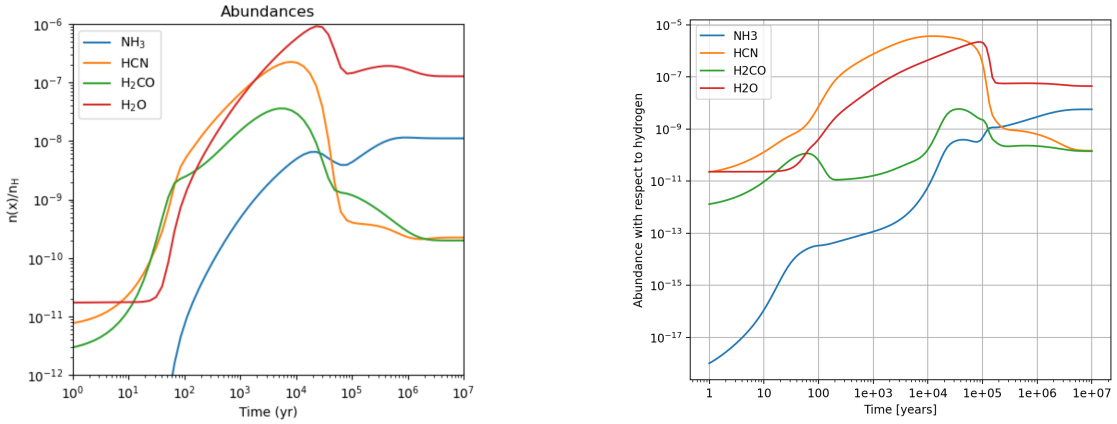

Figure E.7: Abundance temporal evolutions of the glycine precursors linked to the neutral Strecker-like pathway using model 2a. Left: Groyne (2023). Right: this work.

Moreover, as discussed in Groyne (2023), one notices that **the studied precursors appear all quantitatively earlier than in model 1a**. It is consistent since a higher density means a higher collision rate, which means of course a higher kinetics as it was discussed previously in Chapter 2. Additionally, chemical equilibrium is achieved more or less after 10^6 years, the same as in the previous results of Groyne (2023). As discussed in the latter study, this translates into the fact that **the time required to reach equilibrium does not depend on the initial hydrogen density**. This is consistent with the discussion found in Iglesias (1977). What is interesting to note in that paper is that the time scale required to achieve equilibrium is inversely proportional to ξ, the cosmic-ray ionization rate. As done in Groyne (2023), we tried to study this effect by a slight modification of the ξ value. For that, the same physical parameters than model 2a were kept, except that two other values of ξ were tried, i.e. 10^{-16} and 10^{-18} s^{-1} (values studied in Herbst and Klemperer 1973), as shown in Figure E.8. For the higher value of ξ (10^{-16} s^{-1}), the equilibrium is reached before 10^6 years and for the lower value (10^{-18} s^{-1}) it is reached after. The more cosmic rays penetrate the cloud, the more ions will be produced. The **chemistry will therefore be more active**, leading to a faster equilibrium. Keeping

in mind that, for any real molecular cloud, the cosmic-ray flux decreases from the borders of the cloud toward the center.

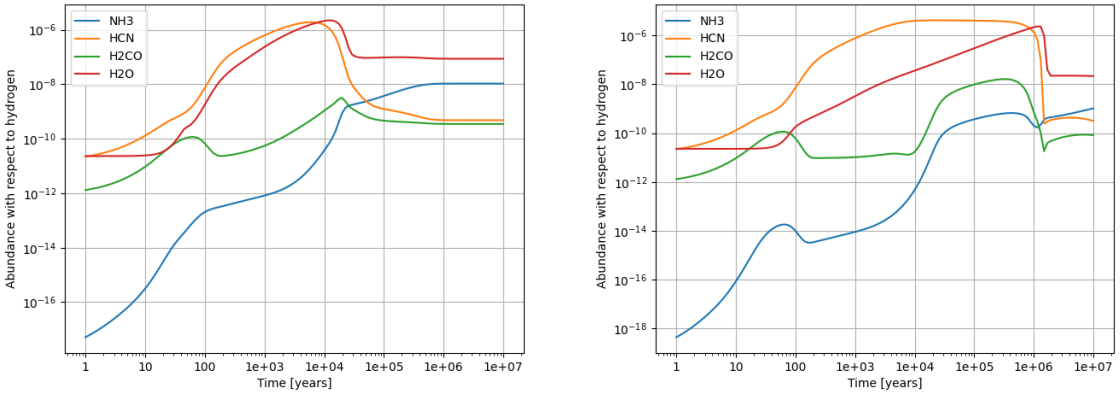

Figure E.8: Comparison (model 2a) of the times at which the equilibrium is reached, using two different values of cosmic ray ionization rate. Left: 10^{-16} s^{-1}. Right: 10^{-18} s^{-1}.

As shown in Table 5.2, the **equilibrium abundances** in models 1a and 2a remain remarkably similar despite the hundredfold increase in initial hydrogen density. At first glance, this aligns with the conclusions of Herbst and Klemperer (1973), which suggest that, since species are continuously formed and destroyed through chemical reactions, an increase in initial density would proportionally enhance both formation and destruction rates, keeping abundances relatively unchanged. However, as Groyne (2023) discussed, this perspective is overly simplistic. A more accurate understanding requires considering additional factors, such as the balance between formation and destruction pathways, reaction types, and the specific order of each process.

We will now discuss the main formation and destruction routes in the case of model 2a, in order to study the effect of a density change on those chemical processes. For the water molecule, except for the first 100 years, the formation chemistry is completely dominated by the dissociative recombination involving H_3O^+. The destruction pathways are also very similar, the early destruction being dominated by reactions with C^+ and the equilibrium chemistry by reactions involving HCO^+. Regarding the formaldehyde molecule, results are somehow different. In the results obtained thanks to model 1a, the dominance of the formation reaction involving O and CH_3 could not be challenged. In those results, we have a drop of the related production rate around 10^5 years, during which the reactions $CH + H_2O \longrightarrow H + H_2CO$ and $H_2COH^+ + e^- \longrightarrow H + H_2CO$ take over. Those reactions showed only a minor contribution in the first model. In comparison with the results from Groyne (2023), the involved reactions are not the same, but the equilibrium chemistry is the same, with the same two dominant formation reactions. The destruction pathways are similar to what was previously obtained. The early destruction is dominated by reactions with C^+ until $\sim$ 10 years, then the reaction with atomic carbon dominates completely until 10^5 years. As before, the equilibrium chemistry involves reactions with HCO^+ and H_3O^+. Looking at the ones of HCN, the dominant formation/destruction routes at equilibrium are the same in both models, as in Groyne (2023). Some new reactions are considered, but with a questionable impact on the final abundance. For ammonia, except for a general displacement of the curve towards the left, nothing has really changed concerning the dominant reactions which are involved.

We will conclude by the results obtained with model 3a, in which T has been increased from 10 K to 20 K compared to model 1a. The abundances at equilibrium and even their temporal evolution stay pretty similar, which is in perfect agreement with the results obtained by Groyne (2023). Indeed, as discussed in that work, a small temperature increment is not enough in such cryogenic conditions to enhance sufficiently the chemistry. In other words, **reactions which were inhibited at** 10 **K will remain inhibited at** 20 **K**. To observe significant differences, one would have to increase the temperature to a higher level, but that would mean leaving the physical conditions of a **quiescent** molecular cloud.

What may be said in conclusion of this first comparison is that although the time-dependent chemistry varies between the results obtained with both codes, **the equilibrium chemistry is always similar**. For comparison, Table 5.2 shows the equilibrium abundances for the four precursors obtained in both works.

Strecker-like synthesis - Activated pathways

As discussed in Groyne (2023) and in Chapter 3, in order to activate the kinetics (i.e. lower the activation barriers) of the Strecker-like formation route, ions can be substituted in the reactions to give the **activated Strecker-like mechanism**. In that context, the following precursors will be considered: H_2CO^+, H_2CO, HCN, NH_3, H_2COH^+ and $NH_3{}^+$.

Let us begin to study the results obtained from model 1a for those precursors. As discussed in the previous section, even though the time-dependent chemistry varies slightly in comparison with the results from Groyne (2023), the equilibrium results are quite similar. The abundances of the cationic/protonated species are about 2 to 3 orders of magnitude lower than the neutral ones, as expected in environments such as molecular clouds, fewer ions being created. Despite their low abundances, ion-involved reactions remain relevant to our study because of their significantly lower activation barriers, which make them much more reactive and thus compensate for their scarcity.

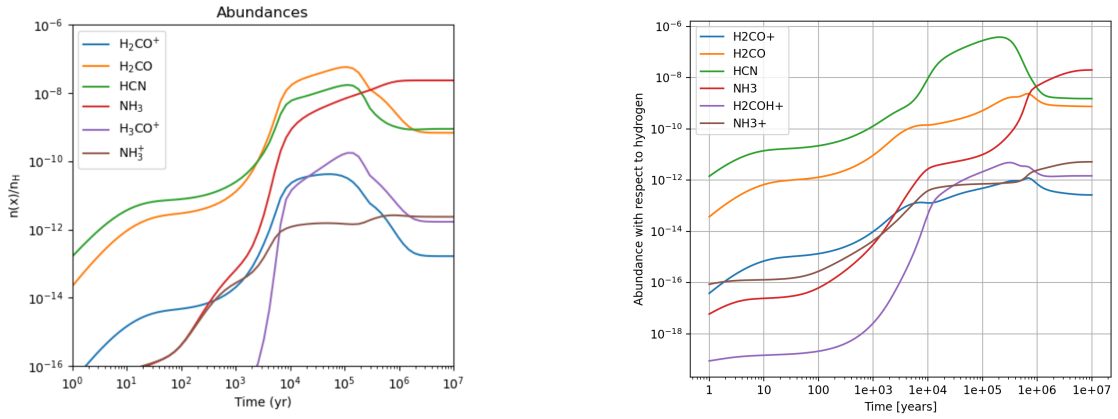

Figure E.9: Abundance temporal evolutions of the glycine precursors linked to the activated Strecker-like pathway using model 1a. Left: Groyne (2023). Right: this work.

Considering the abundances obtained with model 2a, as reproduced in Figure E.10, the conclusions made with the neutral species are no longer valid. Indeed, as one can see

in Table 5.3, we observe a decrease by about 2 orders of magnitude in the ionic equilibrium abundances as compared to model 1a. As discussed in Groyne (2023), this illustrates the restrictiveness of the considerations found in Herbst and Klemperer (1973). The abundances of H_2COH^+, H_2CO^+, and $NH_3{}^+$ are roughly inversely proportional to the initial hydrogen nuclei abundance. This behavior can be understood based on the discussion found in Groyne (2023): "*predicting the impact of an increased initial hydrogen nuclei density on a given species requires considering its involvement in multiple formation and destruction pathways, each governed by specific reaction orders and kinetic parameters*". To fully determine how a species' abundance depends on the hydrogen number density, one must apply the concept of chemical equilibrium, equating its production and destruction rates. In doing so, all density terms in the resulting expression must be rewritten in terms of the hydrogen abundance, which is not straightforward and often necessitates approximations. In quantitative terms, we notice that the equilibrium abundances are very similar to the ones found in the work of Groyne (2023). This agreement might be explained by the **close similarity in terms of the number of pathways in which those precursors are involved in both networks**. Nonetheless, one must not forget the effect of the kinetic parameters on the results. Looking in more detail at those of the dominant formation/destruction pathways plotted by ***Nautilus***, when the parametrization is the same, the parameter values are not always identical; when the parametrization is not the same then the comparison is not really relevant. One has to keep in mind that it is those kinetic parameters and the parametrization of the reaction rates in which they are involved that dictates the chemistry. The fact that they differ, even slightly, between the codes adds a complexity layer on top of this comparison.

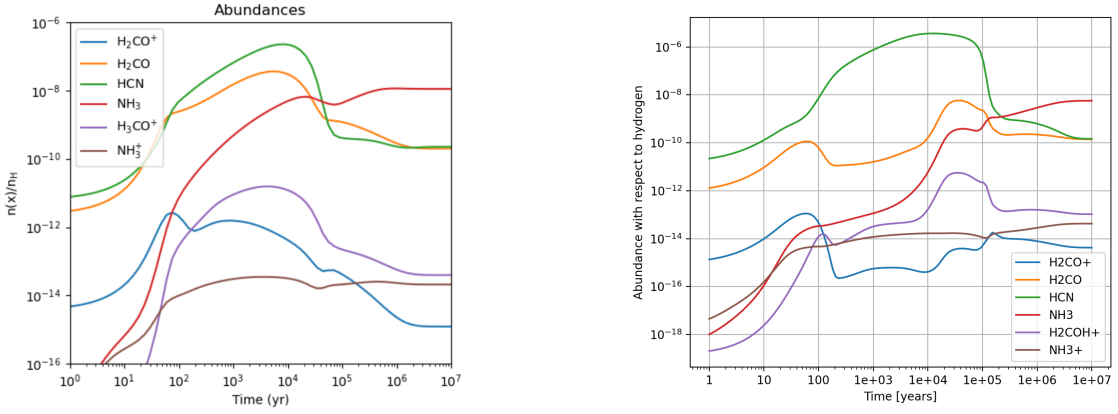

Figure E.10: Abundance temporal evolutions of the glycine precursors linked to the activated Strecker-like pathway using model 2a. Left: Groyne (2023). Right: this work.

The curves obtained for model 3a are this time also pretty similar to those obtained with model 1a as in Groyne (2023). This is further illustrated in Table 5.3, where the abundances from both models are nearly the same except for $NH_3{}^+$ which has an equilibrium abundance enhancement of nearly one order of magnitude. This increase in abundance has already been observed in Groyne (2023), though with a lower amplitude. Looking closer at the networks, the dominant destruction of that species ($H_2 + NH_3{}^+ \longrightarrow H + NH_4{}^+$) is included only one time in ***Astrochem***, but three times in ***Nautilus***, each time with different values of the kinetic parameters but also ranges of temperature validity. For the relevant temperature range (10 to 20 K), though the A parameter is the same, in ***Nautilus*** the B has decreased and C has increased. Differences in the kinetic parameters and the

complex interconnection between various reactions may explain the slight difference in the equilibrium abundance value. It was also checked which formation/destruction pathways are at work for the other compounds, and the important ones are the same in both models. Moreover, the shapes of the abundance curves are nearly the same in the results from both models, meaning that the conclusions drawn previously for model 3a remain valid now. Such a **small temperature increase will not affect much the reactions taking place**, especially reactions involving cationic or protonated species.

Precursors for Woon's mechanism and its variants

The results obtained thanks to model 1a for the first step in Woon's mechanism, named step a in Groyne (2023), are presented in Figure E.11. It must be noted that **the abundance of molecular hydrogen is not plotted**, since it would make the other curves appear insignificant.

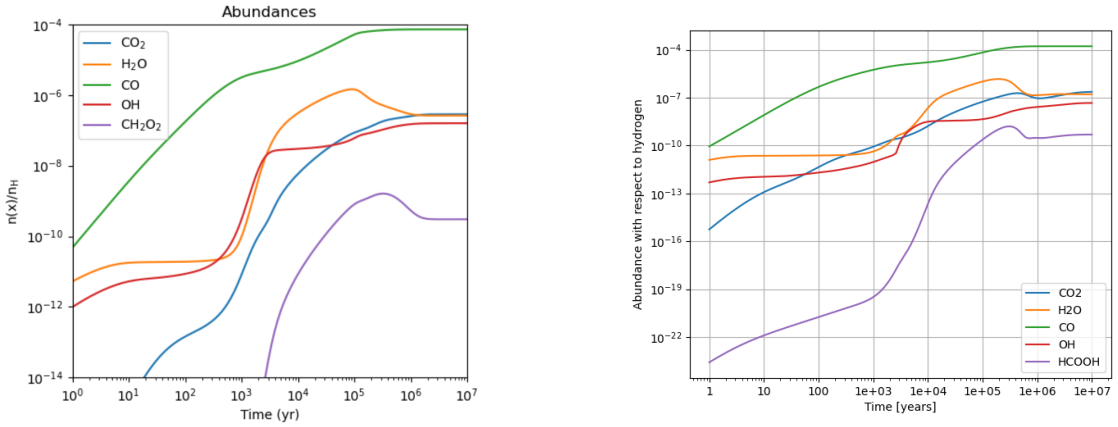

Figure E.11: Abundance temporal evolutions of the glycine precursors linked to the step a of the Woon's pathway using model 1a. Left: Groyne (2023). Right: this work.

The similarity between the two sets of curves may not be immediately obvious due to the difference in scale on the Y-axis, but their overall behavior is remarkably consistent. For instance, we observe characteristic bumps at the same positions, such as the one corresponding to formic acid HCOOH (referred to as CH_2O_2 in Groyne 2023). Additionally, as shown in Table 5.4, the equilibrium abundances are generally comparable. However, some discrepancies exist, particularly in the case of carbon monoxide and the hydroxyl radical. The abundance of CO is slightly higher by nearly an order of magnitude in this work, while OH is lower by a similar factor. This difference is likely due to the greater completeness of the gas-phase reaction network in ***Nautilus***, where both species participate in more than twice as many reactions compared to ***Astrochem***. That could also be linked to variations in the kinetic parameters and related parametrization of the rates, as already discussed in Chapter 5. It is not surprising that CO dominates, since it is the second most abundant molecule in the galaxy thanks to its high stability (and the high relative abundances of C and O). The similarity between OH and H_2O abundance curves, already noted by Groyne (2023), is explained by the same reasons. It has been carefully checked: both molecules are in fact predominantly produced by the same species, which is H_3O^+. The overabundance of water between 10^3 and 10^5 years could be explained by an enhanced destruction of OH, as it has been explained in Groyne (2023) and checked by

computing the destruction routes. The case of formic acid deserves more comments. In the gas-phase network of ***Nautilus***, HCOOH is only involved in **one formation route**, while it was involved in two routes in the work of Groyne (2023). As in that work, some completeness issues may arise concerning this species, and that will have to be kept in mind. Moreover, though it has a higher complexity than the other compounds, it is still found in an appreciable amount, which is beneficial with regard to Woon's mechanism.

Considering now step b, we once again note a clear similarity in the equilibrium abundances. One would expect HCN to dominate regarding its lower complexity as we observe in Figure E.12.

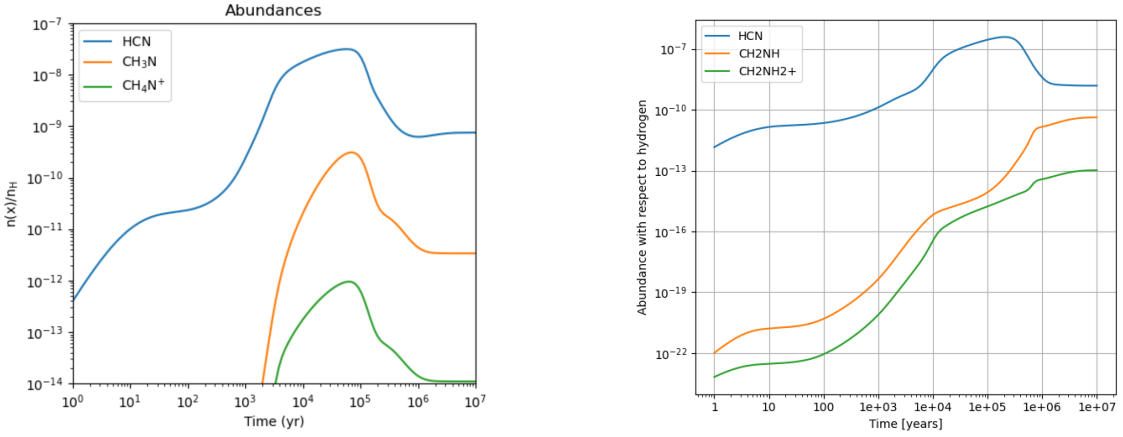

Figure E.12: Abundance temporal evolutions of the glycine precursors linked to the step b of the Woon's pathway using model 1a. Left: Groyne (2023). Right: this work.

As in Groyne (2023) we observe a similar behavior of the abundance curves of methanimine CH_2NH and iminium $CH_2NH_2^+$. This similarity is probably linked to the fact that both molecules are part of the same cationic chain. As explained in Groyne (2023), complementary formation routes involving other ions should be taken into account. The main formation routes of CH_2NH have been studied in the framework of ***Nautilus***, and the dominant ones, i.e. dissociative electronic recombination of $CH_2NH_2^+$, $CH_3NH_2^+$ and $CH_3NH_3^+$, are the same as in the reference work of Groyne (2023). One more reaction has to be taken into account in the context of this work, which is not an ionic reaction and only involves CH and ammonia.

When using model 2a, results are once again quite similar to Groyne (2023). A surprising difference is the higher abundance of formic acid than that of OH. one would have indeed expected the OH radical to be more abundant. This could be related to the fact that it is involved in more destruction reactions in ***Nautilus***, or once again to kinetic parameter considerations. The density being also higher than in model 1a, a reactive radical such as OH would react much easier than a more stable species such as HCOOH. Concerning the decrease in the cationic abundances, one is referred to previous discussions.

For model 3a, the same curves as for model 1a are obtained. This is consistent with what have been said for the Strecker-like synthesis, and we may thus refer to the reasons that have been discussed previously to explain that case.